corrected

CRANFIELD INSTITUTE OF TECHNOLOGY

COLLEGE OF AERONAUTICS

Ph.D. THESIS

Academic years 1984-7

W.G. BROOKS

The design, construction and test of a postbuckled, carbon fibre reinforced plastic wing box.

Supervisor: J.B. Young.

November 1987

This thesis is submitted in partial submission for the degree of Doctor of Philosophy

Contents. Page.

Notation used. 10

Acknowledgements. 13

Abstract. 14

Introduction. 15

Chapter 1. Analysis and design methods for postbuckled composite box structures. 18

1.1. Introduction. 18
1.2. The analysis of plates by closed form solutions. 18
1.3. Design of stiffened panels in the postbuckled range. 20
1.4. Computer based design methods. 21

Chapter 2. The design approach for the wing structure. 26

2.1. The overall design problem. 26
2.2. The design of the stiffened panels. 27
2.3. Steps in the theoretical design process. 27
2.4. Manufacturing considerations. 29

Chapter 3. Nonlinear finite element analysis of stiffened panels. 33

3.1. Introduction. 33
3.2. Panel modelling. 33
3.3. Model development. 39
3.4. The final model, 'panel 6'. 39
3.5. Comparison of LUSAS with experiment. 46
3.6. The effect of different boundary conditions. 51
3.7. Discussion. 52
3.8. Conclusions. 52
3.9. Recommendations. 53

Chapter 4. The theoretical approach for the OPTIMIST Design Program. 54

4.1. Purpose. 54
4.2. Summary of program. 54
4.3. Results for postbuckled panels. 56
4.4. Analytical approach. 56
4.5. Compression buckling of skin panels. 64
4.6. Shear buckling. 64
4.7. Interaction of shear and compression buckling. 65
4.8. Minimum thickness. 65
4.9. Displacement and strain. 66
4.10. Postbuckled stiffness. 66
4.11. Postbuckling amplitude. 67
4.12. Surface strain. 67
4.13 The effect of stiffeners. 69
4.14. Overall buckling of the skin panel. 70
4.15. Weight of the panel. 72
4.16. Optimisation. 72
4.17. Strength reserve. 73
4.18. Use of the program in design. 73

Chapter 5. Finite element modelling of the whole structure. 78

5.1. The development of the method. 78
5.2. Pre-processing of LUSAS data using WEIGHTS. 80
5.3. Considerations when using the method. 80
5.4. Results compared with experiment. 80

Chapter 6. The design of co-cured and adhesively bonded joints in the wing structure. 90

6.1. Peeling effects caused by local buckling at skin/stiffener junctions. 90
6.2. Testing of skin/stiffener joints. 95
6.3. The positioning of assembly joints relative to buckled components. 97

Chapter 7. New Methods of Construction for Composite Box Structures. 104

7.1. Problems with a 'traditional' construction system. 104

7.2. The development of a new method. 104
7.3. The production sequence of the co-cured skins. 105
7.4. Construction of the rib shear webs. 110
7.5. Contruction of the spars. 111
7.6. Assembly of the structure. 112

Chapter 8. The CFRP wing box tooling. 138

8.1. Skin tool production methods. 138
8.2. The resin system. 138
8.3. Mockup construction. 139
8.4. Moulding the CFRP tooling. 139
8.5. Tooling for the rib flanges. 141
8.6. Tooling for the rib and spar webs. 141

Chapter 9. Methods of testing including non-destructive testing. 143

9.1. Structural testing methods. 143
9.2. The whiffle tree. 146
9.3. Non-destructive testing. 148

Chapter 10. Structural weight. 158

10.1. Comparison of the metal and composite designs. 158
10.2. The carbon fibre composite wing in more detail. 160
10.3. Discussion. 160

Chapter 11. Structural load testing. 162

11.1. Introduction. 162
11.2. Test cases. 162
11.3. Positive load test. 162
11.4. Negative load test. 174
11.5. Torsion tests. 178
11.6. Torsion combined with bending. 186
11.7. A comparison of results with theory. 190

Chapter 12. Discussion of the work and suggestions for further research. 193

12.1. General. 193
12.2. Design techniques. 193
12.3. Discussion of the design analysis developed in chapter 4. 193
12.4. The construction method used. 195
12.5. Tooling methods. 195
12.6. Testing. 195
12.7. Conclusions and suggestions for further work. 196

References. 198

Appendix A. Data Input for Finite Element Models. 202

Appendix B. Listing of OPTIMIST program with Flow Diagram and Instructions for Use. 215

Appendix C. Stressing of detail areas. 225

Appendix D. Rejected design approaches. 235

Appendix E. Papers Presented at ICAS and ICCS Conferences. 239

Appendix F. Strain Gauge Positioning and Numbering. 259

Appendix G. Coupon tests for adhesive selection. 272

Appendix H. Drawings. 275

Figures.

Figure No.	Title	Page
0.1	The complete wing box structure.	16
1.1	Direct iteration.	25
1.2	Newton-Raphson iteration.	25
2.1	Finite element wing box model.	30
3.1	Exploded view of LUSAS model "Panel 6".	36
3.2	Panel end element topology.	37
3.3	Panel end node topology.	38
3.4	LUSAS model "Panel 4".	40
3.5	"Panel 6" load/end displacement curves, nodes 1-3.	42
3.6	"Panel 6" load /end displacement curves, nodes 5-7.	43
3.7	"Panel 6" load/end displacement curves, nodes 8-11.	44
3.8	The postbuckled form of model "Panel 6".	45
3.9	LUSAS model "Panel 6" compared with experiment.	47
3.10	Failure mode of model "Panel 6".	48
3.11	LUSAS model "Panel 5".	49
3.12	Comparison of buckling loads and postbuckling behaviour for panel C2.	50
4.1	Sample output graph from OPTIMIST computer program.	55
4.2	Ultimate shear force and net loading for the A1 wing.	57
4.3	Ultimate bending moment for the A1 wing.	58
4.4	Ultimate torque about the wing 25% chord line.	60
4.5	Ultimate running compression and shear loads for the A1 wing.	61
4.6	Ultimate shear flow for the A1 wing.	62
4.7	Postbuckled amplitude calculation diagram.	68
4.8	Postbuckled surface strain diagram.	68
4.9	Postbuckled form with edge restraint at the stiffener to skin junctions.	68
4.10	The effect of variation in proportion of unidirectional fibres in a +-45 plate.	75
4.11	The effect of varying fibre orientation.	76

5.1	Unrepresentative deformations in a finite element model of test box 2.	79
5.2	Test box 2 in the test rig.	81
5.3	Drawing of test box 2.	82
5.4	Cantilever load case for test box 2.	83
5.5	Linear postbuckling model for test box 2.	85
5.6	Positioning of strain gauges on test box 2.	86
5.7	Back-to-back strain gauges 5 and 6 show bifurcation of strains at buckling.	87
5.8	Reversal of strain in gauge 7 at buckling.	88
6.1	Delamination at a skin/stiffener junction.	91
6.2	The corrugated layup.	92
6.3	The bunching problem.	92
6.4	Interleaving and stitching.	94
6.5	The anti-peel strip.	94
6.6	Peel test coupon.	96
6.7	Failure mode of the closely-stitched specimen.	96
6.8	Good and bad locations for joints.	98
6.9	Vacuum clamping.	98
6.10	A typical slotted joint.	100
6.11	A Method of bonding ribs to spars.	100
6.12	Transfer of shear at rib stations.	102
6.13	Aileron pickup design.	102
7.1	The mould is jigged into position.	115
7.2	The plies of prepreg were cut out.	115
7.3	The complete kit of parts.	116
7.4	The complete rib tooling and stiffener cores were positioned.	116
7.5	Junctions in the stiffener cores.	117
7.6	The PTFE release cloth applied to the skin tool.	117
7.7	The first layer of +-45 carbon.	118
7.8	The unidirectional skin plies were added.	118
7.9	The anti-peel strips were set out.	119
7.10	The Rohacell stiffener cores and unidirectional stiffener cap plies were added.	119
7.11	The inner +-45 skin plies.	120
7.12	The anti-peel strips were folded into	

	position.	120
7.13	Kevlar threads define rib positions.	121
7.14	One half of each rib laminate was laid down.	121
7.15	The first half of the rib tool was removed.	122
7.16	The rib tooling was replaced over the rib flange laminate.	122
7.17	The segmented stiffener tooling system.	123
7.18	The stiffeners were covered in a non-porous release cloth.	123
7.19	The tooling almost complete.	124
7.20	The whole area was covered with a breather cloth.	124
7.21	The vacuum bag was attached.	125
7.22	The bag was then evacuated.	125
7.23	The second co-cured skin being unwrapped from the tool.	126
7.24	Detail of a co-cured panel.	127
7.25	Moulding defects.	128
7.26	A rib shear web in the course of construction.	129
7.27	Rib 3706 with aileron pickup showing sandwich panel construction.	130
7.28	The tooling for the rib sandwich panel.	131
7.29	The bobbin used to distribute the load at rib station 3706.	132
7.30	The internal structure of the wing box.	133
7.31	External view showing surface finish.	134
7.32	The mainspar was cut into an angled shape.	135
7.33	The ribs were slid into position.	135
7.34	After inspection, the mainspar was slid into position.	136
7.35	The internal joints and strain gauges.	137
8.1	Rib flange tooling.	142
8.2	The slots for joining components.	142
9.1	The first test box in a three-point beam test.	144
9.2	Construction of a cantilever box beam composite mounting flange.	145
9.3	The loading plate for test box 2.	145
9.4	The whiffle tree.	147
9.5	Positive ultimate load idealisation.	149
9.6	The aileron loading turnbuckle.	150

9.7	Samples of slotted joints for non-destructive testing.	151
9.8	Ultrasonic scans for joints assembled by sliding and slotting.	153
11.1	Acoustic emission versus bending load for the main wing box root area.	164
11.2	Positioning of strain gauges on the main wing box.	165
11.3	Bifurcation of strains for gauges 30.	167
11.4	Bifurcation of strains for gauges 33.	168
11.5	Bifurcation of strains for gauges 31 & 32.	169
11.6	Bifurcation of strains for gauges 19 & 20.	170
11.7	A nonlinear effect at gauge 18.	171
11.8	Positive load test tip deflection.	172
11.9	Positive load test mid deflection.	173
11.10	Root deflection at trailing spar.	175
11.11	Root deflection at leading spar.	176
11.12	Bifurcation of strains in the negative load case at gauges 53.	177
11.13	Bifurcation of strains at gauges 54 & 55.	179
11.14	Stiffening of the panel at gauges 47.	180
11.15	Postbuckling of the skin in bays 1981-2556 in negative loading.	181
11.16	Bifurcation of strains at gauges 39 & 40.	182
11.17	The root area during the negative load test.	183
11.18	General view of the skin postbuckling.	184
11.19	Negative load test mid deflection.	185
11.20	Negative load test tip deflection.	185
11.21	Washout due to aileron loading.	187
11.22	Shear postbuckling due to torsion.	188
11.23	Output from gauges 53 during shear postbuckling.	189
11.24	Tip deflection for the full roll at 0.67 of the positive bending load.	191
11.25	Postbuckling of the wing top surface in the combined torsion and bending load case.	192
C.1	Transmission of shear from ribs to spars.	226
C.2	Design of the aileron pickup ribs.	230
D.1	Construction of the flanged ribs.	238

Tables.

3.1	Material properties for non-linear panel modelling.	35
5.1	Comparison of reduced stiffness linear finite element model with test results for test box 2.	89
6.1	Skin/stiffener junction results.	97
9.1	The strength of coupons taken from a joint specimen.	156
10.1	Wing weight comparison between CFRP and aluminium designs.	159
10.2	Carbon fibre component weights before curing.	161
11.1	Comparison of test results with finite element model prediction for main box.	190

Notation.

The following notation has been used. If more than one use for a symbol is shown, its local meaning is given in the text.

$x \uparrow y = x^y$

A_{ij} = Membrane stiffness matrix terms.

A_s = Stiffener cross sectional area per unit width of panel.

a = Area of cross section, length of plate for buckling analysis. Also postbuckled panel buckling amplitude.

$a()$ = Displacement function.

b = Width of plate.

c = Chord of box.

d_s = Depth of stiffener.

d = Depth of box.

D_{ij} = Flexural stiffness matrix terms.

E_s = Stiffener cap material longitudinal modulus.

E_{11} = Plate longitudinal modulus.

E_{22} = Plate transverse modulus.

$E*$ = Postbuckled longitudinal modulus.

e_{rr} = Error.

e = Strain.

f = Force.

G = Load factor.

G_{12} = Shear modulus.

H = Elastic constant for plate buckling analysis.

I = Second moment of area.

k = Stiffness matrix.

L = Linear operator.

l = Rib spacing, length.

M = Moment.

M_{rib} = Moment applied to rib.

N_x = Running load per unit width in x-axis (spanwise).

N_y = Running load in y-axis (chordwise).

N_z = Running load in z-axis (rib crushing).

N_{xy} = Running shear load in xy axis.

P = Pressure.

P_{aero} = Aerodynamic pressure loading.

P_x = Load in x direction.

P_{cr} = Buckling load.

P_s = Load due to stiffener.

P_{tot} = Total panel load.

q = Shear flow.

R = Radius.

S = Shear force.

T = Torque.

t = Skin thickness.

w = Panel width.

λ = Buckle half wavelength.

θ_1, θ_2 = Angles used in bending strain calculations.

u = Displacement in-plane.

μ = Beam column amplification factor.

Ψ = Sum of internal and external forces.

τ_{cr} = Critical shear buckling load.

ν_{12} = Poissons ratio.

Acknowledgements.

Many people have been indispensable in helping to bring this project to fruition. My heartfelt thanks go to all of them including:

My first supervisor, Ray Butler, for instigating the project and providing support in the early stages. He has continued to take an active interest in the work since leaving Cranfield.

Mike Snell for supporting and monitoring the work from the Royal Aircraft Establishment. He suggested many different lines of research, and has also continued to take an interest since leaving the RAE.

Joe Young, my supervisor at Cranfield in the later stages, who picked up the project in mid-stream. Ken Griffin has also taken an interest at Cranfield.

Richard Potter of the RAE who has ably taken over from Mike Snell.

Maurice Crook of the plastics laboratory at Cranfield, for providing expertise in manufacturing and tireless help. Ian Walton also provided great assistance during construction of the main wing structure. These two people were prepared to work at all hours to complete the layup.

Phil Berkely of Westland Helicopters, who was very helpful in demonstrating all the different types of non-destructive testing techniques for composite materials.

My dear wife Alison, who has meticulously proof-read the manuscript. She has given great encouragement to complete this work.

Abstract.

A postbuckled, carbon fibre reinforced plastic (CFRP) wing box has been designed, manufactured and tested for an aerobatic light aircraft, the Cranfield A1.

Methods of analysis have been evaluated including:

i) Non-linear finite element analysis for the prediction of panel postbuckling.

ii) A simpler technique based on an effective width method. This forms the core of a design program, 'OPTIMIST'. It predicts buckling loads, postbuckled reduced stiffness and overall column failure of co-cured hat stiffened panels. It then optimises the configuration of a box beam for minimum weight.

iii) The use of the effective width method allied to a large scale, linear finite element analysis.

The work includes the development of a new method of construction for composite box structures. The wing skin, stiffeners and rib flanges are co-cured together. Integral slotted joint features are formed in each part. The structure is then adhesively bonded together. A full description of the manufacture of the wing box is included.

The structure was also tested in a specially designed rig. It was tested to ultimate design loads in:

i) Positive bending to 13.5G.

ii) Negative bending to -9G.

iii) Pure torsion resulting from full aileron load.

iv) Torsion with 9G bending.

The compression panels were seen to postbuckle and recover in each load case. Results are compared with theory, and with the original aluminium A1 wing. The structure is 25% lighter than its aluminium counterpart.

Finally, suggestions are made for possible areas of further research.

Introduction.

Carbon fibre reinforced plastic (CFRP) is being increasingly applied to primary aerospace structures because of the reduction in mass possible. However, due to the unusual properties and processing of these materials, new structural concepts have to be developed to realise the advantages to the full. Structural analysis is complicated for these materials by their stratified, directional nature.

In thin-walled structures such as certain wings or fuselages, local buckling of compression or shear skins becomes a problem. The structure can be designed to be stable against this buckling. This may be achieved through closely spaced stiffeners or sandwich construction. These approaches involve extra structural weight in stabilising the thin skin.

Local buckling may occur at a load well below that of the failure load of the structure as a whole. The ratio of failure load to local buckling load, the post buckling ratio, is dependent on the width to thickness ratio of the panel. This may extend up to 15 or more in some cases. As the panels buckle, their compression stiffness reduces. Stiffeners can be arranged at the panel edges to take up relatively more of the load as this happens. Provided that the stiffeners remain stable in the overall and torsional modes, loading may increase.

This post-buckled design concept has been used with success since the 1940s in aluminium alloy structures. At the present time however, designers in composite materials are not confident in exploiting the extra reserve of strength available through postbuckling. A great deal of research effort is being directed towards investigation of the buckling and postbuckling of composite plates. Various analysis techniques have been developed, which are evaluated in this thesis.

There are major problems to solve in transferring and expanding this research to a complete working structure. These include:

i) Delamination of stiffeners from skin panels caused by the buckling.

ii) The need to avoid assembly joints in buckled areas.

iii) The need to avoid interaction between modes of buckling.

Figure 0.1

The complete wing box structure.

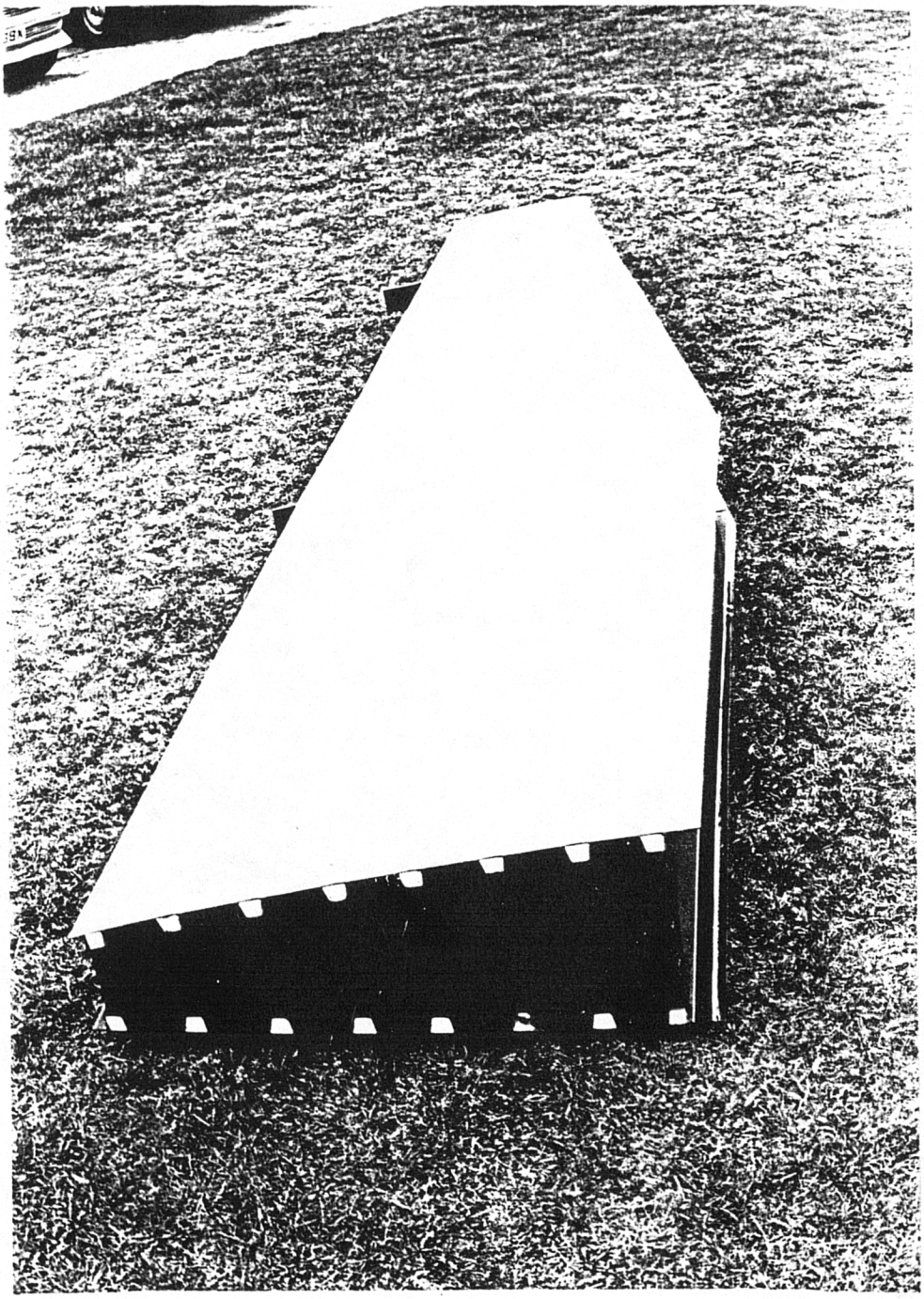

In this work a complete postbuckled CFRP wing box has been designed, manufactured and tested. The completed structure is shown in fig. 0.1. The external geometry and loadings from the existing Cranfield A1 aerobatic light aircraft were used. This was because a close comparison could be made to the original postbuckled aluminium wing, and because of the possibility of fitting a CFRP wing to the aircraft to demonstrate the technology. Two main advantages of the wing are:

i) The reduced weight will improve the climb rate of the aircraft.

ii) The reduced spanwise moment of inertia, coupled with high wing torsional stiffness will improve roll and yaw accelerations.

Details of the Cranfield A1 can be found in ref 27. A series of design notes based on the A1 can be found in refs 28-35.

Chapter 1.

Analysis and design methods for postbuckled composite structures.

1.1 Introduction.

The use of postbuckling in advanced composite structures has only been seriously considered since 1975-80. Now, various means of analysis of postbuckled panels have been developed. However, the accuracy of any theoretical analysis is dependent on the idealisation of the problem. A sound base of correlation with the performance of actual structures is always required. Hitherto, lack of design data and confidence have prevented the use of postbuckling in composite structures.

If possible any method used for analysis should allow the designer to retain a measure of physical insight into the problem. If an involved method of analysis such as non-linear finite elements or finite strips is to be used, then there should be a back-up simplified solution method by which to judge the results. This simplified design check must in turn be compared, and if necessary modified, to correlate with relevant experimental data. This is especially true for non-linear problems such as buckling where the wrong buckling mode may be indicated. Only by completing this cycle is it possible to design in confidence.

1.2. The analysis of plates by closed form solutions.

The theoretical analysis of postbuckled orthotropic plates is being actively pursued. Recently, papers have appeared which deal with complexities of postbuckled plates with non-linear properties or curvature. For example, the analysis of Arnold & Mayers (1) takes into consideration the effects of matrix material non-linearity and transverse shear deformation. The Reisner variational theorem is used to provide differential equations of equilibrium for each layer of the plate. These are then integrated over the volume of the plate. The complexity of this analysis coupled with incomplete information render this work very difficult to use in design . The same comments apply to Stein (2) where a

Newton-based algorithm is used. This provides solutions of Von-Karman equations for large displacements of orthotropic plates. This can be under combined loadings. Kobayashi (3) has developed an analysis technique based on the Galerkin method for postbuckling of curved laminated plates.

For designing postbuckled specially orthotropic plates the author has found a paper by Rhodes & Marshall (4) to be of the utmost value. It provides solution methods for postbuckled stiffness. It is based on an effective width concept applicable to three types of simply supported, specially orthotropic plate. These are where the unloaded edges are:

i) held straight in-plane,
ii) assumed to allow in-plane movement,
iii) free at one edge.

The formulae developed are relatively easy to use and not problem specific. The analysis involves the use of Galerkin's method. This obtains an approximate solution to the differential equations for the strain energy in bending of a specially orthotropic plate. The principle of minimum potential energy is then employed to give the final result.

The effect of allowing the buckling wavelength to shorten as buckling progresses is considered and an analysis method given. The effect of the tendency of the buckles to flatten across the width of the plate is also taken into account. Equations for these two variables are presented. These may be solved graphically, or by numerical minimisation of end load.

The paper also contains graphs of the various solutions compared with the work of others. This paper has enabled the author to develop a computer sizing and optimisation program. This is described in chapter 5.

Finding the buckling load of specially orthotropic composite plates is relatively straightforward. ESDU data sheet 80023 (5) can be used. Alternatively, the solution to the differential equation for bending of such a plate can be found. This is in Cranfield design notes 8050 (6). A similar expression can be obtained for the shear buckling load as in Deitz (7). Using the interaction curve between shear and compression buckling load from Lekhnitski (8), the critical loads for any combination of these may be determined.

Assuming the plate to behave in a linear way before buckling, and applying a reduced stiffness after buckling, the behaviour of the plate can be described. By adding stiffener properties and assuming

strain compatibility, stiffened panels may be designed. This is the basic approach used by the author for initial sizing of the structure.

1.3. Design of stiffened panels in the postbuckled range.

Dickson, Cole and Wang (9) have developed an analysis method for postbuckled composite panels with stiffeners. The design of the stiffeners is of prime importance in postbuckled panel design. Suprisingly, in this paper they have concentrated on the use of open-section stiffeners. Torsional/flexural buckling of these sections is considered. The solution method includes the effect of shear in the postbuckled analysis. This is because the method is mainly intended for the analysis of lightly loaded fuselage panels. The effects of curvature, which are significant, are not included. The analysis method for the skin panel is insufficiently well described and too complex to allow others to use it in design.

Williams, Anderson et al (10) in a survey of recent developments in composite structures have shown the clear superiority of closed-section stiffeners. When stiffened panels are designed to be buckling-resistant, the greater torsional stiffness of these prevents premature failure through stiffener torsional buckling. This gives rise to greater structural efficiency over a wide range of loadings. This conclusion was reached from optimisation of various non-buckled stiffened panel layouts using the program PASCO (11). Avoidance of stiffener torsional failure is obviously of even greater importance in postbuckled design.

In this paper some factors influencing correlation of experimental and theoretical buckling are described. Graphs are presented for the effects on the theoretical buckling strain caused by:

i) transverse shearing of the laminate.
ii) laminate thickness variations from the ideal.
iii) stiffness variations from the ideal.

These factors in combination may account for a 13% discrepancy in the buckling load of typical CFRP stiffened panels.

1.4. Computer based design methods.

1.4.1 Two dimensional panel design approaches.

These design methods all assume uniform properties along the plate, the analysis being of a series of strips linked together to form a desired cross-section. The method has the potential for the analysis of postbuckling in compression. However, the computer programs presently available such as PASCO only design for buckling.

The program PASCO mentioned above is a widely used finite strip buckling program for composite plates. It contains an optimisation routine, CONMIN, for minimising structural weight at buckling. The actual buckling analysis part is called VIPASA (12). Plates (which may be anisotropic) can be linked together in this program to form any desired prismatic cross section.

The theoretical foundation for the VIPASA program is due to Wittrick, Williams et al (13,14,15). Its operation relies on prior knowledge of the plate displacement functions. These are assumed to be sinusoidal along the plate, and polynomial across it. These functions are chosen for compatibility with the boundary conditions between the adjacent strips and at the edges and ends of the plate.

The finite strip analysis works very well for structures loaded in pure compression. When shear loading is introduced, the longitudinal displacement function for each strip has to vary in phase across the plate whilst still satisfying the boundary conditions.

Belgrano (16) has used PASCO for the optimisation of CFRP hat stiffened panels for a range of different compression loading intensities. These panel designs were constructed and tested at Cranfield. He found the panels to possess a considerable range of postbuckled strength. The panels failed either by column buckling, localised fibre 'brooming' at stress concentrations near the edges, or by separation of the co-cured stiffeners from the skin panels.

Separation was caused by the bending and peeling loads imposed by postbuckling, which caused delamination at the skin/stiffener junction. The junction was shown to be an obvious key area of

research for successful postbuckled panel design. Data from Belgrano's work was invaluable in proving design techniques for the wing box. PASCO can only work up to the point of buckling and so does not give insight on these important postbuckled effects.

Snell (17) has shown that VIPASA results tend to predict buckling loads greater than those observed experimentally. A correction factor of 0.7 is recommended to apply to VIPASA results for design purposes. Transverse shear effects and discrepancy between theoretical and actual plate stiffness are suggested reasons for this. The D12 and D23 bending/twisting terms are shown to have a strong effect on the result. Plates tend to have the highest buckling load when these terms are zero.

The same author (18) has found that VIPASA can be used to predict buckling loads of curved panels. This is achieved by linking a number of straight strips to approximate the curve. With a coarse approximation, predicted loads were again too great. However, the prediction improved with increasing number of strips. Hussain (19) has also compared VIPASA results with experiment for curved stiffened panels.

Stroud, Greene & Anderson (20) have compared PASCO results with non-linear finite element analysis using the programs EAL and STAGS. It is stated that for combined loadings of compression and shear, the VIPASA analysis gives conservative results when the buckling half-wavelength exceeds 1/3 of the panel length. For this reason an adjusted analysis is incorporated in PASCO by means of a smeared orthotropic solution. This adjusted solution gives buckling loads that are 25% too high if the buckle half wavelength is over 2.5 times the stiffener spacing. The method is inapplicable if the half wavelength is less than 1.5 times the stiffener spacing.

The advantage of using analyses such as PASCO/VIPASA or the Rayleigh-Ritz based program NEWSGC (21) is in speed of operation, both in processor time and data input requirements. A finite strip or similar analysis for postbuckling would be of great benefit. Graves Smith and Sridharan (22) and Hancock (23) have proposed analyses for postbuckling using a finite strip method. Both of these are presently only applicable to isotropic materials. Snell (26) reports that work is in progress in extending the capability of NEWSCG, a Raleigh-Ritz analysis program, to cover postbuckling.

1.4.2. Finite Element Methods.

A geometrically non-linear analysis can be used to model the postbuckling of composite plates and shells, as described by Zienkiewicz (24). Linear analysis assumes that there is a direct linear relationship between displacement and strain. This is expressed in matrix notation as:

$$e = Lu$$

Similarly, it is also assumed that the stress/strain relationships are linear. These assumptions are clearly not valid in the case of a postbuckling plate. This is because displacements may increase dramatically without a great change in midsurface strain. The load shortening curve can be solved by using an incremental technique. This can be for either displacement of the end nodes or load. At each increment, an iterative solution method is used. The iterative solution determines the reduced stiffness of the plate in its state of deformation at that point. A point on the load curve corresponding to that displacement can then be plotted. The non-linear finite element equations can be written in the form:

$$\Psi(a) \equiv k(a)_a + f = 0$$

If $k^o = k(a^o)$ then an approximate solution may be obtained from:

$$a^1 = -(k^o)^{-1} f$$

This process is repeated as:

$$a^n = -(k^{n-1})^{-1} f$$

until the error, $e_n = a^n - a^{n-1}$ is less than a desired small tolerance. This technique is known as direct iteration, illustrated in fig. 1.1. Another technique which converges to the correct solution faster is the Newton-Raphson method. This method computes the tangent to the curve by forming a tangent stiffness matrix at each approximate solution until

the error is again reduced to a small value. This is illustrated schematically in fig. 1.2. In order to start the out-of-plane deformation at the point of buckling, a small eccentricity or transverse load is required.

Newton-Raphson iteration can be used in the LUSAS finite element program (25). The author has used the program for modelling the postbuckling of a composite stiffened panel. Non-linear finite element modelling is described in more detail in chapter 2.

The great strength of the finite element method lies in its ability to model all the features of the design. Thus such problems as modal interaction of local and stiffener flexural buckling can be tackled, as well as any combination of loading.

The disadvantages lie in the long solution times and large memory space required. Also, in linear problems, there is always one well-defined solution. With a non-linear analysis an incorrect solution may be presented. As previously mentioned, a measure of qualitative insight into the expected solution is required for good results. Small increments of load or displacement are also required. *

The finite element code STAGS as used in (20) has been developed to include a non-linear analysis capability. This has been used by Snell (26) in a programme of research into the buckling and postbuckling behaviour of CFRP panels of different curvatures. Correspondence of predicted and experimental postbuckling behaviour was not achieved unless small compound curvatures were introduced into the panel model. These small curvatures had to be of the same shape as the first eigenvalue buckling mode. This mode shape could be obtained from a linear eigenvalue buckling analysis using the same program.

The problem was very demanding owing to the highly non-linear behaviour of curved panels at buckling. These panels tend to snap through at buckling to exhibit some postbuckled strength reserve if thin and of low curvature. At high curvatures, violent snap-buckling of the panel causes failure. *

* During the course of this work a new technique for non-linear finite element analysis has been developed known as the arc-length method. The method does not require small increments of load or displacement to follow a non-linear path. Further, highly non-linear behaviour such as that found in snap-buckling may be followed.

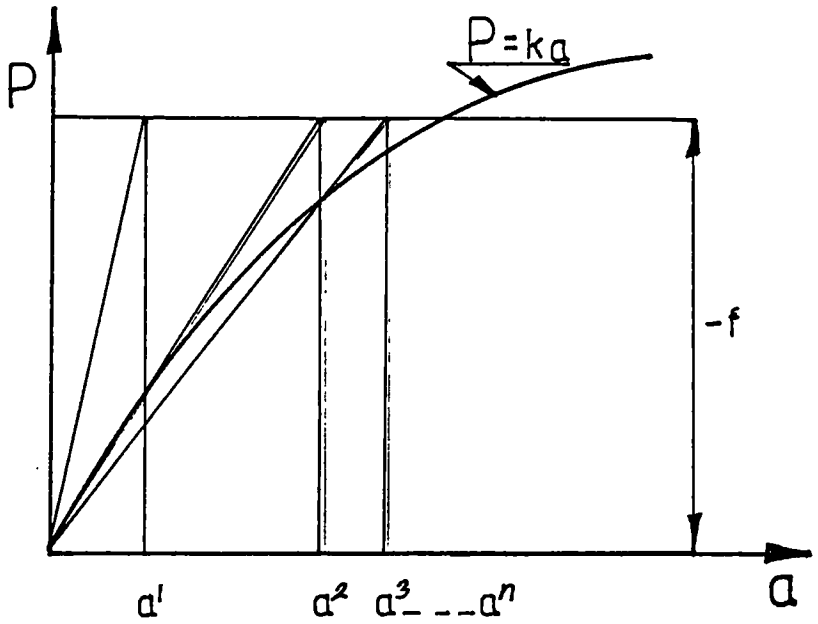

fig. 1.1

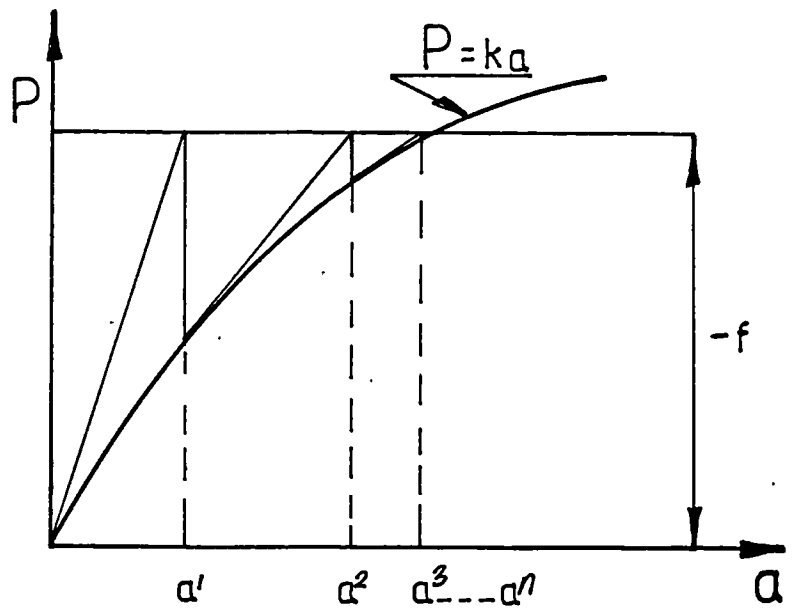

fig. 1.2

Chapter 2.

Design approach for the wing structure.

2.1. The overall design problem.

In order to design the wing the following areas had to be tackled:

a) Effective design of minimum weight postbuckled compression skin as part of a wing box. The design of the compression skin was subject to the following constraints:

i) A maximum overall compression strain limit of 0.4%, which was set to allow for degradation of the material in hot, wet conditions. This also allows for variation in material properties due to manufacturing tolerances.

ii) A Maximum local buckling amplitude of 3% of wing depth at the ultimate design load. This was set as a limit for aerodynamic profile considerations.

iii) Shear strength and stiffness constraints due to torsion of the wing box.

iv) A balanced, symmetric laminate.

v) A minimum gauge of 0.5mm.

b). The design of an efficient structural configuration of ribs, stiffeners and spars to incorporate and stabilise the compression panels.

The positioning of the spars was effectively fixed by the mounting points for the wing on the A1 fuselage. With the deep section and the light loading, two spars were quite sufficient. The spars were designed to be only shear carrying members, as the skins were intended to take all the bending loads. The ribs were designed to resist:

i) Airloading, causing a shear force to be transmitted to the leading and trailing stiffener sidewalls.

ii) Brazier loading caused by the crushing of the two wing skins together as they curve under bending loads.

iii) Loads from aileron pick-up points.

The ribs also had to be stiff enough to provide a simple support condition for the compressed stiffeners in the Euler buckling mode. The ribs must also maintain the desired aerofoil cross section.

c) The complete structure had to be designed in such a way that it could be economically manufactured and assembled. This had to be achieved without undue difficulty and without incurring a large weight penalty. The fact that the structure was postbuckled also introduced special considerations in the design and placing of joints.

2.2. The design of the stiffened panels.

A study was first made of the stiffened panels designed by Belgrano (16). The cross sections of these panels had been optimised at buckling. The optimisation was achieved by the use of the PASCO finite strip panel buckling program. Some exploratory runs were also made by the author using the same program. It was decided to use the same ratios of stiffener external proportions throughout the wing. The stiffeners that gave the best results in the program were of a trapezoidal cross section. The closed cross section would give the stiffeners a high torsional stiffness. Hence, the stiffened panel design would not tend to be sensitive to stiffener torsional/flexural buckling.

For manufacturing reasons, a foam core was incorporated in the stiffener. This allowed easy co-curing of the stiffeners and skin. The foam would also tend to stabilise the thin sidewalls of the stiffener, which are essentially shearwebs. The structural superiority of panels incorporating closed section stiffeners in CFRP has also been confirmed in (10).

2.3. The theoretical design process for the wing box took the following steps:

a) The running compression and shear loads for the wing were determined by calculation from the wing

loading diagrams (28, 32) and the wing geometry.

b) One of Belgrano's panels, No C2, (16) was analysed using a geometrically non-linear finite element model, as described in chapter 3. This panel was also representative of the inner wing loading for the A1 wing design. The purpose of the non-linear finite element study was to try to predict any modal interaction effects. Modal interaction between local skin buckling and stiffener torsional buckling can reduce the failure load. Interaction would not be considered in a more simplified sizing analysis. The non-linear model would also highlight features such as the change in distribution of the load between skin and stiffeners caused by buckling. The computational requirements of non-linear finite element analysis made modelling the total wing structure impractical using the available computing facilities.

c) A special computer sizing and optimisation program, PANSIZE, for postbuckled CFRP stiffened panels was developed. This is described in chapter 4. Incorporation of a weight calculation module, and an optimisation section, enabled different configurations of structure to be compared.

Having determined the best overall configuration of ribs and spars, the minimum weight dimensions for the skin panels and stiffeners at each bay were calculated. The stiffeners were sized to resist long column failure at a set strain limit.

d) Brazier load and air load combined cases were calculated for the ribs. The same PANSIZE program was used to design them to be buckling-resistant at the calculated loadings. The structure was designed so that the shear load from each rib is not transferred directly to the spars in the usual manner. The shear load is transferred to the spars through a bonded joint at the stiffener sidewalls. Because there is no attachment of the spar shear web to each rib, the ribs were designed to incorporate small integral vertical stiffeners. The stiffeners make the ribs independently stable without attachment to the spars.

Load bearing points such as the aileron mountings were designed so that special ribs projected through the rear spar. These ribs incorporate sandwich panel shearwebs and unidirectional material in the top and bottom.

e) The spars were designed as buckling-resistant sandwich panels. The sandwich panel design was chosen for its simplicity of manufacture. It also combined well with the assembly system. A corrugated shear web could work very well here at increased expense.

f) Having determined the types and thicknesses of all parts of the structure, a complete finite element model could be constructed of the whole wing box. The model (fig. 2.1) was constructed with the aid of the WEIGHTS program (38). The WEIGHTS software includes a finite element preprocessor for box beam structures. The model incorporated the reduced stiffness properties for the skin panels obtained from the PANSIZE program.

By using a linear finite element model, overall deflections and strain levels could be checked. Properties of components could then be adjusted and finally fixed. The advantage of this approach for an overall model was that a simple linear/elastic analysis could be used. This consideration, coupled with the use of small-deflection elements, reduced the analysis time to 20 minutes. The process is described in chapter 5.

2.4. Manufacturing considerations.

From this point onward the design was steered by the need to match it to the special characteristics of the material and its production technology. Ciba-Geigy 913 series CFRP prepregs were chosen. The standard XAS-913-27 was used for the unidirectional material, whilst the woven 913-ts-815 was used for compression panel skins and shear webs. The 913 series was chosen for its low curing temperature of 120°C. This made the choice of tooling materials less critical. The woven material was selected for ease of handling in manufacture and superior damage tolerance. In (36) Curtiss & Bishop point out the advantages of 0°(uni)/45°(woven) compression panels. These are:

i) Little degradation in strength and stiffness

ii) Improved strength after damage compared with unidirectional stacked layups.

This part of the design process involved the following areas:

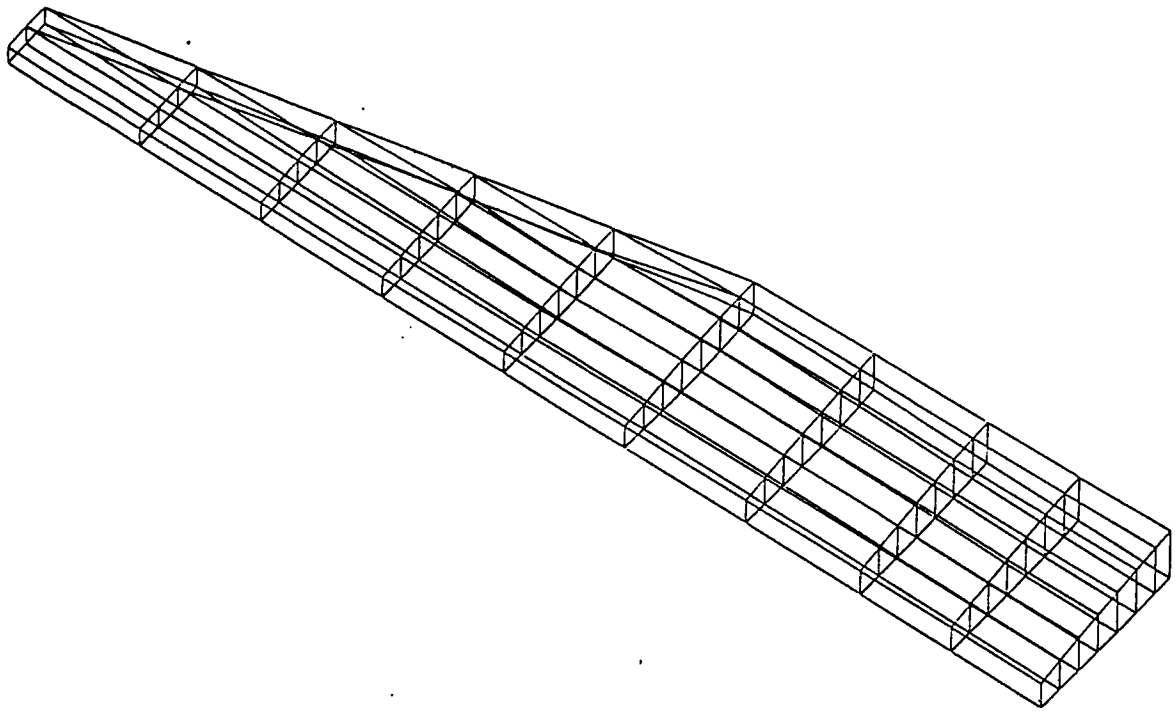

Finite element wing box model

Fig 2.1

a) Joints tend to be a problem in composite materials unless carefully designed and situated. For this reason it was decided to produce as much of the structure as possible as one integrally cured unit. However, a totally co-cured design can introduce considerable tooling and laminating difficulties. The best solution was considered to be to produce each skin complete with stiffeners and rib flanges. All the joints between postbuckled panels and the stiffeners would be co-cured. Assembly joint features could be incorporated into the co-cured skin mouldings. In the final design, the rib shear webs and spar shear webs are designed to plug into these features.

Even when co-cured the transverse strength of the laminate is poor. This causes great concern in the design of a postbuckled structure. The junction between each stiffener and the buckled skin is subjected to transverse peeling and bending effects. Some previously tested panels (16) failed by delamination of the skin from the stiffeners. Research was undertaken to find a way of improving the strength of this junction. Methods included stitching with an interleaved layup, and the development of an anti-peel strip as described in chapter 6.

b) A new method of assembly for the box was designed and tested, as in chapter 7. The assembly method was designed to allow efficient load transfer by adhesives in shear. Bolted connections were not used. The box was also designed so that no large assembly clamps were required. Joints were positioned where they would not be subjected to peel loadings due to local buckling effects. One result of the spar joint location was that the shear loads from each bay could be transmitted to the spar along the leading and trailing stiffener sidewalls. This made the difficult joint between the rib and spar shearwebs unnecessary, making assembly and inspection much simpler.

c) Tooling had to be designed in order to produce the wing, as in chapter 8. Although vaccum bag/autoclave production is now quite standard for flat panels, special tooling had to be designed for the integrally cured structure. The tooling also had to be fairly easy to produce. Methods such as numerical machining of aluminium blocks, for example, were much too expensive.

The main tools were produced by wet laminating

onto a hardboard mockup of the wing. These tools were of CFRP for matched expansion characteristics, but were of fairly light construction. They relied on the autoclave trolley for torsional stiffness. Rib flanges were produced by means of matched tooling moulded from CFRP directly onto the tool surface. The stiffeners, being a fairly simple shape, were produced using segmented sheet steel intensifiers.

d) Testing methods had to be devised for the completed structure, which are described in chapter 9. Some requirements for the testing of composite airframe structures have been published by the CAA (37). Inspection of the structure, especially in the joint areas, is also of great importance. In chapter 9 several non-destructive testing methods have been tried on representative joints.

The root fixing to the test rig was designed as a massive carbon and glassfibre flange. The flange was directly laminated to the root area of the wing after suitable preparation of the surface. No mechanical fasteners were used between the wing and the flange. To apply the load, a whiffle tree was specially designed and constructed. The load was hydraulically applied. A separate turnbuckle was used to apply torque to the wing for the aileron load cases.

e) The wing was instrumented with strain gauges, deflection gauges and acoustic emission equipment. Some gauges were mounted back to back on the skin panels in order to monitor the postbuckling behaviour. A series of tests was completed for the following ultimate load cases:

i) Positive wing bending.

ii) Negative wing bending.

iii) Torsion due to aileron deflection at zero G.

iv) Torsion combined with wing bending.

The test results are described in chapter 11.

Chapter 3.
Non-linear finite element analysis for the postbuckling of CFRP panels.

3.1. Introduction.

In order to judge the potential of the non-linear finite element method, a typical compression panel was modelled and compared with experiment.

A series of stiffened CFRP compression panels were designed and tested by G.Belgrano (16). The panels designed were representative of wing skin compression panels. The design study was based on airliner outer wing loads. This is comparable with the root compression load in the A1 wing skin, 400 kN/m. One of these panels was modelled using LUSAS, a finite element structural analysis system. LUSAS is available on the College of Aeronautics DEC VAX 750 computer at the time of writing.

The LUSAS finite element package is capable of three dimensional analysis of orthotropic materials. A Newton-Raphson iteration process can be invoked for problems with geometric non-linearity, enabling panel postbuckling behaviour to be modelled. The package provides output to a Benson plotter and a graphics terminal. Hence the deflected form may be observed. Belgrano's test panel C2 was selected for modelling, as this was the simplest in having two stiffeners. It still had a central skin panel area in which local buckling could develop.

Belgrano's panel design used top hat section stiffeners which were filled with "Rohacell wf 71" acrylic foam. The foam cores simplified production of the panels, and helped to stabilise the stiffener sidewall skins.

At first, the panel was modelled without any representation of the foam. The model then showed instability of the stiffener sidewalls. Incorporation of the foam into the model stopped the sidewalls from buckling.

3.2.Panel modelling.

3.2.1 Material properties.

The material properties of the three different laminates used for the stiffener web, the stiffener

cap and the main panel skin were evaluated using the laminate analysis program "LAMANAL" developed by R.J.Butler at Cranfield. This gives an output of the membrane, coupling, and bending property matrices A, B, D as well as the moduli Ex, Ey and Exy for the whole plate, based on the fibre orientations and properties of the individual laminae.

The material properties used initially were the standard room temperature properties for XAS 914 carbon fibre in an epoxy matrix. See table 3.1.

3.2.2 Element topology.

The material properties output from LAMANAL were applied to 110 semiloof thin shell elements. These were arranged as 11 elements across the plate, in ten strips along the length as seen in fig. 3.1. The central skin panel area was one element wide, but the elements used were the highest order shell models available, capable of modelling arbitrary geometry. The original modelling had been with 220 elements, but the later inclusion of solid core elements in the stiffeners overran the VAX 750 computer capacity.

The stiffener core effect had to be included since the early modelling indicated an unrepresentative local instability of the stiffener walls. The cores were modelled using the good but computationally expensive HX20 solid semiloof elements. Because of this the model had to be simplified.
The final node and element topology used can be seen in figs 3.2 & 3.3.

3.2.3 Loading simulation.

In order to observe the local buckling progressively developing, the structure was loaded by means of incremental end displacements of one end of the plate, with the opposite end face held stationary. To simulate the test conditions, the compression loaded ends were modelled encastre, and the sides were simply supported along their length, being free to move in-plane. The incremental displacements were in .05mm increments from 1 to 1.7mm or .2-.36% strain, analysed with 10 iterations per increment.

Table 3.1. Material properties used for analysis.

XAS is Ciba-Geigy 913 carbon/epoxy prepreg, 27% resin for the unidirectional and 35% resin for the woven material. R51 and R71 are Rohacell 51 and 71 respectively. These are polymethylacrylate foams.

Materials / Property	XAS u.d.	XAS wov.	R51	R71
0 modulus N/mm^2*10^3	130	69	.07	.092
90 modulus N/mm^2*10^3	9	65	"	"
Poission's 12	0.28	0.1	.3	.3
Shear modulus N/mm^2*10^3	4.8	5.5	.021	.03
0 tensile N/mm^2	1370	600	1.9	2.8
90 tensile N/mm^2	42	550	"	"
0 compression N/mm^2	-1000	-540	-.9	-1.5
90 compression N/mm^2	-200	-510	"	"
Shear ult. N/mm^2	60	60	.8	1.3
Specific Density	1.61	1.65	.05	.07
0 thermal e/C*10^-6	-0.1	5	33.0	35.0
90 thermal e/C*10^-6	28	5	"	"
0 moisture e/%M *10^-3	0.09	0.5	83	90
90 moisture e/%M*10^-3	3.0	0.5	"	"

Figure 3.1.

Exploded view of LUSAS model "panel 6"

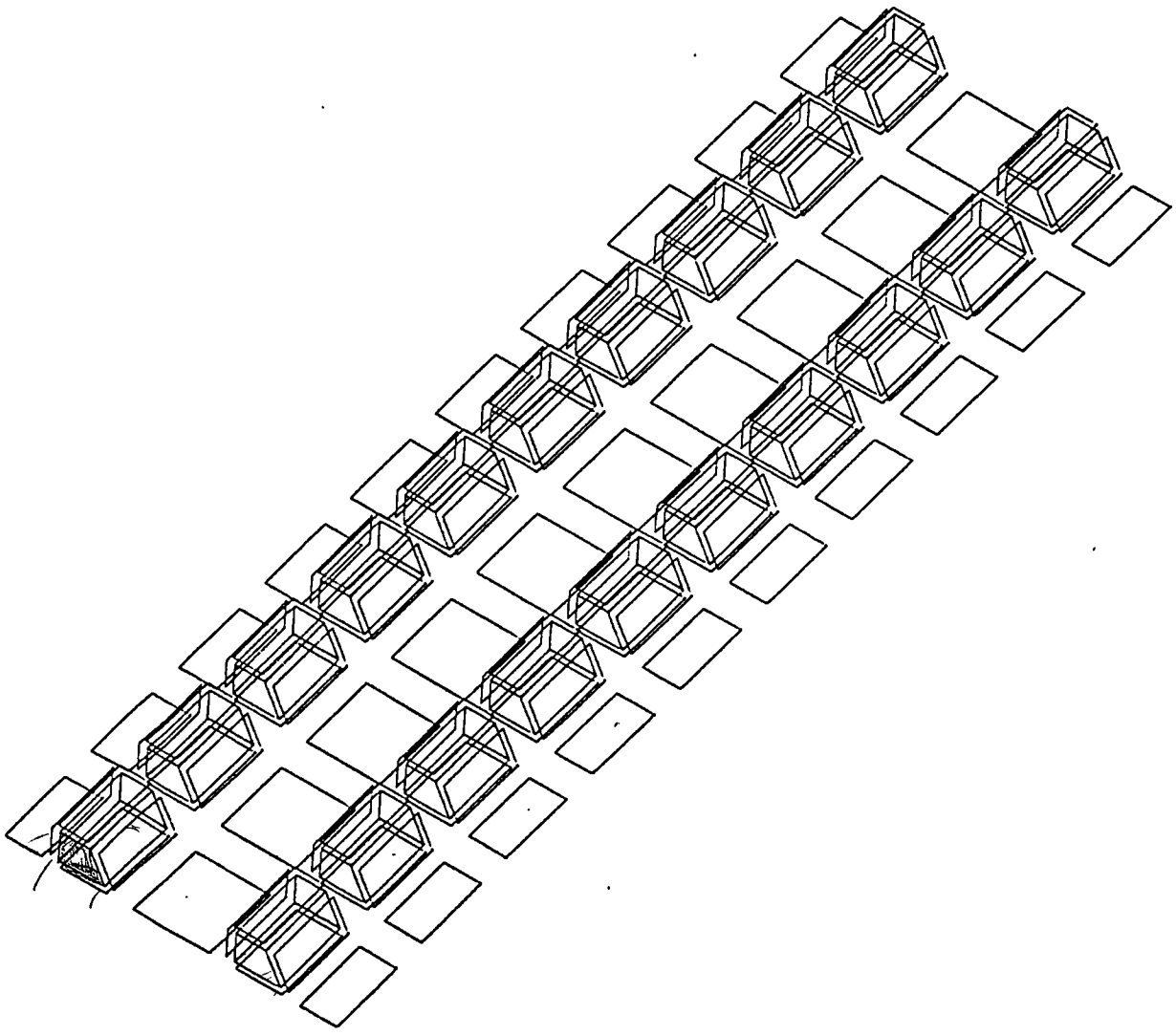

Figure 3.2

Panel end element topology for LUSAS model "panel 6"

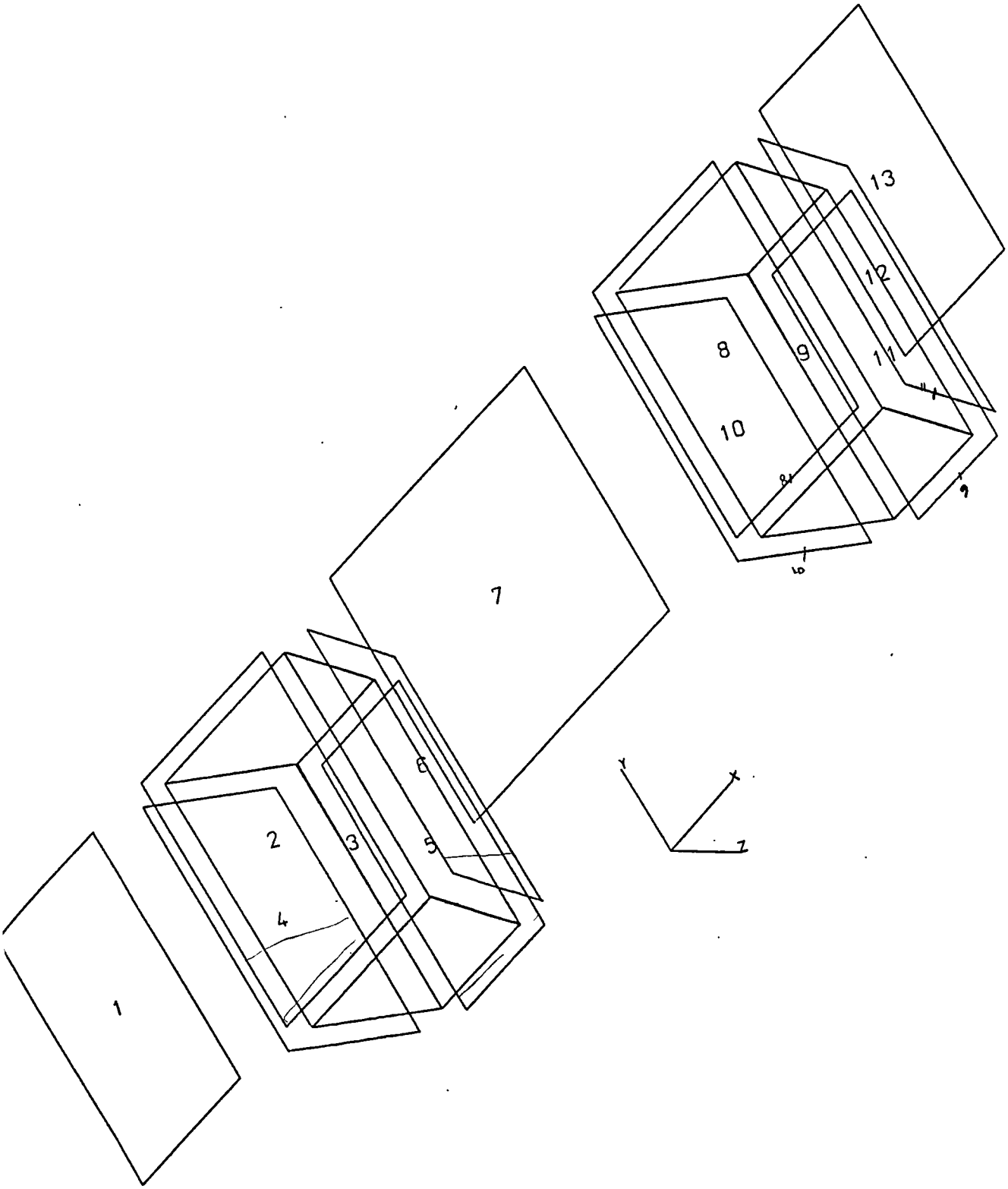

Figure 3.3

Panel end node topology for LUSAS model "panel 6".

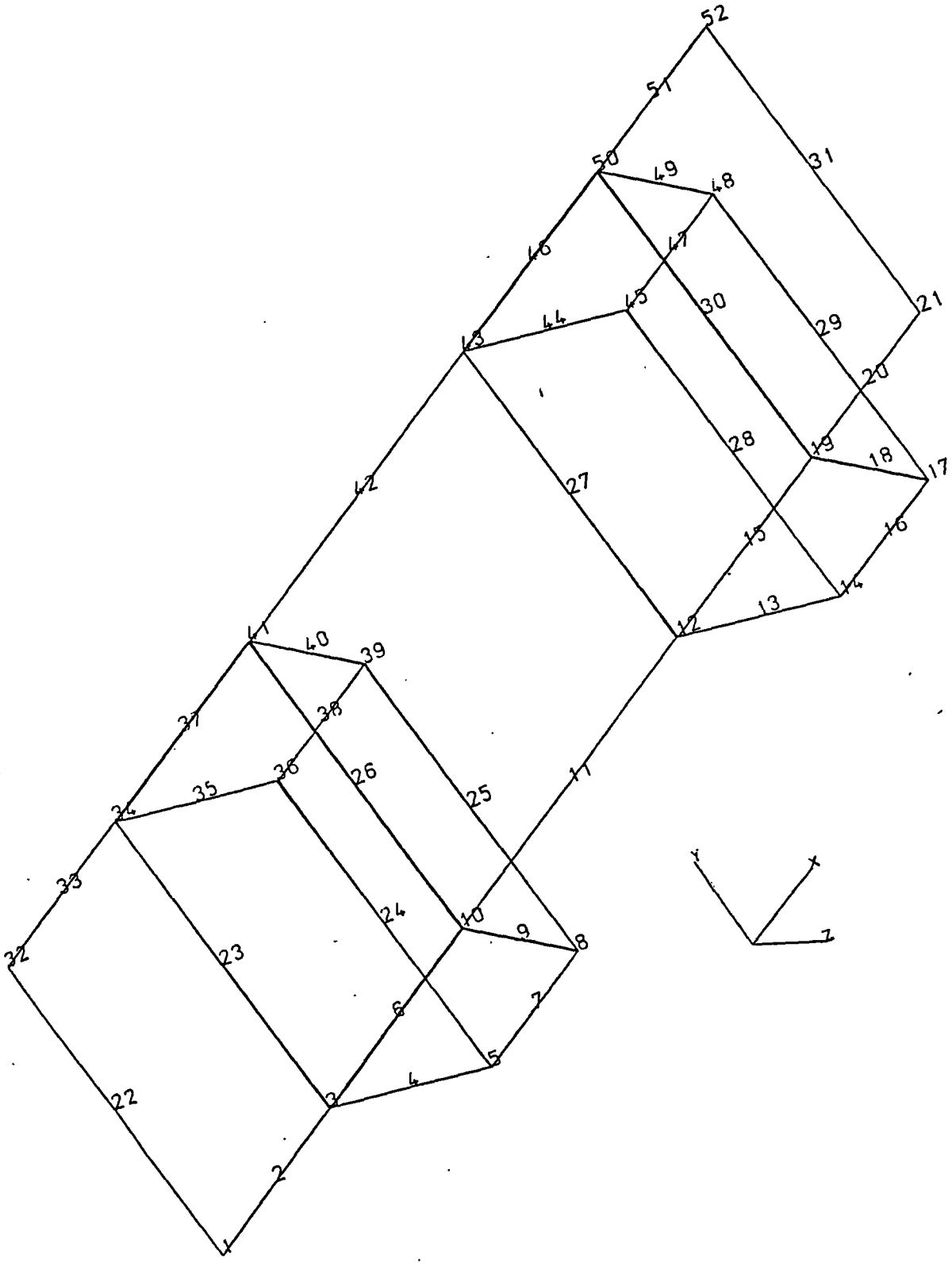

3.3.Model development.

The panel model was developed over 6 runs, during which the effects of stiffener core material, fibre orientation and loading increments were discovered. This culminated in model 'panel 6'.

3.3.1 Loading increments.

It was found that the choice of appropriately small displacement increments was critical in obtaining solutions well into the postbuckled range. With this model, the program would stop running before all the load cases were completed if the strain increments were more than .01%, due to a solution divergence check. This made it necessary to determine carefully the range over which the analysis would be performed, i.e. from just before the onset of local buckling onwards. A PASCO or initial sizing and buckling analysis is useful in determining this point quickly, before embarking on a full non-linear solution.

3.3.2 Stiffener behaviour.

The model was run in the early stages with no representative stiffener foam cores. It was found that the stiffeners themselves would then exhibit pronounced local buckling of the walls, which are quite thin especially at the sides. These walls had a b/t ratio of 52. The side walls of the stiffeners were intended to be very light shear webs, depending on the foam for stability under load. The effect of hollow modelled stiffeners can be seen in fig. 3.4. This resulted in the panel model being reduced in stiffness by 15% from that expected in the postbuckled range from panel tests.

The inclusion of isotropic solid stiffener core elements provided the extra stability required, using Rohacell 71kg/m^3 foam properties.The stiffeners would then remain stable as the skin panels buckled.

3.4. The final model, 'Panel 6'.

This model had a load/displacement curve which

Figure 3.4

LUSAS model "panel 4" showing deformation of stiffeners when no stiffener core was modelled.

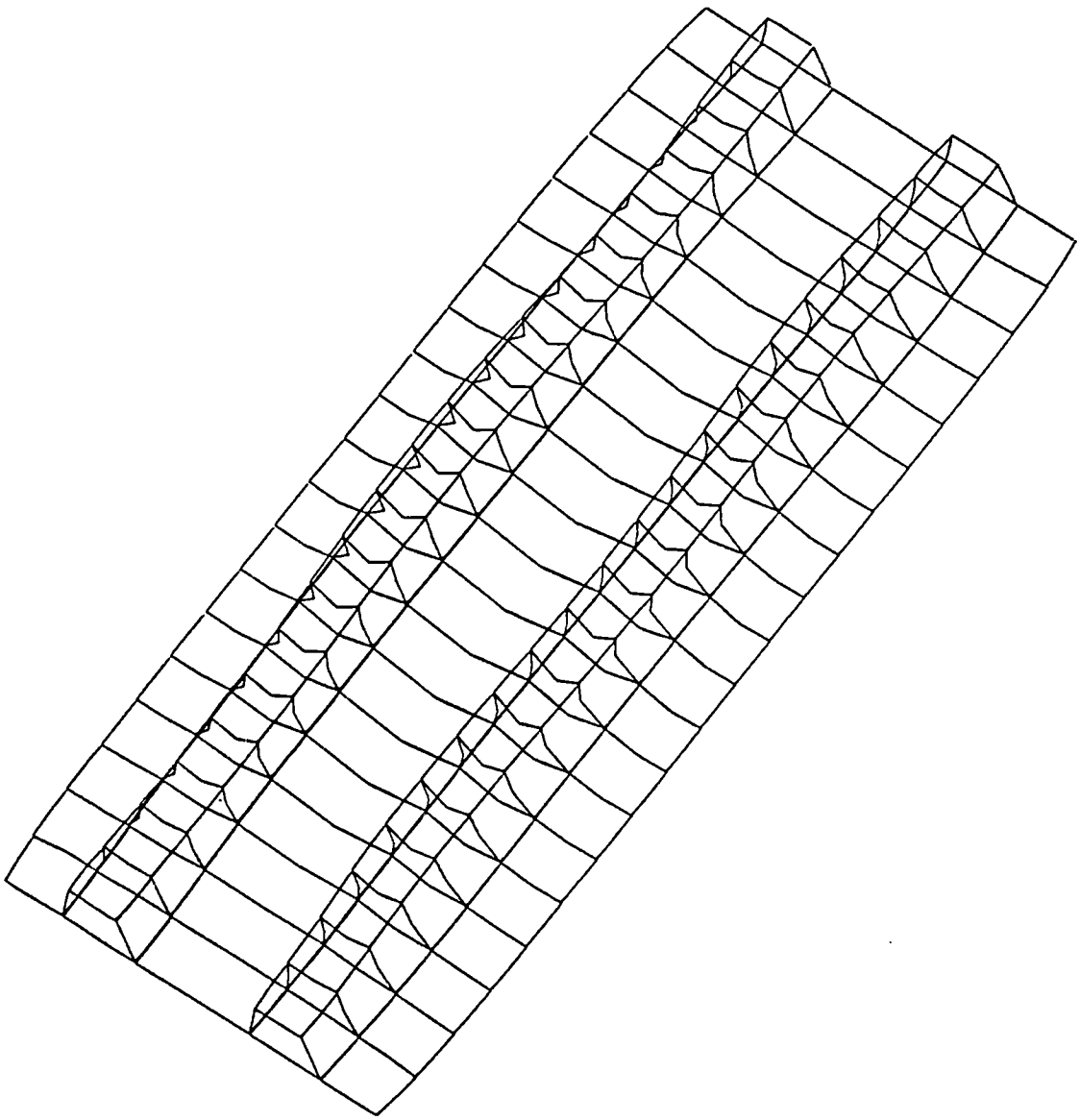

closely matched the experimental result for test panel C2. The data input for this problem is in Appendix A. The panel was modelled using QSL8 semiloof thin shell elements in a geometrically non-linear analysis for uniaxial compression.

3.4.1 Stiffener behaviour.

The stiffeners, when stabilised by a representative core, exhibited no large changes of shape as the panel was compressed. They appeared to be stable enough to resist failure both in the overall Euler mode and in the torsional mode, allowing the skin panels to postbuckle progressively, as was intended in this design.

3.4.2 The postbuckled form.

This took the form of a series of local buckles in the areas of skin panel between the stiffeners and the edges of the panel. The half-wavelength of these buckles was of the order of the width of this part of the panel, so this area buckled into a series of squares typical of postbuckled behaviour.

3.4.3 Load/displacement behaviour.

The detail possible in the finite element analysis enabled the load/displacement behaviour of the panel to be observed for each node across the width of the plate. The reduced stiffness behaviour of a postbuckled, stiffened compression panel is very complex. The load/displacement behaviour of the whole panel is a macroscopic indication of many different effects.

These effects can be seen in the load/displacement curves for each nodal end reaction, figs 3.5 to 3.7. At node 2 the most obvious indication of postbuckling behaviour can be observed. This node is positioned in the centre of the outer skin panel between the stiffener and the edge of the panel, where the local buckles were seen to develop as seen in fig. 3.8.

The load/ displacement curve can be seen to rise linearly up to 1.4mm displacement where the buckling commences and the stiffness of this part of the panel can be seen to progressively reduce. Its complement can be observed in the load/displacement curve for

Figure 3.5

LUSAS model "panel 6" load/end displacement curves.

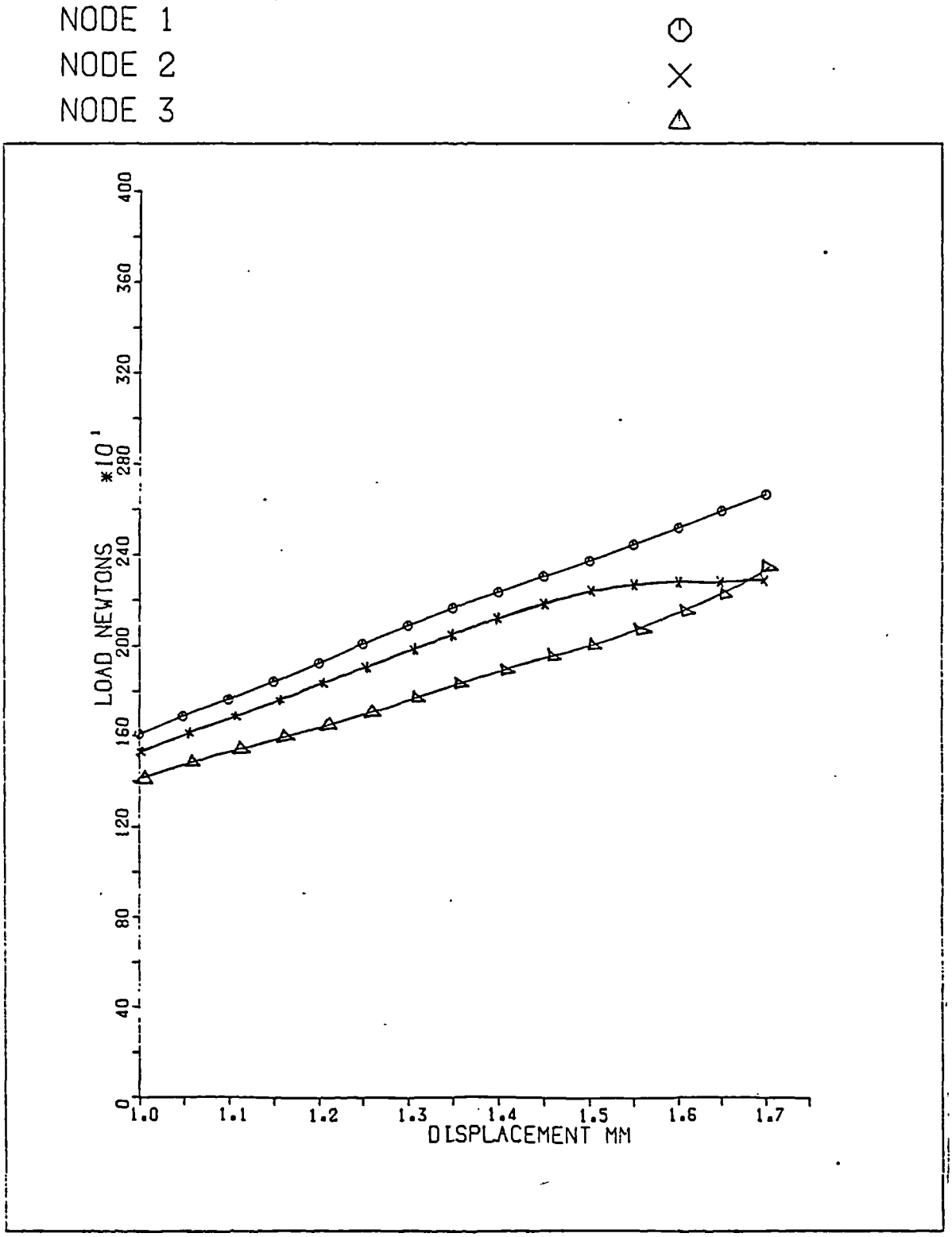

Figure 3.6

LUSAS model "panel 6" load/end displacement curves.

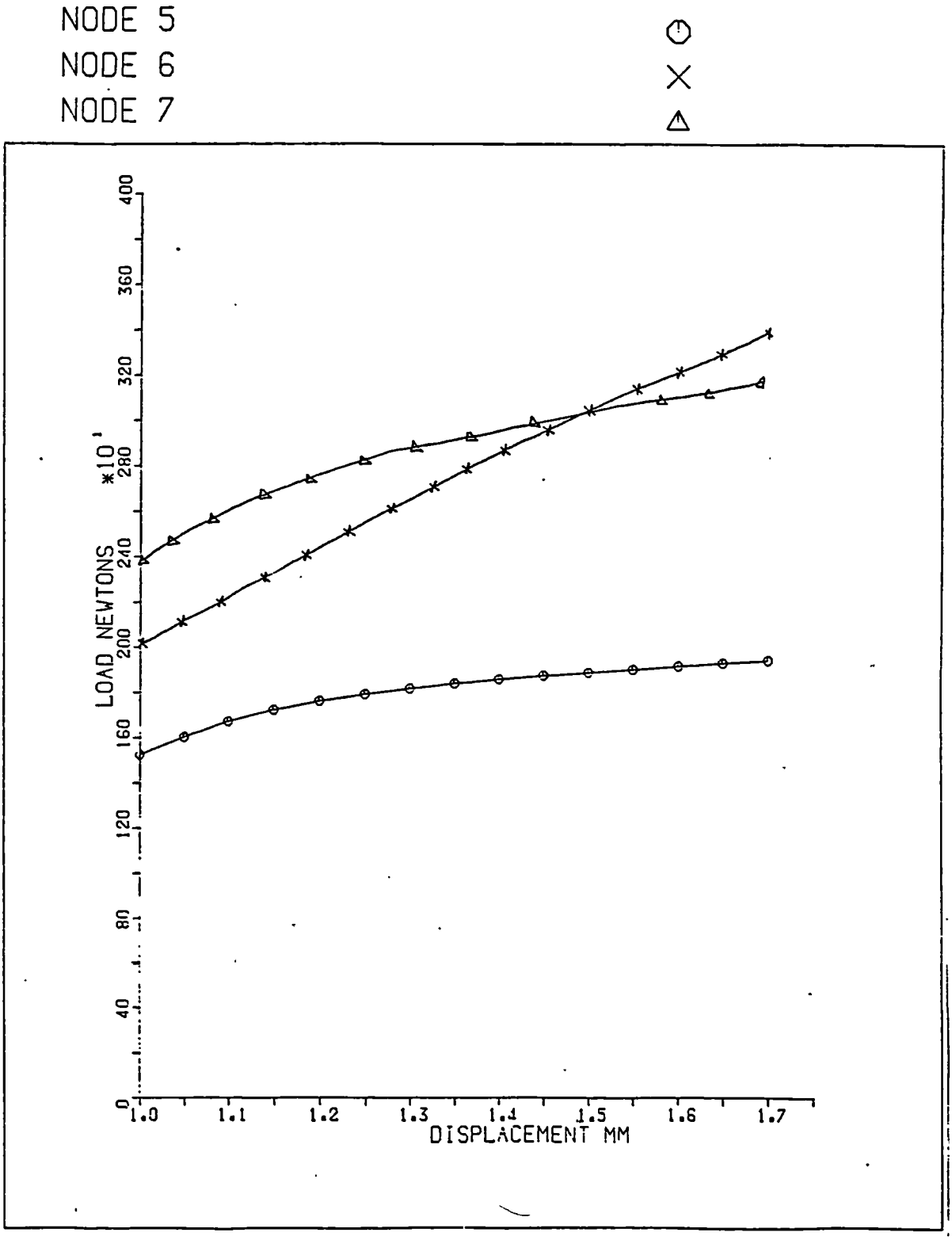

Figure 3.7

LUSAS model "panel 6" load/end displacement curves.

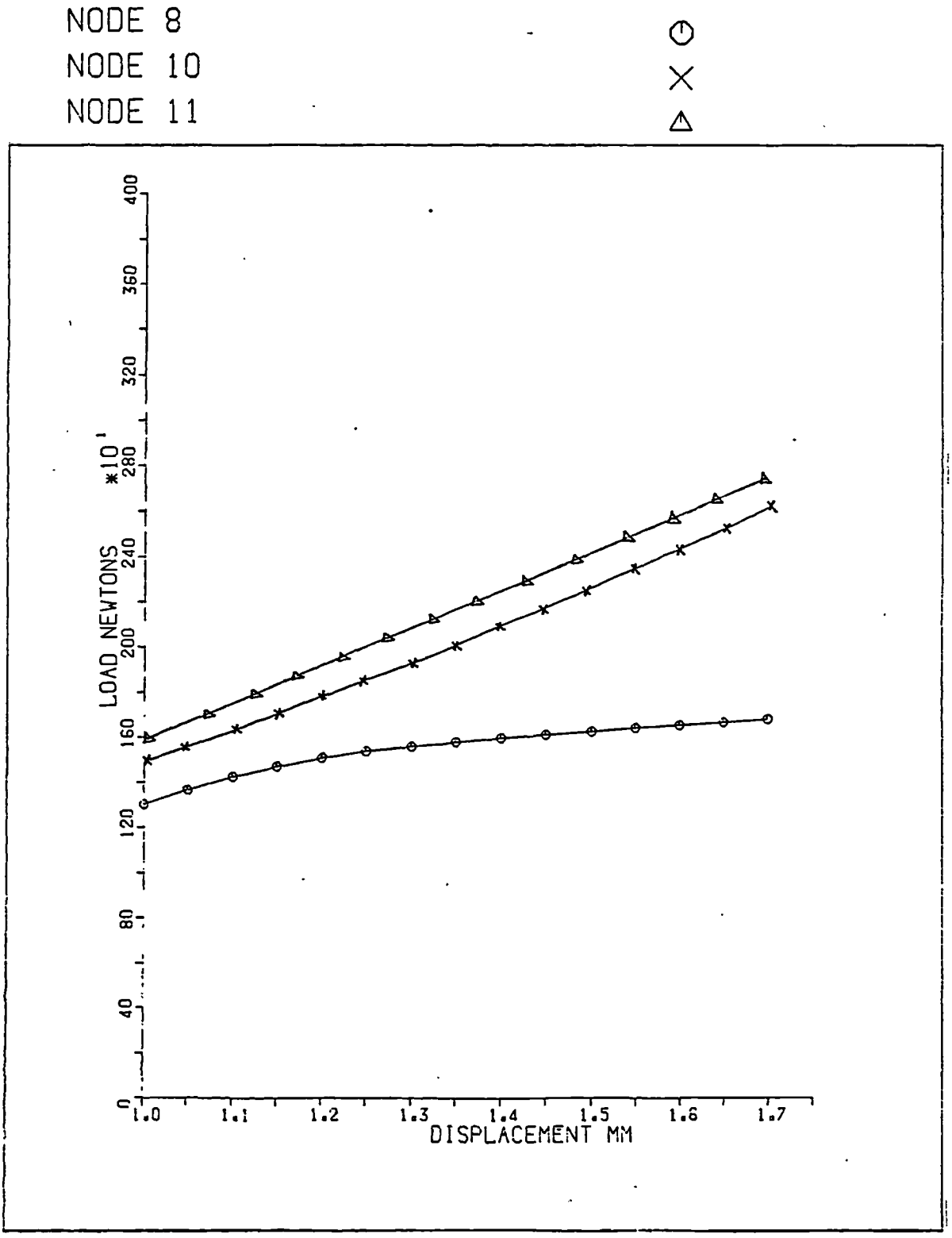

Figure 3.8

Showing the exaggerated postbuckled form of LUSAS model "panel 6". Panel sides simply supported.

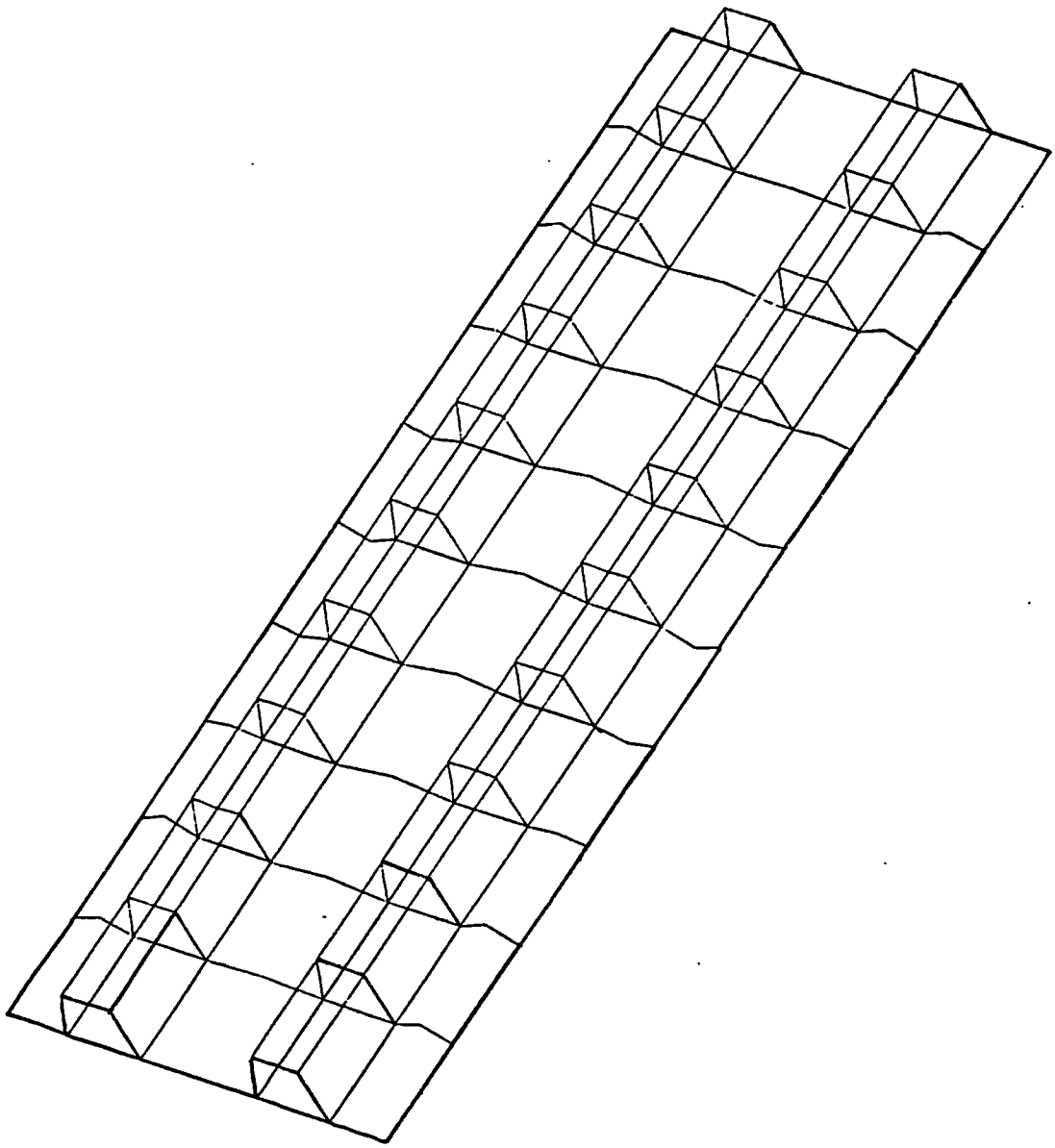

node 3, at the edge of the stiffener. Here the load reacted by this part of the panel rises non-linearly as the displacement increases beyond 1.4mm. Other parts of the panel can also be seen to react to the load in different ways.

When the load/displacement curve for the whole panel, fig. 3.9, is observed, a progressive decline in stiffness can be seen. This is caused by the combination of these various effects across the plate.

3.5. Comparison of LUSAS with experiment and effective width analysis.

In fig 3.12, the model is compared with experimental readings from the test on panel C2 in (16), pgs. 103 & 104. Results from an effective width design method for postbuckled composite panels is also shown. The effective width method is described in chapter 4.

3.5.1 Strain gauge readings.

The top curve of fig 3.12 indicates mean readings from strain gauges 7 & 8 in the longitudinal axis. These were positioned at the centre of the plate, one on each side. This curve has an approximately linear trend over the range examined, being similar in this respect to the LUSAS P6 graph for node 11, the middle end node.

3.5.2 Platen displacement.

The lower curve is that produced by platen displacement readings from dial gauges during testing of panel C2. The reduced stiffness over the range observed can be attributed to movement of the panel end fittings and local brooming of the fibres near the ends. In this test the panel failed locally at a corner near an end fitting before a failure of the panel occurred by buckling effects. When the end fitting area failed, the support conditions changed and so the test panel failed in an overall Euler mode. Belgrano concludes that this localised failure was exacerbated by over-tightness of the knife-edge side supports.

Figure 3.9

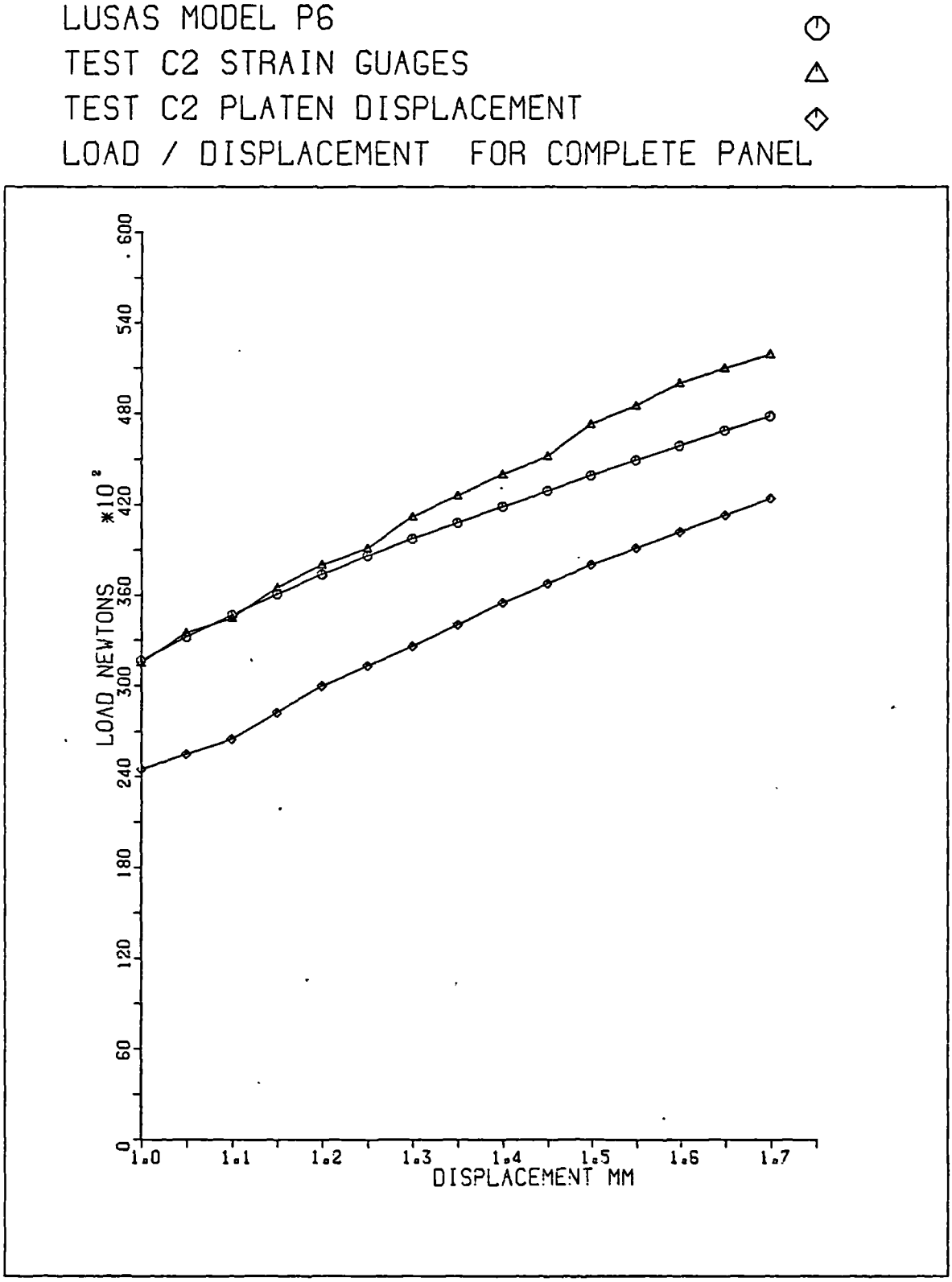
LUSAS MODEL P6
TEST C2 STRAIN GUAGES
TEST C2 PLATEN DISPLACEMENT
LOAD / DISPLACEMENT FOR COMPLETE PANEL
LOAD NEWTONS *10²
0
60
120
180
240
300
360
420
480
540
600
1.0
1.1
1.2
1.3
1.4
1.5
1.6
1.7
DISPLACEMENT MM

Figure 3.10

Failure mode of LUSAS model "panel 6" when the simply supported sides are constrained against spreading widthwise.

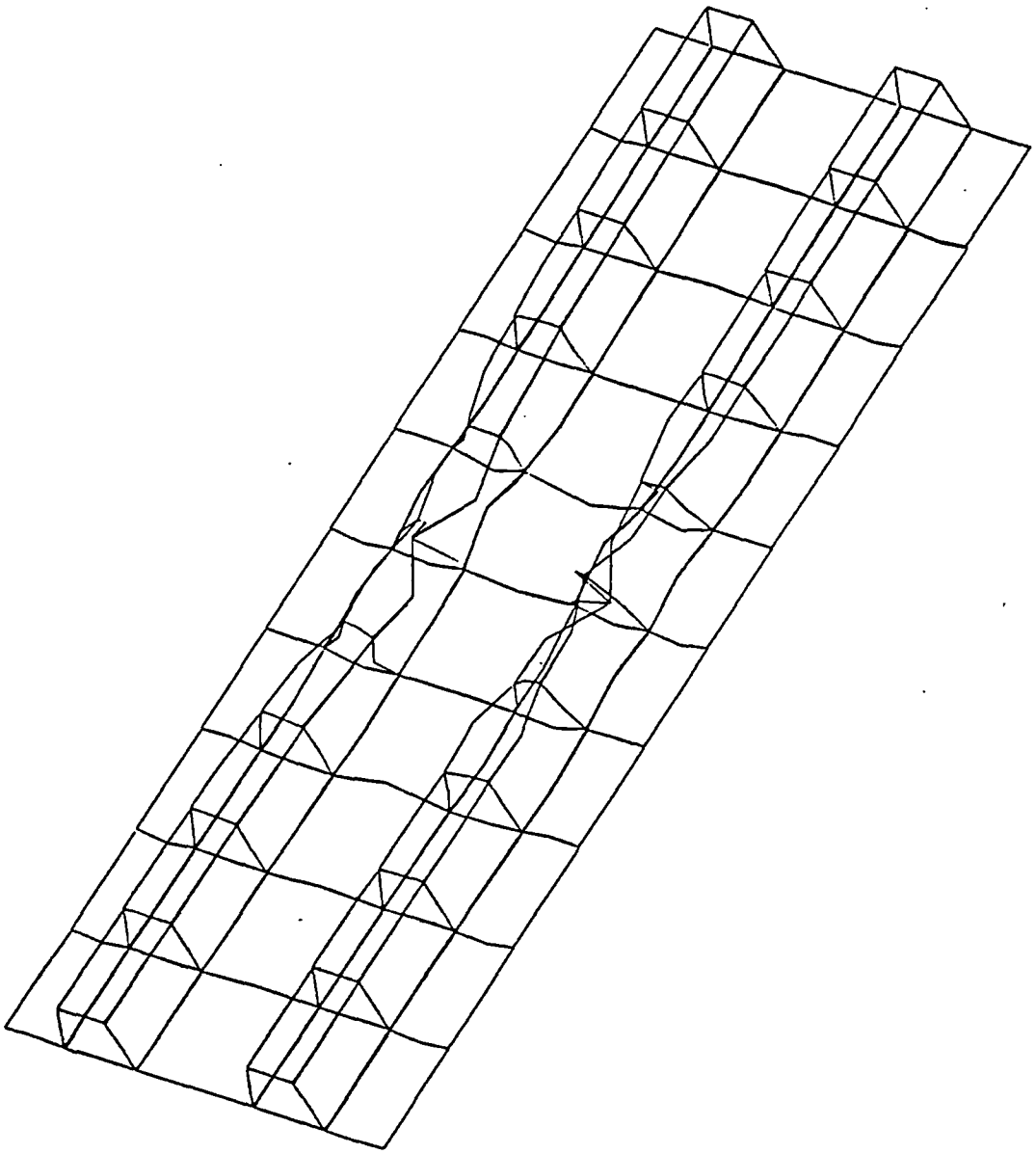

Figure 3.11

LUSAS model "panel 5". This shows the exaggerated postbuckled form when the sides are free to wave.

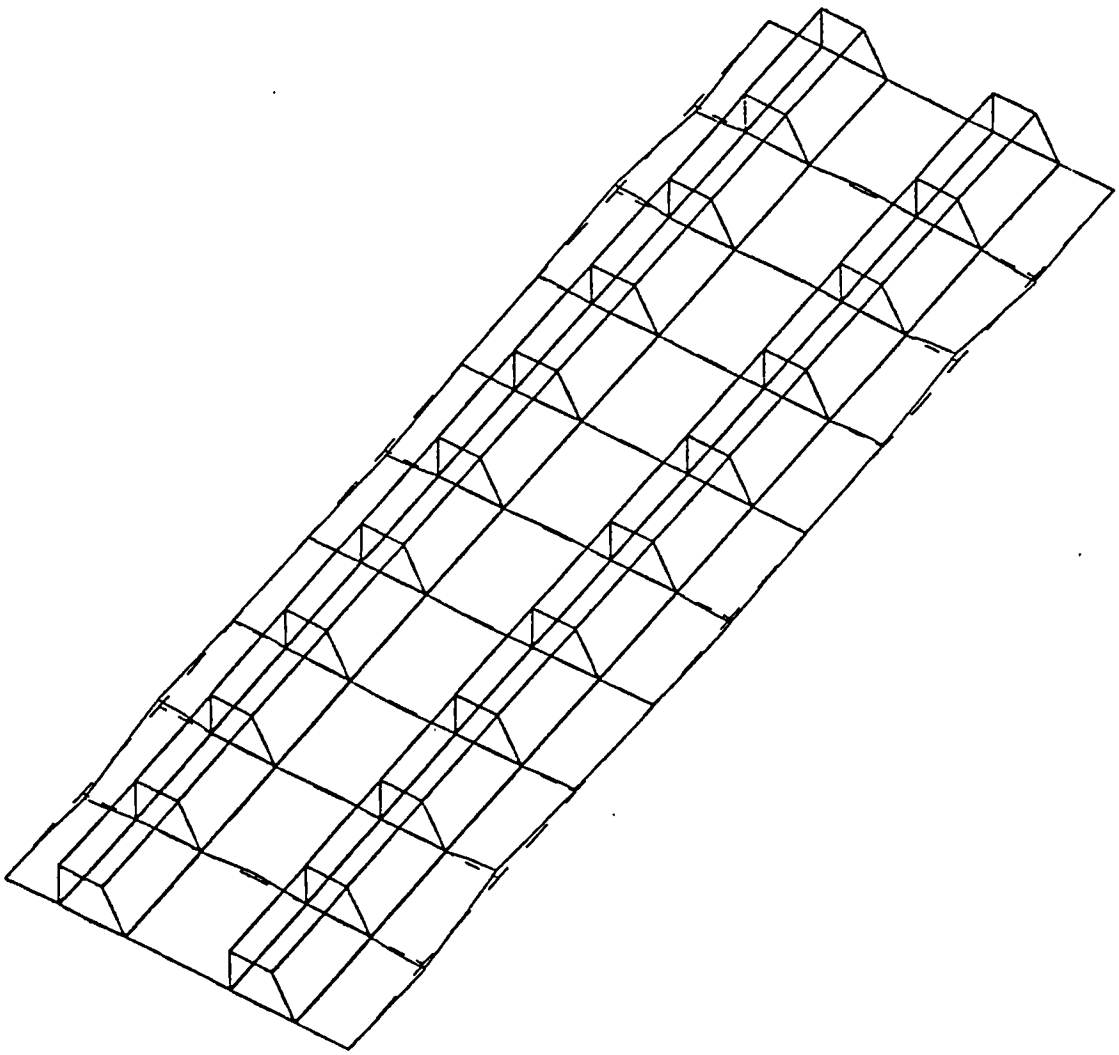

Figure 3.12

Comparison of buckling loads and postbuckling behaviour for panel C2. Non-linear finite element analysis and the effective width method of chapter 4 compared with experiment.

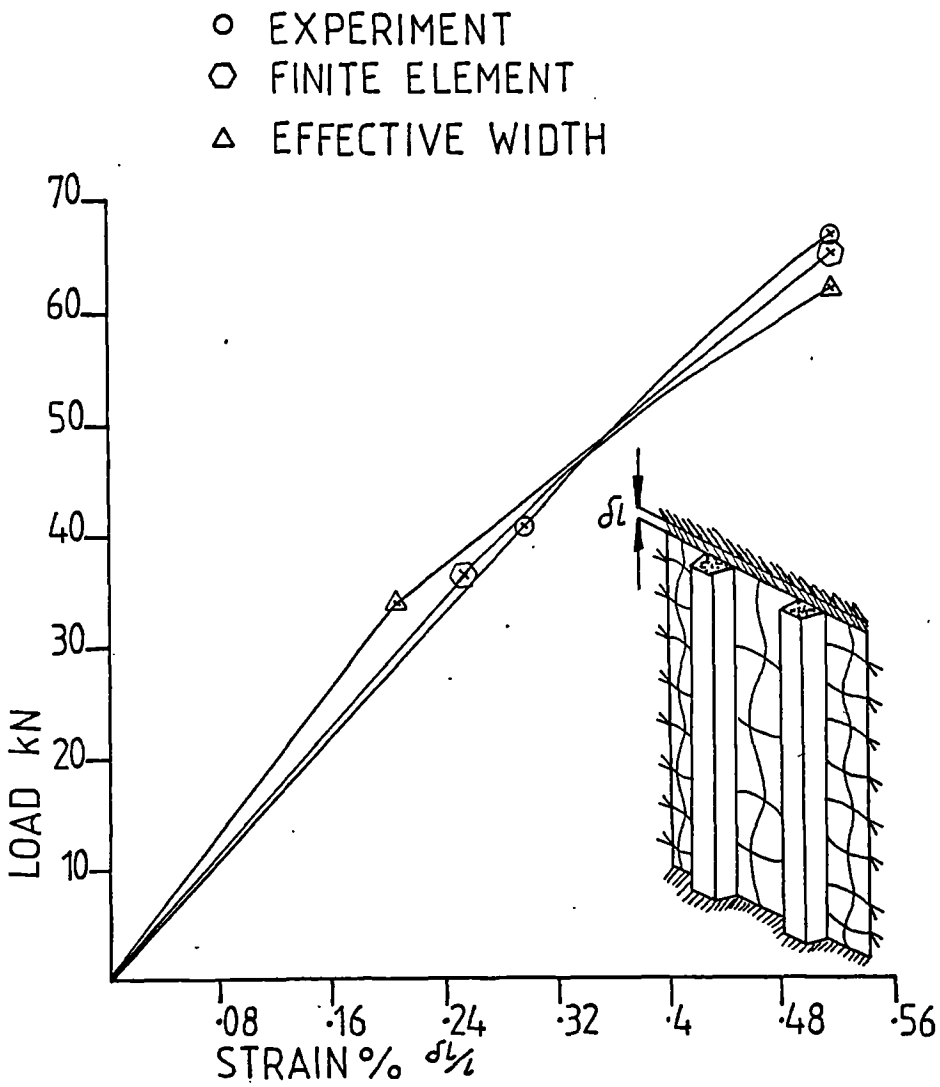

3.5.3 Experimental loads and postbuckling range.

During the test, initial buckling was first observed at 47.5kN, after which a local buckling mode appeared between the stiffeners of half-wavelength 63mm. The load on the panel continued to rise to a maximum of 65kN when the failure occurred. The end displacement of the panel was 2.4mm at failure.

3.5.4 Model results.

The load/displacement curve of the model fits in between the effective width analysis and the experimental results. Definite non-linearity of response develops from 40kN onwards. It is interesting to note the closeness of the finite element solution to the experimental results, even though a lower postbuckling mode was indicated compared with the testing.

3.6. The effect of different boundary conditions.

The theoretical postbuckling behaviour of the plate was found to be critically affected by the prescribed support conditions at the plate edges. The best correlation was obtained with:
i) rigid end supports in all three axes
ii) simply supported sides allowing in-plane expansion of the panel.
These support conditions were also the most representative of the actual test conditions.

3.6.1 Plate ends free to spread in-plane.

In this case buckling was very much delayed, and was not apparent in up to 2mm displacement, while the whole plate expanded across its width. The stiffness of the plate was lower than in the case of constrained ends.

3.6.2 Plate ends rigid, sides constrained against spreading.

With these conditions the postbuckled range of the plate was reduced, and failure of the stiffeners was indicated at 1.5mm displacement. However, the stiffness of the plate was greater than in the free-expansion cases. The failure mode indicated by this can be seen in fig. 3.10.

3.6.3 Plate sides free to move out of plane.

This effect can be seen in fig. 3.11 where waving of the free edges takes place. The stiffness of the panel was reduced due to the lower buckling load of the side panels, the panel taking 48kN at .4% strain. After this the panel developed an overall failure in an Euler mode, the load dropping to 42kN at .45% strain.

3.7. Discussion.

The main area of concern was the difference in postbuckled modes between the finite element model (shown in fig 3.8) and the panel tested. This could be considered to be affected by a Poisson's ratio effect due to constraint of the end nodes in in-plane expansion. Alternatively, the long wavelength form of the mid-panel buckle could be driven by the onset of overall Euler instability of the stiffeners, as was the case when the panel sides were modelled free. Fig 3.8 shows mixed bowing of the centre panel combined with a short wavelength buckling of the panel edges.

3.8. Conclusions.

It has been shown in this chapter that close correlation can be demonstrated between experimental and finite element model results for a representative composite wing skin compression panel. This has been shown over a postbuckling range, with the F.E. results becoming gradually more conservative as the buckling develops. At the onset of buckling, correlation was within 1%, diverging to 7% at a postbuckling load ratio of 2.24.

The chief advantage of using a finite element technique lies in the detail of the results available, making it possible to:

i) Examine the re-distribution of load across a plate as local buckling develops.

deformations can be observed.
iii) Find areas of high stress concentration where failure due to delamination may occur.
The major drawbacks of the finite element method, at present, are:
i) The detail of data input required
ii) The very long processor time required to solve a non-linear postbuckling analysis.
The processor time is typically 10-12 hours for these panels using a DEC VAX 750 computer.

3.9. Recommendations.

Non-linear finite element analysis should be used to discover problem areas such as modal interaction and to refine a design. It seems unsuited for initial design work, where a much faster, simpler approach is required for initial sizing and configuration studies. Its use is also restricted with the equipment described to the analysis of small parts of the overall structure.

However, finite element modelling and the experimental work in (16) has allowed deeper insight into the problem of postbuckling analysis. It has become possible to formulate a simpler technique now that the behaviour of a typical composite panel has been established.

Chapter 4.

The theoretical approach behind the OPTIMIST program for the initial design of postbuckled CFRP box beams.

4.1. Purpose.

The program uses a relatively simple approach to obtain initial design information. The advantages of using it in the initial stages lies in the speed of operation, which allows rapid parametric and configuration studies. This is due to the short run time, the convenience of using a desktop computer and the simplicity of the data input.

4.2. Summary of program.

The program contains routines for compression buckling, shear buckling and the interaction between these loadings. The program calculates the buckling load for a chosen plate thickness. It also calculates the minimum thickness required to resist buckling at a given loading.

Reduced stiffness for compression postbuckling, and the effect of stiffeners are calculated. A desired strain value is input and compared with the critical strain to give the postbuckling ratio. From comparison of these two values the postbuckling amplitude of skin panels is calculated. Increased surface strain due to bending caused by the buckling is also calculated.

From the box geometry and loading, shearing and crushing loads on the ribs are calculated. By use of the buckling module, the minimum thickness of rib required to resist buckling is calculated for a given rib spacing.

The program then minimises the weight of the structure. This is achieved by calculating the required stiffener dimensions to resist column buckling over a range of rib spans. The required minimum rib thickness to resist buckling for each of these spans is also calculated. At each cycle, the weight of the structure per metre span is calculated. When the weight reaches a minimum value, the optimum values are output. Convergence to the mimimum weight is also shown graphically in fig. 4.1.

Figure 4.1

Sample output from the OPTIMIST program (appendix B). Showing minimisation of weight per unit span with change in rib spacing.

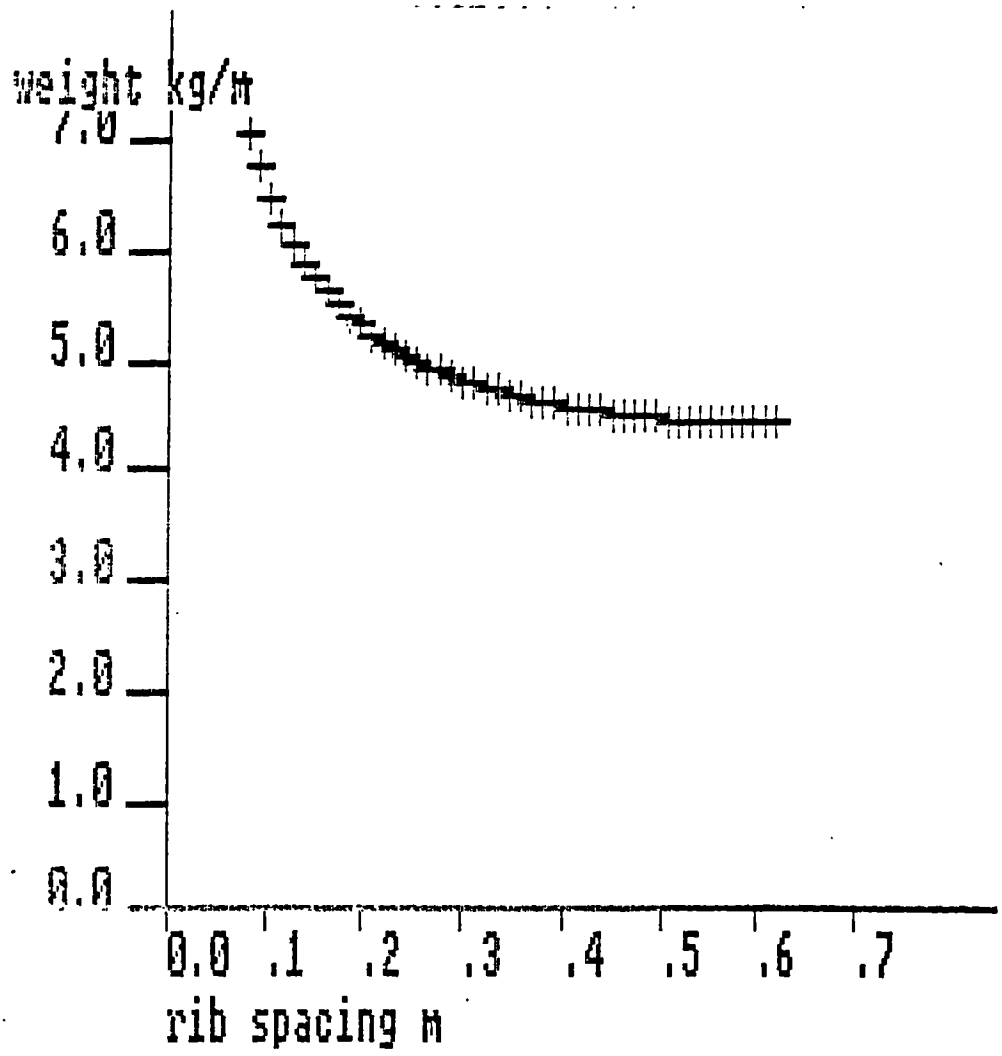

4.3. Results for postbuckled skin panels.

Fig. 3.12 shows that the results for the postbuckled skin panels correlate well with experimental and finite element results for the panel investigated. The assumptions made in the program confine its use to the analysis of specially orthotropic box structures. These incorporate postbuckled compression panels using foam-filled stiffeners of approximately square cross section.

4.4. Analytical approach.

4.4.1 Material Choice.

In the program a family of laminates is used, which may be selected from a menu. These laminates all have +-45° woven carbon outer plies and 0 unidirectional inner plies. These laminates vary from being almost 100% unidirectional material to 100% +-45° material. The properties for these laminates at a unit thickness were calculated using a standard laminate analysis program such as "LAMANAL" and incorporated as data statements. The A, B & D matrices used to describe the stiffness properties of the material have different dependences on the thickness.

This program assumes a specially orthotropic laminate, so the B matrix terms are all zero. The A terms describe membrane behaviour of the laminate. In this program it was more convenient to use the membrane engineering properties Ex, Ey and Gxy. The D matrix terms are factored by the cube of the desired thickness. This allows a variable thickness to be used for sizing purposes without the constant need to re-evaluate the material properties. Later, when choosing a practical laminate it may be found that slightly different thicknesses of uni- and woven materials have to be used. In this case, when fine tuning the design, the actual properties of that laminate will be calculated separately. These properties can then be inserted in the program for a final analysis.

4.4.2. Loading section.

Loadings of the wing structure have been obtained from ref. 28 and converted into metric units in figs 4.2 & 4.3. Torque loadings from aileron deflections

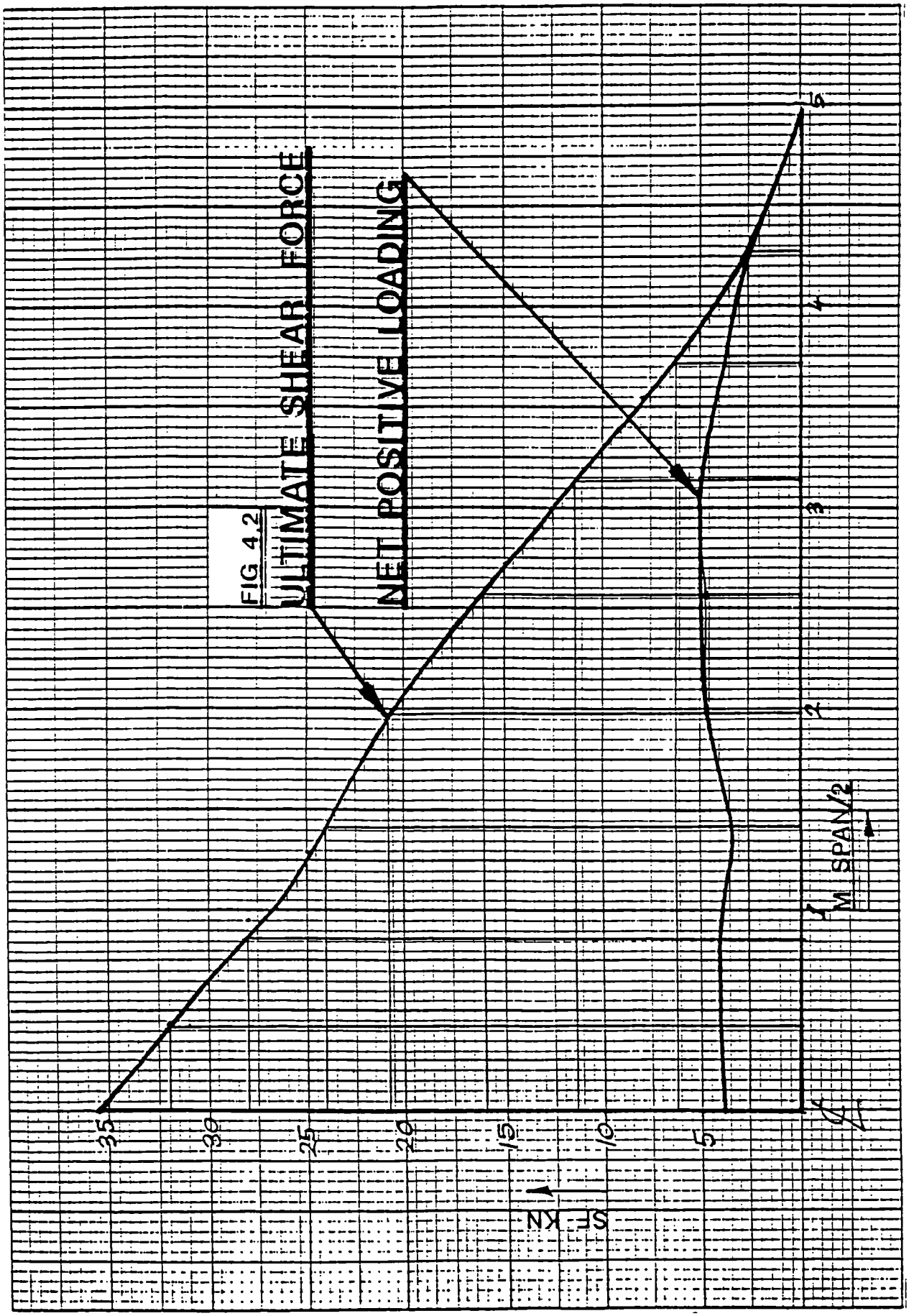
ULTIMATE SHEAR FORCE
NET POSITIVE LOADING
SF KN
35
30
25
20
15
10
5
1
2
3
4
5
M SPAN/2

FIG 4.2

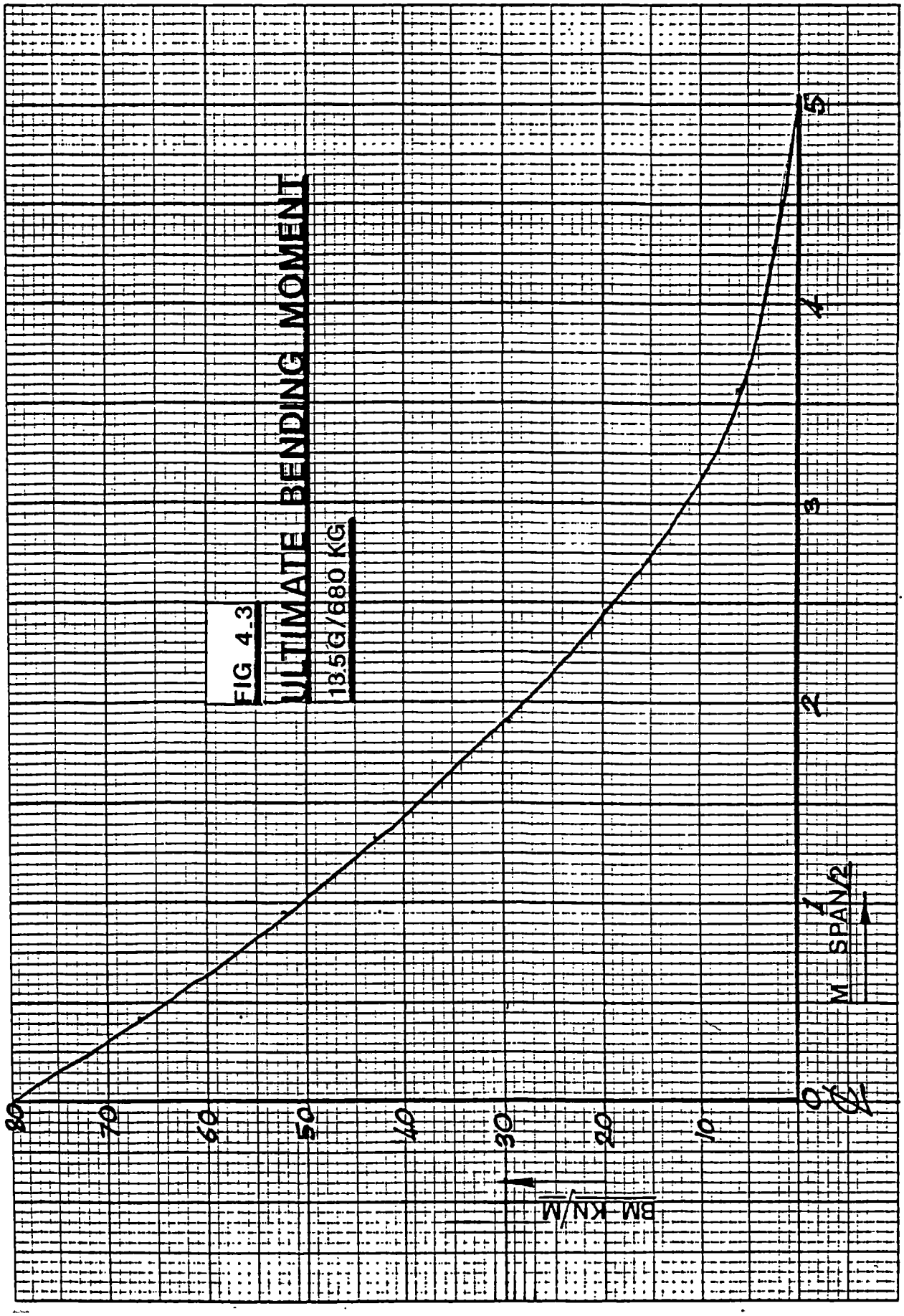
ULTIMATE BENDING MOMENT
13.5G/680 KG
BM KN/M
80
70
60
50
40
30
20
10
0
1
2
3
4
5
M SPAN/2

FIG 4.3

have also been evaluated in fig 4.4. These loads have been converted into the running loads Nx, Ny, Nxy, Nxz as shown in figs 4.5 & 4.6. For example,

$$Nx = \frac{M}{cd}$$

$$Nxz = \frac{S}{d}$$

where c=chord and d=depth of the box.
The familiar expression for torque-induced shear flow was also used i.e

$$q = Nxy = \frac{T}{2a_s}$$

These running loads are all required for operation of the program.

4.4.3. Secondary structure.

The wing ribs were sized by means of analysing the combination of crushing load and shear load. These are applied by the Brazier forces due to wing curvature and shear load due to airload distribution. From hoop tension theory (40) it can be shown that:

$$\frac{1}{R} = \frac{e_t + e_b}{d}$$

Where:

e_t, e_b = top,bottom strains respectively.

R = radius of curvature.

d = depth of structure.

The pressure over the surface is then given by:

$$P = \frac{N_x}{R}$$

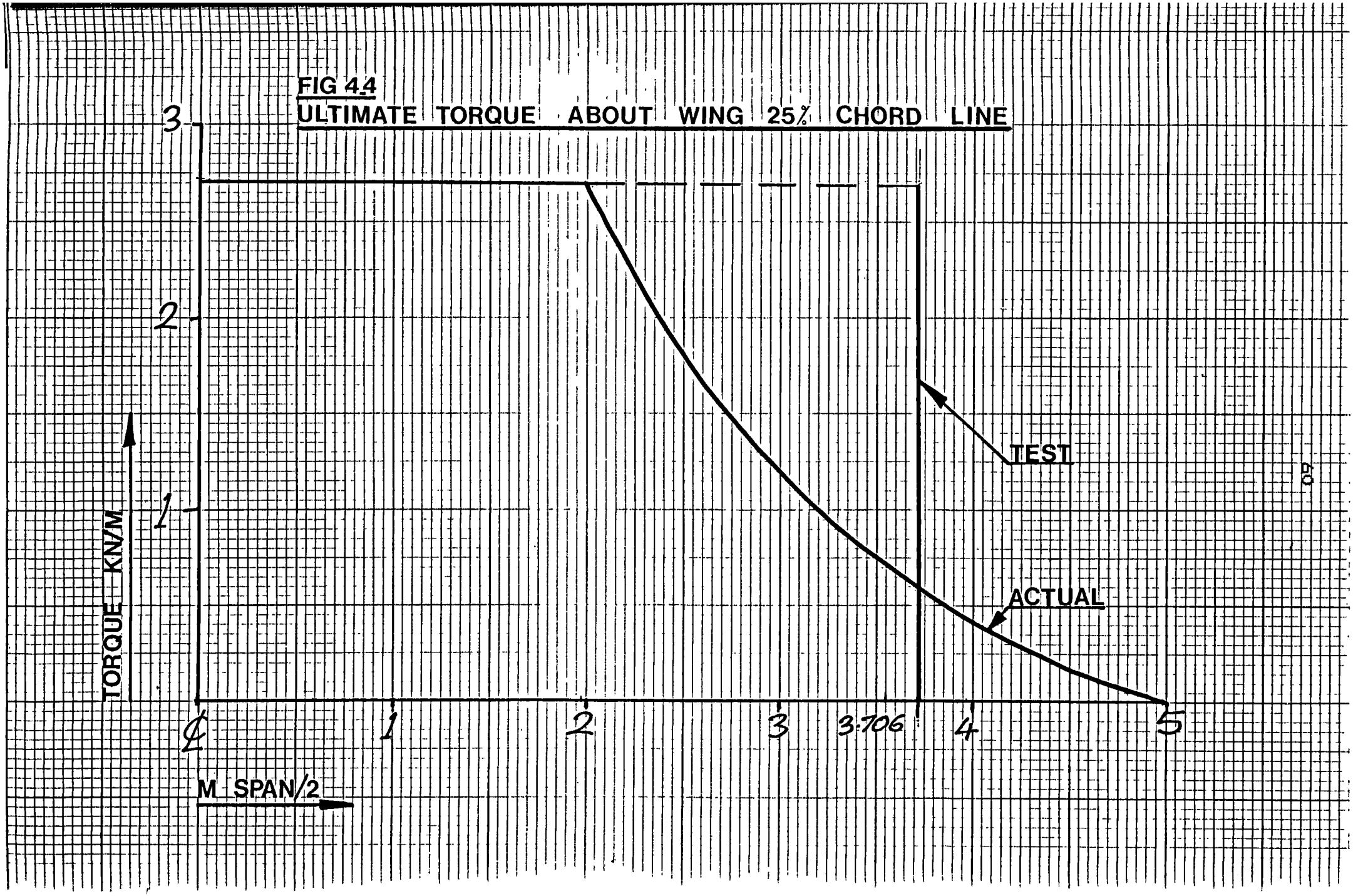
FIG 4.4
ULTIMATE TORQUE ABOUT WING 25% CHORD LINE
3
2
1
TORQUE KN/M
TEST
ACTUAL
¢
1
2
3
3·706
4
5
M SPAN/2
60

FIG 4.5

$N_x = \frac{M_x}{cd}$

$N_{xz} = \frac{S_x}{d}$

FIG 4.6

$q = N_{xy} = \frac{T}{2a}$

TEST CASE

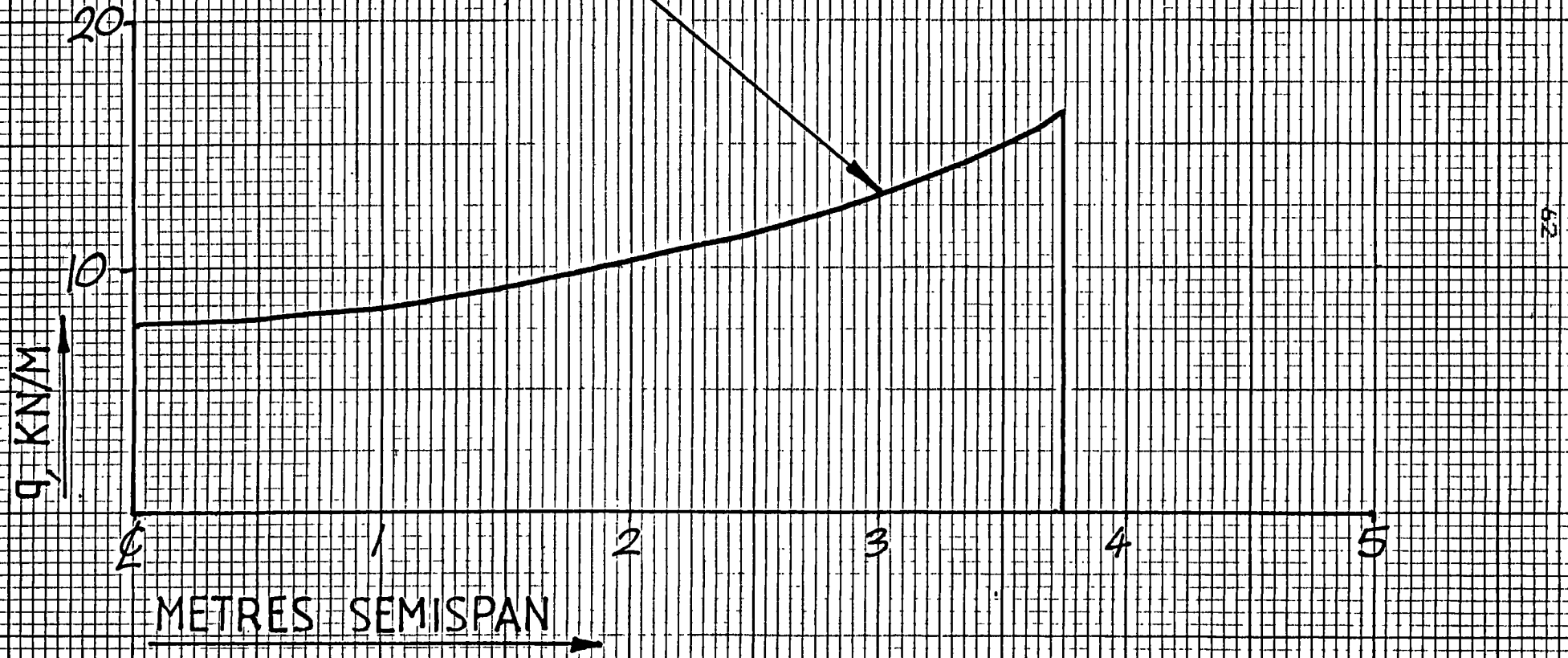


FIG 4.4
ULTIMATE TORQUE ABOUT WING 25% CHORD LINE
TORQUE KN/M
3
2
1
TEST
ACTUAL
℄
1
2
3
3.706
4
5
M SPAN/2

FIG 4.5
$N_X = \frac{M_x}{cd}$
$N_{XZ} = \frac{S_x}{d}$
N_X
N_{XZ}
LOAD / WIDTH KN/M
400
300
200
100
1
2
3
4
5
METRES SEMISPAN

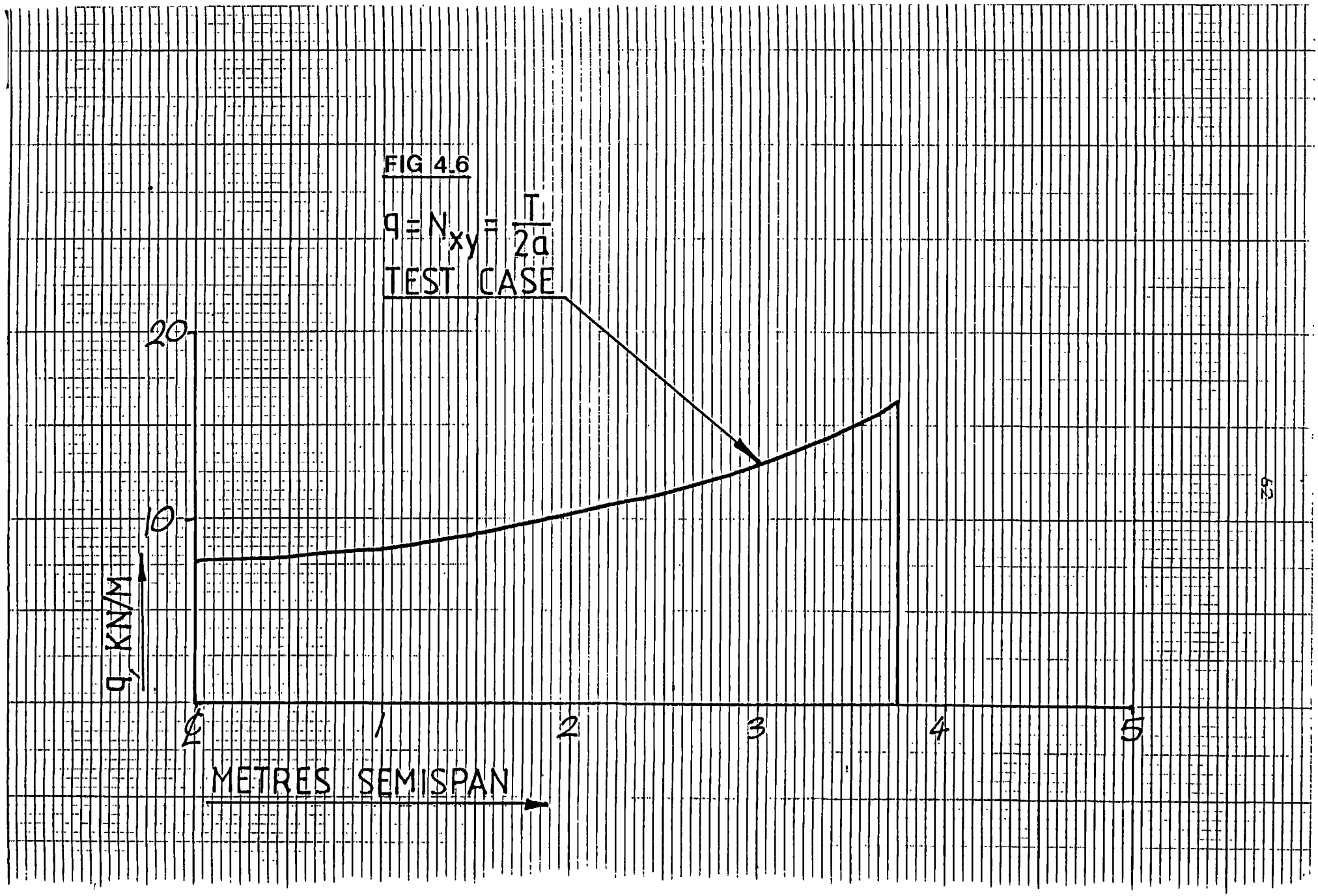
FIG 4.6
$q = N_{xy} = \frac{T}{2a}$
TEST CASE
20
10
q KN/M
℄
1
2
3
4
5
METRES SEMISPAN

The crushing load per rib follows as:

$$P_{rib} = P_{CL}$$

where:

P = surface pressure.

P_{rib} = crushing force per rib.

C = flange length.

l = rib spacing.

The aerodynamic loading per rib assuming constant loading between front and rear spars is:

$$N_z = P_{(avg)} L$$

Which gives rise to the shear of the rib:

$$N_{yz} = \frac{P_{avg} L C}{2d}$$

The bending moment applied to the rib by the airloading is:

$$M_{rib} = \frac{N_z C^2}{8}$$

This gives a chordwise loading on the rib flanges of:

$$N_y = \frac{M_{rib}}{d}$$

These values were computed and the loading conditions used to design non-buckled stiffened panel type ribs. The program contains a subroutine which calculates the thickness required to resist buckling.

4.4.4 Compression Panels.

In the experimental results for all of the test panels in ref.16 it was noticed that the stiffeners remained stable up to overall failure. The high torsional stiffness of the stiffeners prevented them from rolling. The only non-linear effect of the stiffeners was in taking up relatively more of the panel loading as the skin panels buckled. For these reasons it was assumed that the stiffeners could be considered to be a linear-elastic part of the structure until overall failure occurred.

The behaviour of the whole stiffened panel was thus approximated to that of a series of plates which would locally buckle, held in simple support at each side by a series of linear-elastic stiffeners.

4.5. Compression buckling of the skin panels.

The length of the panel is allowed to vary, and the buckling load is determined for simple-support conditions by the equation below. The equation has been derived from the usual differential equation describing the free vibration of a specially orthotropic plate.

$$P_{cr} = \frac{\pi^2}{b}\left\{D_{11}\left(\frac{b}{a}\right)^2 + 2(D_{12} + 2D_{33}) + D_{22}\left(\frac{a}{b}\right)^2\right\}$$

4.6. Shear buckling.

The critical load on the plate for shear buckling is given by the equations below, also derived from the overall plate differential equation, from ref. 6.

When:

$$D_{11}D_{22} > (D_{12} + 2D_{33})^2 ,$$

for $D_{11} D_{22} > (D_{12} + 2D_{33})^{1/2}$,

$$\tau_{cr} = \sqrt{\frac{2D_{22}(D_{12} + 2D_{33})}{\left(\frac{b}{2}\right)^2 t}} \left\{ 8.3 + 1.525 \frac{D_{11} D_{22}}{(D_{12} + 2D_{33})^{1/2}} \ldots . \right.$$

$$\left. \ldots - 0.493 \frac{D_{11}^{1/2} D_{22}^{1/2}}{(D_{12} + 2D_{33})^{1/4}} \right\}$$

When: $D_{11} D_{22} < (D_{12} + 2D_{33})^{1/2}$,

$$\tau_{cr} = \sqrt[4]{\frac{D_{11} D_{33}^{1/3}}{\left(\frac{b}{2}\right)^{1/2} t}} \left\{ 8.125 + 5.64 \sqrt{\frac{(D_{12} + 2D_{33})^{1/2}}{D_{11} D_{22}}} \ldots . \right.$$

$$\left. \ldots . - 0.6 \frac{(D_{12} + 2D_{33})^{1/2}}{D_{11} D_{22}} \right\}$$

4.7. Interaction of compression and shear buckling.

From Leknitski (5) it has been shown that the plate buckles when:

$$\frac{P_x}{P_{x_{cr}}} + \frac{P_y}{P_{y_{cr}}} + \left(\frac{P_{xy}}{P_{xy_{cr}}} \right)^{1/2} \geq 1$$

4.8. Minimum thickness.

The buckling load is directly proportional to the size of the D matrix terms. These in turn are proportional to the cube of the thickness. Thus the required thickness to resist buckling is given by:

$$t_{cr} = \sqrt[3]{\frac{N_x t^3}{N_{x_{(+)cr}}}}$$

4.9. Displacement and strain.

The displacement of the plate in compression at buckling is given by:

$$u_{cr} = \frac{P_{xcr}\, a}{t E_{11}}$$

from which the strain at buckling follows from:

$$e_{cr} = \frac{u_{cr}}{a}$$

4.10. Postbuckled stiffness.

This is analysed using the approach found in ref.4.

First the elastic constant H is found:

$$H = \left(\frac{1}{G_{12}} - \frac{2 D_{12}}{E_{11}} \right)$$

This is applied to the following equation for the reduced stiffness of a simply supported plate with

edges free to wave in plane:

$$\frac{E_{xx}}{E} = \frac{2+\left(1+E_{11}H\left(\frac{b}{a}\right)^{12}+3\,\frac{E_{11}}{E_{22}}\left(\frac{b}{a}\right)^{14}\right)}{2+3\left(1+E_{11}H\left(\frac{b}{a}\right)^{12}+3\,\frac{E_{11}}{E_{22}}\left(\frac{b}{a}\right)^{14}\right)}$$

4.11. Postbuckling amplitude.

An assumption is made that the centre of the plate does not experience increased membrane compression strain after buckling. Thus, the difference between the critical plate end displacement and the postbuckled end displacement can be used to calculate postbuckled amplitude. The deformation is assumed to take a sinusoidal form.

Taking a sine wave from 0 to $\pi/2$ as in fig. 4.7, the length along this portion of the wave is given by:

$$l = \int_0^{\pi/2} \sqrt{\delta x^2 + \left(a\sin\left(2\frac{(x+\delta x)}{\pi}\right) - a\sin\left(\frac{2x}{\pi}\right)\right)^2}$$

This is solved in the program by choosing a small finite length, $\delta x = \pi/200$ say. A small amplitude, a, is chosen and incremented upwards after summating L. This process continues until:

$$l = \frac{\pi}{2} + \frac{\pi}{2}(e - e_{cr})$$

The postbuckling plate amplitude is then output.

4.12. Calculation of surface strain due to buckling.

This is calculated at the same time as the postbuckled amplitude. To explain the method, fig 4.7 is expanded in fig 4.8. Firstly the thickness of the plate from mid surface to outer surface is given by:

FIG 4.7

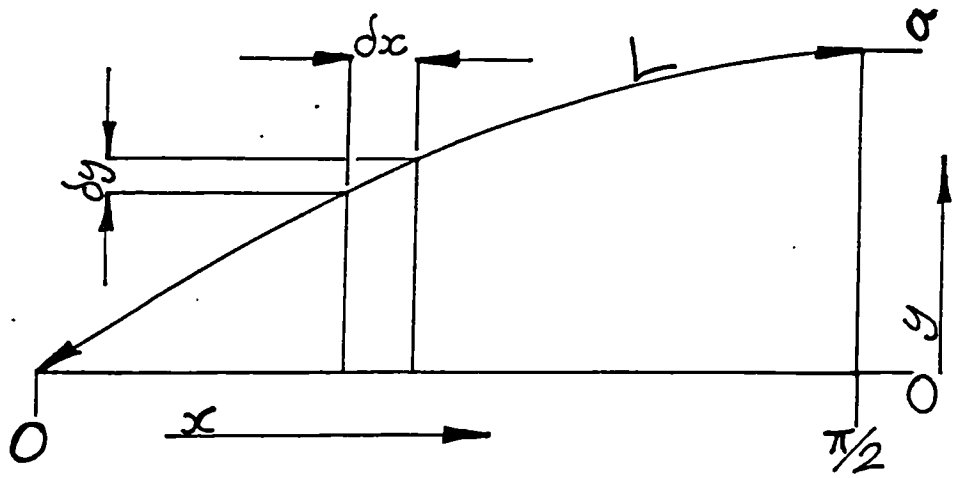

FIG 4.8

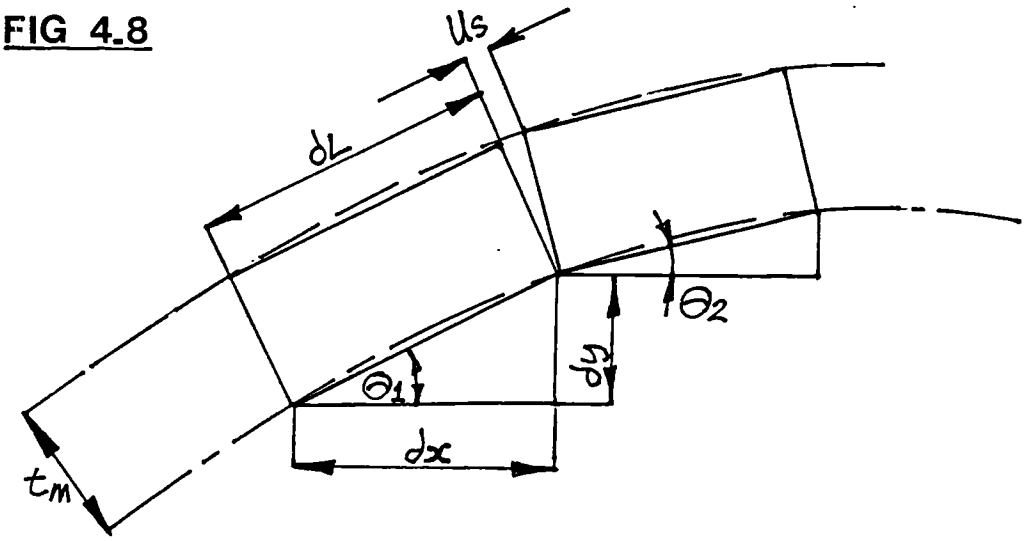

FIG 4.9

semi-thickness for plate length π,

$$t_m = \left(\frac{0.5t}{\lambda}\right) \times \pi$$

The displacement caused by the bending of the plate for each small element of the plate is then:

$$u_s = t_m \times \sin(\theta_2 - \theta_1)$$

The surface strain due to the sinusoidal curve at this position is then:

$$e_s = \frac{u_s}{\delta l}$$

This is calculated for the whole sine wave from x=0 to There is a maximum compressive strain at x=0 and a maximum tensile strain at the buckle peak. At the buckle peak, a reasonable result is given in the sample run shown of 0.265%. However, at the edge of the plate there is a discontinuity. This results in a high strain, 1.5% in the sample run. It is probable that the plate curves more gradually into the sine wave as in fig 4.9. The buckle peak values are used as a failure criteria if above 0.4%.

4.13. The effect of stiffeners.

The stiffener areas and properties are then superimposed on those for the skin panels to obtain the whole plate stiffness. This can be determined at the point of buckling, and for any desired strain level above this.

The stiffener area is assumed to be 90% unidirectional fibres in the stiffener cap. The other 10% is assumed to be 45 degree fibres in the stiffener sides, which constitute shear webs. These are assumed not to contribute significantly to the compression stiffness. This assumption is justified by the non-linear finite element analysis.

The loading due to the stiffeners is thus:

Stiffener Loading:

$$P_s = A_s E_s u$$

so that the total panel loading per unit width is given by:

$$p_w = N_{xc} = P_s + w p_{skin}$$

4.14. Overall buckling of the panel.

Here the stiffener/skin combination is considered to act as a beam column due to transverse loading and end compression. The skin and stiffener caps are assumed to be thin so that the second moments of area are calculated from the centroids of their areas.

The bending rigidity of the panel as a long column is taken to be:

$$EI = A_s\left(\frac{d_s}{2}\right)^2 E_s + t \times w\left\{\left(\frac{d_s}{2}\right)^2 E_{11} \times \left(\frac{E_{11}^*}{E_{11}}\right)\right\}$$

From this, the critical length for overall Euler type panel failure is found from:

$$l = \sqrt{\frac{\pi^2 EI}{P}}$$

However, the panel is also subjected to transverse forces. These arise from the airload and Brazier

loading effects. This reduces the axial load the panel can carry to:

$$l_{bc} = \sqrt{\frac{\pi^2 EI}{(P+b_c)}}$$

where bc is the reduction in load which can be carried due to beam column effects. The approach used is based on Timoshenko, ref. 41. To calculate the maximum bending moment an amplification factor has to be calculated . This is dependent on how near the axial load is to the critical. This is given by:

$$u = \frac{\pi}{2}\sqrt{\frac{P}{P_{cr}}}$$

The maximum bending moment is calculated from:

$$M_{max} = \frac{P_{tr} l^2}{8}\left(\frac{2(1-\cos(u))}{u^2\cos(u)}\right)$$

Where P_{tr} = transverse Load.

This enables the maximum strain at the stiffener cap to be calculated:

$$\frac{M_{max}}{d_s} \times \frac{1}{A_s} \times \frac{1}{E_s} = e_{sc}$$

The solution procedure for the beam column is to increment the rib spacing downwards from the pure Euler length until the panel can also resist the transverse loading. This is limited by a maximum strain of 0.4% in the stiffener cap caused by the bending of the panel.

4.15. Weight of the panel.

The stiffeners are assumed to be of square cross section, and to be filled with 51 kg/m^3 foam. The cross sectional area of carbon in the stiffener caps is already known, as is the skin thickness. The stiffener sidewalls are assumed to be 0.5 of the skin thickness. With this data the weight of the stiffened skin panel at a given stiffener depth can be readily determined.

The rib thickness is proportional to the cube of the buckling load for a given rib panel length and width. Thus we can say that the panel thickness required for buckling at the desired load is:

$$t_{rib} = \sqrt[3]{\frac{N_z t^3}{N_{z\,crit}}}$$

4.16. Optimisation.

In the program the weight of the skin/stiffener/rib configuration is then calculated. This is performed for progressively increasing rib spacings starting from a lower bound. The required stiffener depth to resist beam/column failure is calculated at each rib spacing. The crushing load on each rib is proportional to the rib spacing. Thus the required thickness of rib required to resist buckling up to each rib spacing is given by:

$$t_{rs} = \sqrt[3]{\frac{t_{rib}^3 \times l}{l_{t\,crit}}}$$

When the weight reaches a minimum value, the optimum values are output. A plot of weight per unit structural span versus rib spacing is produced at the same time. This is shown in fig 4.1.

4.17. Strength reserve.

The strength reserve for design purposes is calculated by the ratio of postbuckled strain to allowable stiffener cap strain of .4%. The strain at the buckled panel surface is also calculated and used as a failure criterion if above 0.4%. The postbuckled panel surface strain is used as a guide only at present. Buskell, Davies and Stevens (45) did some experimental work on the failure of postbuckled panels under simple support conditions. The panels tended to fail at the edges by transverse shearing stresses in the material. Transverse shearing stress is at a maximum where the postbuckled amplitude is zero, i.e. between buckle peaks. For the testing in ref. 45, the plate edges were cut off close to the simple supports in the testing machine. It was proposed that the effect of cutting off the panels just outside the simple supports tends to increase the tranverse shear effect due to Kirchoff edge stresses.

All the panels except C4 in ref.1. tended to fail at approximately .4% strain by localised splitting or delamination around the stiffener edges, especially at the stress concentrations caused by the end fittings, or by actual failure of the end fittings. Panel C4 failed in an overall mode at .4% strain.

4.18. Use of the program in initial design studies.

4.18.1. Skin panel design.

The first approach was to investigate the effect of varying stiffener pitch on panel weight. Generally, it was found that the wider the stiffener pitch and the higher the postbuckling ratio, the lighter the structure. In the limit, the compression carrying material would all be concentrated in a few stable booms, the skin being just thick enough to take shear loads.

This approach gives rise to unacceptable out-of-plane displacements of the skin panels due to the postbuckling. A criterion of no more than 3% of the section depth in out-of-plane displacement was fixed. This was to prevent delamination of the skin panels and for reasons of aerodynamic performance. This gave a postbuckling load ratio of between 2 and 4 progressing from root to tip.

The skin panel design was investigated to see the effect of different laminates and ply angles on buckling and postbuckling behaviour. The postbuckling curves are shown in figs 4.10 & 4.11. These curves have been produced by the OPTIMIST program. It can be seen that the +-45 degree layups have the highest buckling loads, but a purely +-45° laminate has rather poor axial stiffness. The effect of adding progressively more unidirectional fibres to the laminate is shown in fig 4.10. As can be seen, the buckling load for the same plate thickness reduces and the stiffness before buckling is increased. The ratio of postbuckled to non-buckled stiffness also becomes smaller.

This information is important in the design of the wing, because the relatively thick root skin sections buckle at a much higher strain than the thin tip sections. This allows more unidirectional material to be used towards the root without an unacceptably large postbuckling ratio for the panels. At the tip sections just +-45° material is used to obtain the lowest postbuckling ratio for a given axial strain of the stiffeners.

4.18.2. Rib pitch.

The effect on the weight of varying the rib pitch was examined. A structure with too few ribs tends to be heavy because of the large stiffener cross section required to resist column failure. The use of many ribs also gives a non-optimum solution because of the weight of numerous joints, and the requirement for unrealistically thin rib shear webs. The optimum rib pitch varied from .4m at the root to .6m near the tip, but was not found to be very critical. Ribs were thus positioned in areas where loads were to be fed into the structure such as the undercarriage, main fuselage mountings and aileron hinges. In addition a rib positioned at the kink in the mainspar is most important in this wing because of the interaction between bending and torque at this station.

4.18.3 Stiffener cross section.

Optimisation of the stiffener cross section was found to be very critical. The wing box was designed with

Figure 4.10

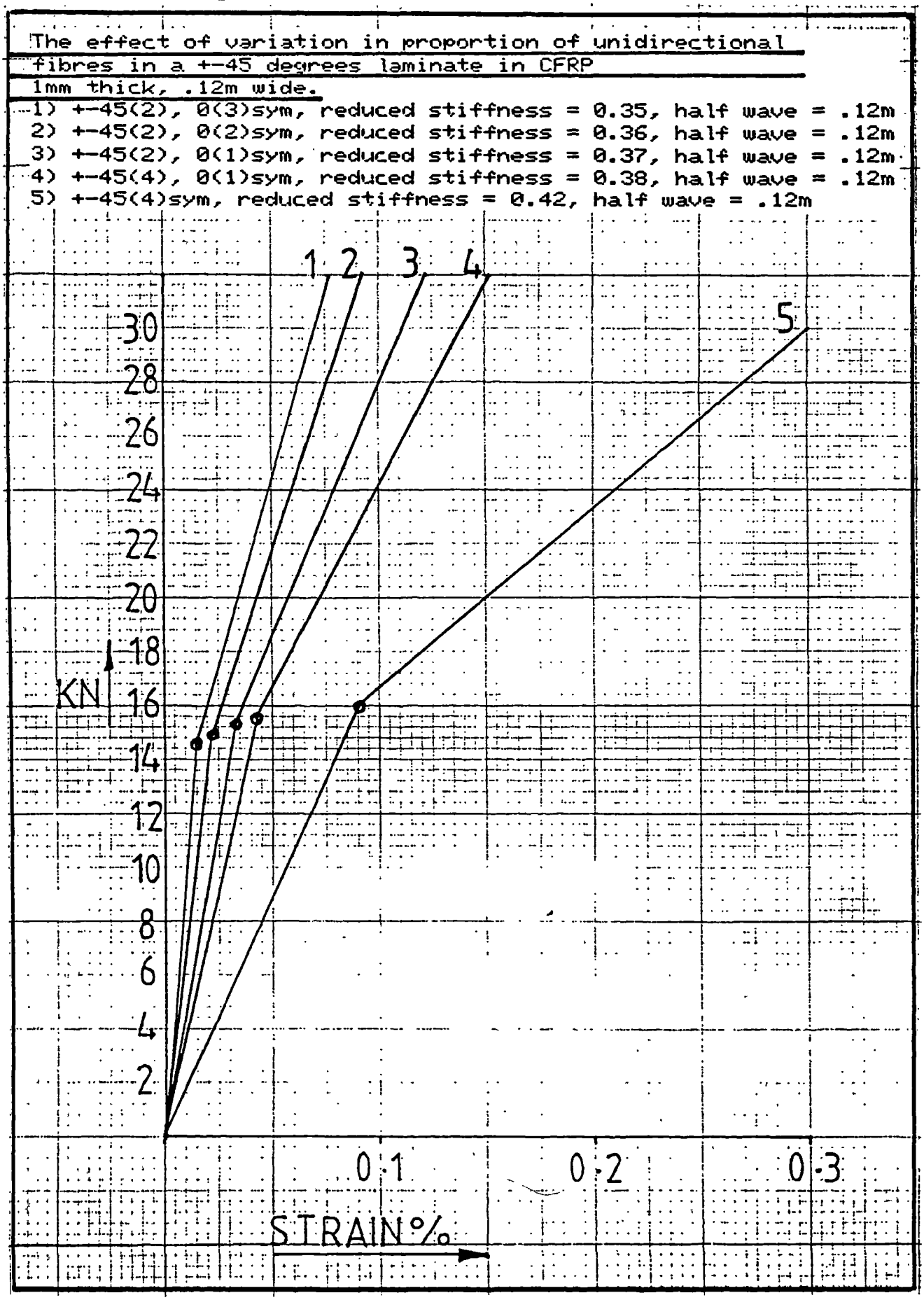
The effect of variation in proportion of unidirectional fibres in a +-45 degrees laminate in CFRP
1mm thick, .12m wide.
1) +-45(2), 0(3)sym, reduced stiffness = 0.35, half wave = .12m
2) +-45(2), 0(2)sym, reduced stiffness = 0.36, half wave = .12m
3) +-45(2), 0(1)sym, reduced stiffness = 0.37, half wave = .12m
4) +-45(4), 0(1)sym, reduced stiffness = 0.38, half wave = .12m
5) +-45(4)sym, reduced stiffness = 0.42, half wave = .12m
1
2
3
4
5
30
28
26
24
22
20
18
16
14
12
10
8
6
4
2
KN
0·1
0·2
0·3
STRAIN%

Figure 4.11

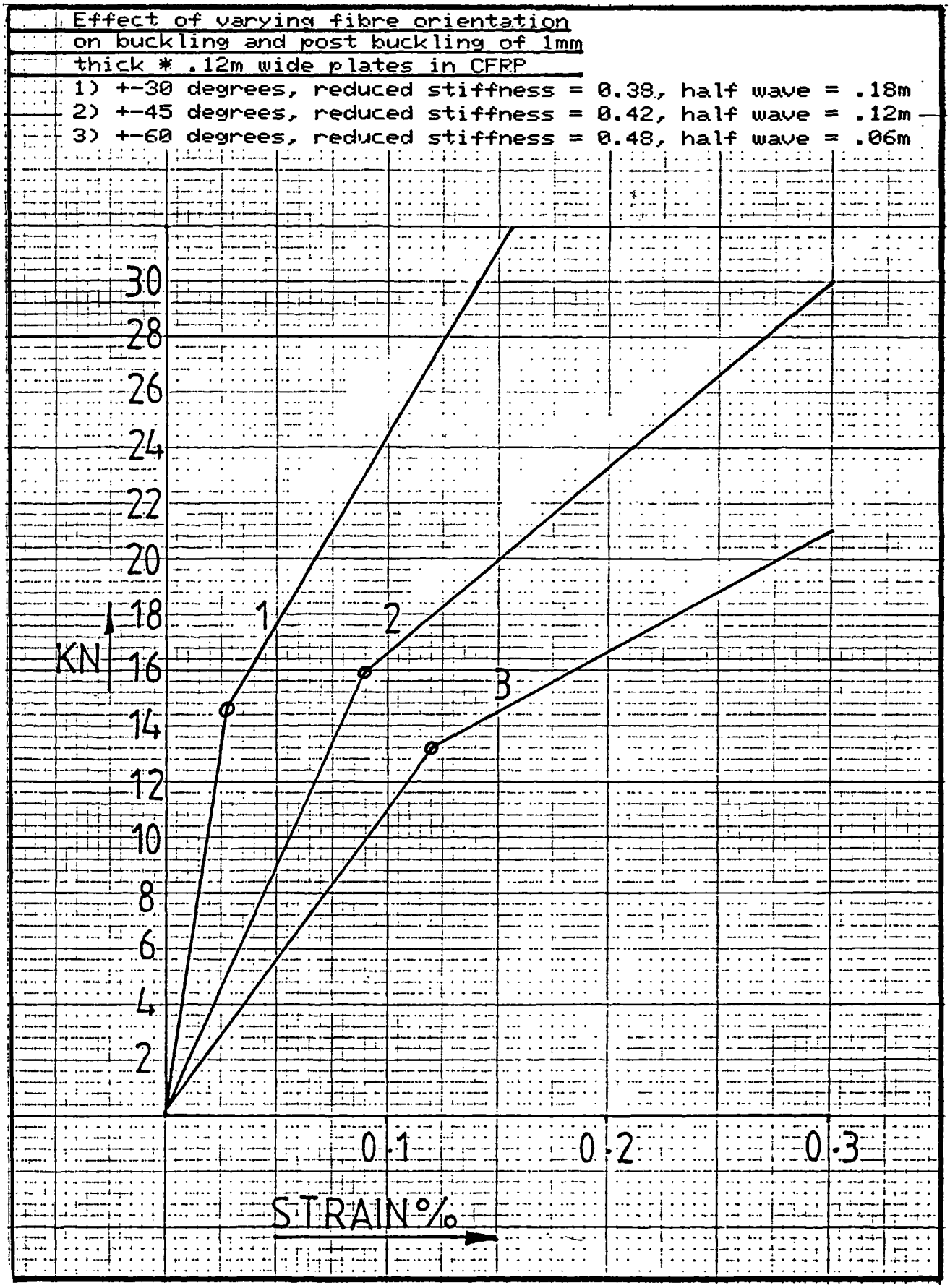
Effect of varying fibre orientation
on buckling and post buckling of 1mm
thick * .12m wide plates in CFRP
1) +-30 degrees, reduced stiffness = 0.38, half wave = .18m
2) +-45 degrees, reduced stiffness = 0.42, half wave = .12m
3) +-60 degrees, reduced stiffness = 0.48, half wave = .06m
30
28
26
24
22
20
18
16
14
12
10
8
6
4
2
KN
1
2
3
0.1
0.2
0.3
STRAIN%

beam/column failure of the stiffeners to occur at 0.4% strain or lower. An over-large stiffener cross section resulted in a weight penalty. The increased weight is due to the weight of the foam core used to stabilise the stiffener, and the weight of the stiffener sidewall material. The design when optimised had a variable stiffener size through the span so that they would be just stable at ultimate load. When this was rationalised to three sections as shown in the main drawing A1-CFRP-01 in Appendix H, a weight increase of .5kg resulted.

Chapter 5.

Finite element modelling of the whole structure.

5.1. The development of the method.

In chapter 2, large scale non-linear modelling of the structure has been shown to require very large computer memory and running times. This problem was partly the motivation behind the OPTIMIST postbuckling sizing program. The program can quickly provide an optimum structural configuration for each loading condition along the span. It also provides reduced stiffness values for the postbuckling skin panels.

By using the reduced stiffness properties calculated by the OPTIMIST program, a finite element postbuckling model of the total structure could be formed. A linear analysis is used which incorporates the reduced stiffness properties for the skin panels. In this way a linear finite element model can be used to simulate postbuckling. All three test boxes designed and constructed in this work have been modelled in this way.

Initially, semiloof thin shell elements were employed to represent the skin panels. These elements were connected such that the mid-side nodes were unsupported. Transfer of edge moments from one element to the next caused them to deform. The deformation was totally unrepresentative as shown in fig 5.1.

To solve this problem, simpler SMI4 quadrilateral membrane elements were tried. These formed the skin elements whilst BRS2 bar elements were used to represent the stiffener unidirectional material. This approach was much more successful as all skin element nodes were interconnected by ribs. Skin element material properties were defined simply by the laminate stiffnesses Ex, Ey, Gxy and v12. Flexural behaviour of the skin elements was not being modelled. This made the "D" matrix bending stiffness terms unimportant.

The model could be run either with pre- or postbuckled stiffnesses for the skin panels. The differences in overall deflections and strains caused by the buckling could then be monitored. The increased levels of strain taken by the stiffener elements after buckling was of particular interest. Stiffener elements were modelled simply as units of cross-sectional area. The same stiffener properties were

Figure 5.1

Unrepresentative deformations caused by edge moments with eight-noded semiloof thin shell elements.

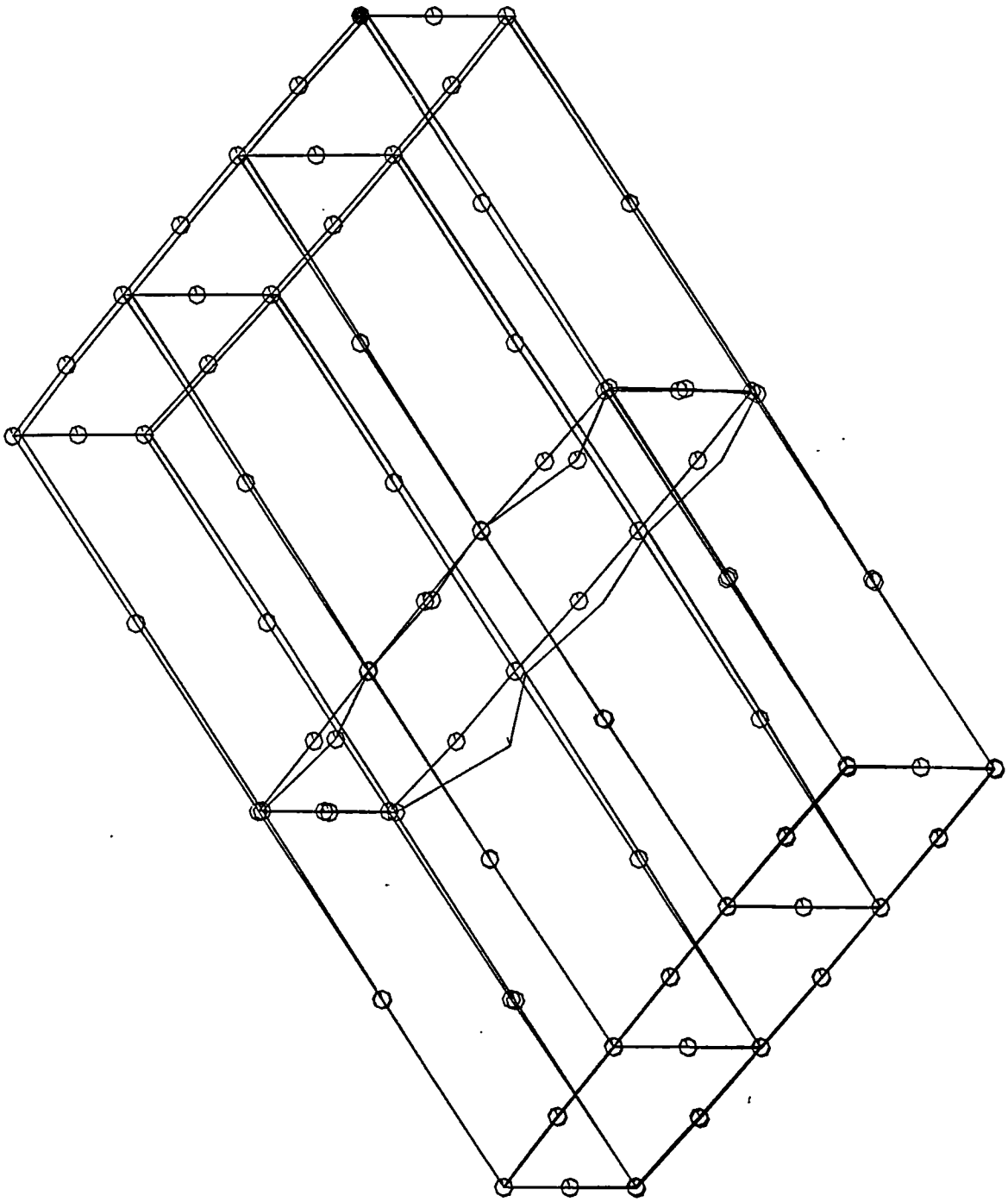

used for buckled or non-buckled analyses.

5.2. Pre-processing of LUSAS data using WEIGHTS.

For small, simple test boxes manual data preparation is quite straightforward. In the case of a complex wing box, it becomes rather laborious. This is especially true if different configurations of ribs and stiffeners need to be examined.

For this application, use of the WEIGHTS software developed by Murphy (38) is recommended. The data preprocessing module allows a wing structure model to be generated quickly. Data is only required for key points such as the root, tip and kink positions. Ribs are then generated by spacing ratios along the span. A similar method is used for the stiffeners. All the variables in the A1 wing can be accommodated. Variation of sweep, dihedral and washout along the span are also possible. The model used in the design of the wing box has been generated by WEIGHTS.

5.3. Considerations when using a linear F.E. model with reduced skin stiffnesses.

The method described is a simplified technique to allow easier analysis of complete postbuckled box structures. Naturally, many assumptions have to be made about the postbuckled behaviour of the structure. Before using this method it is essential to determine overall stiffener buckling behaviour by some other means first. The OPTIMIST program will calculate stiffener buckling as well as rib buckling. Spar shear buckling must also be investigated. Modal interaction effects between stiffener and skin buckling should also be checked. Modal interaction can be modelled by non-linear finite element techniques, as described in chapter 3. Experimental panel testing may also be required.

If these areas have been addressed, the method can be very useful. Good agreement for deflections and strains can be obtained. A model of the whole wing box can be solved in about 20 minutes DEC 750 computer processor time.

5.4. Results compared with experiment.

The linear finite element/reduced stiffness technique was first proven in the design and test programme for box 2, which is shown in fig 5.2. This

Figure 5.2

Test box No.2, shown in the cantilever load test rig. This was the first box to be built with co-cured skin/stiffener panels. It incorporated experimental stitching of stiffeners to the skin.

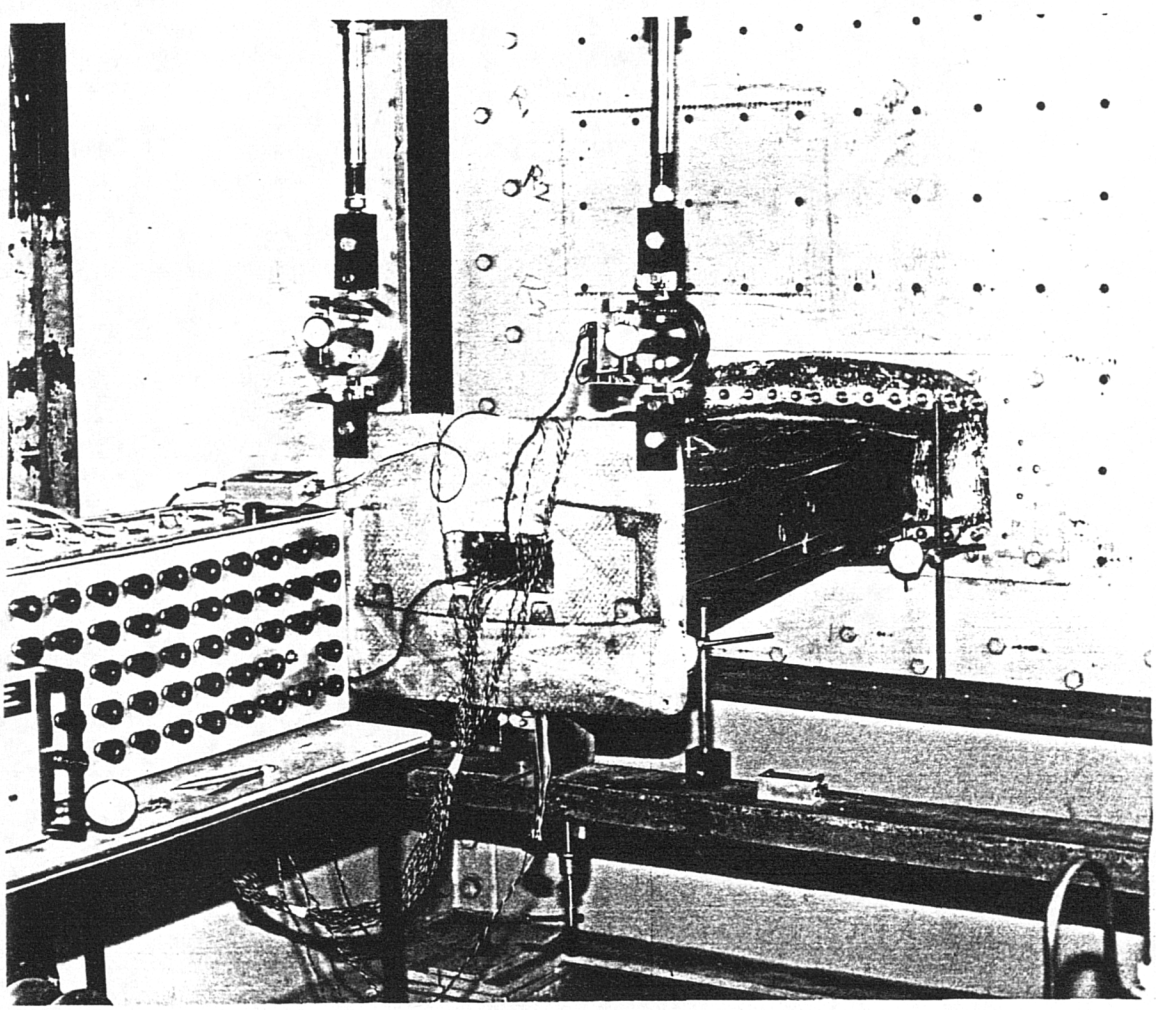

Figure 5.3

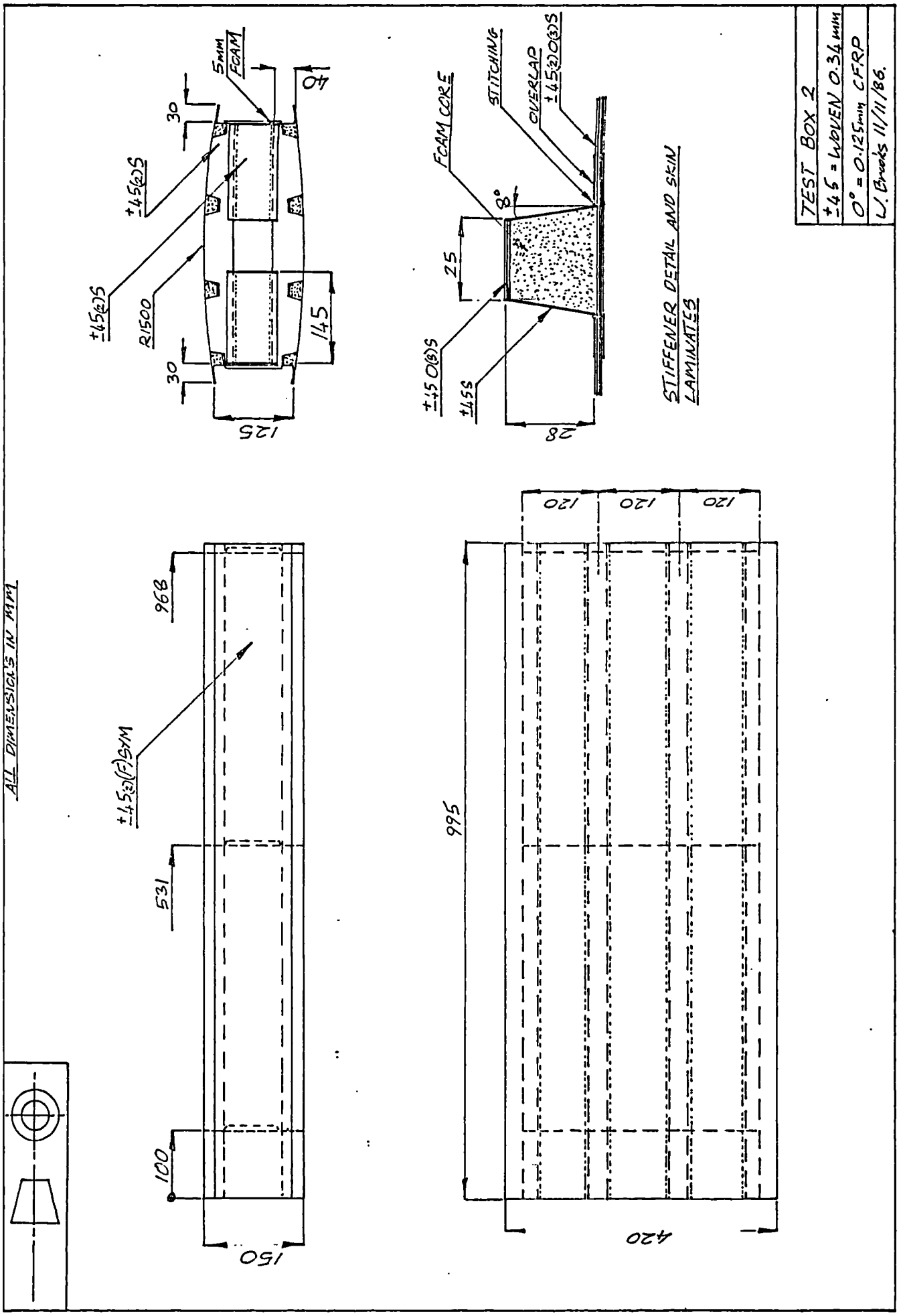
TEST BOX 2
±45 = WOVEN 0.34 mm
0° = 0.125mm CFRP
L. Brooks 11/11/86.
ALL DIMENSIONS IN MM
STIFFENER DETAIL AND SKIN LAMINATES
FOAM CORE
STITCHING
OVERLAP
±45(2)0(3)S
±45(2)S
±45(3)(F)SYM
±45S
968
531
100
150
995
420
120
120
120
125
145
30
30
5MM FOAM
40
R1500
25
28
8°

Figure 5.4

Cantilever load case and deflections for test box 2.

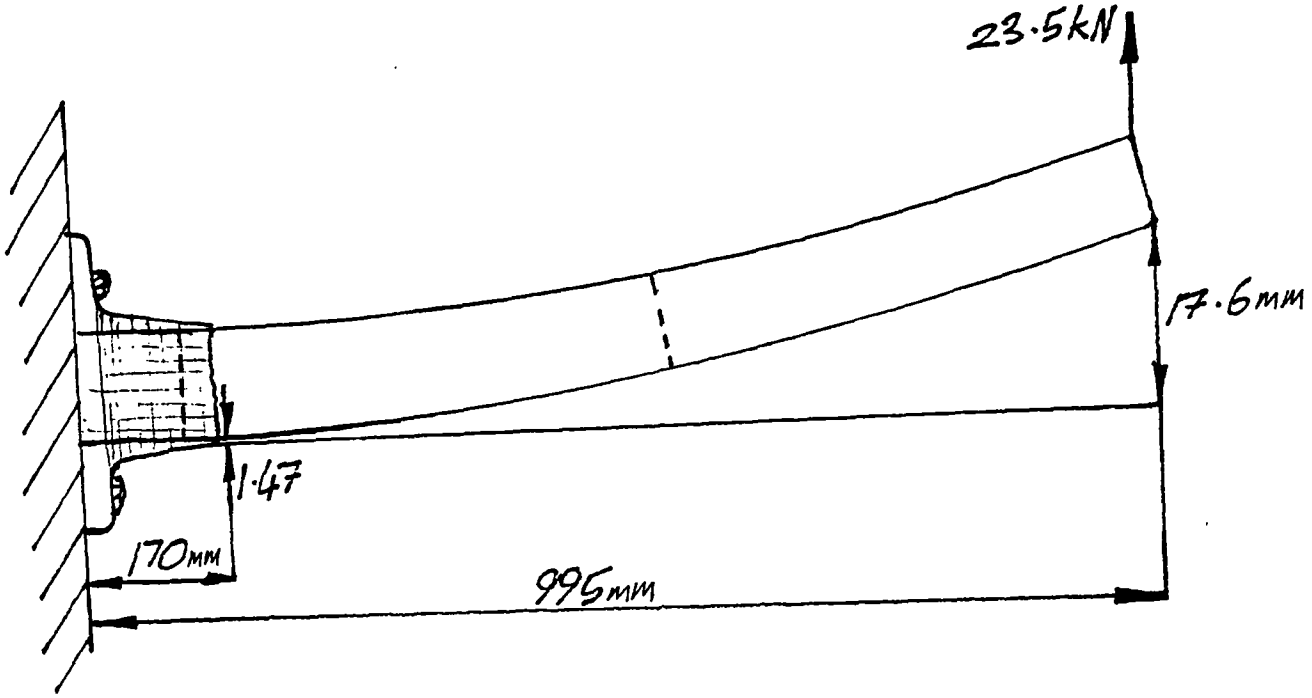

testbox is representative of the wing root area, with a skin running load of 400 KN/m and a skin thickness of 2mm. It has a constant small chordwise skin curvature of 1500 mm, representing that of the wing. It was the first to be produced using the co-curing method devised for the main box. It incorporated some experimental features such as Kevlar stitching of the skin/stiffener junction, which is covered in chapter 6. The stitching was combined with an interleaved skin layup. Test box 2 is shown in fig. 5.3. It was loaded as a cantilever as shown in fig 5.4.

Test box 2 was designed by using the OPTIMIST program to supply thicknesses and postbuckled stiffness properties. The linear postbuckling model is seen in fig. 5.5. The element numbering is shown. It was loaded and restrained in exactly the same manner as the actual box. The data input for the model is in Appendix A. The box was instrumented with strain gauges at critical points, positioned as in fig. 5.6. These strain gauges were 10mm long to give a good average strain value on the surface.

Table 5.1 overleaf shows reasonable agreement between the predicted strain in the skin and the experimental. The main descrepancy is in the low experimental strain in the stiffener caps. The low strain is thought to be the effect of shear lag. Due to the shortness of this test box, the full axial strain is not transmitted to the stiffener caps. Gauge 7, axis 1, situated at the junction of a stiffener sidewall and the skin, gives a better indication of the true compression strain in the skin.

The results from the back to back strain gauges nos. 5 and 6 are shown in fig. 5.7, which clearly shows the bifurcation of strain in inner and outer surfaces. The bifurcation occurs as the skin panel buckles, commencing at approximately half the ultimate design load. The box had been designed by the OPTIMIST program to have a postbuckling strain ratio of 2.3, with a maximum strain level of 0.3%. Another indication of the onset of buckling is given by gauge no. 7, fig. 5.8. Gauge 7, axis 2, is positioned across a junction between a skin panel and a stiffener. The gauge records a small tensile loading before buckling due to the Poisson's ratio of the material under compression. Above the buckling load the tensile strain reduces, due to the outward bowing of the skin panel here. The indication of buckling by gauge 7 appears at a slightly later stage than with the bifurcation method.

Figure 5.5

Linear postbuckling model for test box 2.

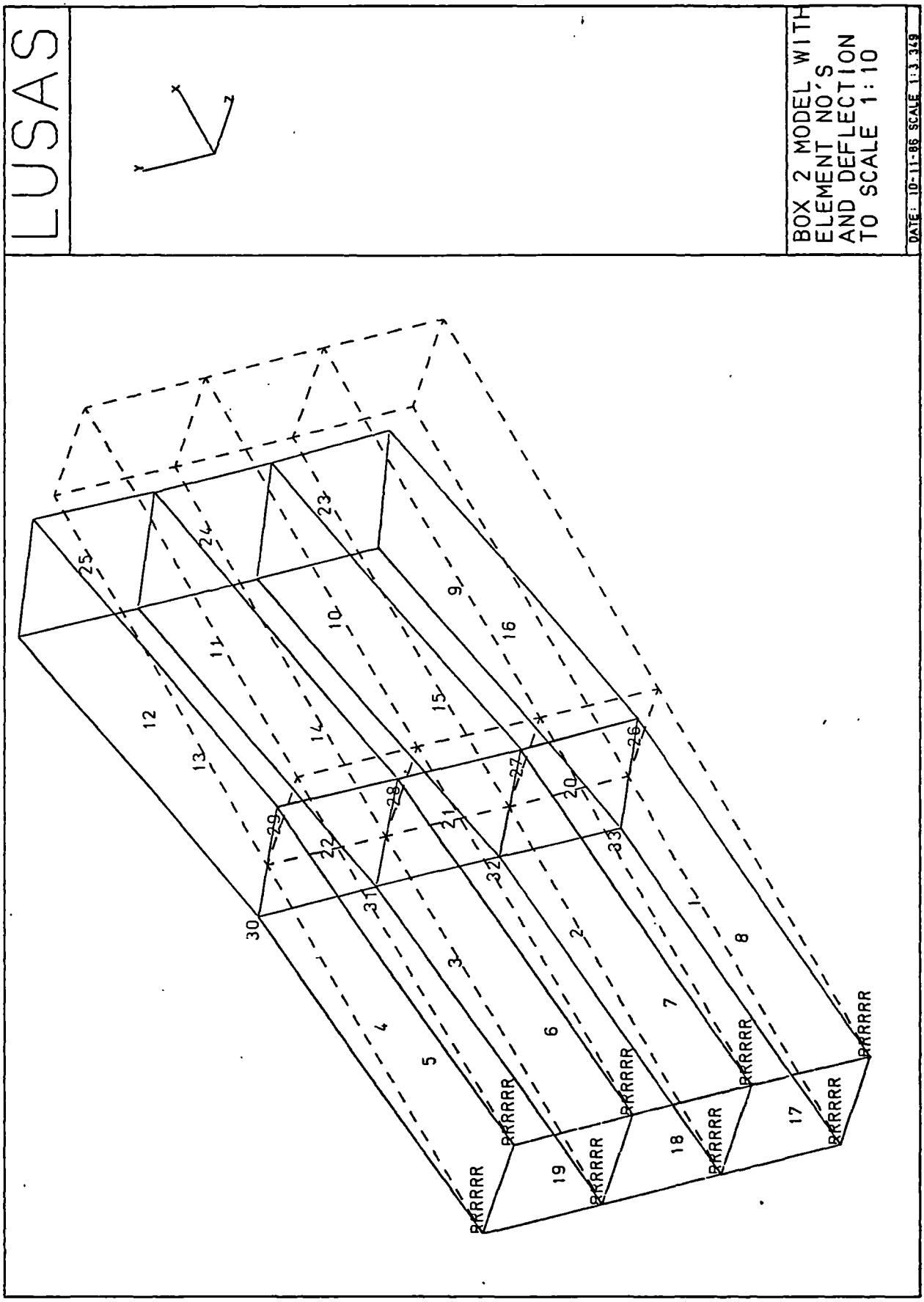

Figure 5.6

Positioning of strain gauges on test box No. 2.

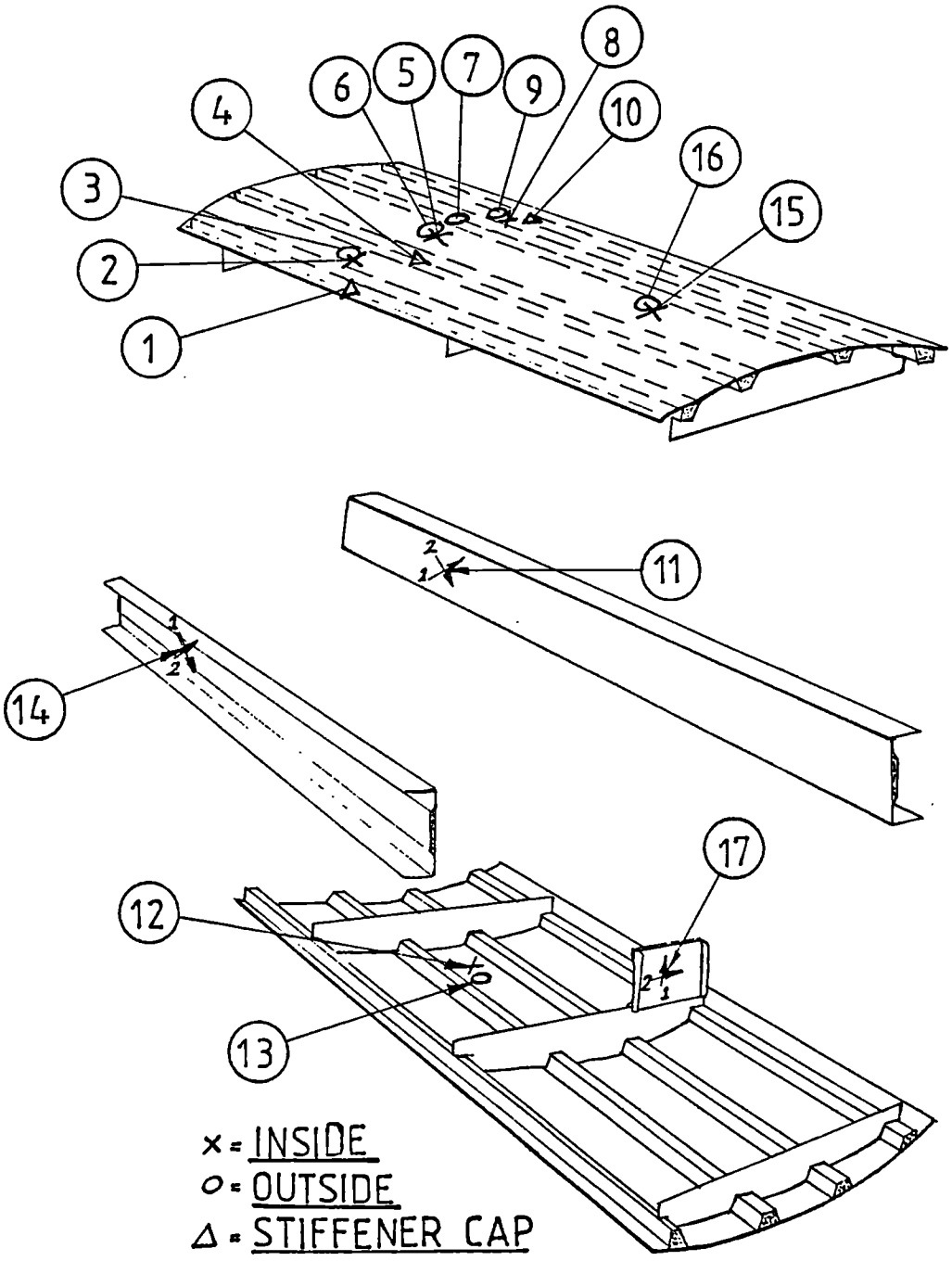

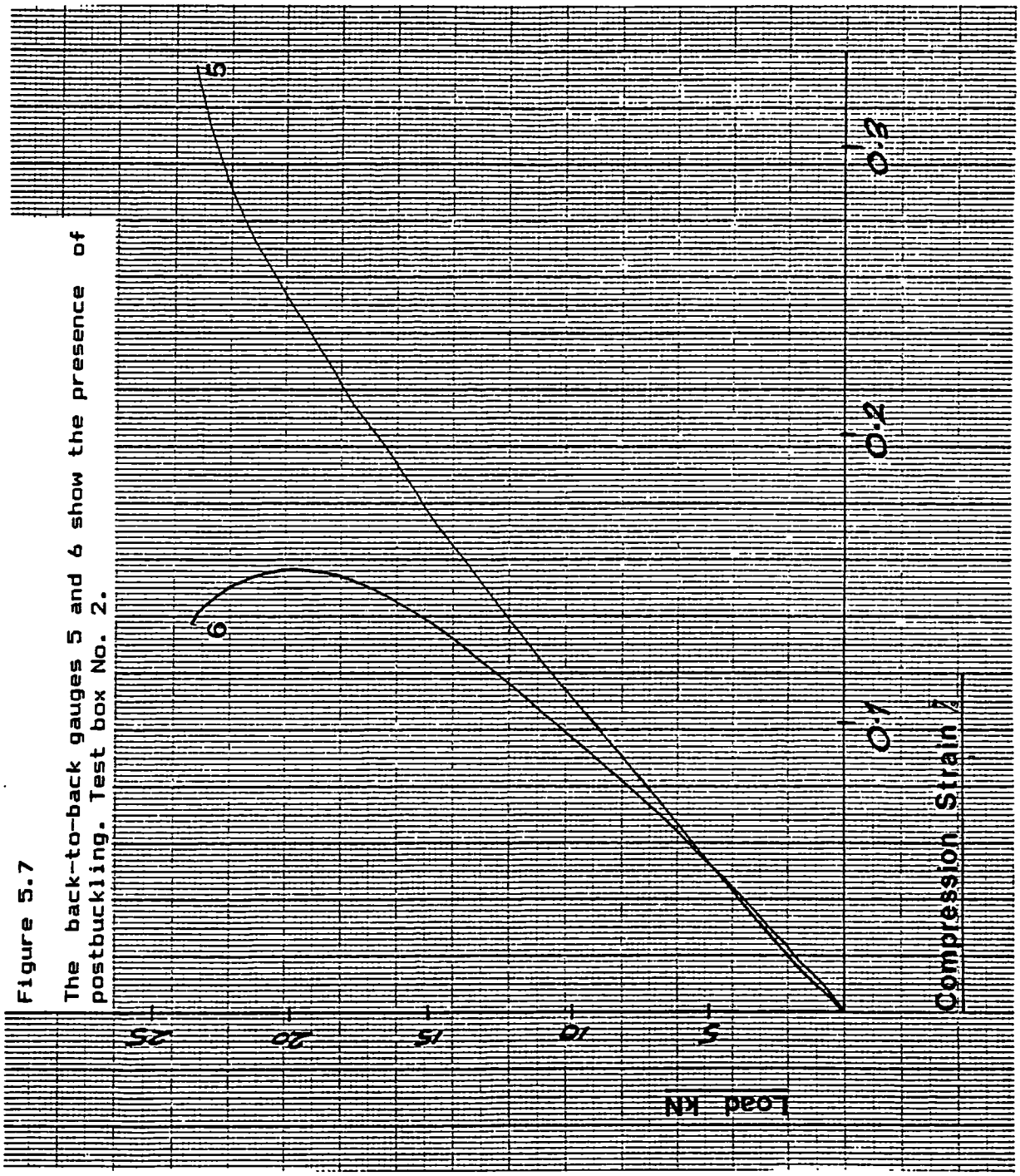

Figure 5.7

The back-to-back gauges 5 and 6 show the presence of postbuckling. Test box No. 2.

Figure 5.8

Reversal of strain in gauge 7. This gauge is located at a skin/stiffener junction near a buckle peak.

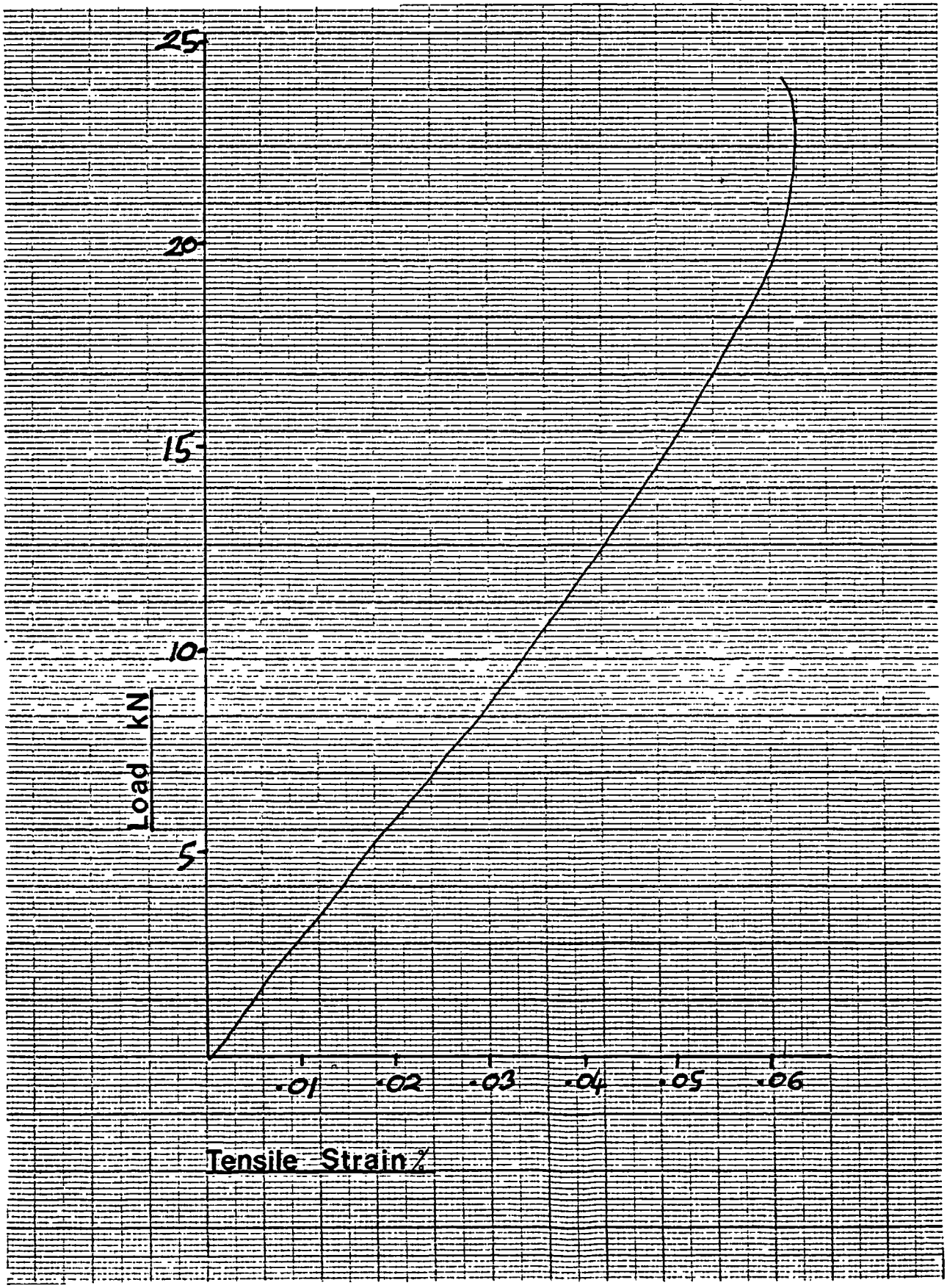

Table 5.1.

Comparison of the reduced stiffness linear finite element model with test results for test box 2.

Gauge no.	Element	Strain gauge	F.E. Strain
1 (x-axis)	26	-1.46e-3	-3.72e-3
2&3 ""	1	-2.16e-3	-2.5e-3
4 ""	27	-4e-4	-1.5e-3
5&6 ""	2	-2.32e-3	-2.5e-3
7 ""	28	-2.48e-3	-2.8e-3
8&9 ""	3	-2.33e-3	-2.5e-3
10 ""	29	-7.63e-4	-3.72e-3
15&16 ""	10	-8.3e-4	-1e-3
11 (shear)	4	1.04e-3	2.8e-3
14 (shear)	8	9.17e-4	2.8e-3
12&13 (x)	6	1.6e-3	1.1e-3
17 (z axis)	22	3.38e-5	1.7e-4
17 (y axis)	22	-1.69e-4	-1.9e-4

The model showed a deflection of 17.6 mm as compared to the actual measured tip deflection of 17.7mm. This does not account for the 1.47 mm deflection at the end of the attachment flange, however.

Success in the design and test of this box gave confidence in the method for the main wing. Data input for the main model is in Appendix A. Some key results of the F.E. models compared with actual test results are given in chapter 11.

Chapter 6.

The design of co-cured and adhesively bonded joints in the wing box structure.

6.1. Peeling effects caused by local buckling at skin/stiffener junctions.

One cause of failure of the panels in (16) was separation of the skin from the stiffeners due to the effects of local buckling. As the skin panels buckle, both bending and peeling loads are generated at the skin/stiffener junction. These panels had the stiffeners co-cured to the skin as integral members. However, they were constructed in such a way as to produce a weak peel-loaded junction between the stiffener and the skin as shown in fig. 6.1.

The OPTIMIST program contains a method for calculating the strain due to bending at this junction. This strain, with the attendant peeling effects, limits the possible extent of postbuckling in many cases. Three methods have been explored to prevent or delay the peeling mode of failure.

6.1.1 The corrugated method.

This method of panel layup is shown in fig. 6.2. It was intended to prevent stiffener separation from the skin by putting most of the skin plies into the stiffener sidewalls. Continuous fibre paths would then exist across the junction. The corrugated method was used in the construction of the first testbox which developed a postbuckling ratio of 5.

The main disadvantage of the corrugated layup arises when the panel has more than two stiffeners. It then becomes extremely difficult to form the prepreg so that it conforms exactly to each stiffener profile. Excess material is forced to bunch together, usually at the stiffener corners (fig. 6.3). Bunching occured despite the use of tooling that was completely successful when used on a single stiffener panel.

There is also a large proportion of $+-45^{\circ}$ fibres placed into the stiffener walls by this method. These fibres are used in the skin panels to give a high buckling load. They are not required in the stiffeners, which are essentially beam-columns. Their function is to take up axial loading as the skin

Figure 6.1

Delamination at a skin/stiffener junction caused by postbuckling.

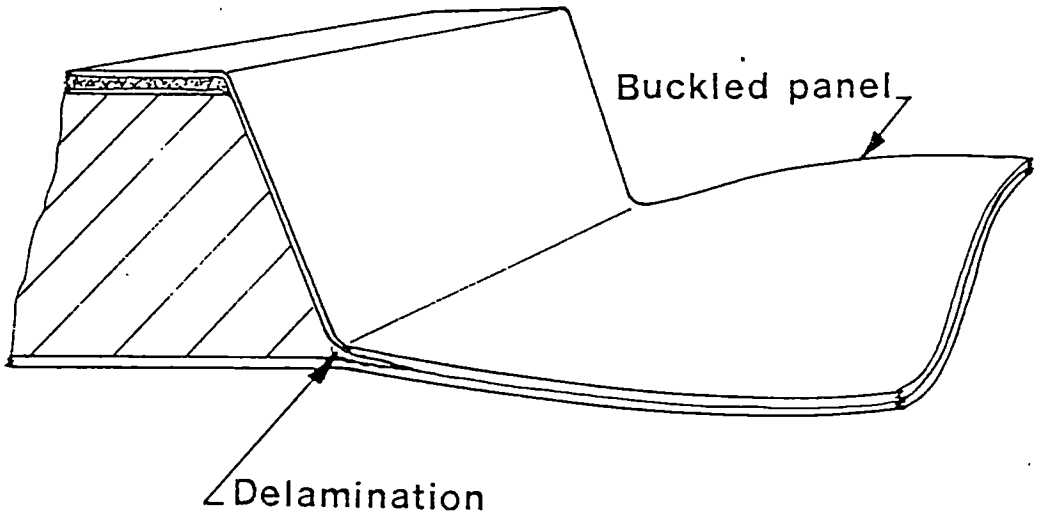

Figure 6.2

A corrugated layup to prevent skin/stiffener delamination with postbuckling.

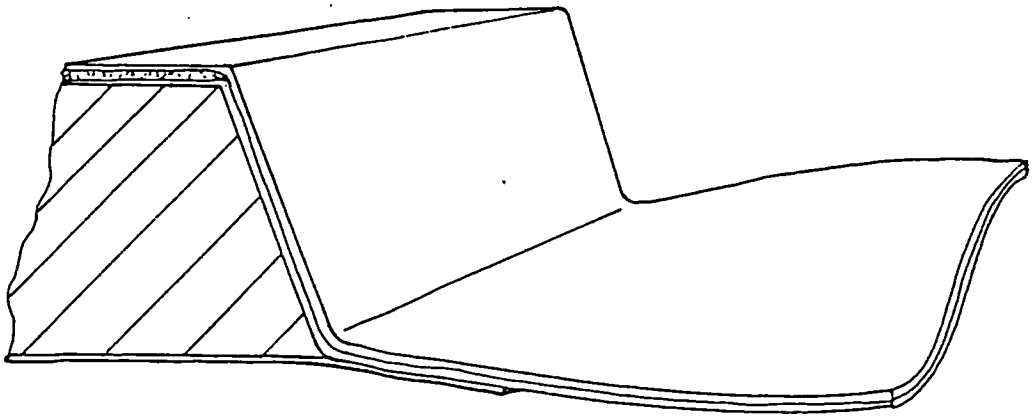

Fig 6.3.

If a corrugated layup is attempted in a multi-stiffener panel, bunching tends to develop.

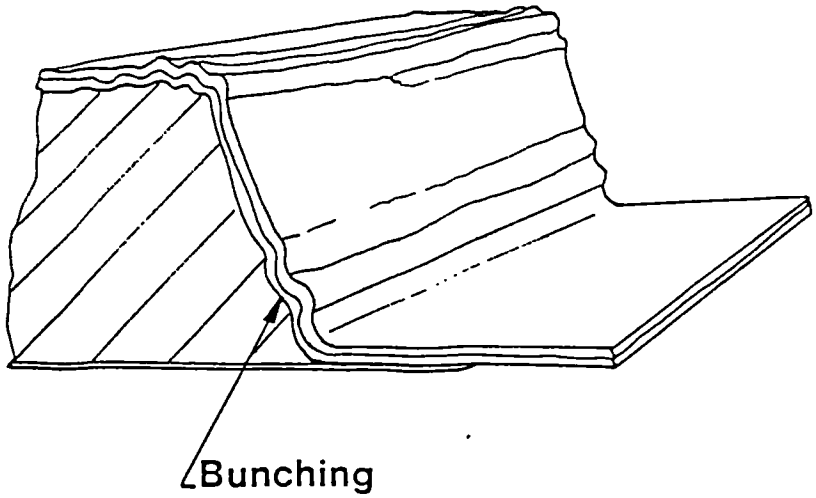

panels buckle, and to provide structural stability in the long column and torsional modes. For high column stiffness, unidirectional material is required at the stiffener top and base. Thin shear webs are required between them. This provides the necessary shear stiffness and gives a torsionally stiff section.

6.1.2 The stitching method.

Stitching of the panel at the skin/stiffener junction was seen as a means of achieving two aims. These were to make the prepreg conform tightly to the stiffener profile at the layup stage, as well as to improve the strength of the joint. A standard industrial sewing machine was used. A 70 tex spun Kevlar thread was used with an ultimate tensile load of 57N. Due to the limited throat of the machine, a layup technique had to be developed which used sub assemblies. The sub assemblies were then co-cured together. An interleaving technique was devised for sewn construction as shown in fig. 6.4. Interleaving has the advantage of allowing adjustment of the stiffener spacing on the tool. It also allowed the laminate to settle into position during the cure. Settling removed the problems of the laminate bridging or bunching at stiffener corners, as with the corrugated panel layup.

The compression skin panel of testbox 2 (fig 5.2) was successfully produced and tested using the stitching method. Testbox 2 is representative of the wing root area and has a postbuckling ratio of 2.5 .

Although the stitching method was successful, the manufacturing process is rather labour intensive. Slow stitching rates have to be used to allow the viscous resin to flow as the needle passes through; typically 150 stitches per minute at 20° C. Faster speeds result in more damage as more fibres are broken rather than flowing around the needle. Sleath (42) has experimented with these parameters . Increasing the temperature of the prepreg reduces the viscosity but increases the amount of resin which adheres to the needle. An acetone solvent pad can be used to keep the needle clean. The solvent may affect the properties of the cured laminate in this area.

Testing of specially prepared joint samples proved that very close stitching pitches are necessary. This was typically 0.6mm. The positioning of the stitching relative to the junction is also very critical.

Figure 6.4

Stitching was used to improve the skin/stiffener junction peeling strength. The interleaving technique was devised to enable a standard sewing machine to be used.

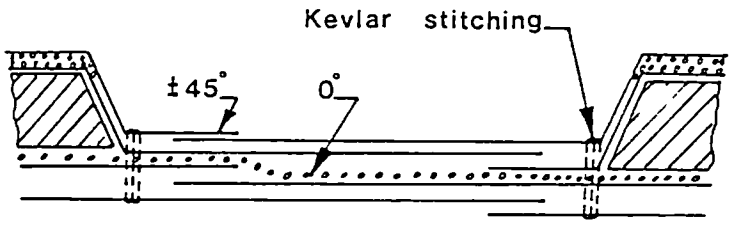

Interleaving and stitching

Fig 6.5.

The anti-peel strip reduces the stress concentration in the matrix at the junction. This feature was incorporated in the final design.

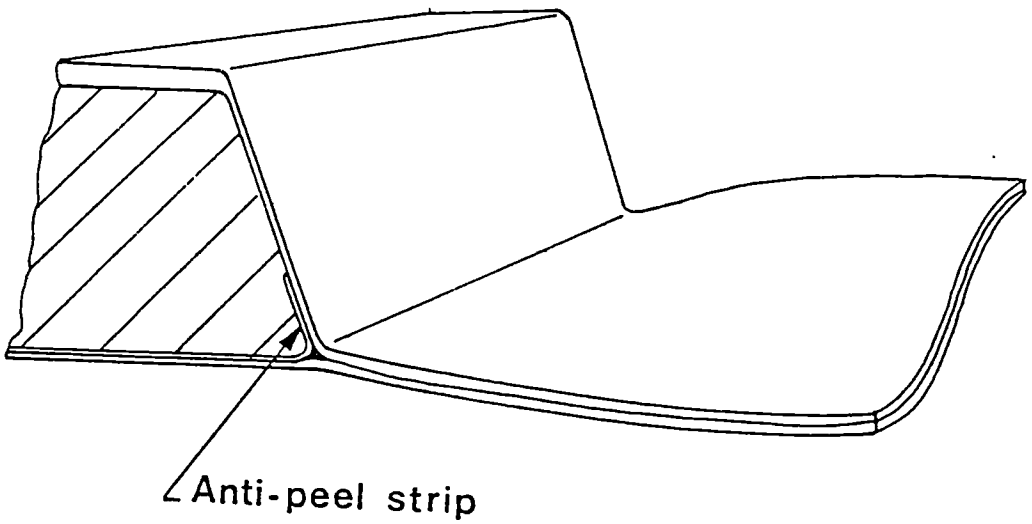

6.1.3 Co-cured joint design.

The junction strength can be considerably improved by the incorporation of an anti-peel bridging strip as shown in fig. 6.5. A single ply of woven +-45° carbon has a great effect on the peeling strength compared with the simple joint. The bridging strip can be incorporated into the construction under the stiffener foam core, bending upwards into the stiffener sidewall. The void at the junction between the strip, the stiffener sidewall and the skin is filled with resin or a bundle of unidirectional fibres. Ref. 43 shows that increasing the corner radii here increases the joint peeling strength.

To solve the problems of stiffener spacing adjustment and float of excess material, the stiffener sidewall plies have been designed to overlap at the stiffener cap. The stiffener cap is a structurally stable area. A joint here is not liable to failure through delamination caused by local buckling effects.

In the actual main wing box design this anti peel strip is oriented at 0/90° to the stiffener longitudinal axis. One ply only is used. The scheme was to allow the 90° fibres to prevent peel failure. The 0° fibres contribute to the compression stiffness. Just using 90° fibres here could be the best solution.

6.2. Testing of the skin/stiffener joints.

A special test coupon has been devised to duplicate the peeling and bending loads at the junction, as seen in fig. 6.6. Using this method, various configurations of co-cured joint were tested, with results shown in table 6.1. In the case of the stitched joints it was found that the stitching pitch had to be in the order of 1mm or less to realise an advantage over the plain control specimen. The stitches had also to be made within 0.5 mm of the junction in order to provide an improvement.

The very great improvement in strength from the use of an anti-peel strip can be seen. It allows the interlaminar tensile loads to be distributed over a large area instead of the load acting on the stress concentration at the joint in the brittle matrix.

The first specimen was co-cured together in a simple L-type joint. This is the simplest way of joining the stiffener sidewall to the skin. It fails because of the high stress concentration in the resin

Figure 6.6

This special test coupon was designed to prove peel-loaded joints.

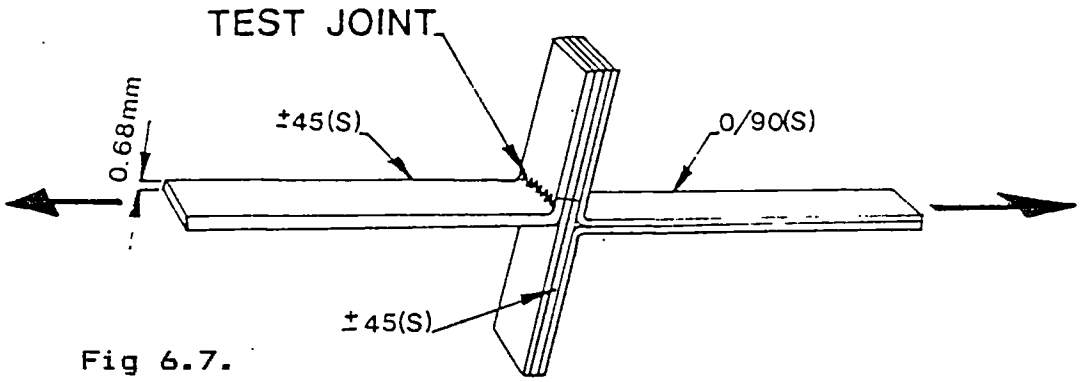

Fig 6.7.

The closely stitched specimen. This shows that failure has occurred by delamination of the whole transverse surface. The stitching has stayed intact.

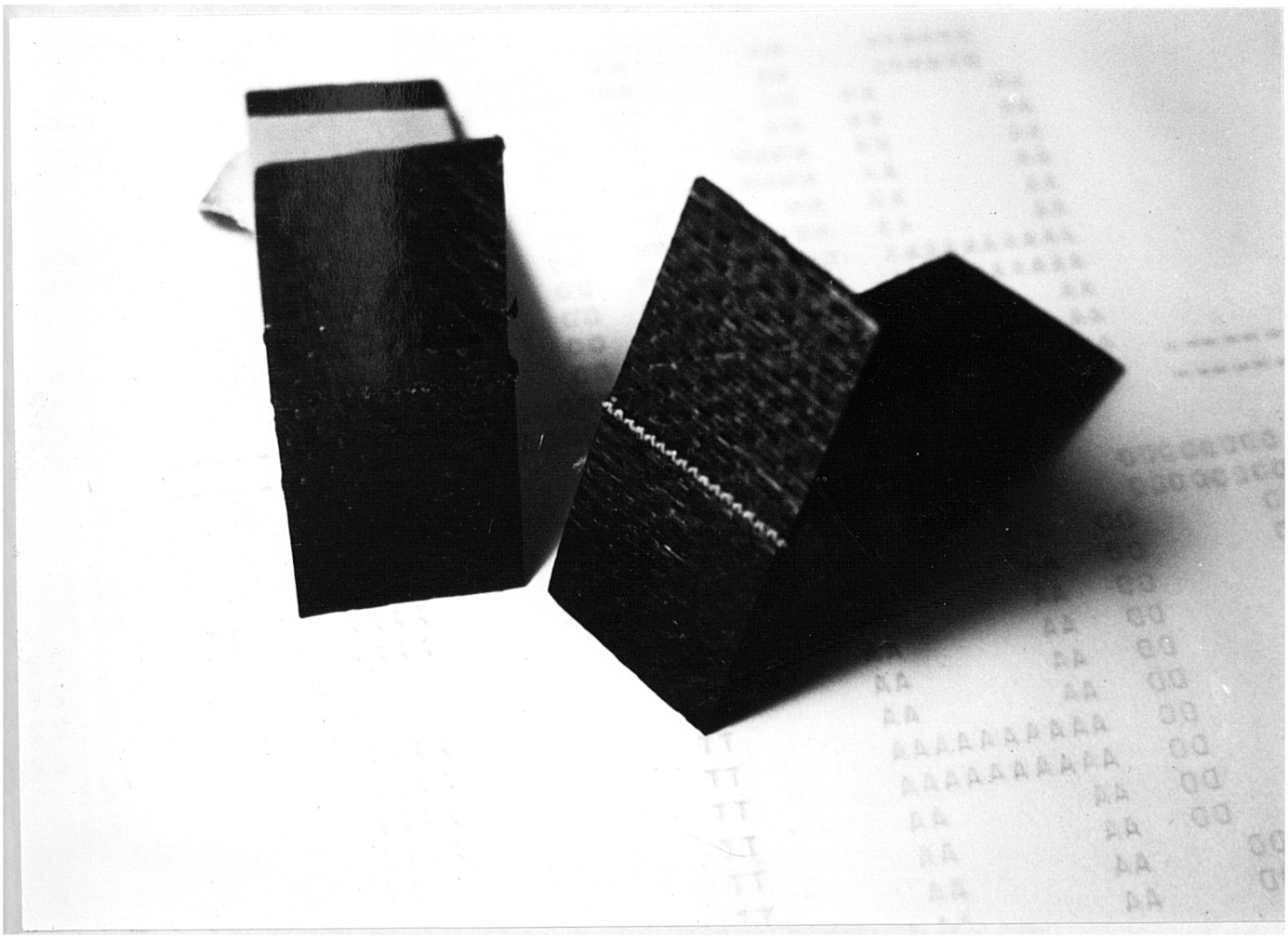

at the junction, which is due to peeling stresses. All the other specimens change the failure mode. In these cases the whole area under the junction has to separate. The greater surface area implies greater failure load and reduced stress concentrations in the matrix. This is the reason why the results fall into two bands. There is no great advantage in increasing the number of anti-peel plies once the failure mode has changed.

Table 6.1. Skin/stiffener junction results.

Specimen	Load/width N/mm.
Control- simple co-cured peeling joint	78
Zig zag stitched, 0.6mm feed, 1.8mm wide stitches using 70 tex spun Kevlar. Delaminated under the stitching.	100
With anti-peel strip 1 ply woven cfrp at junction. Did not peel-delaminated under the joint.	104
With anti-peel strip 2 plies woven CFRP at junction. Delaminated under the junction.	118

The stitched specimen had the closest stitching of all the samples. There were three others where the stitching pitch varied from 1-2.5mm. These all failed at virtually the same load as the peeling control specimen, in the following sequence:
i) Peeling stresses in the matrix at the junction would start a crack.
ii) The crack would propagate to the stitch line.
iii) The stitches would then fail.
The required combination of close stitching and critical positioning makes the method difficult. The closely stitched specimen is seen separated into two parts after failure in fig. 6.7.

6.3. The positioning of assembly joints relative to buckled components.

Good and bad methods of joining a spar to a postbuckled skin panel are shown in fig. 6.8. Joint geometry should also be simple unless the two

Figure 6.8

Good and bad locations for bonded spar joints in a postbuckled structure.

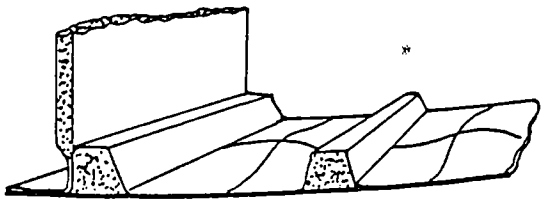

Good

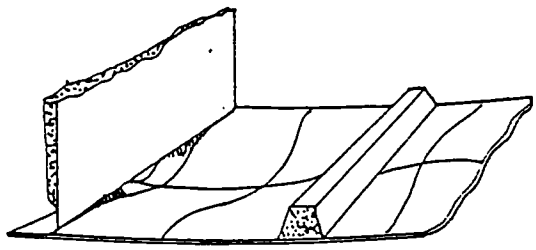

Bad

Fig 6.9.

For clamping the spar joints of test box 2, a partial vacuum was drawn as shown.

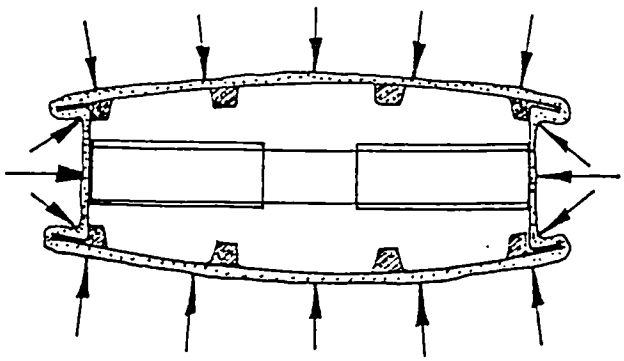

Vacuum clamping

components to be joined have been produced on very precise matched tooling. This is one reason why it has been found better to co-cure the rib flanges with the skin. The box structure can then be completed by the use of rib shear webs.

6.3.1 Clamping of simple lap joints.

Clamping of lap joints for assembly, particularly if one side is blind, can be a major problem. This is particularly true for thin sections where the clamping force has to be distributed along the length of the component. The spar joints of testbox 2 were clamped by means of a partial vacuum drawn inside the box as shown in fig. 6.9. This technique is acceptable for boxes of near square section. Boxes of long chord require reinforcement to avoid crushing. An alternative solution is to design a large clamping jig, the cost of which is too high to justify for a one-off structure. This type of simple lap joint also incorporates no means of controlling the bondline thickness. The joint may be clamped too tightly, making the bondline too thin, with a consequent reduction in strength.

6.3.2 Slotted joints.

The above disadvantages led the author to investigate slotted joints as shown in fig. 6.10. This type of joint can be co-cured as a feature of the structure. It can be designed to be self-clamping with bondline thickness control. Slotted joints can also locate the components together in the desired position. These joints load the adhesive in pure shear without the peeling effects which can occur in single lap joints.

6.3.3 Spar joints.

Continuous slotted joints are used to join each spar shear web to the stiffened skin panels. In the final wing design a sandwich stabilised shear web is used, which is designed not to buckle. This 'slot together' joint concept could work particularly well with a sine wave stabilised shear web, requiring very little strength from the adhesive.

Figure 6.10

A typical spar to skin joint used in the final design.

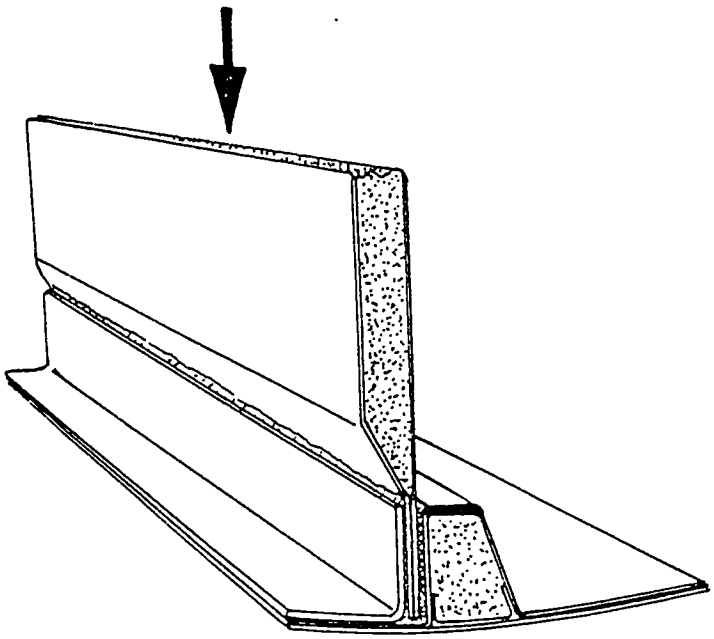

Fig 6.11. Slotted joint

In test box 2, this method was used to bond rib shear webs to spar shear webs.

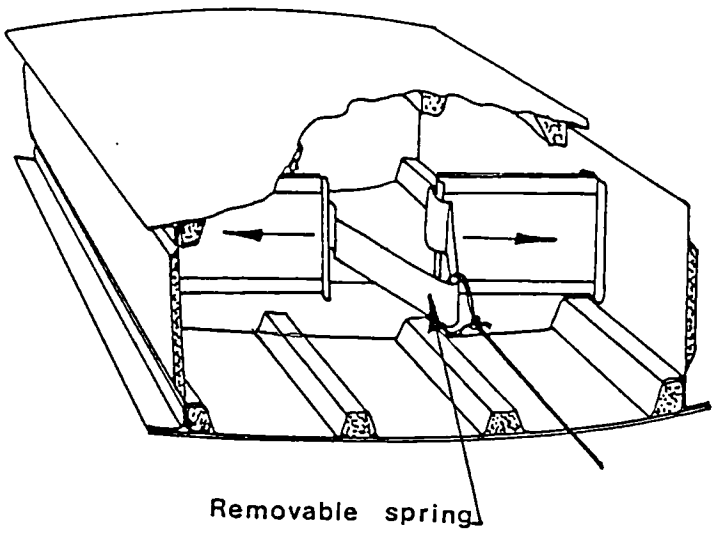

6.3.4 Rib joints.

The ribs are joined together by means of a slotted joint similar to that of the spars. However, in the case of the ribs there can be a need to form a bond between the ribs and the spar shear web (fig. 6.11). This is accomplished by cutting the rib into two sections. The bond clamping force is then provided by means of a removable hairpin spring. The spring slides the two rib sections apart along their slotted joints.

Joining the ribs to the spars was found to be quite difficult in practice. With long ribs, a considerable spring pressure was required to overcome friction. The springs also made assembly difficult. The ribs kept pushing out into the path of the spar when assembly was attempted. Finally, once the structure was complete, this joint was very awkward to inspect. Other solutions such as the use of separate "L" sections to form the joint seemed to offer little advantage.

A solution appeared to the problem once the slotted joints for the skin/spar connections were devised. It was realised that because the spar was attached to the stiffener sidewall, a load path already existed here. The load path starts from distributed airloading gathered on to each rib (fig. 6.12.). The air load is fed into the spar by shear at the spar/stiffener joint. The load is diffused between each rib because of the bending stiffness of the stiffeners.

Calculations showed (Appendix C) that there was ample area to transfer the load through the adhesive. With regard for the concentrated loading in the vicinity of each rib, this scheme should work on many other wing structures.

Because the rib shear load is taken through the stiffener sidewalls, there is no need for direct connection between the rib web and the spar. With no connection here, the ribs had to be designed as free standing members. They are stabilised by moulded integral stiffeners to resist shear and compression buckling. This provided few problems in construction as sections of Rohacell core were incorporated into each rib.

Where pickup points such as those for the aileron hinges are required, the spar shear web is cut. This allows the rib web to come through as a continuous member. The rib web is designed as a beam, incorporating unidirectional material at the top and

Figure 6.12

Distributed airload is taken to the leading edge stiffener by the rib. The shear load is then transmitted to the spar by the slotted joints along the stiffener sidewalls. Note also the stiffeners moulded in to the rib shear web.

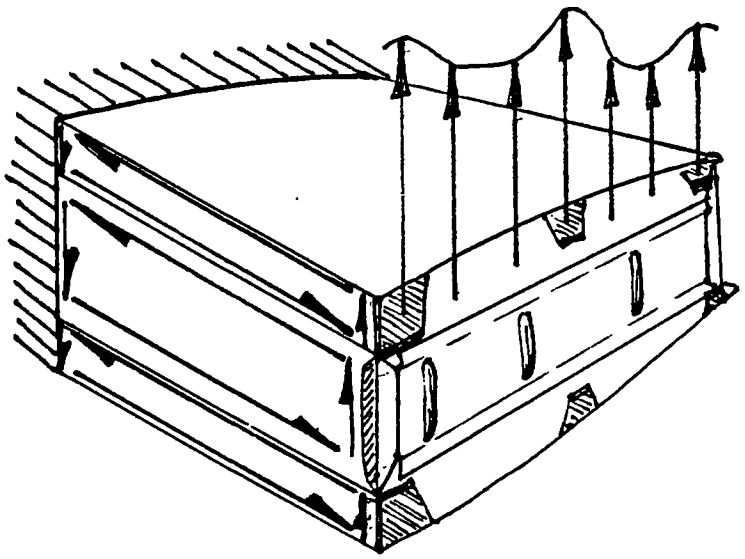

Fig 6.13.

At aileron pick-up points, the rib continues through the rear spar shear web. Small angled sections then transmit the spar shear across the rib.

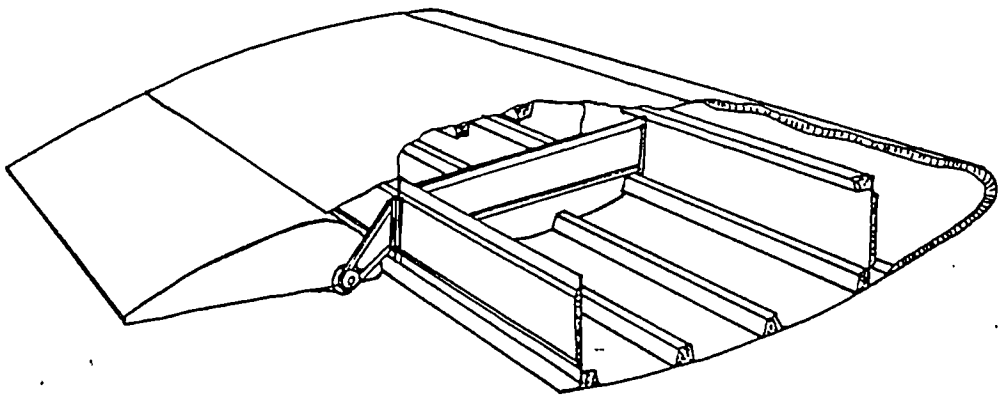

bottom. The rib then diffuses the load into skin shear through the slotted joints and co-cured rib flanges (fig 6.13). Since only the spar shear web has been cut, no problems exist with discontinuity of the spar caps. Small angled sections are used to transfer spar shear across the rib.

Chapter 7.

New methods of construction for composite box structures.

7.1. Problems with a "traditional" construction system.

The initial scheme employed integrally stiffened, co-cured flat panels. These would be curved to shape. Separate ribs would be used to assemble the box and provide the desired cross section. "C" section spars would be used to transmit the shear from top to bottom skin.

The objective of this initial scheme was to minimise on tooling requirements for a one-off structure. The first testbox was constructed in this way. With the relatively thin wing skin and the gradual chordwise curvature, curving the skins to take the form was practical. The curvature was gradual enough to prevent very large bending stresses being built into the skin.

In the A1 wing, the mainspar is kinked. Furthermore, the stiffeners do not follow the camber lines but run parallel to the trailing edge. This implies that the stiffeners must bend along their length. In the metal A1 wing, the stiffeners were simply bent to shape. This would leave inbuilt stresses in a carbon structure.

Apart from this drawback, the use of traditional ribs caused difficulties. It proved difficult to match the complex skin and stiffener profile to the ribs. The joint was also difficult to clamp without the use of rivets.

The usual method of joining a "C" section spar to a skin was also unsatisfactory. In the first testbox, the spars were joined to the free skin edges as in fig. 6.8. Postbuckling effects then caused the joint to separate under peeling loads. This caused the box to fail. These rejected schemes are detailed in Appendix D.

7.2. The development of a new method.

These joining problems can be overcome by co-curing as much of the structure together as possible. A curved skin tool is obviously required. Co-curing of the whole top skin, spars and ribs seemed feasible.

Joining of the lower skin could then prove problematic. Flat, peel-loaded joints could be used. These would probably have to incorporate bolts or rivets to a) clamp the joint together and b) improve the peel strength. If plug-in, shear loaded joints were used, then the geometry of the upper and lower skin joint features would be very critical in this case. The complete skin/spar/rib scheme would also make vacuum bag consolidation difficult. Removable tooling blocks may have been required.

7.2.1 The construction method used.

A compromise between full co-curing and the discrete component design was appropriate. If the structure was not to be all co-cured, then assembly joints would have to be made. It was decided to move these to effective locations. Large, shear loaded bond areas could then be designed into the joints. Peel loading of assembly joints was avoided after experience with the first box. The scheme eventually used was to co-cure stiffened skins with the rib flanges. The tooling for this design could be produced quite simply, as in chapter 8.

7.2.2 Forming of assembly joints.

The rib flanges were arranged to protrude upwards from the skin and end at a straight edge. Slots formed in the straight edge of the separate rib shear webs engage in the rib flanges. A similar scheme was employed for the skin/spar joints. A slot was formed at the side of the leading and trailing edge stiffeners. The spar web was then plugged or slid into position. Provided that both the slot and the web are well coated with adhesive, a very firm joint can be made. No clamps are required to close the joint, and the adhesive is loaded in pure shear.

7.3. The production sequence of the co-cured skins.

7.3.1 Preparation.

The tool was first aligned by fitting the original wooden plug onto the surface. Since the wood plug was split at the centreline, this mid surface could be

used to true the mould. The mould was mounted on adjustable dexion supports. These supports were in turn rested onto two levelled rails (fig. 7.1). The mould was clamped via these mounts to the autoclave trolley bed for curing. This kept distortion during the cure to a minimum.

All the prepreg layers required to produce the whole wing were cut out. They were stored in the freezer until needed (fig 7.2). This took the author two weeks. All the parts were cut out on a hardboard surface using Mylar polyester film patterns. Mylar lays flat, is transparent and is quite dimensionally stable. A roller press system using a blade set into a plywood block would work well in production. The complete kit is shown in fig 7.3.

The completed foam stiffener cores were cut out on a bandsaw. They were layed onto the tool surface with the completed rib tooling as in fig 7.4. Stiffener runoffs were joined with an epoxy/microballoon paste. The paste was used to blend the junction together as shown in fig 7.5. The tooling used to consolidate this area was moulded from carbon/epoxy. The stiffener cores were covered in PTFE tape for the purpose of moulding these parts.

7.3.2 Laying up.

The tool was next covered in a non-porous PTFE release cloth, fig 7.6. A high temperature wax release could have been used here. However, using PTFE was a simple way of being sure of an easy release from the tool.

The first layer was rolled onto the tool, fig 7.7. This is a woven +-45° layer. Overlaps of material were 50-70 mm where joints were required. These were arranged not to coincide with joints in other layers.

The centre plies of unidirectional material were layed into position, as in fig. 7.8. These were followed by the stiffener anti-peel strips. The stiffener spacing was regulated by the rib tooling, as shown in fig 7.9.

Next, the stiffener cores of Rohacell foam were positioned. The cores were then capped by the stiffener cap plies of unidirectional material (fig. 7.10). The unidirectional plies had been previously layed up to the correct thickness in a sheet form. They were then cut into strips, and coiled onto a large diameter drum for freezer storage.

7.3.3 Anti-peel strips.

The anti-peel strips were layed in position under each stiffener core. These strips are designed to fold upwards to lie against the stiffener sidewalls.

Using the rib tooling to control the stiffener spacing, the inner skin plies of woven material were added (fig 7.11). These plies were positioned as separate strips for each stiffener bay. Each inner skin ply strip overlaps at the stiffener cap with the adjacent strip. The full stiffener cap width is used for the overlaps.

A "zip up" technique was used to fold the anti-peel strips along the stiffener sidewalls and position the inner skin plies. The technique used two PTFE coated plates as in fig. 7.12. The first plate would bend the strip upwards, followed by the second plate to press the skin ply into the corner at the stiffener base. The two plates were moved smoothly along the stiffener length, continuously attaching the laminate.

Once the joint had been pressed together in this way, the laminate stayed together. This is due to the fairly high tack of the Ciba Geigy 913-815 woven material. The process may be more difficult with non-woven materials. Some difficulty was experienced if the anti-peel strip reached less than half way up the stiffener sidewall. It was also found most important to maintain the correct stiffener spacing. This was essential to maintain the correct ply overlaps at the stiffener caps.

7.3.4 Jigging.

For the wing to assemble properly, it was important to ensure correct rib spacing on each skin. A series of jigging holes were drilled into the tools. The holes were carefully measured to be in matched positions on each skin tool. A tolerance of +-1mm on all measurements was used. Kevlar threads were then stretched between the holes. The thread was locked in position by inserting tapered pins between the jigging hole and the thread. These threads were used to define the position of each rib flange (fig. 7.13). The rib tooling controlled the positioning of the front and rear spars. However, since this tooling is segmented, the overall spacing was regularly checked during the layup. During certain phases of the layup, clamps were used to lock the leading and trailing stiffeners in

the correct positions.

7.3.5 Rib flanges.

The rib flange laminations were then positioned in the following way. The rib flange tools for one side were first positioned against the Kevlar line. Half the rib laminate was then laid into position. The rib flange laminations were cut out so that they fitted around each stiffener. At the junction with the skin, they flanged outwards 20mm to provide a joint with the skin and stiffeners (fig 7.14). The rib flange tooling for this side was placed over the laminate. The first side of the rib flange tooling was then removed (fig 7.15). The opposite half of the rib laminate was then positioned, flanging out in the opposite direction. Finally, the original side of rib tooling was replaced over the laminate (fig 7.16). The Kevlar line was cut and either pulled through or allowed to remain in the laminate.

This method provided a means of laying up a rib-to-skin joint which flanges outwards in both directions. This type of joint is much stronger in peel than a single direction flange. With the flanges being co-cured to the stiffener sidewalls and caps, the rib flange can be considered a structurally integral part of the skin. The carbon rib tools were coated in PTFE tape for an easy release from the cured components. Note the continuous PTFE tape strip along the top of the rib tooling, and the segmenting of the tooling to allow even consolidation, as shown in fig. 7.16.

7.3.6 Stiffener tooling

The stiffener tooling was required to consolidate the stiffener whilst preserving a desired cross section. Work by Belgrano (16) and Hussain (19) has shown problems of bunching of material when elastomeric tools were used. The use of silicone based tooling was also questionable, because of the risk of contaminating the laminate surface. This could make bonding unreliable.

To solve these problems, a system of segmented rigid tooling was devised as in fig 7.17. This system allows the autoclave pressure to consolidate the whole cross section. The critical top and bottom corners are well formed, and a good surface finish can be

achieved. Fig 7.18 shows the stiffener tooling being positioned over the PTFE non-porous release cloth. Fig 7.19 shows the tooling almost complete, including the specially moulded sections for the stiffener runoff areas. In the photograph the strips forming the joint on the leading stiffener are being positioned. The sidewalls of the leading and trailing stiffeners were cut at special angles. This allowed the flat surface of the spar shear webs to meet the flat side of the stiffeners. Between these joining strips and the stiffener sidewalls, a PTFE surfaced steel slot tool was inserted. The laminate was compacted in this area with a folded steel angle section (fig 7.19).

7.3.7 Vacuum bagging.

The whole laminate was now ready to be covered in a glass felt breather cloth (fig 7.20). Separate sections of breather were used for the rib flange areas and the rest. A heavy duty breather was used over the rib tools. This was to prevent the edges of the tooling from puncturing the vacuum bag. A light material was quite sufficient for covering the stiffener tooling. After this stage, a large vacuum bag was positioned over the tool (fig 7.21). The bag incorporated large "rabbits ears" at each rib station. Although the bag looks very large, it fitted the contours of the moulding without undue slack when a vacuum was applied (fig 7.22).

7.3.8 Curing.

The layup was transported to the autoclave under vacuum. Very little leakage occurred once the bag had bedded down. At the autoclave the tooling was clamped down to the trolley to minimise distortion. The cure cycle was to the standard Ciba-Geigy specifications for the 913 system. A curing pressure of 40psi was used. This is mainly limited by the capability of the foam stiffener cores at 120° C. However, the quality of the cured parts appeared to be good. The rigid tooling seems to intensify the pressure where it is required, i.e. at tight radii.

The first skin to be co-cured had a single vacuum takeoff point at the root. A vacuum gauge line was positioned at the opposite end. During the cure, a back pressure of 10psi built up at the gauge end,

reducing the differential to 30psi. This must have been due to a small leak towards the wing tip. For the subsequent skin, two vacuum lines were fitted at each end. The gauge was situated in the middle. This time, full pressure differential was maintained throughout the cure cycle.

7.3.9 Construction time and results.

With everything prepared, the first skin took 9 man-days to lay-up for curing. The second took 5, and was a better quality moulding. Distortion of the two skins was within 2 degrees of twist and 10mm bow over the length of 4.4 metres. Fig 7.23 shows the second co-cured skin being unwrapped. The small gantry above the tool is a support for the spar tooling. The two sandwich construction spars were cured in the same autoclave cycle.

Fig 7.24 shows the generally high quality of the finished panel. One manufacturing problem occurred in the areas of the stiffener runoff tooling. This tooling needs modification so that the tool acts as a pressure intensifier. An elastomeric material would help in this area.

Another moulding defect was the wrinkling of the skin around the spar attachment slot. The tool used to make the slot may have been too low. Consequently, the skin was not compressed below the slot. Some experimentation with slot tooling is required to solve this problem. Neither of these two defects were serious from a structural point of view. They are shown in fig 7.25, which shows the mainspar at station 3706.

7.4. Construction of rib shear webs.

The rib shear webs incorporate integral stiffeners to resist crushing. The stiffeners are produced by inserting Rohacell cores into the layup. The rib shear webs also incorporate slotted edges for joining to the rib flanges.

Fig 7.26 shows a rib during the course of laying up. All the ribs except for station 4281 were of $+-45^{\circ}(2)_{sym}$ construction. In this figure the first two layers have been positioned. The PTFE covered steel slot tools and the stiffener cores are also added. Note the addition of a single ply of unidirectional

material laid along the stiffener cap. The next stage is to lay on the next two plies. The rib is then cured in the normal way using a PTFE non-porous release cloth and a vacuum bag. Again, a 40 psi cure is used in the autoclave. No tooling is required to produce these components apart from a flat surface.

Rib stations 3706 and 1981 were designed to pick up aileron loadings. Stressing for these details is in Appendix C. The ribs are shown in drawing A1-CFRP-03, Appendix H. The aileron pickup ribs project aft of the trailing spar, to a hole where the load is applied. The design approach was to incorporate a sandwich panel into the rib here. At the top and bottom edges of each rib, unidirectional material was added. The unidirectional plies transferred the direct loads caused by bending of the rib into the rib flanges.

The pickup rib features are shown in fig 7.27 during the course of laying up. The specially cut 'ears' on the lower plies were folded over the sandwich section. By folding continuous +-45° plies around the sandwich core, torsional stiffness and transverse shear stiffness were both improved. The folded aluminium segmented tooling is shown in fig. 7.28. The load was transmitted to the sandwich section by means of a bobbin. The bobbin is shown in fig 7.29 before installing in the rib with Ciba-Geigy 2005 adhesive. The pick-up ribs gave no trouble during testing whatsoever.

7.5. Construction of the spars.

The spars, like the ribs, are simply shear webs. All the direct loads are taken by the skin and stiffeners. This allows a very simple spar design. The spars are of simple sandwich panel construction as shown in drawing A1-CFRP-02, Appendix H. The sandwich core is 5mm Rohacell wf 51 foam, which is bevelled at the edges to allow the prepreg to conform smoothly to shape. The foam core is narrower than the total spar width, so leaving a margin of solid laminate at each edge. On assembly of the wing, the solid laminate edge engages in a slot. The slot is formed in the leading or trailing edge stiffener sidewall as an integral part of the skin moulding.

The spars were produced on low-cost chipboard tooling. To solve the problem of porosity, the tool was fully enclosed in the vacuum bag. By fully enclosing the tool, the fire risk presented by the

chipboard was reduced. The mainspar was originally designed to incorporate the kink at station 1981. Due to assembly problems, the spar had to be modified to incorporate a joint in the kink area.

7.6. Assembly of the structure.

7.6.1 Choice of adhesive.

A decision was made to assemble the box using a cold-curing epoxy paste adhesive. The construction technique is also well suited to the use of a hot-cure adhesive. The author, however, wished to avoid the cost and time involved in arranging oven facilites. The strain gauges and wiring would also have been damaged by the heat of the curing process.

The advantages of a hot-curing adhesive would be i) unlimited assembly time and ii) improved strength of joints. Film adhesives could work in principle, but do not provide lubrication for sliding components together.

Tests were made on two possible adhesives, Redux 403 and Araldite 2005, both Ciba-Geigy products. Coupon testing as in Appendix G showed the latter was 80-100% stronger than the former in a representative joint. The 2005 was also attractive as it is a high peel strength adhesive. A typical shear strength of 30 MPa was recorded. The best film adhesives are capable of 50-60 MPa. However, joint areas required for 30Mpa are still very small. The joints in the wing were designed for 10 Mpa at ultimate load.

7.6.2 Assembly sequence.

The general internal structure of the wing box is seen in fig. 7.30. Here, all the rib webs and spar sections have been slotted into one skin. The co-cured skin/stiffener/rib flange system can be clearly seen. When assembled, the smooth surface finish can be seen in fig 7.31.

The use of Araldite 2005 gave a pot life of 1.5 hrs in which to assemble the structure. Several 'dry runs' were made to see if this was practical. The original scheme for assembly was:

i) Install mainspar into lower skin slot.
ii) Position ribs on rib flanges on lower skin.

iii) Engage mainspar in upper skin, and gently lower the trailing edge of the upper skin. The rib/upper flange joints would be made progressively.
iv) Slide trailing spar into slot to close the box.

This scheme proved very difficult indeed. All the ribs had to be located simultaneously as the top skin was lowered. In addition, the two pickup ribs prevented sliding the rear spar into position. The spar between these two ribs had to be plugged in. This made all the joints between these ribs blind. Correct engagement of the slots would be impossible to check. Effective inspection would also have been impractical.

To solve these problems the mainspar was cut at the kink. The slot for the outer mainspar was continued here so that it could be slid into place from the inboard end. The spar was cut into a diamond shape, as in fig 7.32. This ensured a positive shear connection between the two spar sections. A flat panel was also bonded to each side of the spar on assembly, to transfer the shear. The inner panel was bonded to one section of spar first. It was clamped for bonding during assembly by self-tapping screws.

With the mainspar in two sections, assembly became much easier. All the joints can be inspected before closing the box. Also, ribs can be slid into position one by one. This eases the problem of limited adhesive pot life. The assembly sequence, which is shown on the video tape is as follows:
i) Plug in the two pick-up ribs to the lower skin.
ii) Plug in the trailing edge spar between the two ribs.
iii) Position the top skin to plug into these three components.
iv) Slide the remaining trailing spar sections into position.
v) Slide in the root rib into the top and bottom flanges.
vi) Jig the assembly by temporarily inserting the mainspar between the two skins.
vii) Allow the assembly to cure before proceeding.
viii) Remove mainspar and slide remaining ribs into position (see fig. 7.33).
ix) Install systems and check all joints.
x) Slide mainspar outer sections into position (see fig. 7.34).
xi) Slide in the mainspar inner section.
xii) Complete the box by making the mainspar kink joint.
xiii) Apply gentle pressure (shot bags) to the whole

surface. The washout of the wing is jigged by resting the whole box on the lower skin tool during assembly.

The internal joints, together with the strain gauges, can be seen in fig 7.35. The strain gauges were positioned on each rib and on a selection of skin and spar panels. Layout and type of these gauges is shown in Appendix F.

Figure 7.1

The mould is jigged into position on an adjustable bed and trued by means of a spirit level.

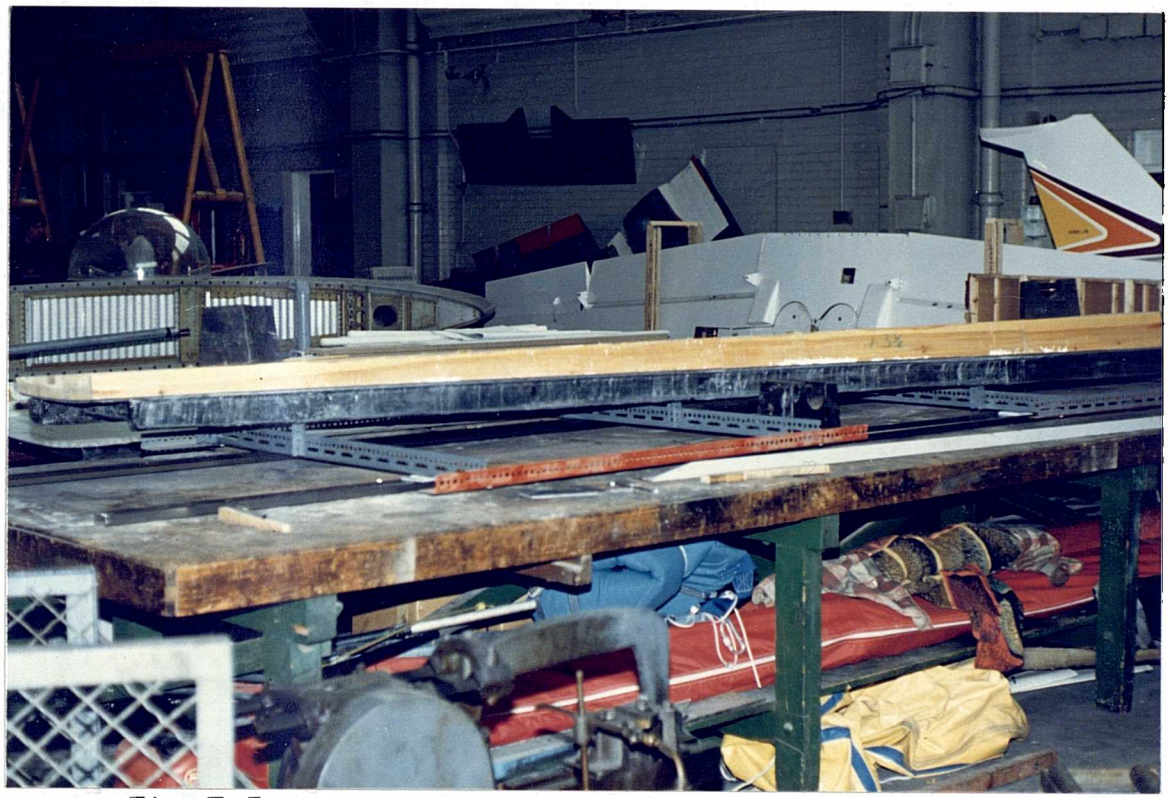

Fig 7.2.

The plies of prepreg were cut out using mylar patterns. Here, material for the rib flanges is being prepared.

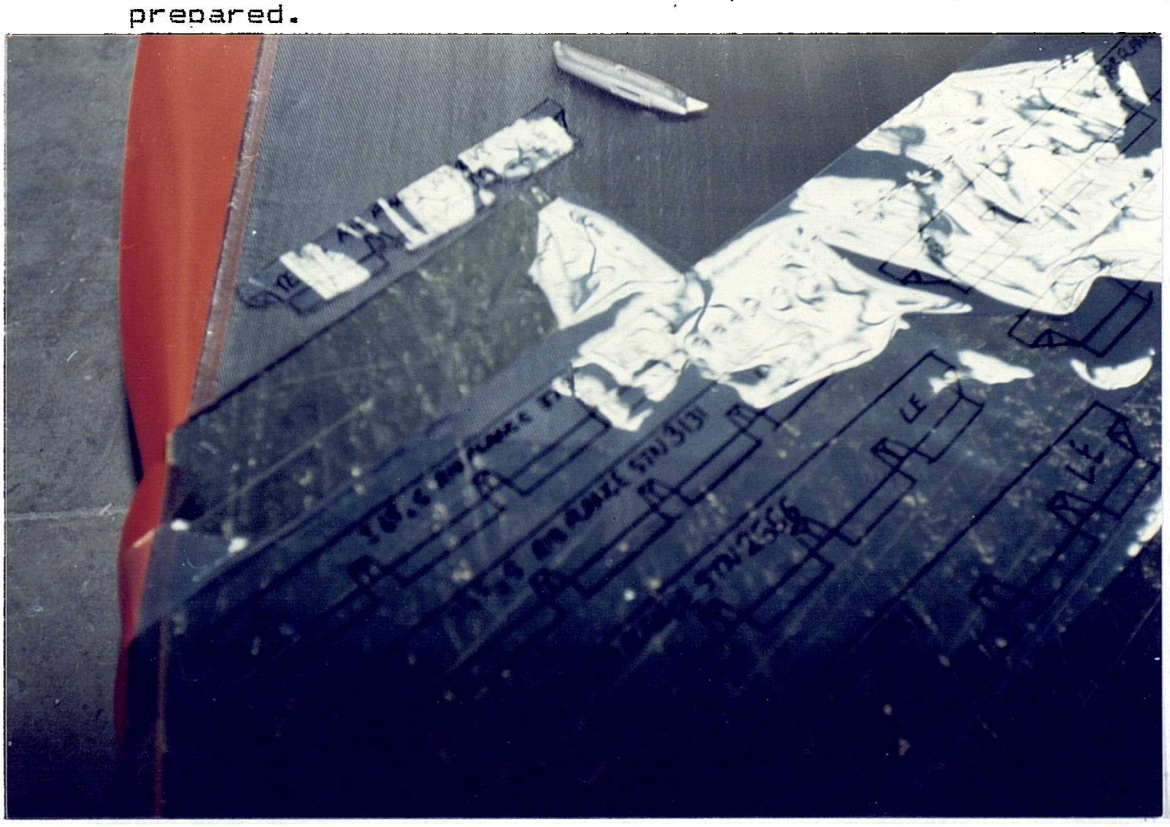

Figure 7.3

The complete kit of prepreg parts for constructing the wing box.

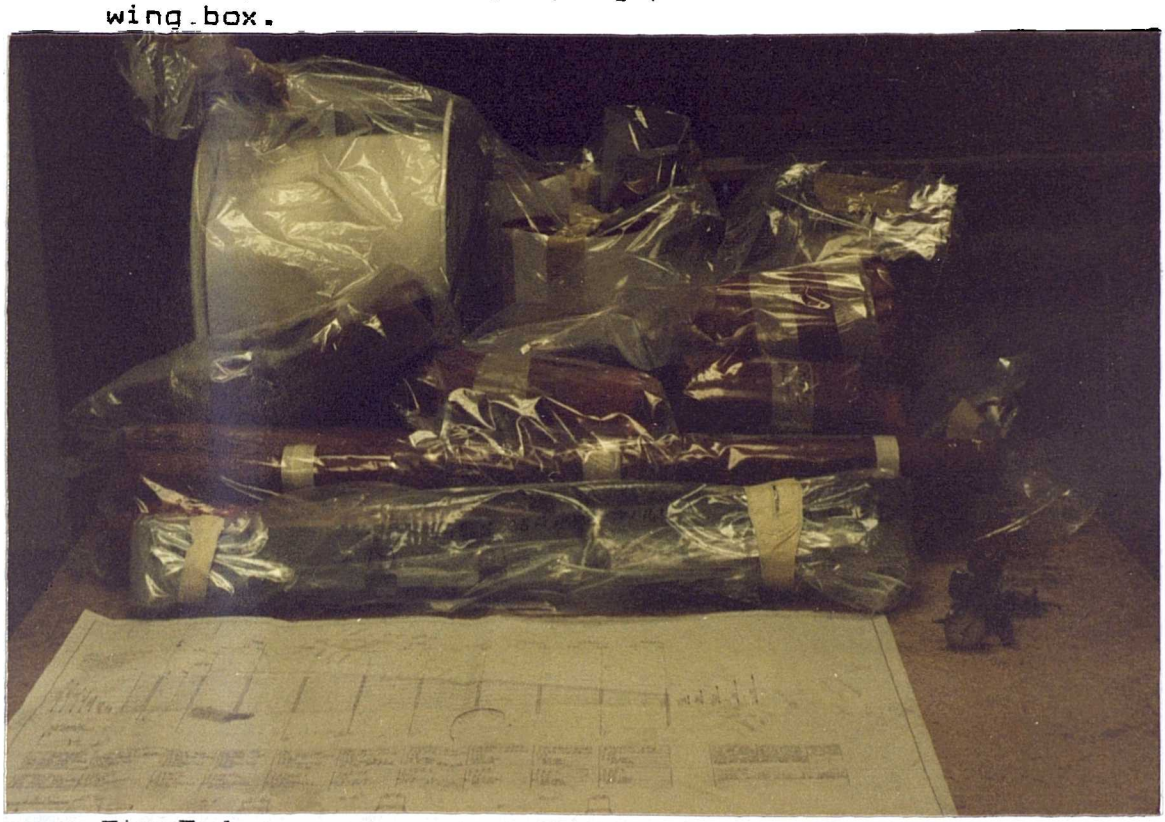

Fig 7.4.

The complete rib tooling and the stiffener cores were positioned upon the skin tool.

Figure 7.5

The junctions in the stiffener cores were joined and faired together with an epoxy/microballoon mix.

Fig 7.6.

A layer of non-porous PTFE release cloth was placed onto the tool surface to ensure an easy release.

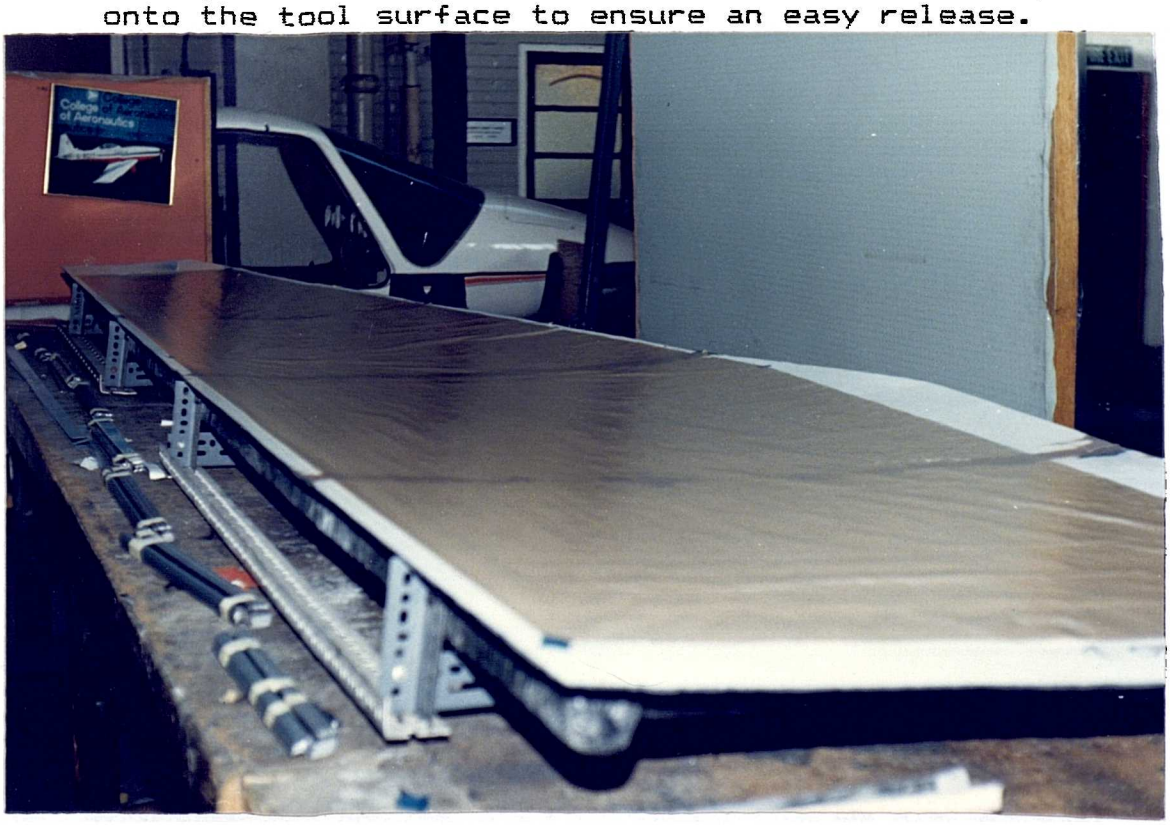

Figure 7.7

The first layer of +-45 woven carbon was rolled into position.

Fig. 7.8

The unidirectional skin plies are added to the layup.

Figure 7.9

The anti-peel strips for the stiffeners were set at the correct spacing by use of the rib tooling.

Fig 7.10.

The Rohacell stiffener cores were placed on the layup, followed by the stiffener caps of unidirectional CFRP.

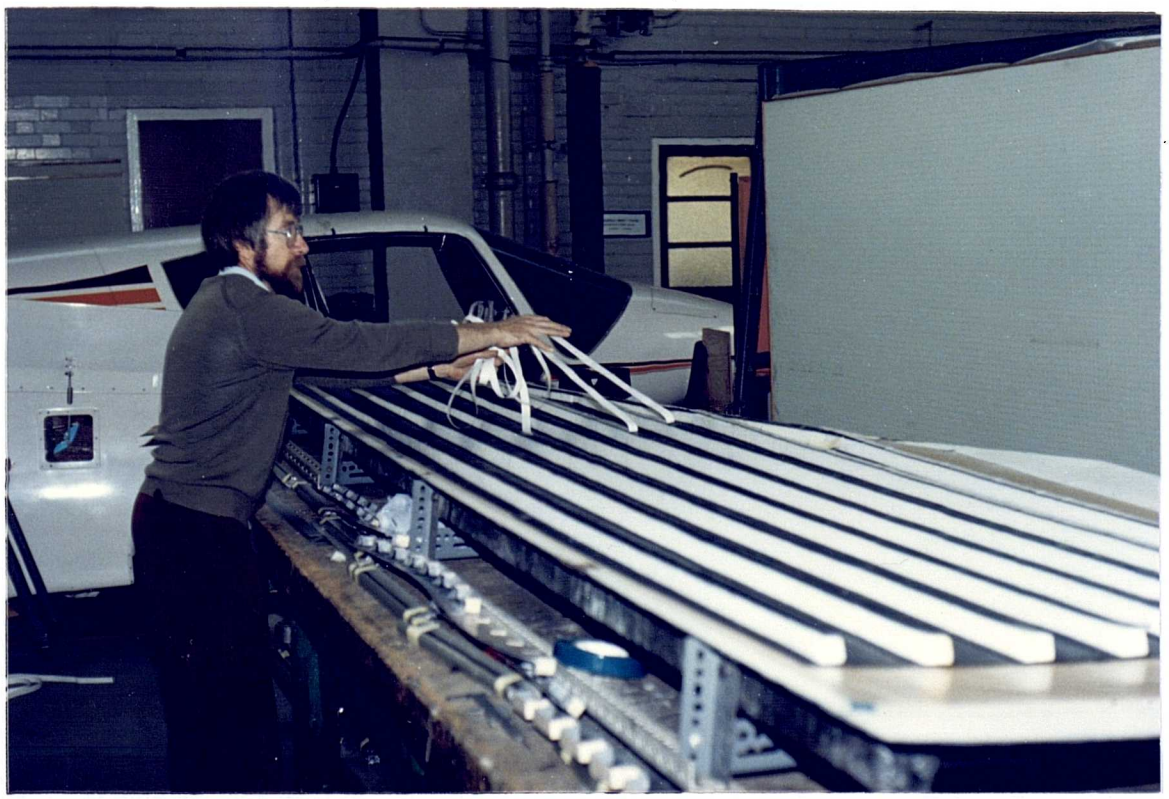

Figure 7.11

The inner skin plies of +-45 woven carbon were added.

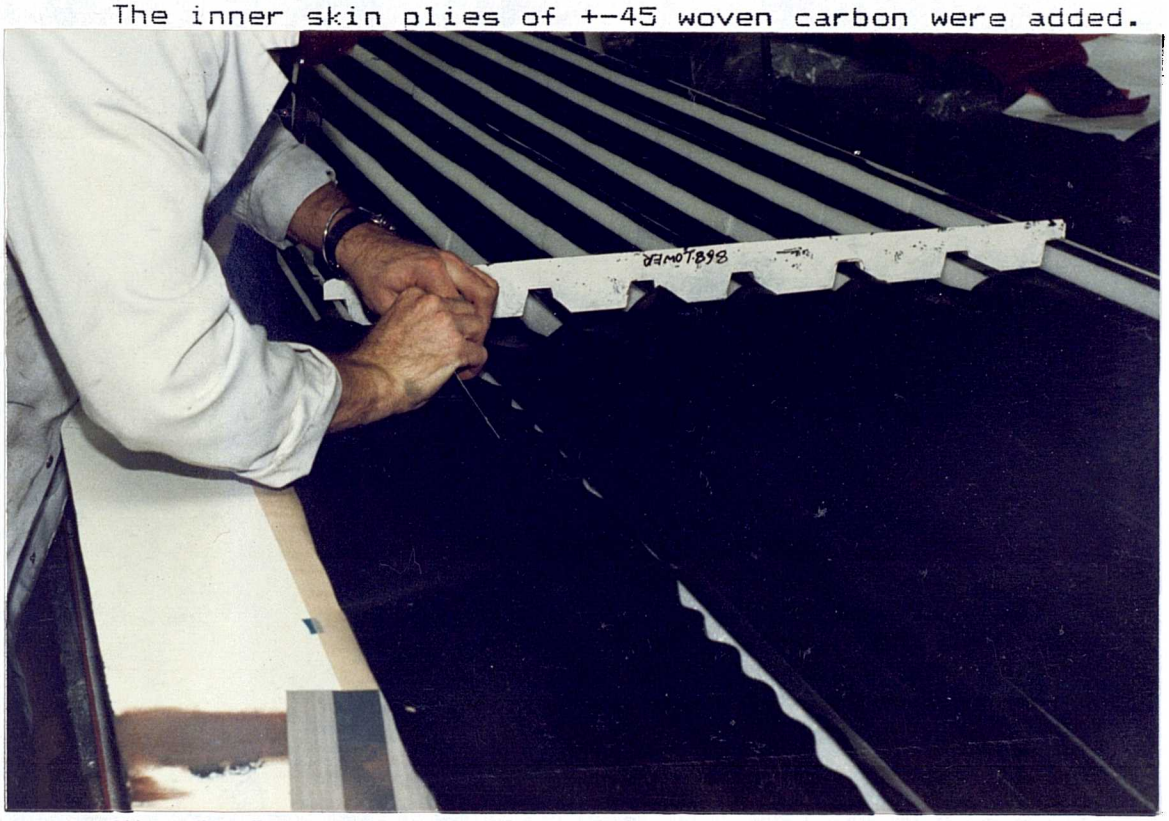

Fig 7.12.

Using two PTFE coated aluminium plates, the anti peel strips were folded into position.

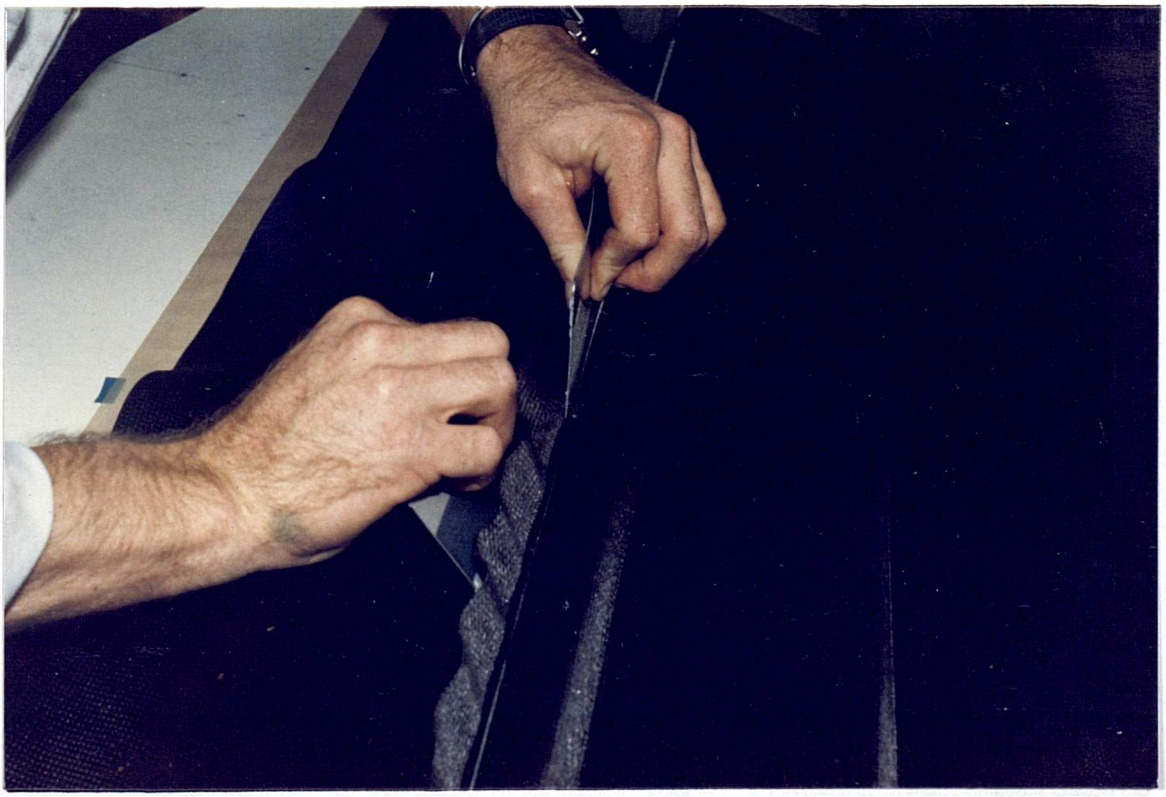

Figure 7.13

Kevlar threads were used to define the position of each rib.

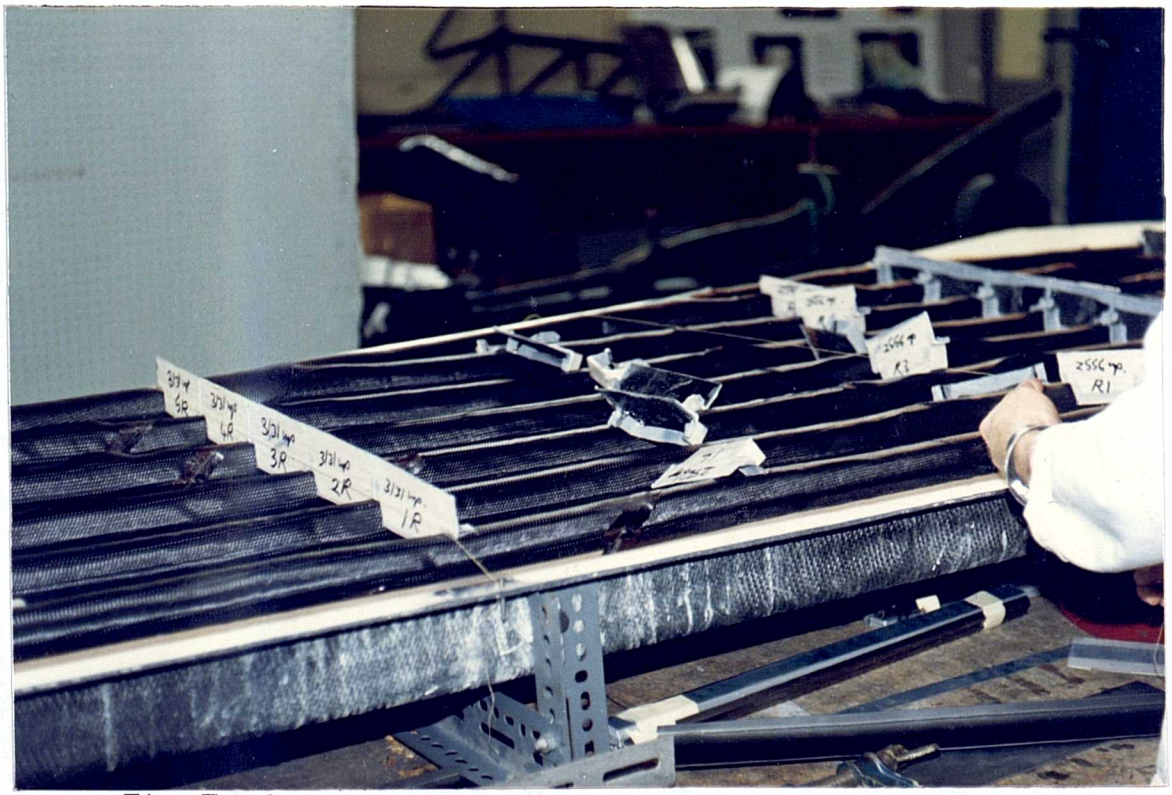

Fig 7.14.

One half of each rib flange laminate was laid down.

Figure 7.15.

The first half of the rib tool was removed to allow the second half of the laminate to be positioned.

Fig 7.16.

The rib tooling was replaced over the second half of the rib flange laminate to complete this lay-up.

Figure 7.17.

The folded steel segmented stiffener tooling system.

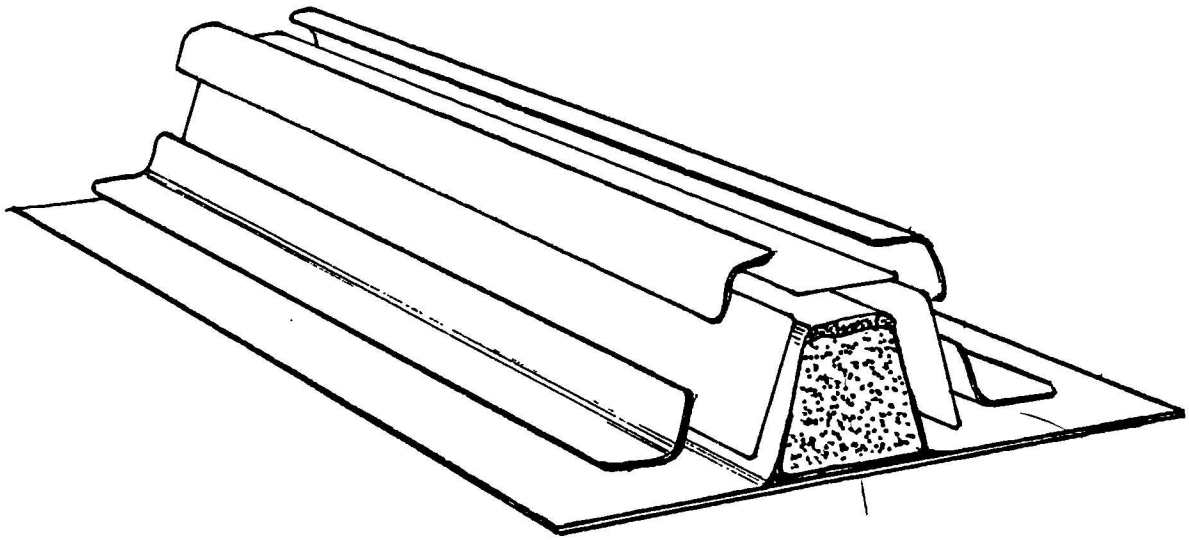

Fig 7.18.

The stiffeners were first covered in a non-porous release cloth.

Figure 7.19.

The tooling almost complete.

Fig 7.20.

The whole area was then covered with a breather cloth.

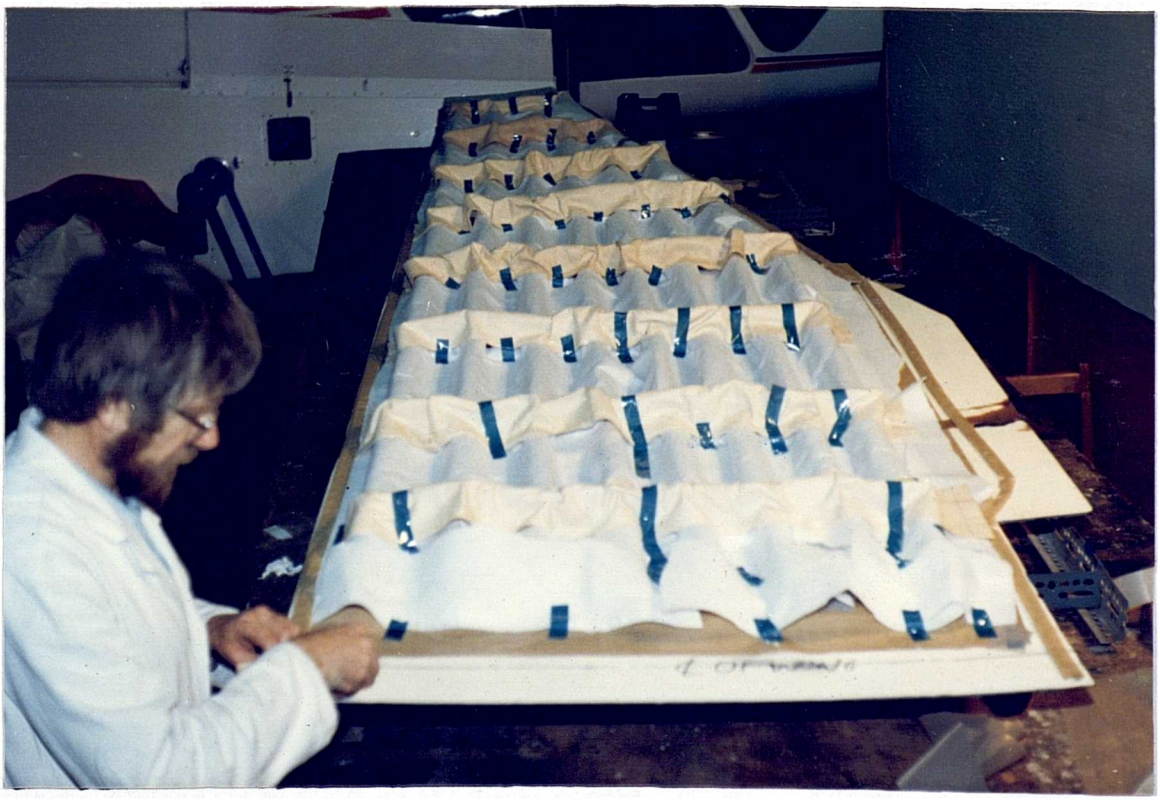

Figure 7.21.

The vacuum bag was attached with a mastic strip. Note the large folds near each rib.

Fig 7.22.

The bag was then evacuated and checked for leakage.

Figure 7.23.

The second co-cured skin shown being unwrapped from the tool.

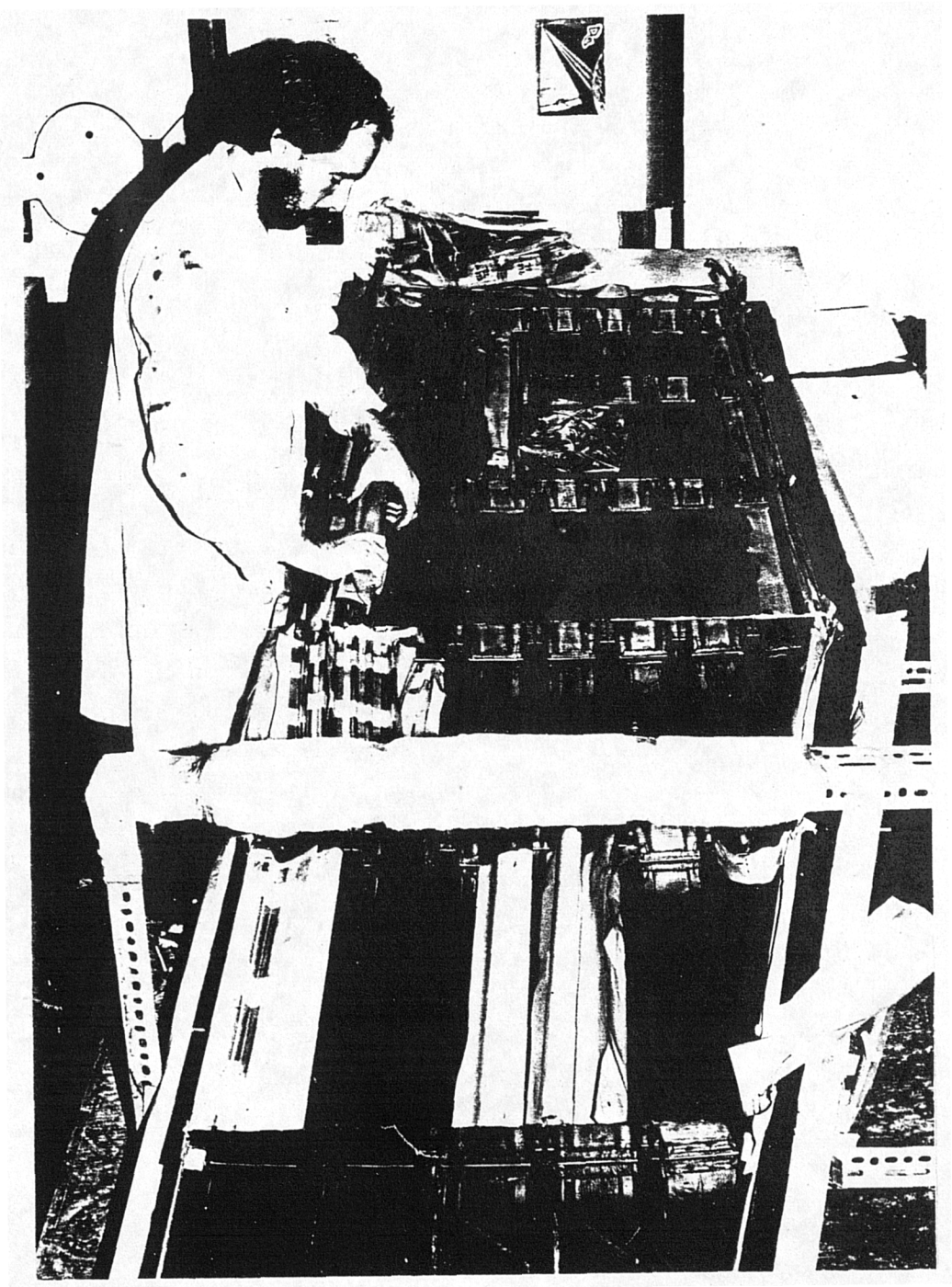

Figure 7.24.

Detail of a co-cured panel showing good surface finish and consolidation.

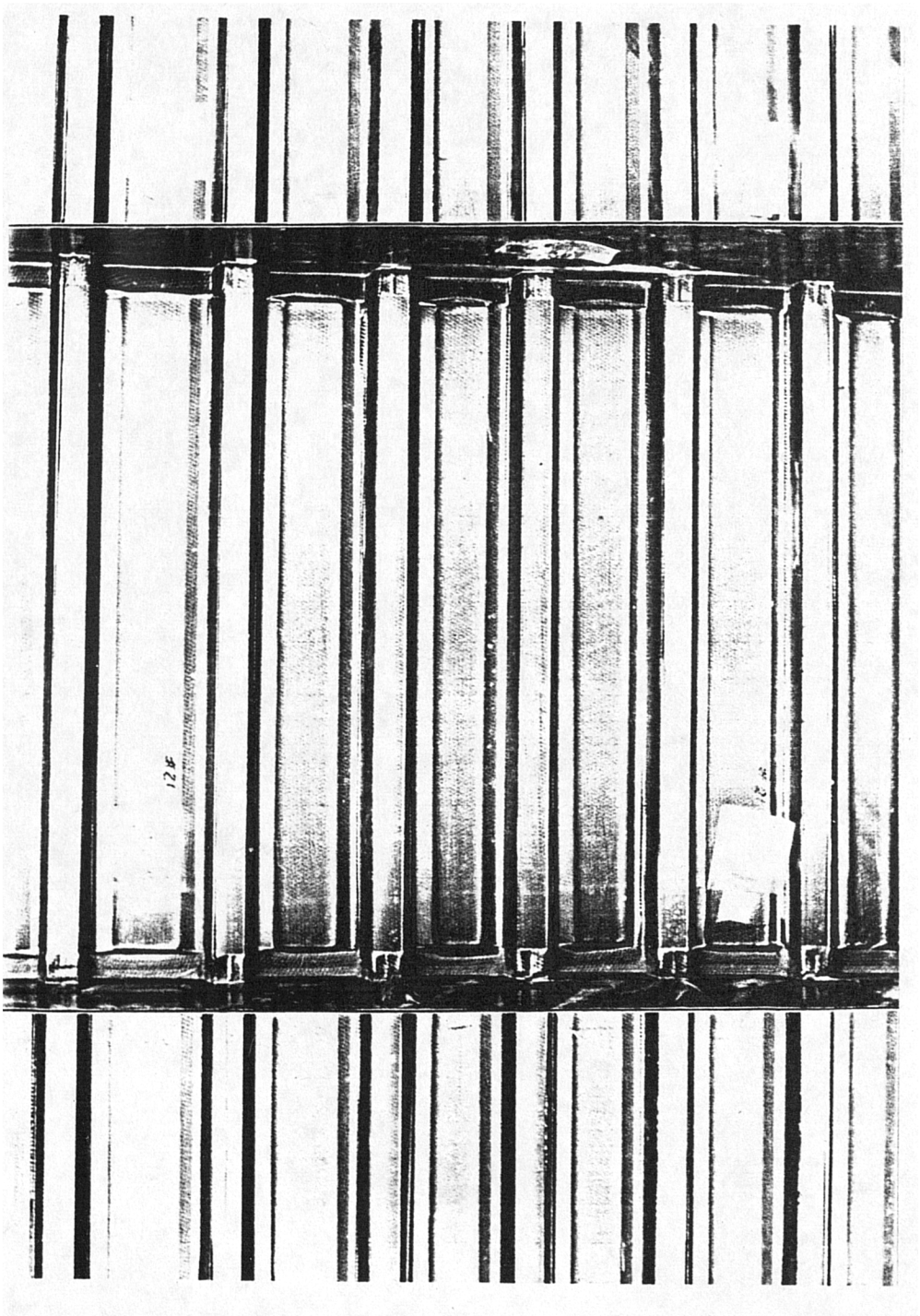

Figure 7.25.

Moulding defects in the skin above the stiffener run-out. This did not affect the strength of the structure.

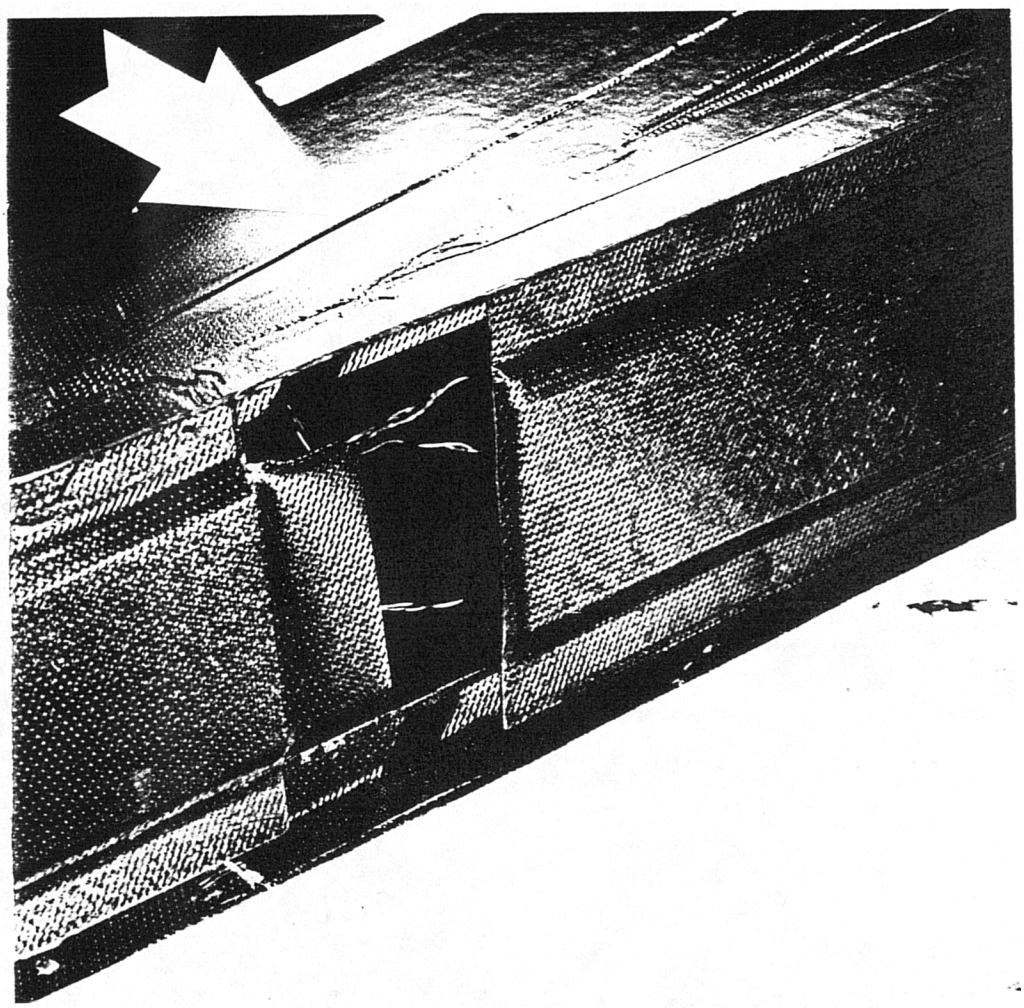

Figure 7.26.

A rib shear web in the course of construction. Note the vertical stiffeners with Rohacell cores.

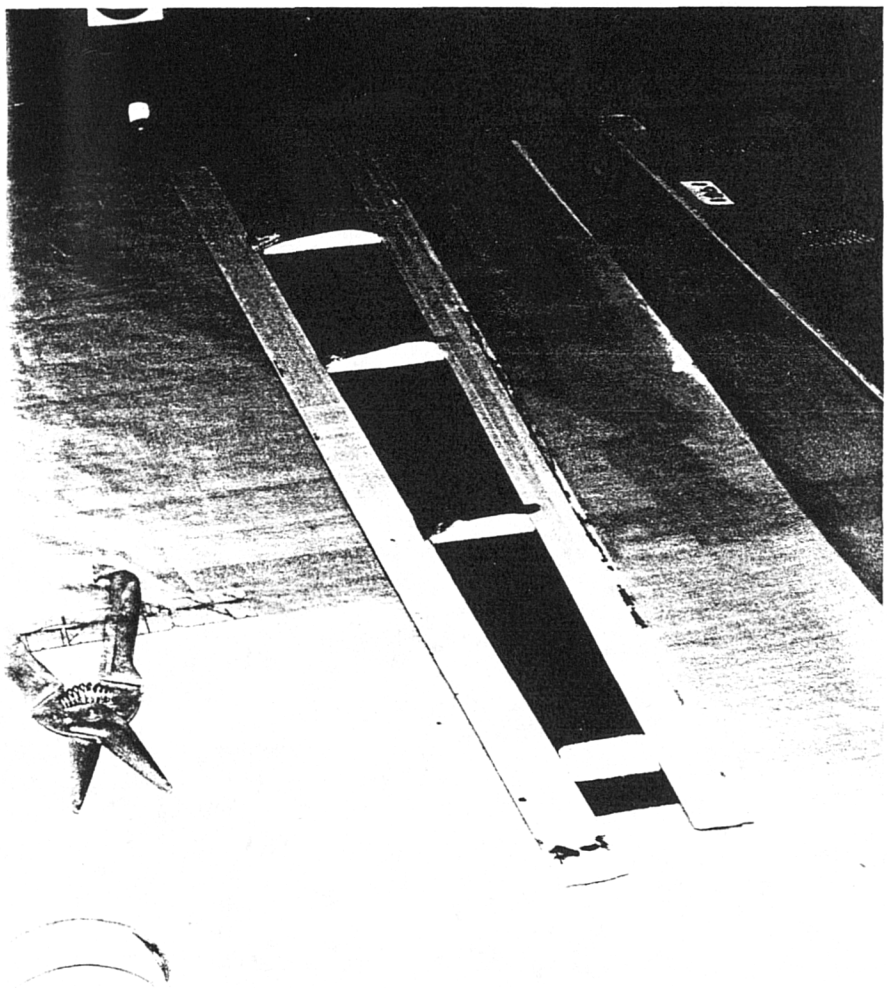

Figure 7.27.

Rib 3706 showing the sandwich panel construction for the aileron pick-up point. Note the unidirectional material at the top and bottom of the rib. The outer plies wrap around the whole sandwich core.

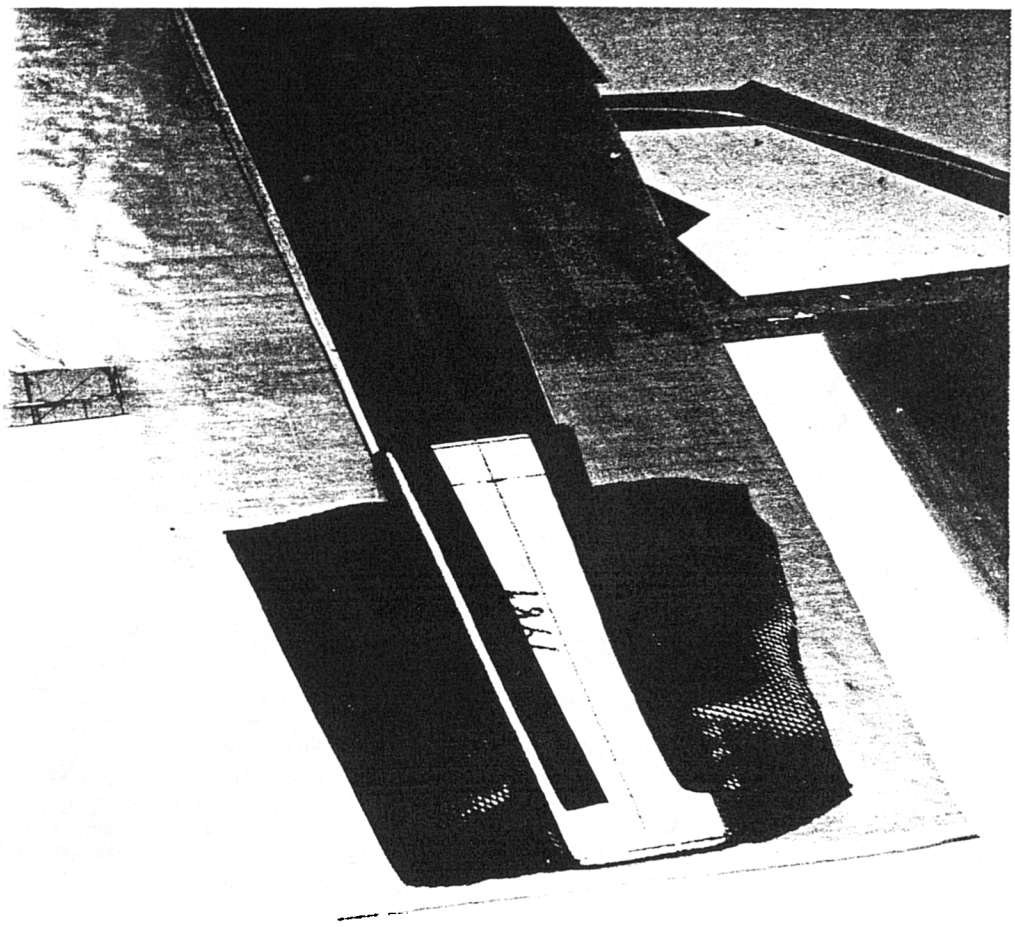

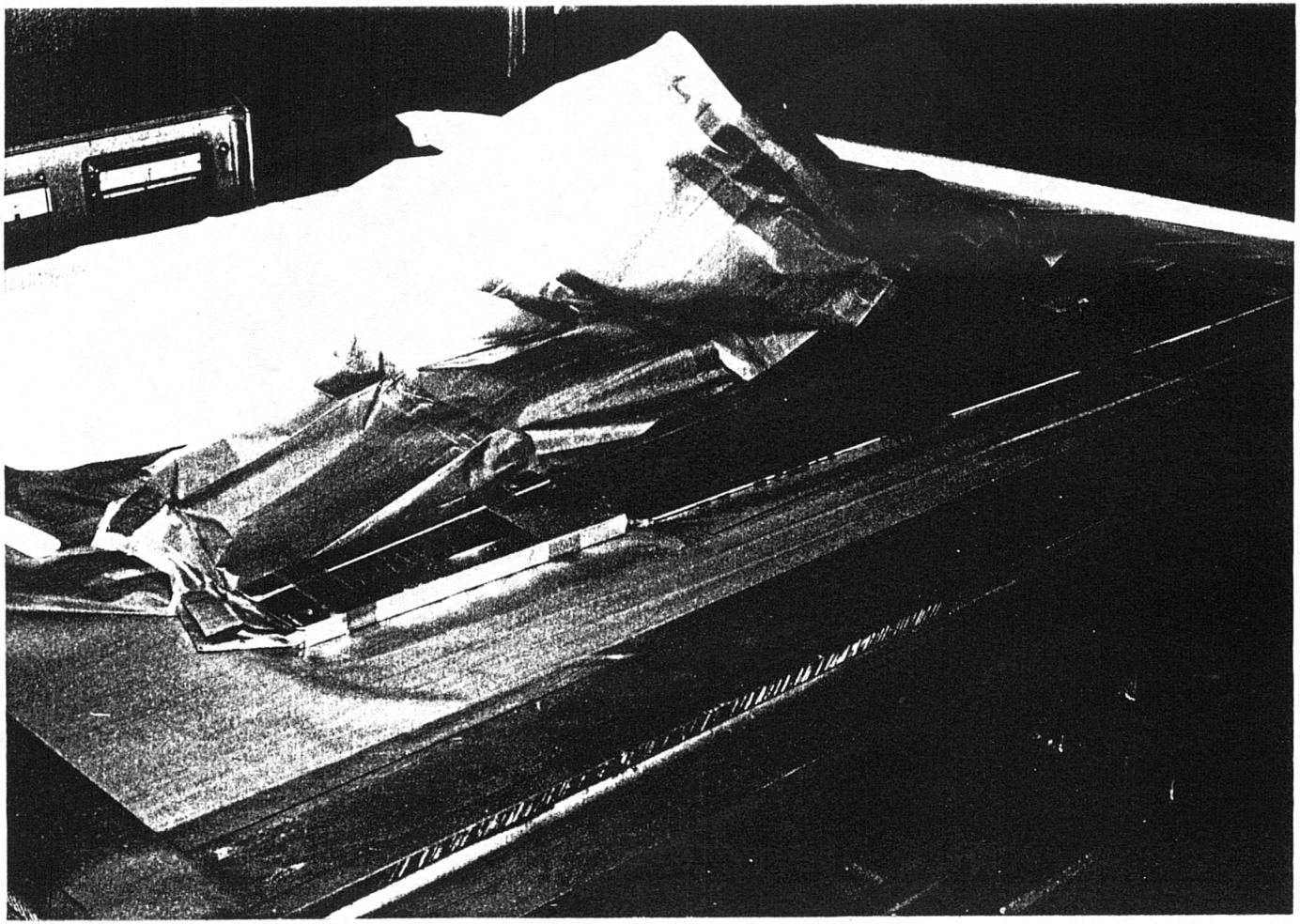

Figure 7.28.

The sheet aluminium tooling for the sandwich panel part of the rib is shown here.

Figure 7.29.

The bobbin used to distribute the load from the aileron to the rib was installed in the prepared hole. Araldite 2005 was used to bond it into position.

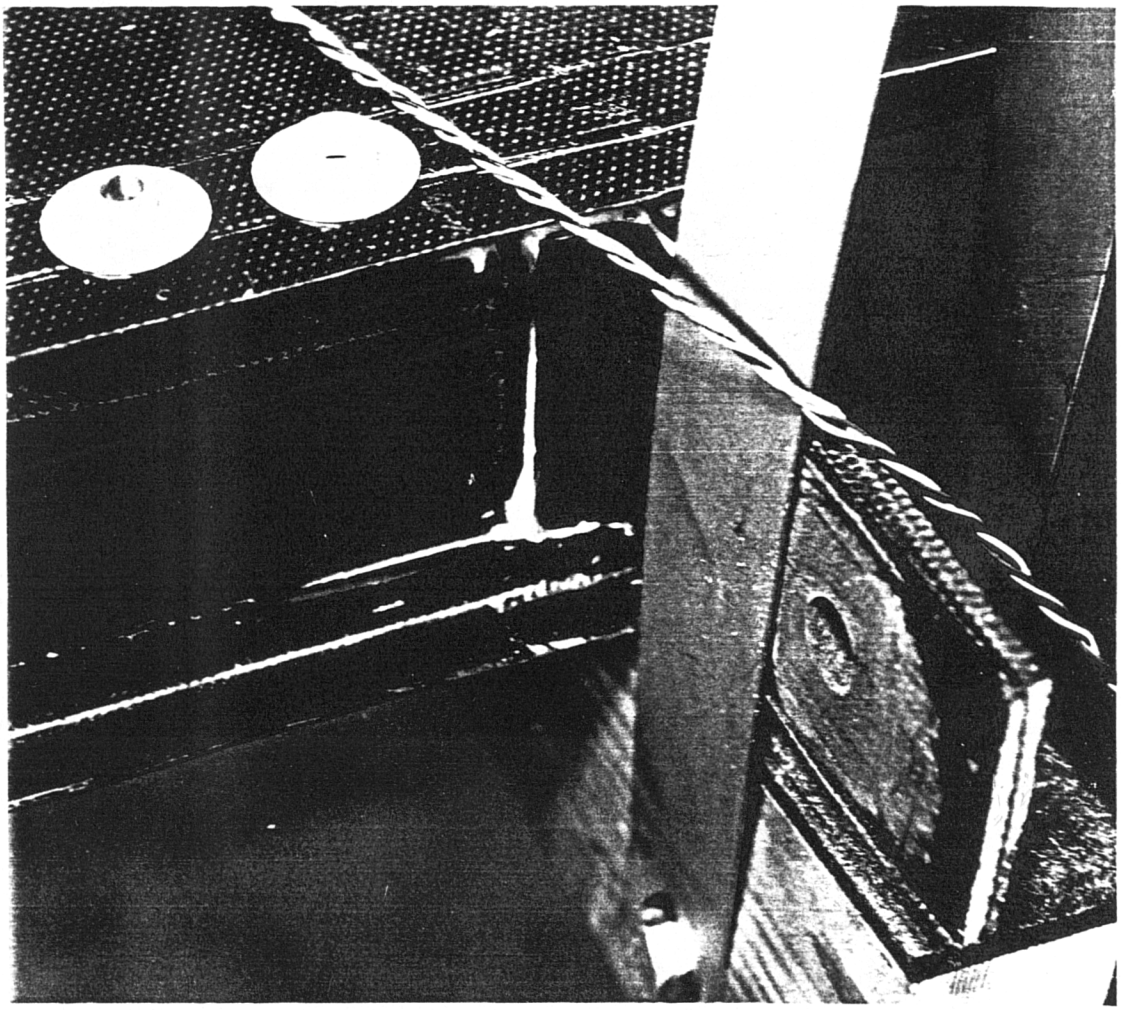

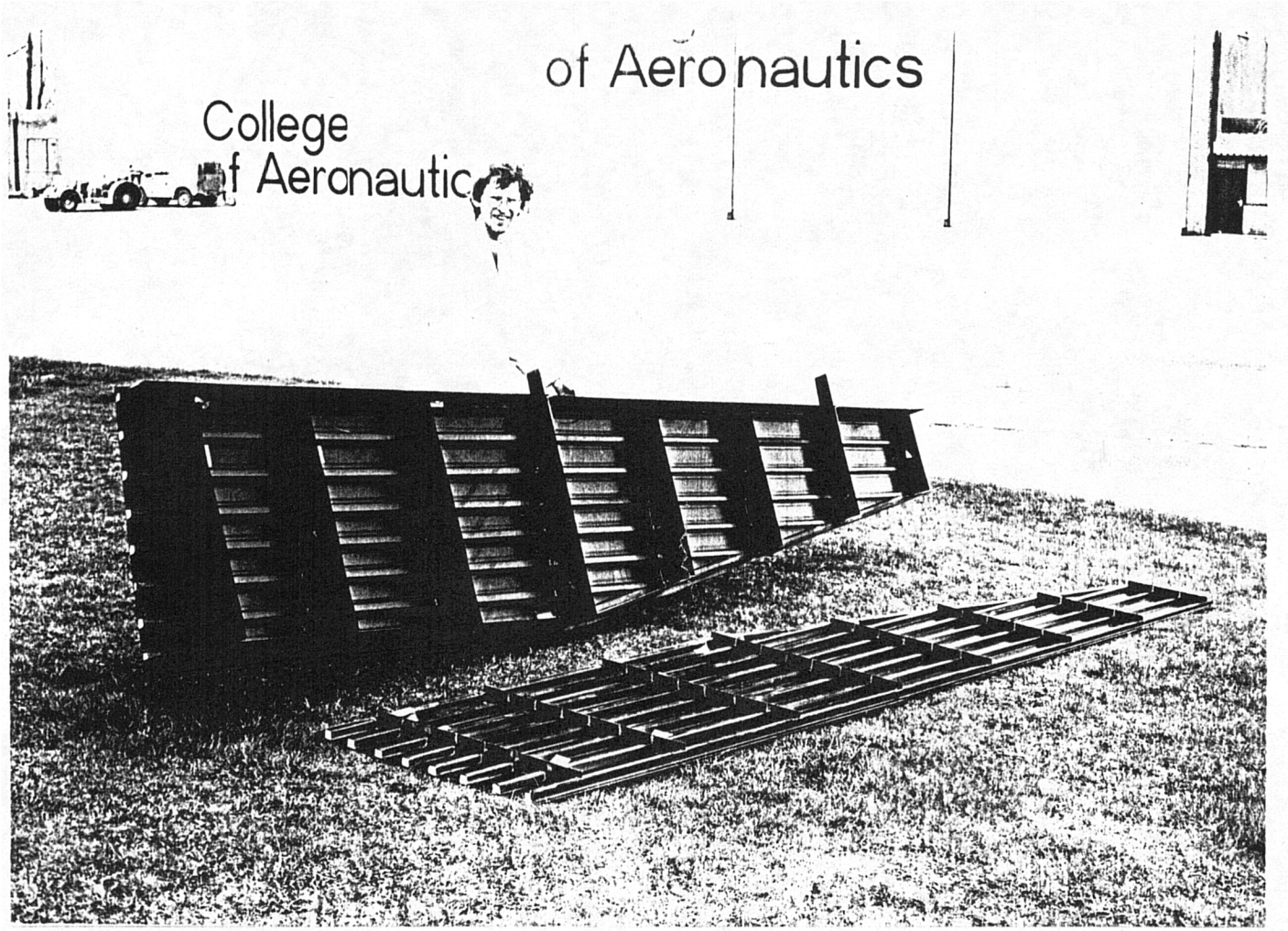

Figure 7.30.

The internal structure of the wing box.

Figure 7.31.

External view showing the good surface finish achieved. Note the two projecting aileron pick-up ribs.

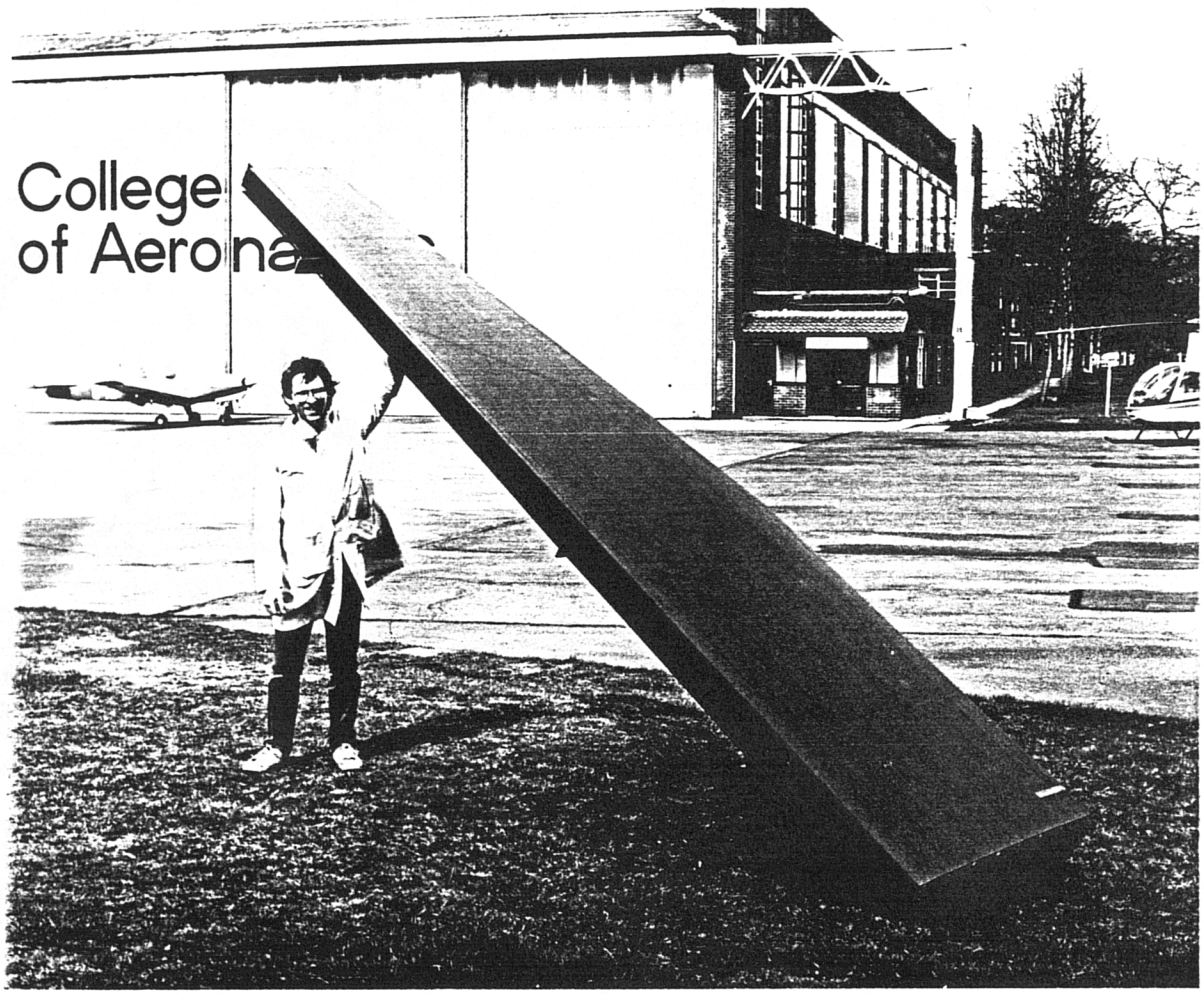

Figure 7.32.

The mainspar was cut into an angled shape to ensure good mechanical transfer of shear.

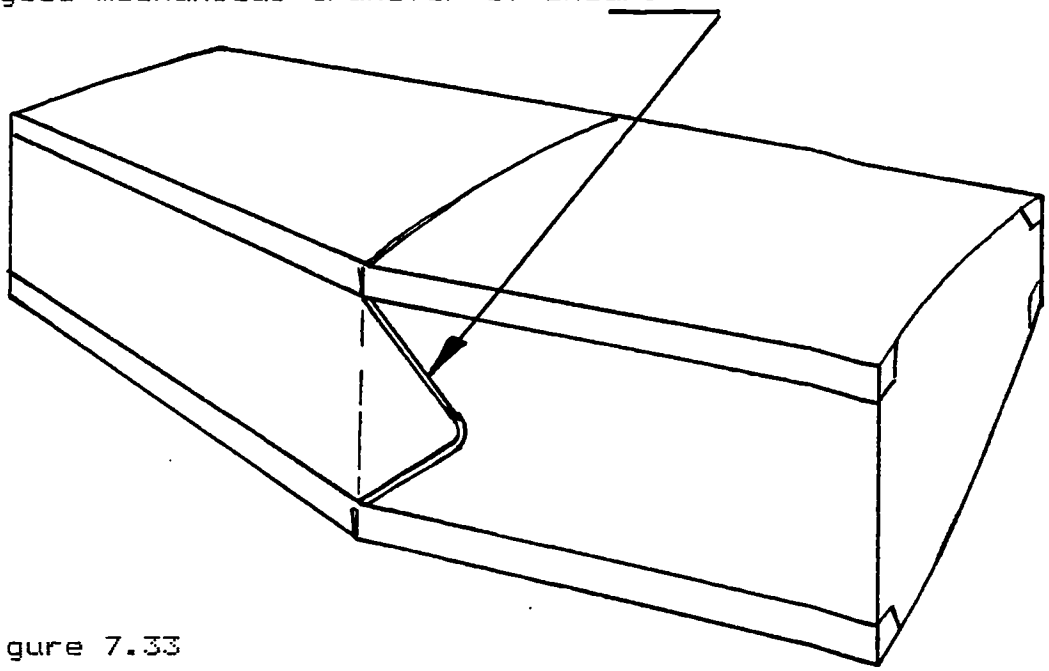

Figure 7.33

The ribs were slid into position from the leading edge.

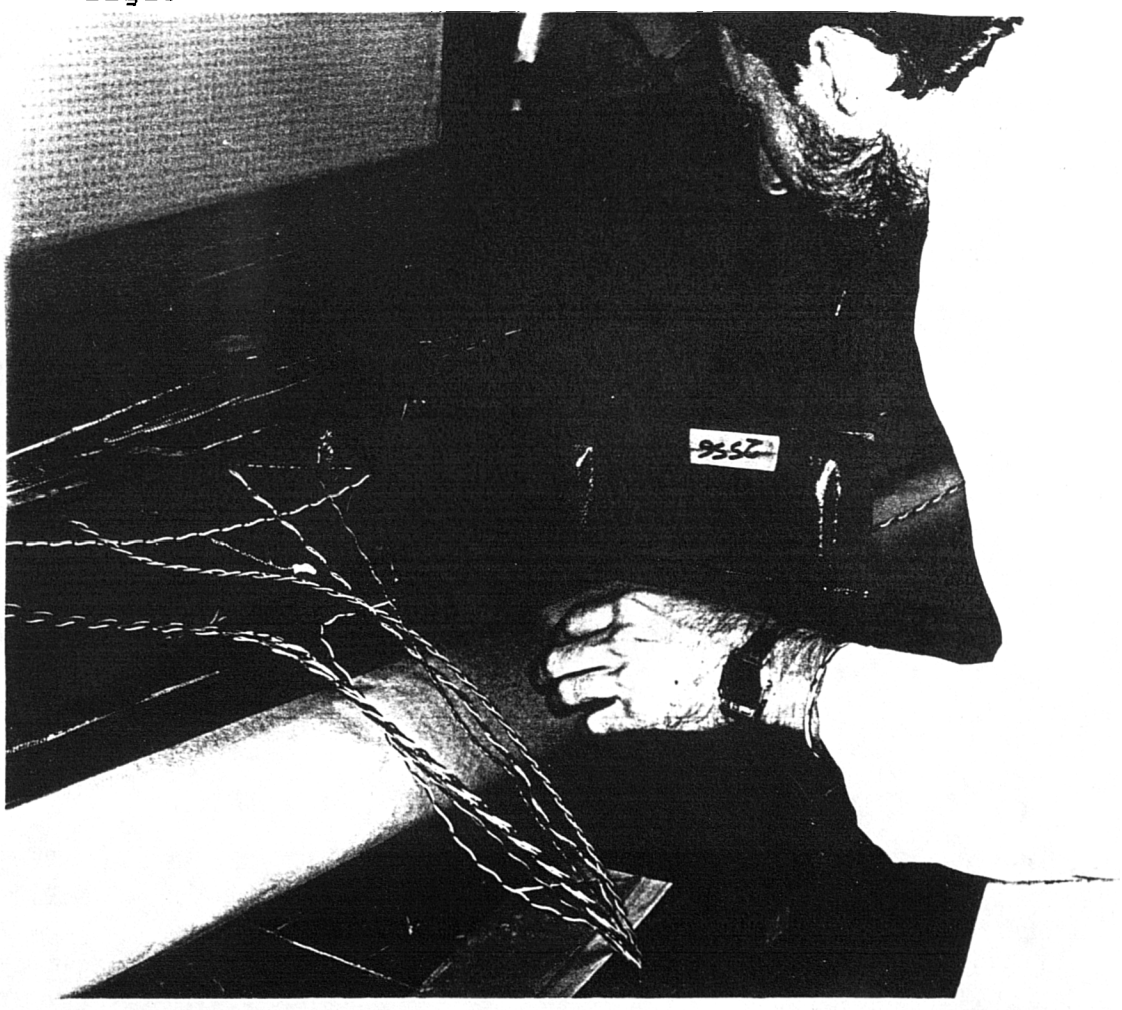

Figure 7.34.

After inspection of the joints, the mainspar was slid into position.

Figure 7.35.

The internal joints and strain gauges.

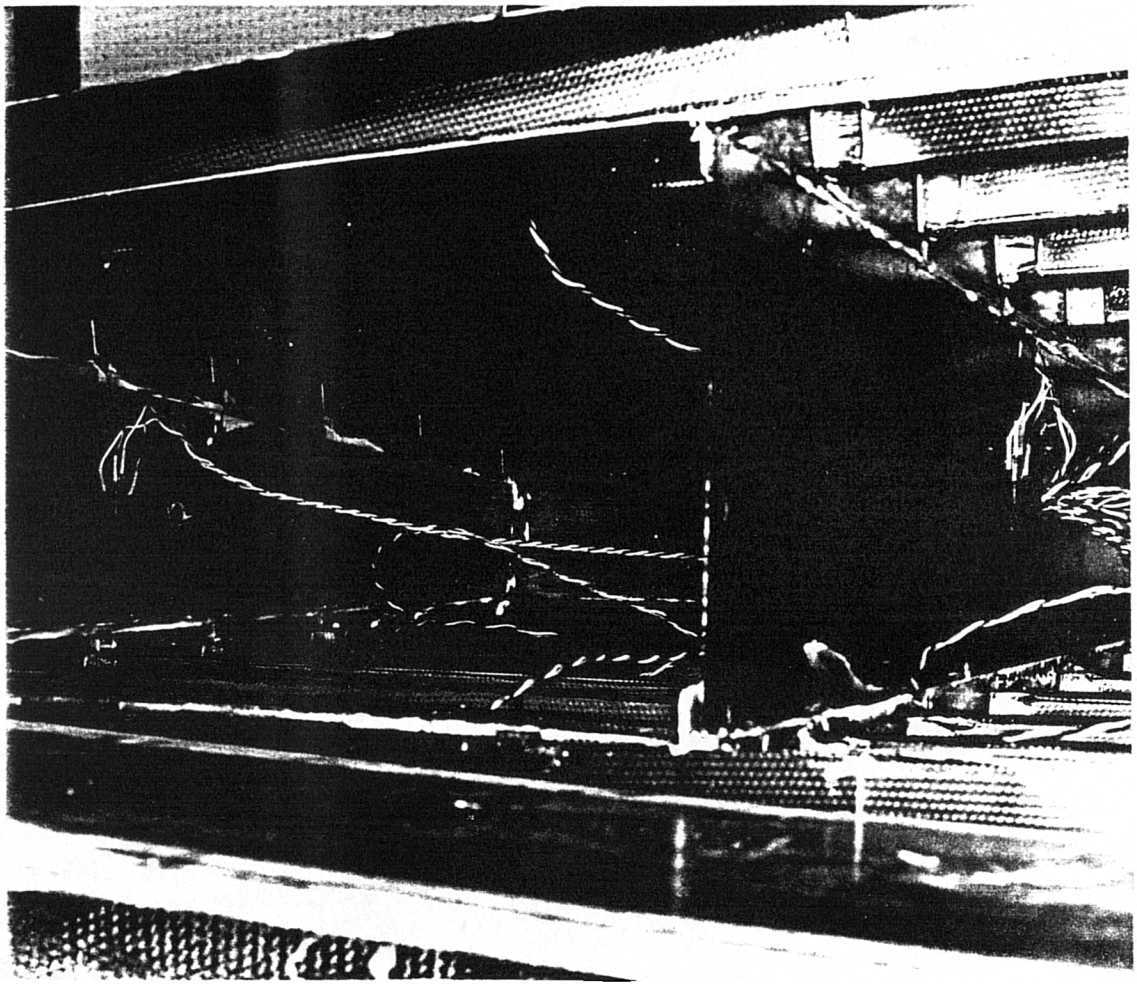

Chapter 8.
The CFRP wing box tooling.

8.1 Skin tool production methods.

Originally, the tooling for the wing box was to have been moulded directly from the existing A1 wing. However, this would necessitate removal of the wing for moulding of the undersurface. The tool would also have to be resurfaced by hand to remove the rivet head impressions. It became obvious that it was quicker to construct a wooden mockup on which to mould the skin tools.

The choice of using CFRP as a tooling material was due to the matching expansion characteristics and high stiffness. It is possible that woven GRP could have been used, with a considerable cost saving. Expansion against the tool could have been taken up by float on a suitable release film. However, more material would have been required to obtain the desired rigidity.

8.2. The resin system used to produce the tooling.

The tooling itself was moulded from a high temperature wet layup epoxy resin with woven carbon fibre reinforcement. The resin system was Structural Polymers SP 690 gel coat and SP 590 laminating resin. This system, when cured at room temperature, has a similar heat deflection temperature (HDT) to that of most epoxy resins at 80°C. This is the temperature at which the resin will creep under load. However, when the resin is post-cured by progressive heating to 130° C over five hours, further cross-linking of the polymer takes place. By this process the HDT is raised to the same level. At this slow rate of heating, the HDT always stays above the ambient oven temperature.

Once post-cured, the tooling is suitable for autoclave curing of prepreg components at up to 120° C. This was one of the major reasons for choosing a low temperature curing prepreg for the final structure such as Ciba Geigy 913. By using the post-curing technique with a special resin, the production of the tooling is greatly simplified. Normally, prepreg tooling has to be produced at much greater cost.

8.3. Mockup construction.

Using the author's wing coordinates program, full scale plots of the wing ribs were produced. These were drawn on the College of Aeronautics' large Benson plotter. Plots were checked for accuracy and found to be better than +-0.1% in both axes. They were then used directly as cutting templates for the blockboard ribs.

The mockup was completed with leading and trailing edge sections and stringers to maintain the profile between the ribs. A sized hardboard material was used for skinning. This had sufficient thickness to give a smooth contour between each stiffener. The mockup was produced in four sections which were bolted together for ease of construction and transport. Since the wing section of the Cranfield A1 is very nearly symmetrical over the chord of the main structure box, it was decided to produce the tooling with a symmetrical section. This allows the tooling to be used to produce a complete span if ever the opportunity should arise.

The tooling incorporates enough chord to enable integral undercarriage mountings to be built into the wing skins if desired. The tool, which is shown in the drawings, has a 90mm margin around the component to allow room for vacuum bagging.

Before moulding, the finished mockup was aligned on a table using spirit levels. No washout was incorporated, so that a complete span could be built on this tooling if desired. It was given four coats of release wax. This was tested and found to give an easy release of the moulding with an acceptable surface finish.

8.4. Moulding the CFRP tooling.

A gel coat was applied to the surface using a 30cm wide wool roller. The coating was brushed out to remove air holes. This part of the operation had to be finished within 30 minutes to avoid an exothermic reaction of the resin in the application roller. A period of three hours was then required to allow the gel coat to cure to a light tack before continuing further.

A kit of woven material was previously cut out, with the fibre orientation at 0/90° to the rear spar axis. The laminate was formed of two different weights

of reinforcement. In order to provide a fine surface texture, two layers of 200 g/m↑2 material were applied to the gel coat surface. This was followed by four layers of 400g/m↑2 . A further two layers of 200g/m↑2 served to form a balanced, symmetrical laminate. The resulting thickness was 6mm. From experience with testbox 2, this was found to be sufficient to maintain the correct skin contours.

Each woven layer of the tool laminate was wrapped around a large cardboard tube. The tool surface was then wetted with resin by means of a wool roller. The layer could then be unrolled from the tube onto the surface. By this process, distortion of the weave was avoided. A serrated 30cm long aluminium roller was used to consolidate the resin into each ply.

The completed laminate was finished by using a squeegee to remove excess resin from the surface. The wet layup skin plies took three people four hours to finish. Resin was mixed in 1.3 kg batches using a food mixer. If the resin was distributed in trays to a depth of less than 2cm and used immediately, no problems occurred with exothermic reaction of the resin.

After the basic tooling skin had been allowed to cure overnight, a stiffening structure was added to the outside face. This structure was formed by laying two spanwise lengths of 100mmx50mm section softwood onto the tool. The wooden stiffeners were placed along the leading and trailing edge spar positions. The stiffeners had a 10mm radius along each top corner, which allowed a wet laminate to follow the profile. After liberally coating the wood with resin, three plies of the 400g/m↑2 woven carbon were applied.

Ten chordwise chipboard stiffeners were also placed onto the surface at the actual rib stations. These were laminated into position with one layer of each type of reinforcement.

Following a room temperature cure over three days, the tool was released from the mockup. This was accomplished by inverting the tool and then removing the mockup by unbolting each section in turn. The tool was trimmed with a portable grinder fitted with a diamond edged cutting disc. The flashing at the junctions of the mockup sections was removed, leaving the tool ready for post-curing and subsequent use. The cost of the two skin tools in materials was £5000 in early 1986. The use of wood in the tooling was considered to constitute a negligible fire risk. However, several firms approached for autoclave

facilities refused to allow the use of wood. This should be borne in mind for future projects.

8.5. Tooling for the rib flanges.

By using composite materials, complex forms can be produced quite easily. In order to produce a co-cured rib flange, a dummy rib was set onto the face of the tool at the desired rib station. The dummy rib was also fitted with dummy stiffeners as in fig 8.1. A wax release agent was then applied to the area. A wet layup CFRP moulding was then formed on each side of the rib. In order to obtain sharp corners to the mouldings, the first layer is a very resin-rich layer of glass fibre finishing tissue. The tissue is followed by the woven CFRP reinforcements.

The rib tooling components were then cut into segments at the centreline of the stiffeners. Splitting up the rib flange tooling allowed for some variation in the stiffener cross section. Each segment was trimmed to size and then covered in a PTFE tape. The tape gave an easy release from the prepreg component after curing.

8.6. Tooling for the rib and spar shear webs.

The rib webs and spars are very simple, being flat plates or sandwich panels. They can be produced on any flat surface. The rib webs have a slot incorporated in the edges for joining to the rib flanges. This involved inserting a PTFE coated steel strip into the edge of the layup, as in fig 8.2.

Figure 8.1

Rib flange tooling. This is produced by placing a dummy rib and stiffener upon the skin tool surface. The CFRP tool is then produced by laminating around this dummy rib. The tool is cut into segments at the apex of each stiffener. One of these segments is shown here.

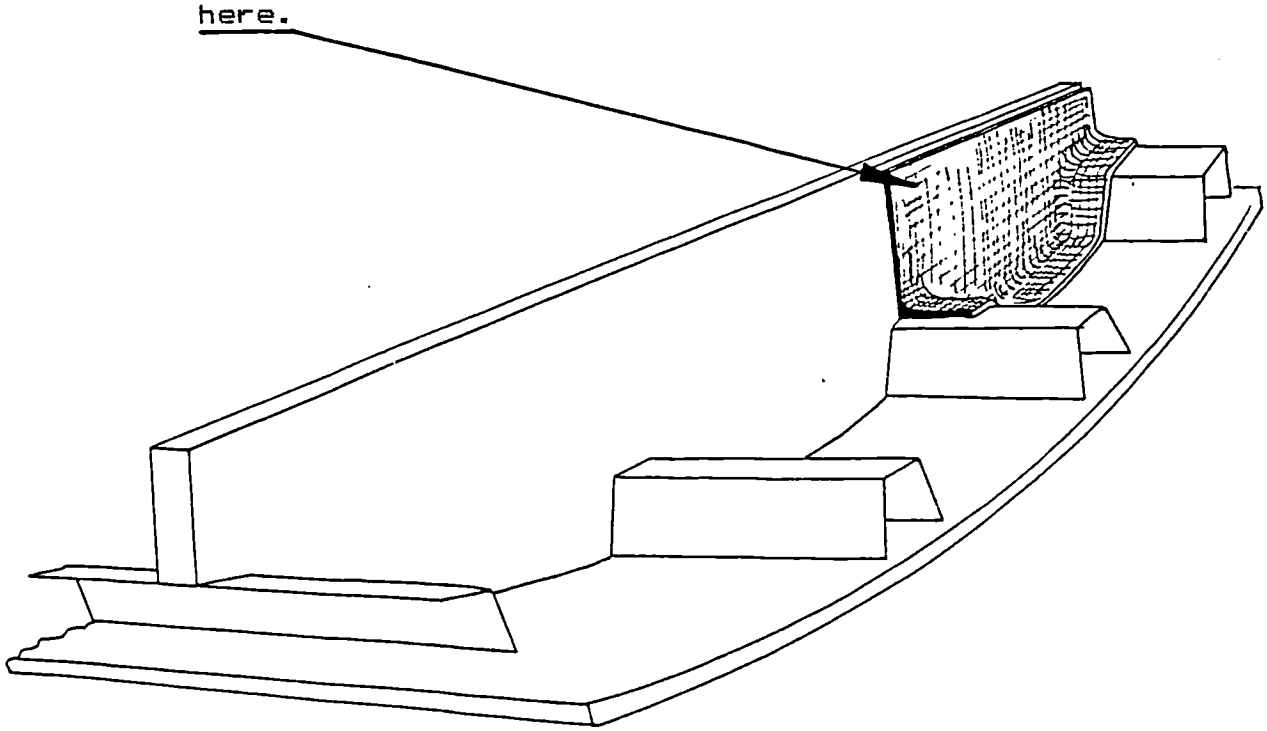

Figure 8.2.

The slots for joining components together are formed by means of a PTFE coated steel strip. It is removed after curing.

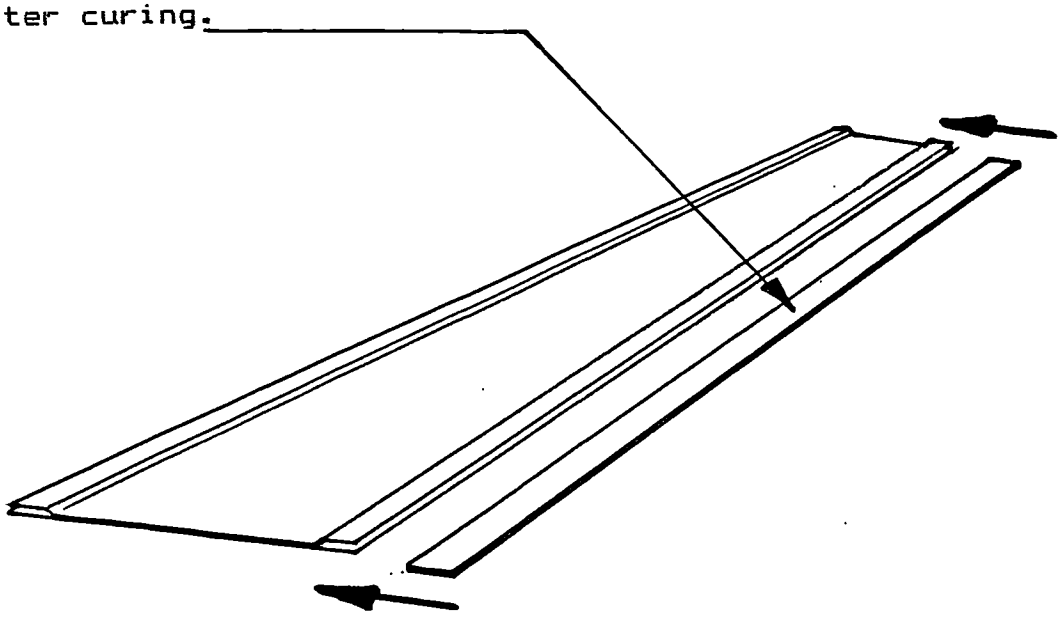

Chapter 9.
Methods of testing including non-destructive testing.

9.1. Structural Testing Methods.

The first box constructed was tested as a three point beam (fig. 9.1). Loading was applied by a turnbuckle to the contour board at the mid span of the box. This is possibly the easiest method of subjecting a box to bending, as no end fittings are required.

Twice the load and twice the length of structure is required to generate the same maximum bending moment as for a cantilever beam. For this reason, in order to induce the desired direct loading in the compression skin of the first box, a very high shear loading was required. This was not representative of the actual wing load case.

To solve this problem the second box, with skins representative of the wing root, was tested as a cantilever. Two basic multipurpose rigs exist at Cranfield. Each comprises a massive block from which two large and very stiff 'I' beams project at the base. A test box can be bolted rigidly to the block, and the load applied via the beams.

The problem of root attachment was solved by constructing a carbon and glass fibre root flange. The method of producing it is shown in fig. 9.2.

The area required for the bond formed between the box and the flange laminate was calculated on the basis of work by Webber & Murphy (39). Here, the technique of laminating glass/epoxy directly onto cured glass/epoxy was evaluated for the repair of sailplane spars. The resulting adhesion shear strength was significant but inferior to that of a purpose-designed adhesive on a ready-cured laminate. A conservative value of 5 MPA was assumed, and the required surface area calculated. The thickness of the flange laminate was tapered to avoid a large stiffness change between the box skin and the end of the flange. This avoided the problem of large stress concentrations in the bond causing premature failure here. Simple stressing calculations were used to determine the number and type of bolts required, and the thickness of the flange required at the bend.

In the case of test box 2, the load was applied by two hydraulic rams with dynamometers in tension. The load was taken into the box using a loading plate of glass/epoxy. The loading plate was made in the same

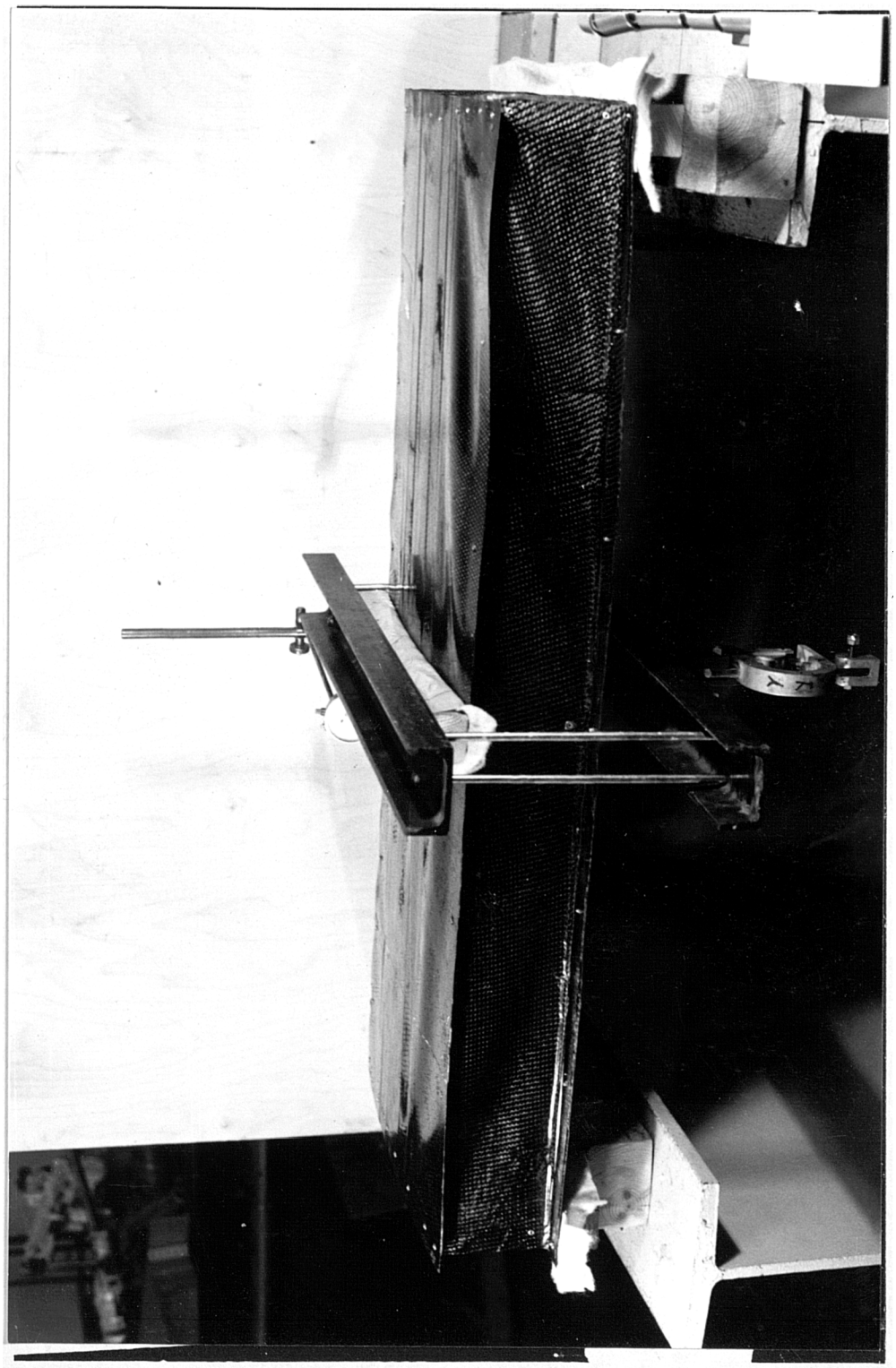

Figure 9.1

The first test box was loaded as a three point beam.

Figure 9.2

The box is placed onto a PTFE coated, flat surface. The flange is laminated into place.

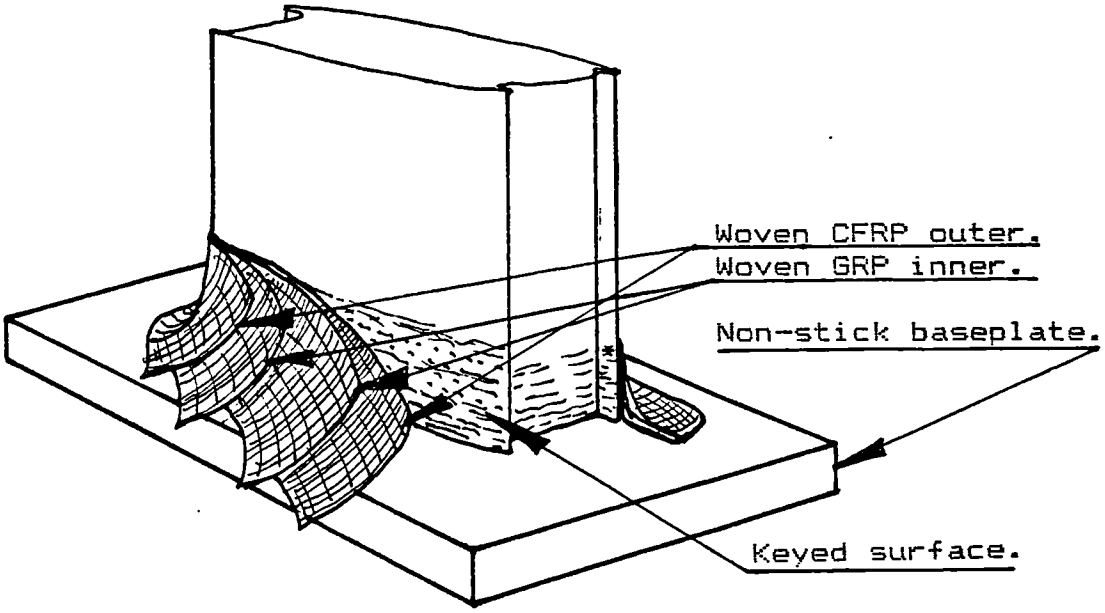

Figure 9.3.

The load was transmitted into test box 2 by means of this loading plate.

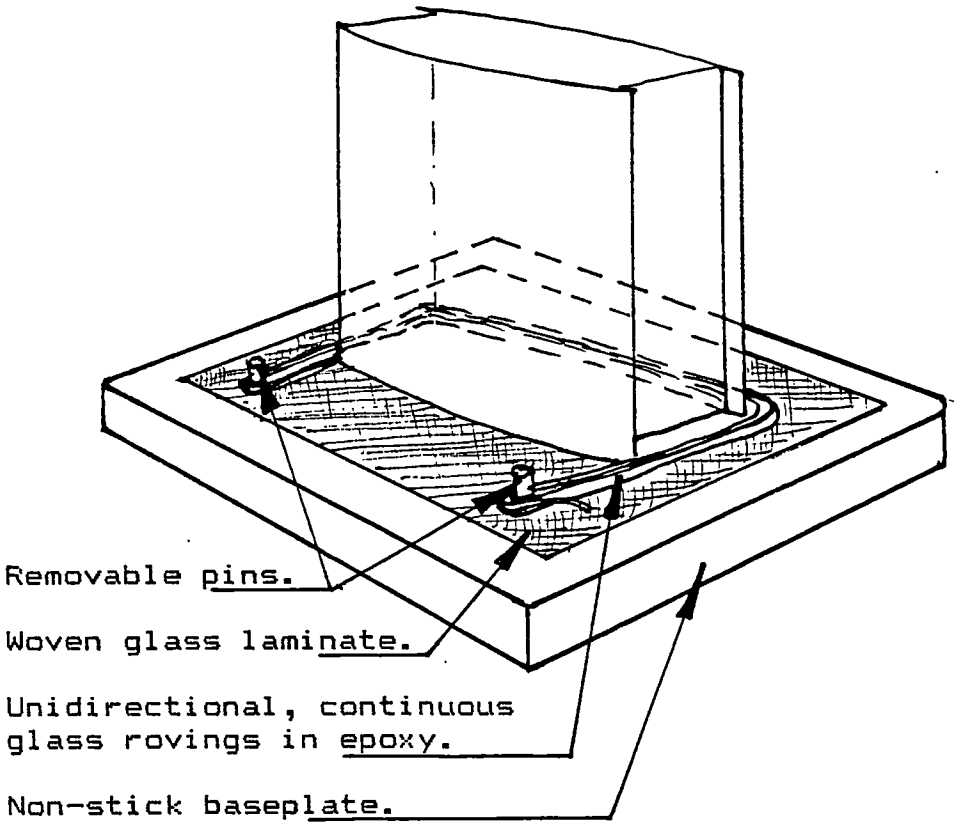

manner as the flange. However, the baseplate incorporated pins in the loading locations. Unidirectional glass/epoxy tows were then wrapped around the box and the pins, as seen in fig 9.3. After cure, the pins were removed and bolts with shackles attached to transmit load from the rams.

These means of attaching the box to the rig were very successful. With no bolted joints in the connection from box to flange, a smooth transfer of load resulted. The strains measured across the width of the box were quite uniform. The design ultimate load for the box was achieved without any failure of the flange or loading plate.

One significant problem arose during testing. The relatively poor quality of the flange laminate and the consequent voids tended to cause acoustic emission. The noise coming from this area tended to mask the ultrasound from the box during loading. This problem could be solved by the use of acoustic sensors in the flange area, which could be set to lock out the noise. To accomplish this obviously requires more sophisticated equipment than the single channel detector which was available.

A similar approach to flange design was used in the testing of the main wing box. Owing to the use of another test rig, a wider bolt pitch was dictated. There was also greater offset between the box and the boltline. The large offset implied the use of an impractically thick flange, so strengthening webs were introduced between each bolt. The strengthening webs introduced some complexity in design, so it was analysed by a simple finite element model. The webs were constructed by laying shaped Rohacell foam web cores onto the flange laminate after the first few layers were applied. To maximise the bending stiffness of the flange, the bulk of the thickness was of 0/90° glass/epoxy with woven and unidirectional carbon for the outer layers. Again, testing up to the ultimate design load cases for the box has not caused failure here.

9.2. The whiffle tree.

A whiffle tree was designed to load each rib station. This is a system of beams which is intended to simulate the effect of air loading on a wing. The whiffle tree is shown in drawing A1-CFRP-05 (Appendix H) and in fig 9.4. In the case of the original

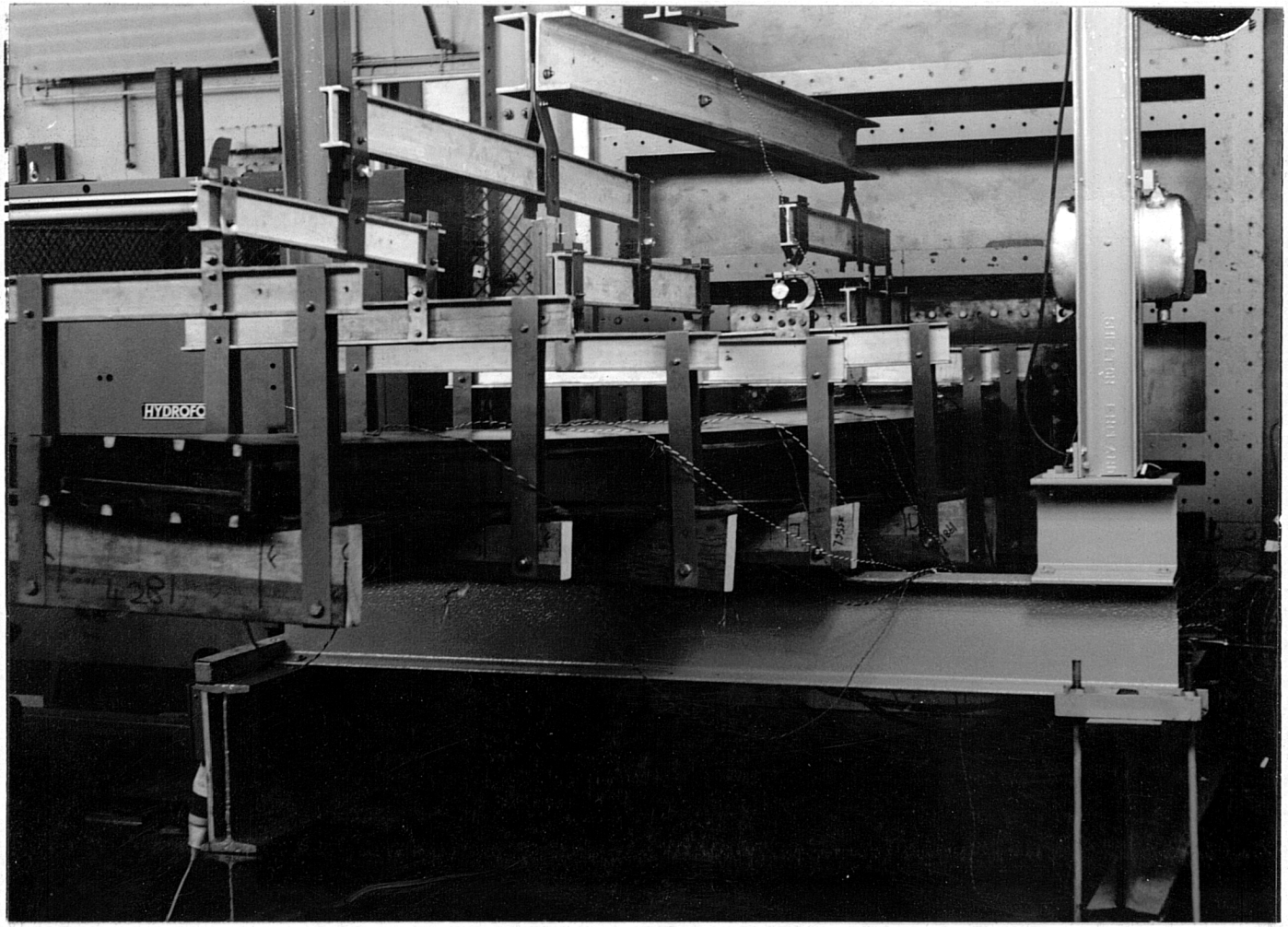

Figure 9.4

The whiffle tree shown with the wing box under positive load.

aluminium wing, five stations were loaded by independent turnbuckles and dynamometers. The difficulty with this system is that the turnbuckles interact, and that the rate of loading is slow. Due to the comprehensive test programme envisaged with the CFRP design, the effort of producing a whiffle tree was worthwhile.

A hydraulic loading system, incorporating dual rams with a manual pump and bleed valve had already been constructed for test box 2. This was found to have sufficient capacity and stroke for loading the main wing. Load was transmitted to the wing by means of a series of aluminium beams to wing contour boards. It was not considered important to link the beams together at their centrelines. This was due to the small extent of relative swinging expected. The whiffle tree was designed with a minimum reserve factor of 2 with respect to the maximum design load of 28.25 kN.

The spanwise load distribution was taken from the net shear force diagram for the 680kg, 13G case. It was simulated by a point load at each rib as shown in fig. 9.5. The chordwise load distribution was 2/3 on the front spar, 1/3 on the rear. This was distributed to the wing surface by foam padding on the 50mm wide contour boards.

Aileron loadings were applied by means of a turnbuckle, and were measured by means of a hook dynamometer. The turnbuckle and dynamometer were attached to a gantry passing over the wing as shown in fig. 9.6.

9.3. Non-destructive testing (NDT).

Since the box was to be assembled by adhesive bonding, suitable joint testing methods had to be investigated. To evaluate different NDT techniques, two test samples were constructed. The samples were of similar configuration to the actual wing joints. The samples were plates 600mm long and 100mm wide, joined together by a 20mm deep double lap joint, as in fig. 9.7. The laminate was $+-45(2)^{\bullet}$,SYM.

One of these samples was assembled by wetting both surfaces with adhesive, and then slotting the two sections into each other. This simulated assembly of the rear spar onto the stiffened wing panel. A second specimen was assembled by wetting with adhesive and sliding the two parts together from one end. This

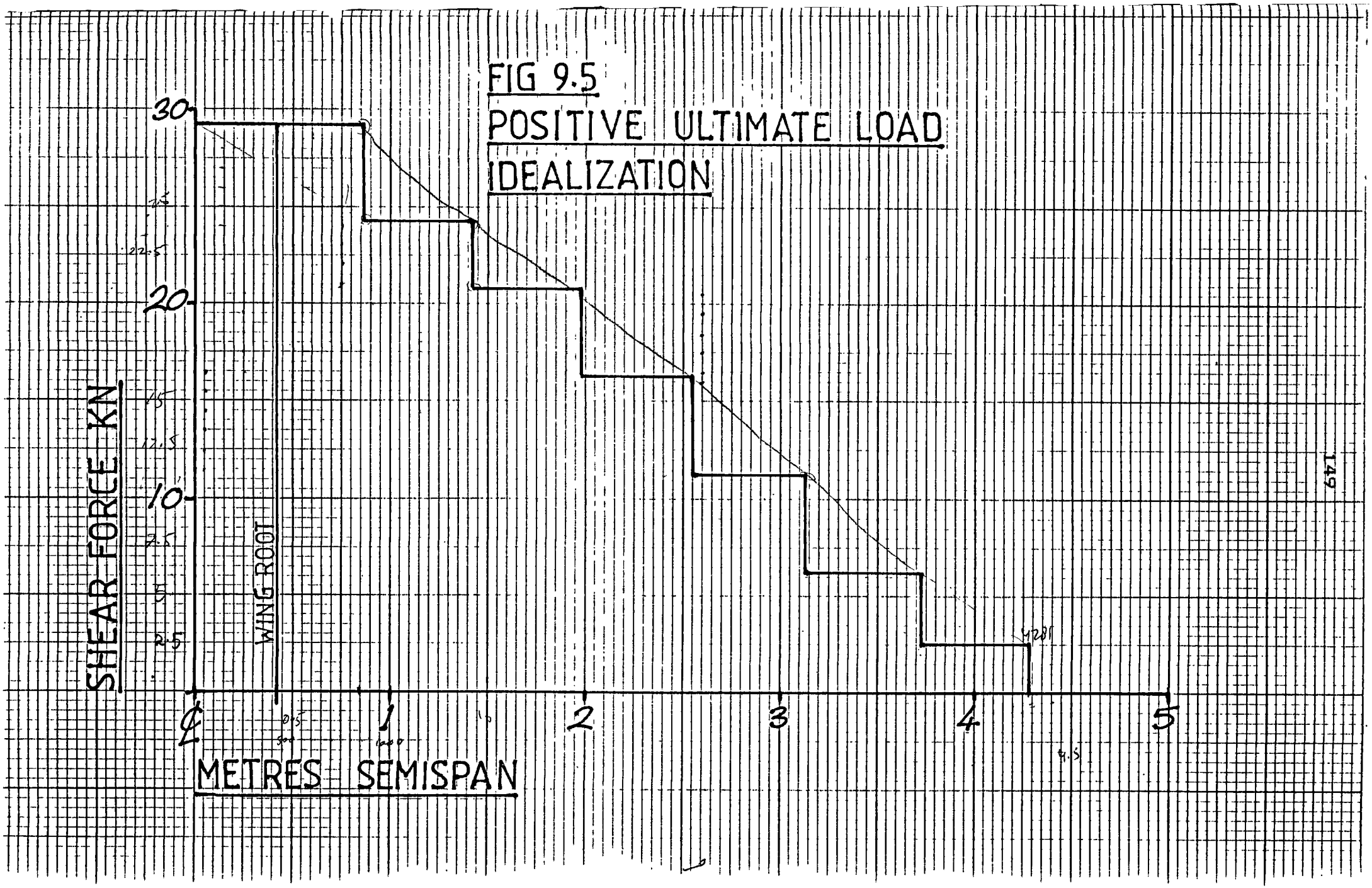
FIG 9.5
POSITIVE ULTIMATE LOAD
IDEALIZATION
SHEAR FORCE KN
30
20
10
WING ROOT
℄
1
2
3
4
5
METRES SEMISPAN

Figure 9.6.

The aileron loads were applied by means of a turnbuckle and measured by a hook dynamometer. Aileron loads could also be combined with bending loads by using the whiffle tree.

Figure 9.7.

Samples of typical rib and spar slotted joints were constructed for NDT examination. Where a poor joint was suspected, they were cut into coupons like those below. The coupons were then tested for tensile strength.

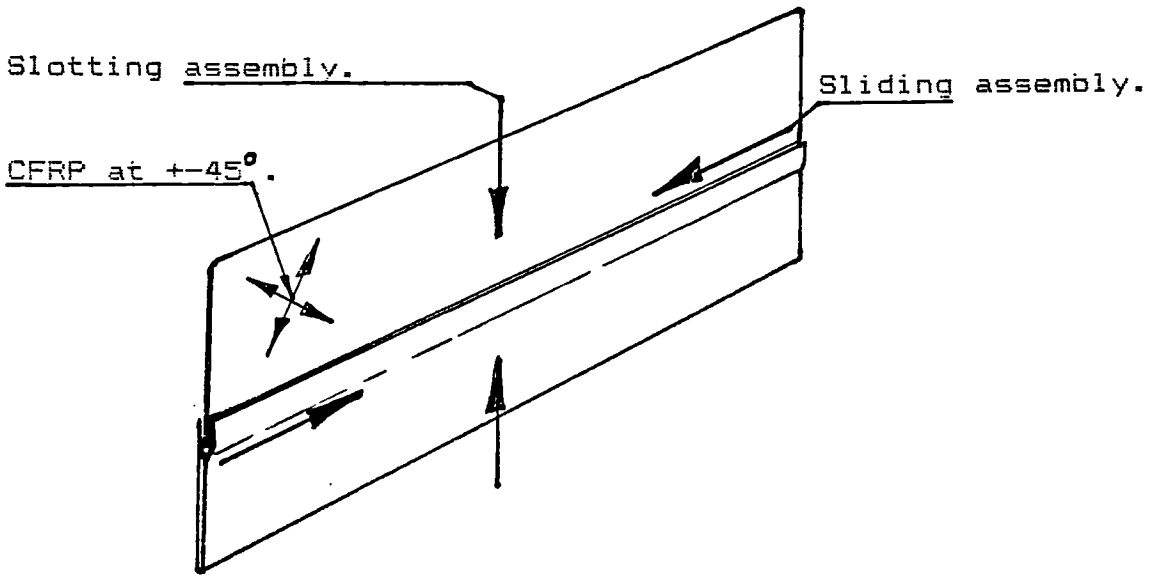

simulated sliding the front spar into position when assembling the wing box. As in the actual wing assembly, no clamping was used apart from that given by the fit of the two components.

The slotting assembly technique was expected to allow complete filling of the joint with adhesive. The sliding technique was expected to be less reliable, as the adhesive could be pushed out of the joint during assembly. Following an offer from Westland Helicopters' NDT department, the samples were examined by the following different methods:

9.3.1. Ultrasonic scanning in a water bath.

The sample was placed in a water tank on top of a 20mm thick block of glass. The water gives good coupling of the sample to an ultrasonic probe. The probe contains a focussed ultrasonic piezo-electric transmitting crystal. This sends out pulses of very short duration at a frequency of 5MHz. A receiving crystal in the same probe picks up the reflected pulses. The pulses are reflected from:

i) The top surface of the sample.
ii) The lower surface of the sample.
iii) The bottom of the glass block.

The amplitude of pulse (iii) is of the most interest. The amplitude of this pulse is affected by the energy absorption of the sample. If an area is disbonded, then the amplitude of the returning pulse is attenuated. The effect is caused by the energy absorbed in the disbonded area of the sample.

The amplitude of the returning signal is plotted by scanning across the sample as shown in fig. 9.8. The dark areas indicate a strong returning wave and hence a good bond. For the specimen which was slotted together, there is a continuous line of good adhesion along the length of the joint. The joint does not appear to be properly bonded over the whole depth of the slot. In the sample which was slid together, an area of low transmission is shown indicating a poor bond.

This equipment is capable of producing a clear indication of the permeability of the part, but suffers from a number of drawbacks in this application:

i) Due to the small thickness of the component, the time taken by the pulse to travel through the material is very short. This demands very high

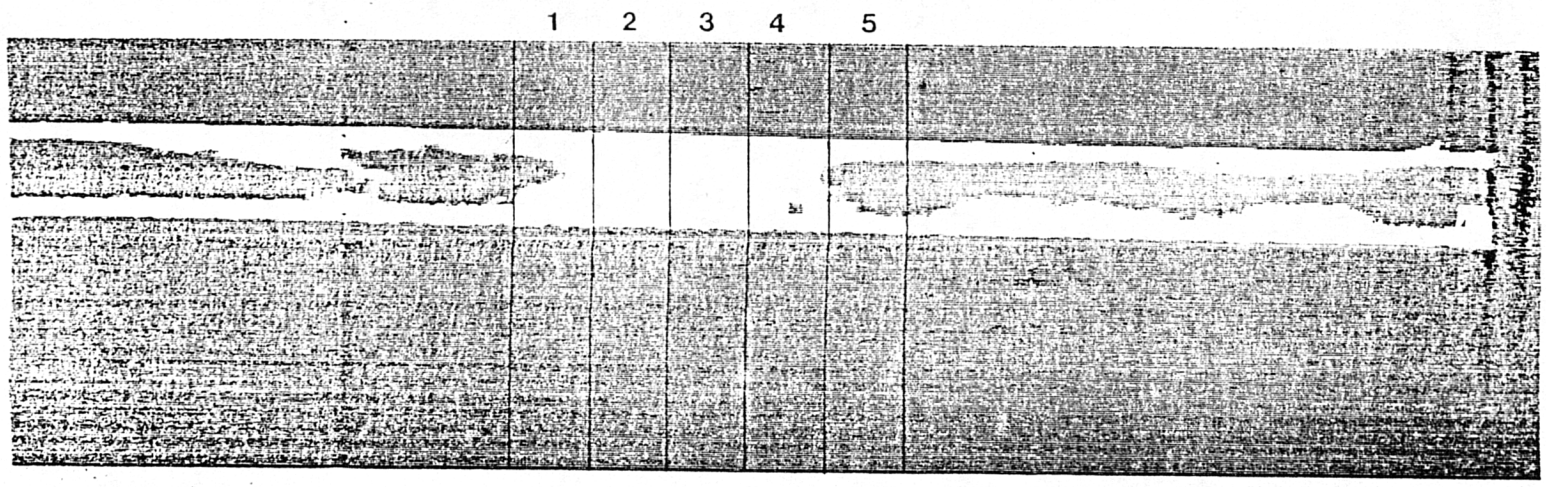

Figure 9.8.

The ultrasonic scans for the slid together specimen (top) and the slotted together specimen (bottom). The top specimen was cut into coupons as shown. The tensile strength of these is given in table 9.1.

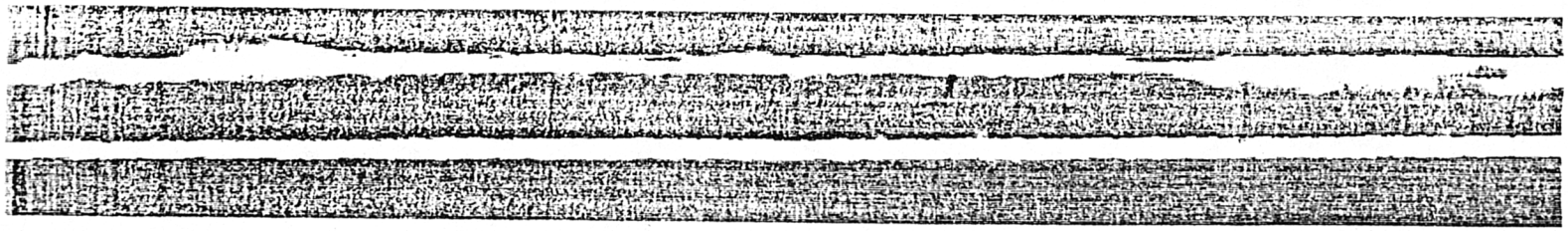

resolution equipment to separate the top and bottom surface pulse reflections. The glass block allows the returning signal to be readily distiguished from the top surface reflection. In the case of the spar joints, no rear surface access is possible to install such a block.

If the necessary resolution is available, separate reflected pulses may be seen for the top surface, the two adhesive layers, and the bottom surface. Positive identification of the bottom surface wave is given by pressing the rear surface with a soft block. This attenuates the rear surface wave. Again, this is not possible without access to the rear surface.

ii). For consistent results, a smooth surface finish is required on both sides. The finish cannot be guaranteed for the rear surfaces of these spar joints. This is because they are formed against a Rohacell foam stiffener core.

The drawback of having to immerse the assembly in water can be solved by a number of means. A water jet probe can be used. Here the probe contains a jet nozzle so that a continuous water connection is always made with the specimen.

A good ultrasonic coupling can also be made using a coupling jelly, usually based on glycerol.

For components where access can be obtained on both sides, two water-filled rubber rollers can be used. These rollers contain a probe on each side, pointing towards the specimen. The quality of bonding is then determined by the degree of through transmission.

9.3.2. The acoustic flaw detector (AFD).

The AFD is a device operating in the audio range. A long probe contains a piezo-electric transmitting crystal, and a receiving crystal. The receiving crystal is situated some distance from the transmitting crystal, which is at the tip of the probe. A sound wave is applied to the specimen, and the amplitude and phase of the returning wave is measured.

The AFD gave inconclusive results when tested on the suspect area of specimen no.2. This was due to harmonic waves being set up in the testpiece, because of its thin section and high stiffness.

9.3.3. The Fokker bond tester.

This ingenious device gave by far the best results. A probe is used which is coupled to the specimen by the use of a jelly. The probe incorporates a large barium titanate crystal at the tip. This crystal forms part of the tuned circuit of an oscillator running at 900 Khz in free air. When the crystal is coupled to the specimen its resonant frequency is altered. If the specimen is homogeneous, the frequency will be reduced by the mass of the area coupled to the probe. If a disbonded area is encountered, the frequency will not be reduced by as much. The amplitude will also be reduced by the energy absorption of the part.

The frequency change was shown by a small cathode ray tube display on the instrument. This was synchronised to show a single stationary pulse when the probe was in contact with a good section. When a disbond appeared, the waveform moved to the right and reduced in amplitude.

When the probe was passed over the suspect area discovered in the ultrasonic test, the instrument gave a clear and unmistakable indication of this. No access was required to the opposite side. Since the device excites a comparatively large area at a time, (10 mm^2), the smoothness of the surface texture on the rear surface is not too important. Westland Helicopters use this technique as a routine production inspection for composite rotor blades. The postbuckled wing could be inspected in a very similar fashion.

9.3.4. Thermography.

Thermography was not tried on the specimen as the equipment was part of a large, automated inspection rig for helicopter rotor blades. The technique uses an infra-red- sensitive video camera. The specimen is first heated, and then filmed whilst being allowed to cool. With glass/epoxy the method is very successful because of the low conduction of the material. With carbon, the heat tends to be conducted rapidly along the fibres.

Thermography is ideally suited to rotor blade inspection, where a thin skin is bonded to a massive spar. The heat then soaks back through the thin skin. If a disbond exists between the skin and spar, a

marked drop in skin temperature results. This is observed by the camera.

In the case of the postbuckled wing, no large sections exist for the heat to be stored in this way. The carbon fibre material may also mask the effect. One possible approach is to scan the part at high speed for the initial period of cooling. The cooling phenomenon can then be seen in slow motion before the temperature equalises. If a technique could be developed, this would be a very quick means of inspection.

9.3.5 Testing the suspect area.

Although a suspect area of disbonding had been discovered by some of these methods, the physical implication of this was not known. By visual inspection, both sides of the joint appeared to be satisfactory. In order to determine the strength of the bond in this area, five 20mm wide coupons were cut from the centre of the suspect area. The results of the testing are shown in table 9.1.

Table 9.1.

The strength of coupons taken from a joint specimen. (See fig 9.8 for location of coupons in the specimen.)

Coupon No.	Tensile load *KN*
1	6.2
2	6.02
3	4.013
4	4.28
5	6.26

It appears from the testing that only one side of the joint was disbonded. The joint still possessed substantial strength in this area. The fact the

disbond was only on one side is a consequence of the slotted joint configuration. Providing there is sufficient adhesive in the joint, a disbond on one side implies increased pressure for bonding on the other side. Further, if this flaw could be easily detected, a fault of real consequence should be easy to find with the Fokker bond test. In all of the tests in the above table, the disbond was on the flat side of the joint. On the overlapping side, the adhesive held. Failure occurred by fibre breakage at the bend.

9.3.6 Conclusions.

The adhesive joints in the wing can all be inspected by means of the Fokker Bond Tester. The equipment is not highly expensive, and provides a clear indication of disbonded areas. It is well suited to the inspection of typical thin joints found in the structure. No immersion or rear surface access is required. The rough surface texture of the material in contact with the foam cores is of little concern due to the averaging effect of the large excited area.

Inspection of all the joints in the wing would take about 12 hours. The thermal imaging technique has the potential to reduce this considerably. However, this technique suffers from a number of fundamental problems in thin-walled CFRP structures.

Chapter 10.
Structural weight.

10.1. Comparison of the metal and composite designs.

The aluminium and composite designs are subject to the same external geometry and loading conditions. This has enabled a comparison to be made between the weight of the two structures. Although the original metal design was postbuckled, there was also a substantial spar boom. Not all of the direct bending loads were taken by the skins. The aluminium wing had 16 ribs on each side, with 8 Z-section stiffeners across the chord at the root. The geometry of the section, and the positioning of the spars, was kept identical in the CFRP design. The wing was proof-loaded before flight as in ref. 44.

The weight of the aluminium wing box was calculated from the original drawings. The leading edge of the wing does not contribute very much to the bending strength, as only the wing box from front to rear spar is continuous across the fuselage. The weight of each bare aluminium wing, including undercarriage mounts, was 68kg.

The weight of the CFRP wing was calculated in three parts:

i) Integrally stiffened skin panels.
ii) Ribs.
iii) Spars.

The weight of the skin panels was analysed by a module in the OPTIMIST program. This took the optimised proportions of a typical skin/stiffener from the PASCO program as in ref. 1. The stiffener was assumed to be of square cross section, filled with 70kg/m↑3 foam. The stiffener sidewalls were assumed to be one third of the thickness of the main skin. The rib weights were calculated as buckling-resistant panels designed to take shear and Brazier loading.

Table 10.1 Wing weight comparison.

Part	Aluminium (calc)kg.	CFRP(calc)kg.	CFRP(actual)kg
Ribs	.313	.498	.323
"	.310	.478	.299
"	.555	.457	.266
"	.307	.452	.314
"	.287	.419	.180
"	.397	.329	.138
"	.371	.254	.180
"	.206	.082	.030
"	.267	-	-
"	.185	-	-
"	.158	-	-
"	.127	-	-
"	.102	-	-
"	.074	-	-
"	.050	-	-
Ribs total=	3.714	2.969	1.730
Top skin	6.830	12.950	14.160
stiffeners	5.000	-	-
Bot skin	6.830	9.960	12.650
stiffeners	5.000	-	-
Skins tot.=	23.660	22.910	26.810
Front spar booms	10.020	-	-
Front spar web	3.140	1.600	2.067
			.250
Rear spar web	2.197	.800	.687
			.532
			.104
Rivets	.700		
Adhesive	-	.600	.600
Total=	43.431	28.879	32.780
Weight % saving=	0	33%	25%

10.2. The carbon fibre composite wing in more detail.

In the actual wing, the rib weights are lower and the skin weights higher than calculated. This is because part of each rib is an integral part of the skin panel. The overlapping of material at the stiffener caps required for a practical layup was not considered in the original weight breakdown. Some extra material was also required to form the slotted joint features in the skin. The anti-peel strips also contributed some weight.

Overleaf is a table taken from weights of components before curing. These include the backing film. As supplied, 16% of the weight of the woven material is backing film. 16% of the weight of the unidirectional material is backing film and paper. The stiffeners are numbered from rear to front. "P.S. 7" consists of all the inner woven panel material between stiffeners 7 & 8.

10.3. Discussion.

As can be seen, there is a difference in the weight of the prepreg and the actual structure weight after curing. The difference of .95kg is accounted for by the following:

i) The stiffener cap plies and anti-peel strips were all cut to one length. They were trimmed to size on laying-up.

ii) Trimming of the mouldings after cure.

iii) Escape of volatile substances from the prepreg during cure.

The extra material in the actual wing box increased the stiffness of the wing as well as the weight. In the test results it can be seen that the strains and deflections are lower than expected. This gave rise to increased buckling loads, especially on the inner panels. See chapter 11 for the results. Ultimate strength has also been increased, as shown by the negative bending case. At the time of writing, the box has not been loaded to failure.

Table 10.2.

Carbon fibre wing component weights before curing.

Part	Weight kg (with backing film).	Weight kg (Net).
Top and bottom skin components.		
P.S. 1 and 2	4.2	3.5
P.S. 3 and 4	3.4	2.9
P.S. 5 and 6	3.3	2.8
P.S. 7	1.6	1.3
Spar joining strips	1.25	1.05
Anti-peel strips	1.5	1.26
Main external woven plies	7.84	6.6
Bottom unidirectional skin plies	1.93	1.04
Top unidirectional skin plies	2.89	1.56
Stiffener cap u.d. plies	3.4	1.84
Rib Flanges	2.3	1.98
Skins total	33.61	25.83
Rib webs total	2.13	1.78
Rear spar components.		
Rear inner	.91	.76
Rear mid	.65	.56
Rear outer	.16	.14
Rear spar total	1.72	1.46
Front spar components.		
Front inner	2.15	2.04
Front outer	.18	.14
Front spar total	2.33	2.18
Total Carbon Prepreg Weight	39.79	31.25
Adhesive		.6
Stiffener cores		1.8
Total structure weight		33.65

Chapter 11.
Structural load testing.

11.1. Introduction.

The whiffle tree described in chapter 9 was used for all tests. The wing box was mounted by means of a flange that was bolted onto a plate at the root. The bolt spacing in this was symmetrical, allowing the wing box to be rotated for negative tests. The contour boards and beams were removed and replaced at 180 degrees in this case.

For the aileron loadings, a gantry which spanned the wing box was used. Aileron loads could be applied by means of a turnbuckle as in fig 9.6.

11.2. Test cases.

The wing was tested to ultimate design loads in the following cases:

1) Positive wing bending for the 13.5G case at 680kg maximum aerobatic weight. Ref. 28 was used to give the load distribution and inertia relief. A loading idealisation was used to supply load at each rib station, as shown in fig 9.5. The total load applied was 28.25 kN.

2) Negative wing bending for the -9G case at the same weight. Here the same loading distribution was used, with the applied load factored by 9/13.5.

3) Torque due to maximum aileron deflection at Vd, stick force limited. This is the zero G accelerated roll case as in ref. 32.

4) Maximum aileron deflection at +.67 x 13.5G, stick force limited.

5) Maximum aileron deflection at -.67 x 13 G, stick force limited.

11.3. Test Results.

11.3.1 Positive Load Test.

The wing structure was loaded up to a maximum of 28kN. Up to 20kN this was in 5kN increments, and was then reduced to 2kN steps. At each increment a full set of readings was taken. 75 strain gauges were

monitored, along with deflections at the flange, mid-span and tip. A single channel acoustic emission recorder was also used.

11.3.2 Behaviour of the structure under test.

Loading progressed smoothly up to 19kN. Visible skin buckling started to appear from 12kN upwards. This started in the skin panels between stations 2556 and 3706, near to the trailing spar. At a load of 19kN, a loud bang was then heard from either the root rib area or the mounting flange. The sound was thought to have come from rib station 868mm because of the concentrated loading at the contour board.

As the load had not reduced after the bang, loading of the structure was continued. No further loud sounds were heard up to the ultimate design load of 28.25 kN. However, as can be seen from the acoustic emission trace (fig. 11.1), there was considerable noise emanating from the mounting flange. For this reason it was decided not to increase the loading beyond 28.25 kN. Eventually, failure would probably occur at the mounting flange area. This is not representative of the actual wing, which is a continuous structure across the centre section.

11.3.3 General strain gauge results.

For decoding strain gauge results, fig. 11.2 shows the positioning of all the gauges fitted. In each load case, the ribs, spars and compression skin were monitored. Two gauges only were used on the tension side, to record the highest values in the root area.

Gauges were fitted back-to-back at one predicted half buckle wavelength outboard from each rib. Generally, the actual buckle peaks were very close to the gauges. Some interesting plots of bifurcating compression strain have been recorded from postbuckled skin panels.

All the rib webs except stn 1981 showed a small tensile strain in the vertical axis. The ribs had been designed for Brazier-induced compression loads. The tensile loading is thought to be due to the method of loading the box. The contour boards tended to concentrate the loading near the spars. This loading resulted in vertical compression of the spar webs and tension of the rib webs. In all cases except for

Figure 11.1.

An acoustic emission plot versus positive bending load for:
1) The mounting flange adjacent to gauge 19.
2) The wing skin adjacent to gauges 22/23.

Both traces are at the same scale, which is:
i) Amplification 75 db.
ii) Delay 0.2 milliseconds.
iii) Window of 0.2 milliseconds.

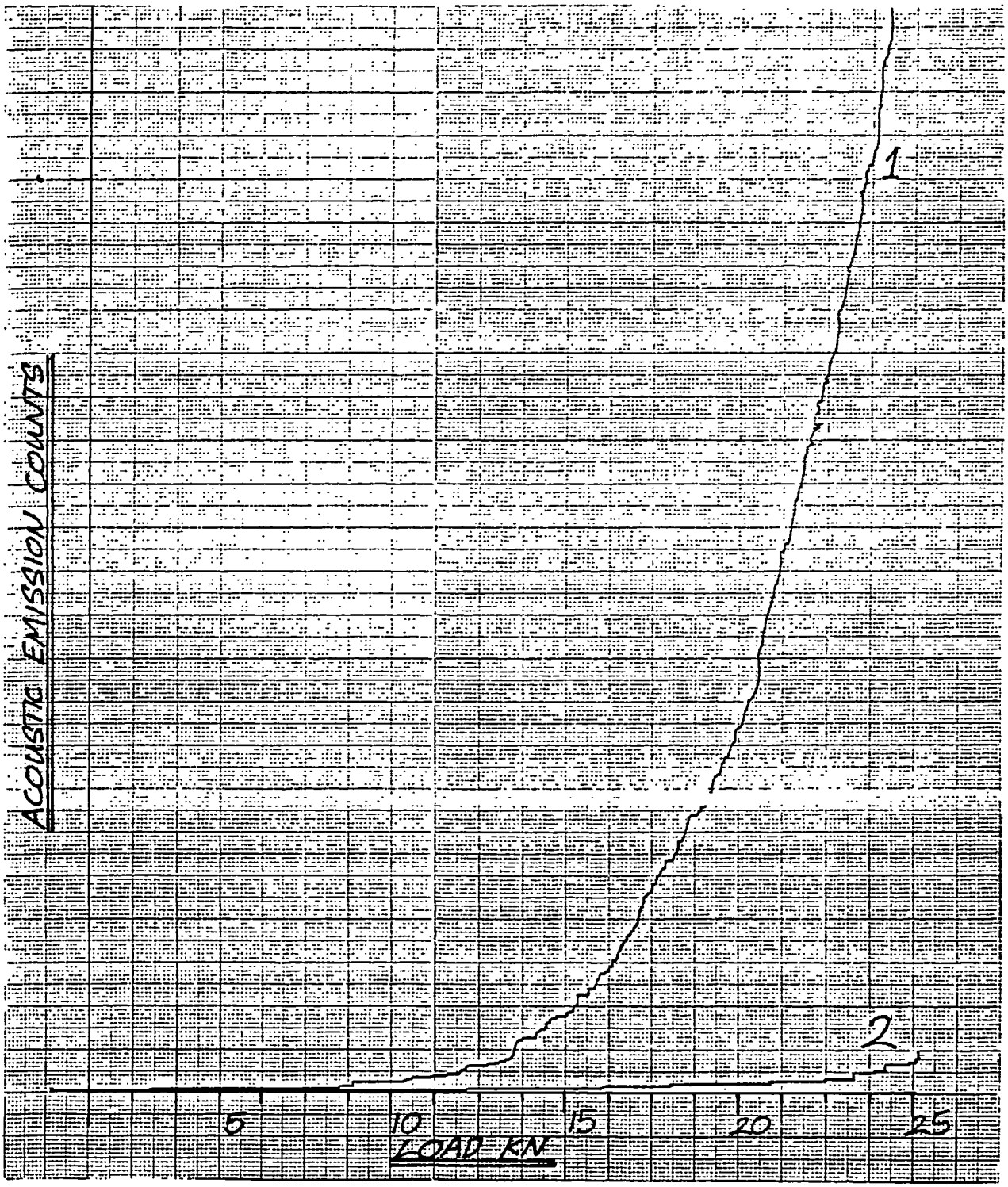

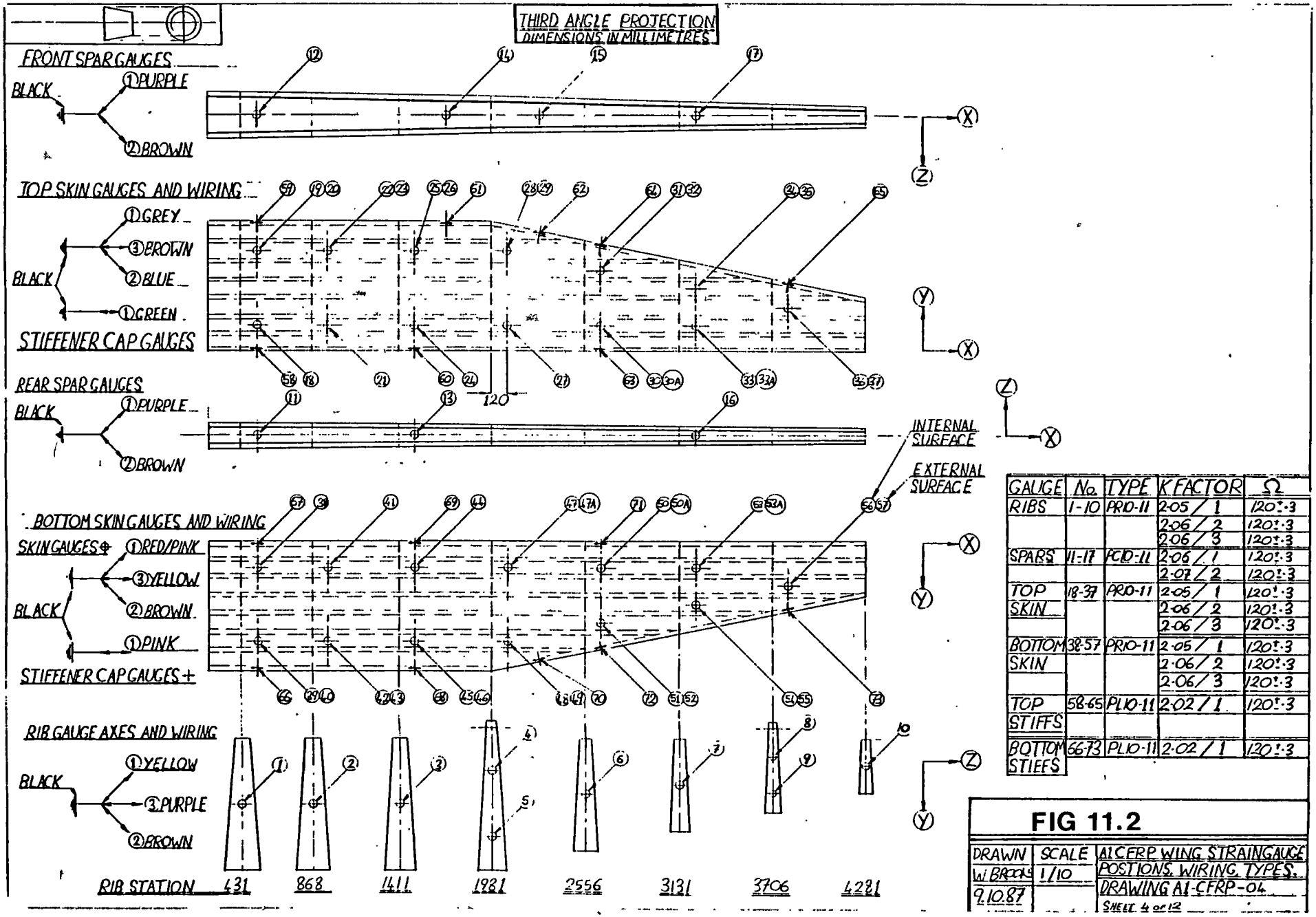

GAUGE	No.	TYPE	K FACTOR	Ω
RIBS	1-10	PRD-11	2·05 / 1	120±·3
			2·06 / 2	120±·3
			2·06 / 3	120±·3
SPARS	11-17	PCD-11	2·06 / 1	120±·3
			2·07 / 2	120±·3
TOP SKIN	18-37	PRD-11	2·05 / 1	120±·3
			2·06 / 2	120±·3
			2·06 / 3	120±·3
BOTTOM SKIN	38-57	PRD-11	2·05 / 1	120±·3
			2·06 / 2	120±·3
			2·06 / 3	120±·3
TOP STIFFS	58-65	PL10-11	2·02 / 1	120±·3
BOTTOM STIFFS	66-73	PL10-11	2·02 / 1	120±·3

FIG 11.2

DRAWN	SCALE	A1 CFRP WING STRAINGAUGE POSITIONS, WIRING, TYPES.
W BROOKS	1/10	DRAWING A1-CFRP-04
9.10.87		SHEET 4 OF 12

station 1981 this effect overrode the Brazier loading.

The complete numerical strain gauge results are available in Appendix F. The highest compression strain recorded for the positive load case was 0.265%. The predicted design value was 0.3%. The experimental strain was recorded by gauge 19, which is on the compression skin close to the root of the box.

11.3.4. Postbuckling of the skin.

The non-linear effects on surface strain caused by postbuckling were monitored. The most clearly marked postbuckling was at gauge 30. Fig 11.3 shows load versus strain for an external and internal gauge here. An inward buckle is indicated. The externally mounted gauge shows increasing strain as buckling progresses. The behaviour was entirely elastic and could be repeated many times. Similar results are shown by gauge 33, fig 11.4, which again shows an inward buckle.

Postbuckling was suppressed to a degree near the front spar. This is probably due to the effect of curvature. From the centreline to stn 1981, the first stiffener behind the mainspar is also more closely pitched. However, gauges 31 & 32 do show some postbuckling as in fig 11.5. No postbuckling could be detected between stn. 868 and 2556. From stn. 2556 inboard two extra skin plies are built into the laminate. This made the skin flexurally rigid enough to resist buckling. A smaller increase in thickness here was not possible. This is due to the relatively thick woven material (0.34mm) and the need for laminate symmetry.

Towards the root area some postbuckling effects emerged again. Gauges 19 and 20, outboard of stn 431, show non-linear behaviour in fig 11.6. The curves indicate outward bending of the skin here. Gauge 18 in fig 11.7 shows the stiffness reducing up to 20kN and then increasing again. This change is likely to be due to end effects caused by the proximity of the mounting flange.

11.3.4 Load /deflection behaviour

The tip deflection was very close to being linear throughout the range as shown by fig. 11.8. The mid span deflection, fig. 11.9, shows a slightly greater

Figure 11.3.

Bifurcation of strains versus positive loading for strain gauges 30 internally and externally mounted on the compression skin.

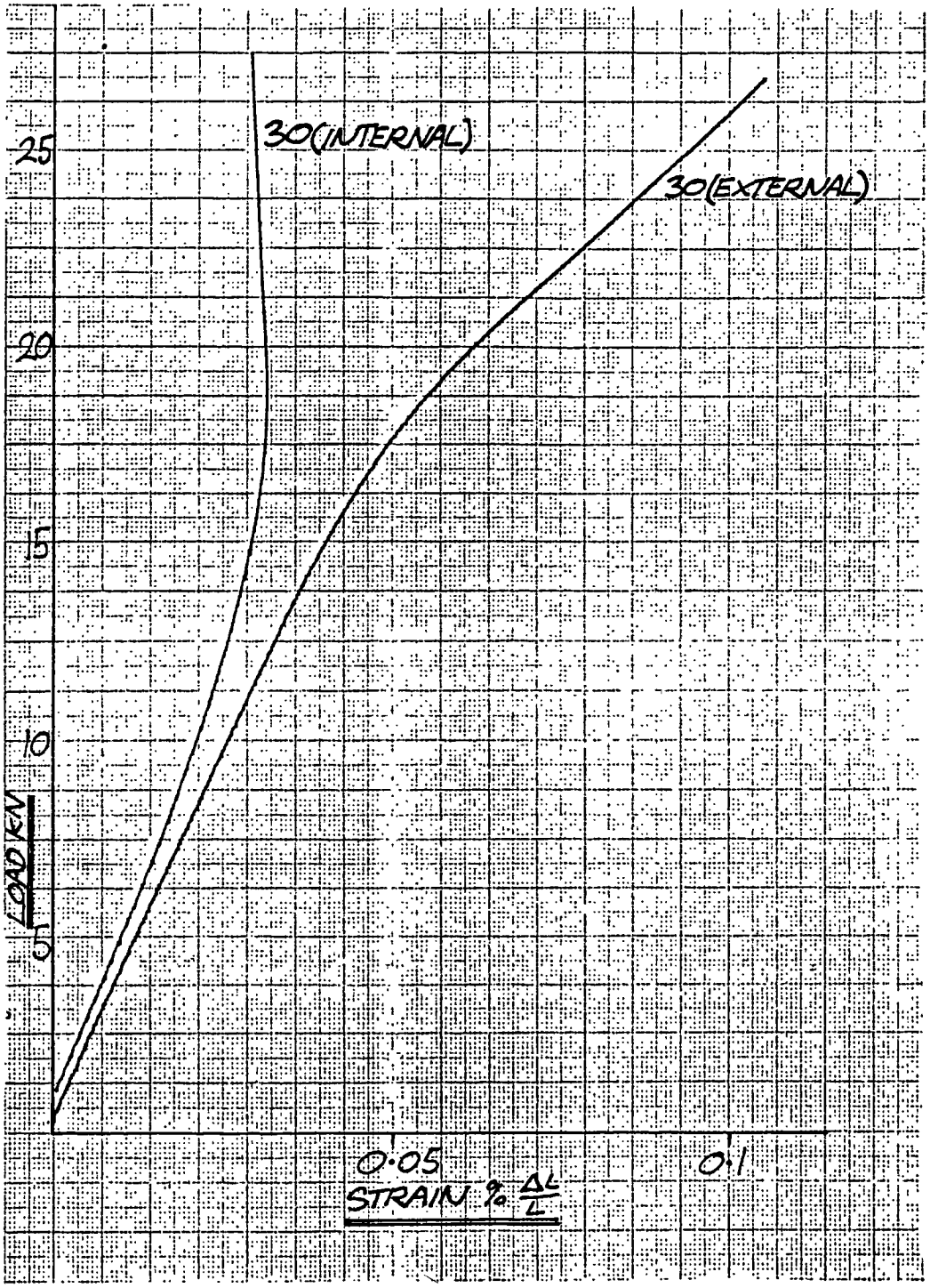

Figure 11.4.

Bifurcation of strains versus positive loading for strain gauges 33, internally and externally mounted on the compression skin.

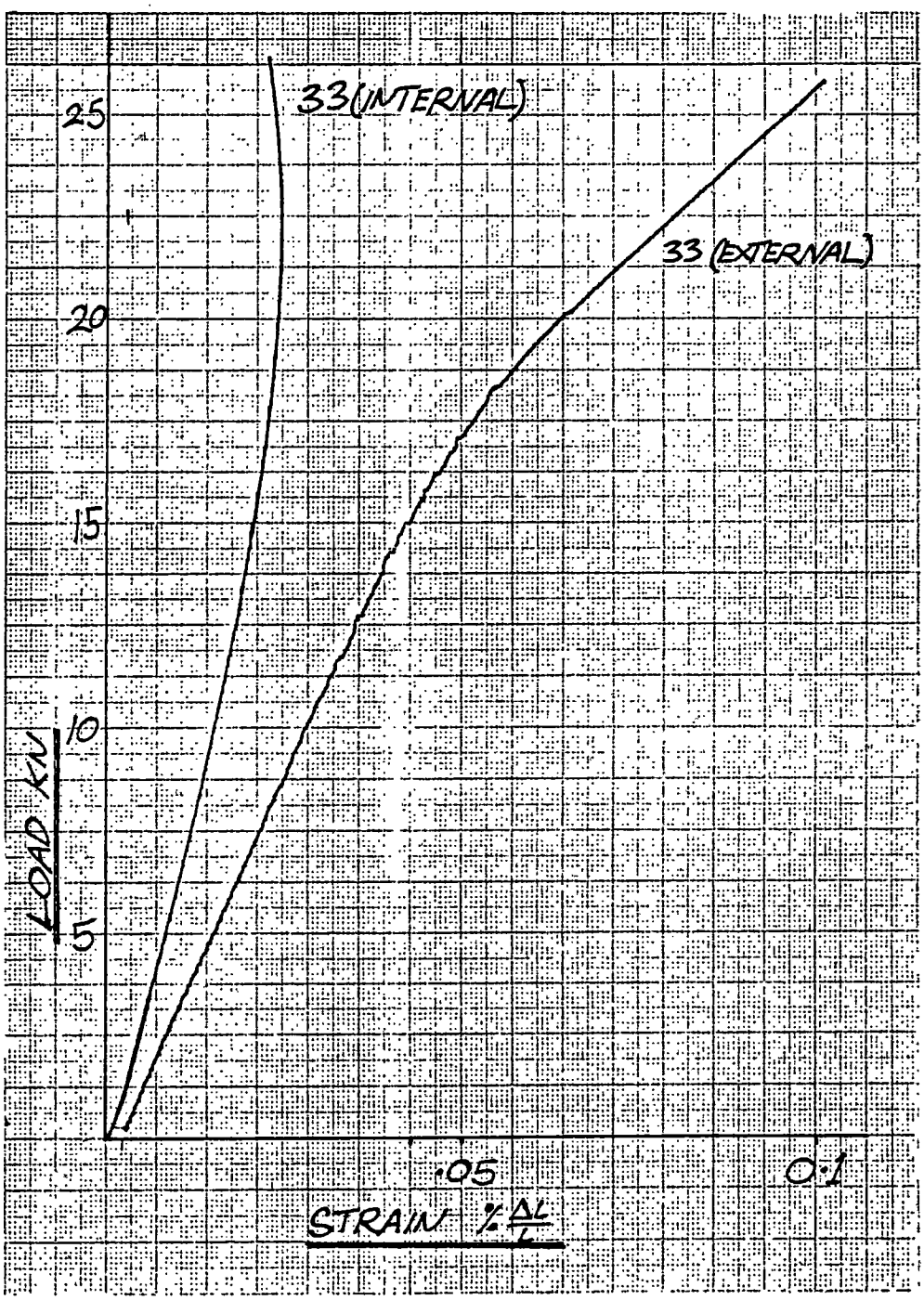

Figure 11.5.

Bifurcation of strains versus positive loading for strain gauges 31 and 32. Postbuckling was reduced to some extent near the front spar, as shown by this figure.

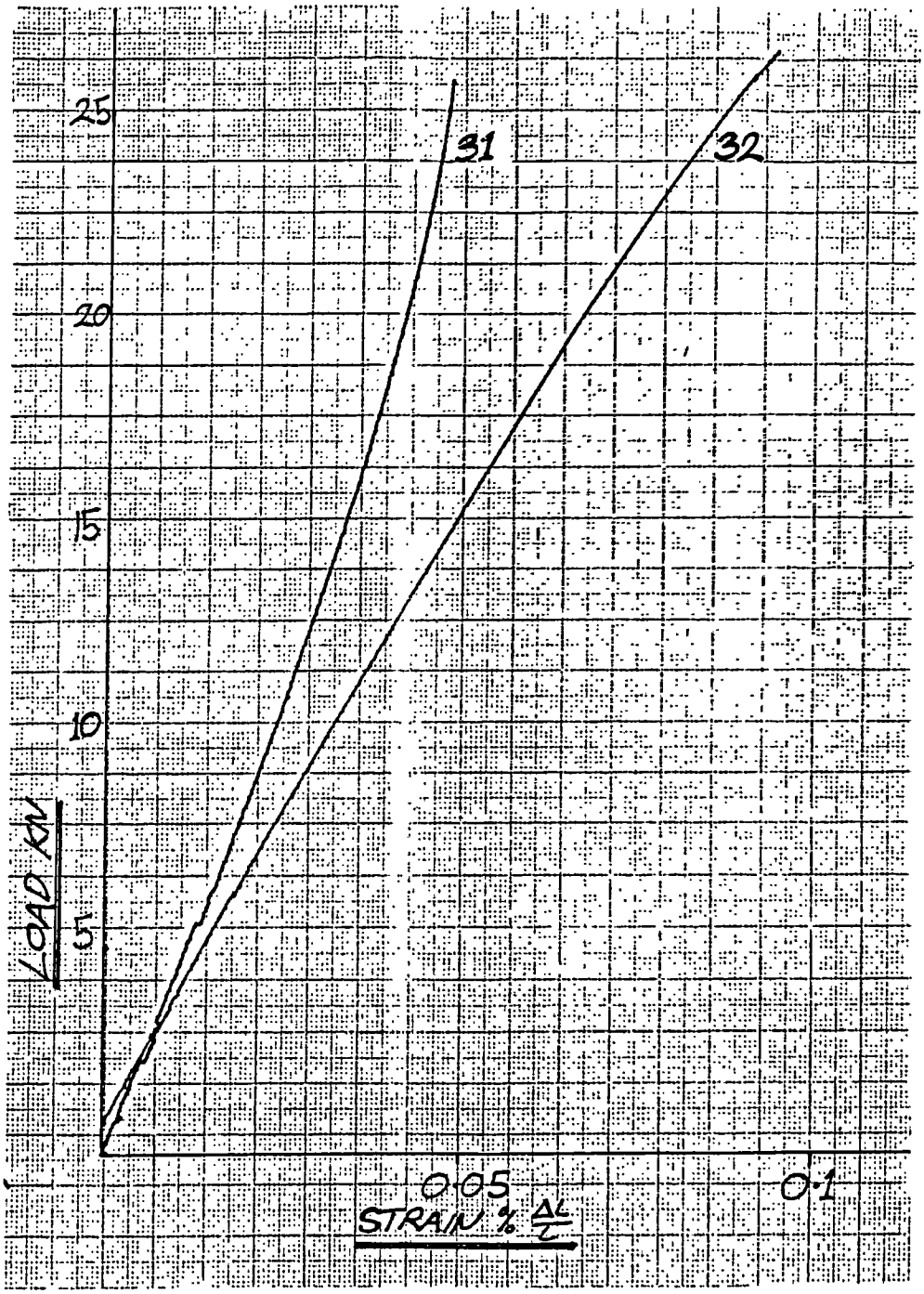

Figure 11.6.

Bifurcation of compression strain versus positive load for gauges 19 and 20. These gauges are at the wing root.

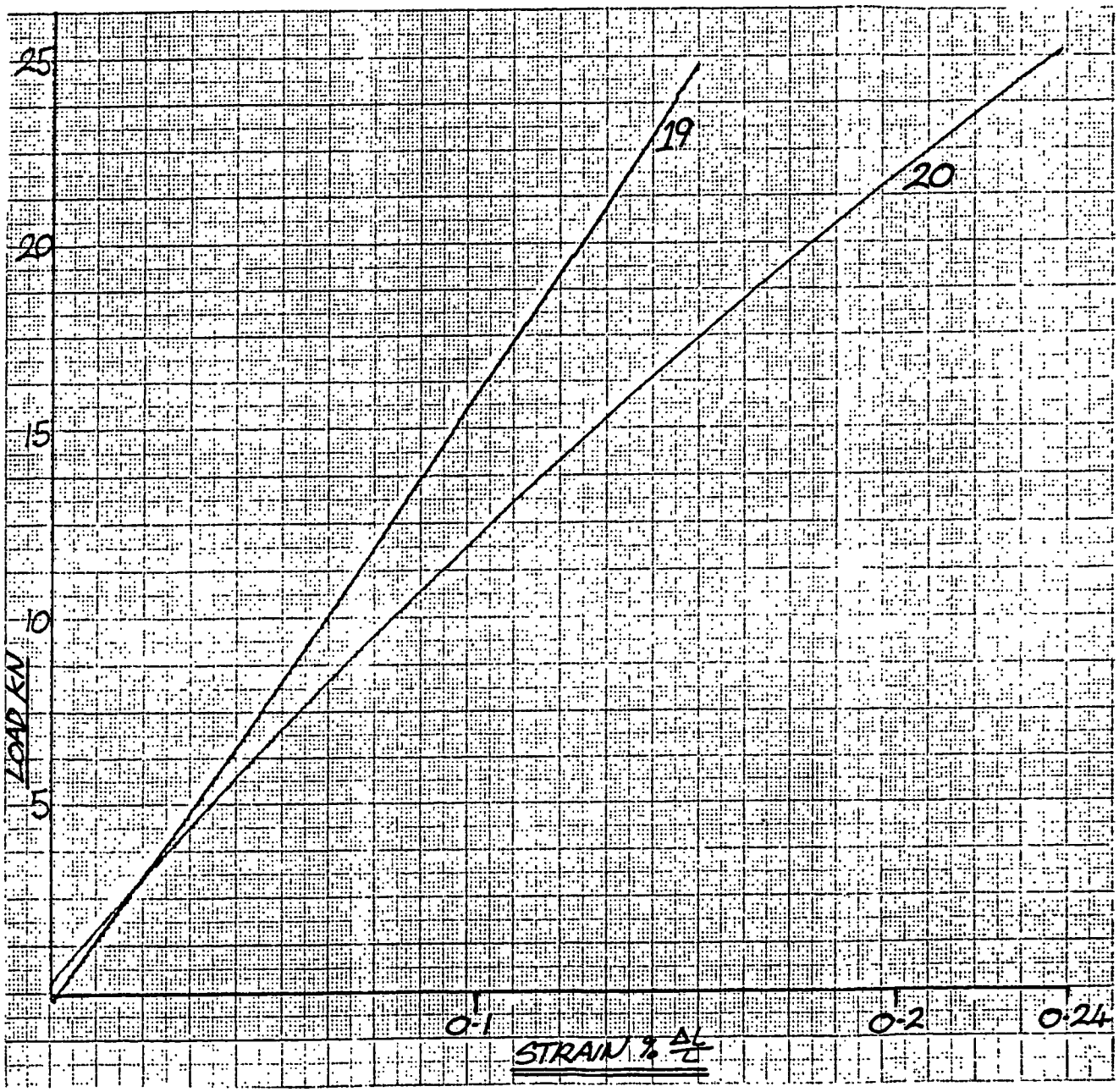

Figure 11.7.

A nonlinear relation between compression strain and positive load is shown by gauge 18. The gauge is close to the wing root at the trailing edge.

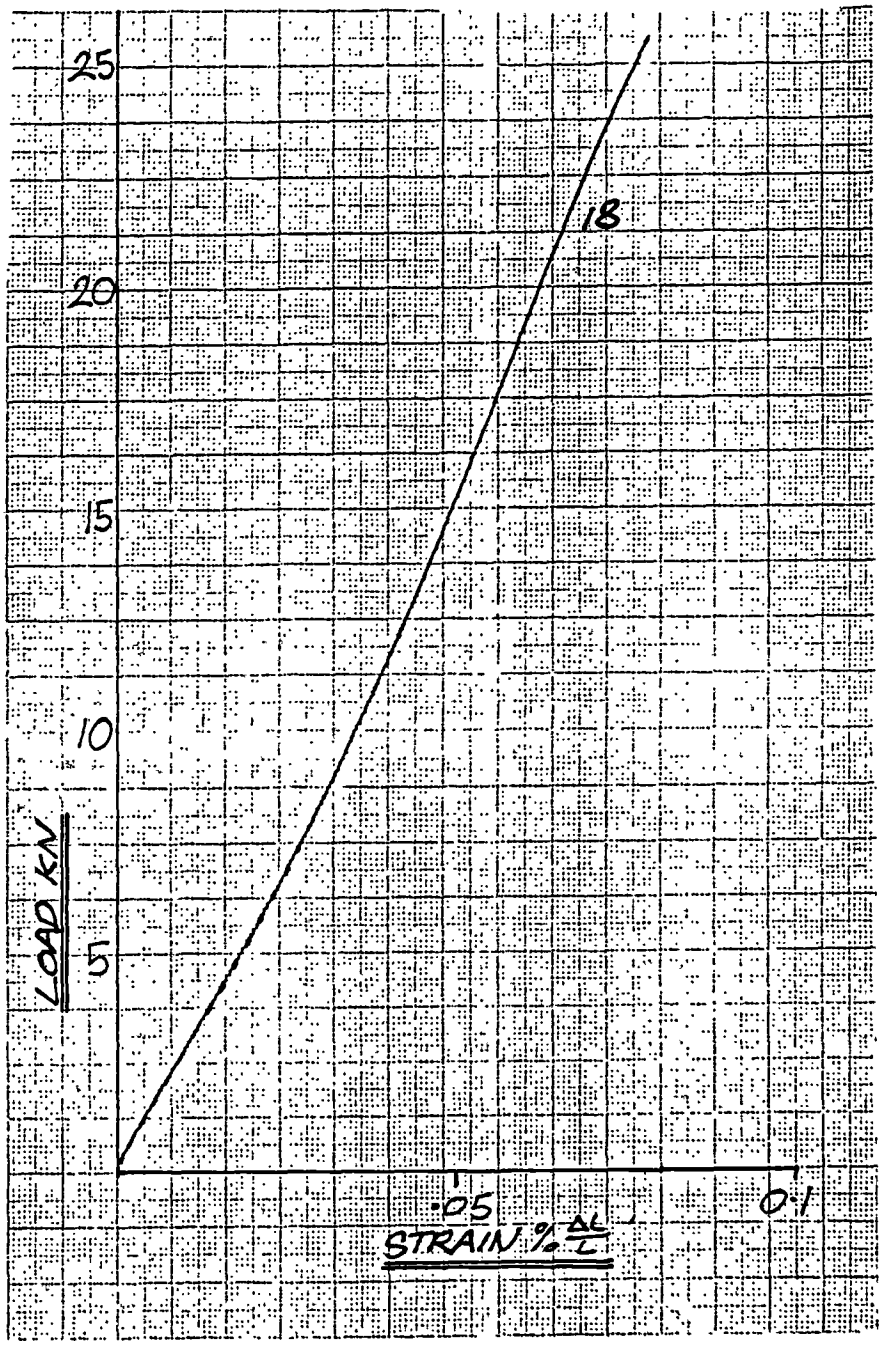

Figure 11.8.

Tip deflection of the wing for the positive load case. The arrow shows the jump in deflection at the point where a loud bang was heard during testing.

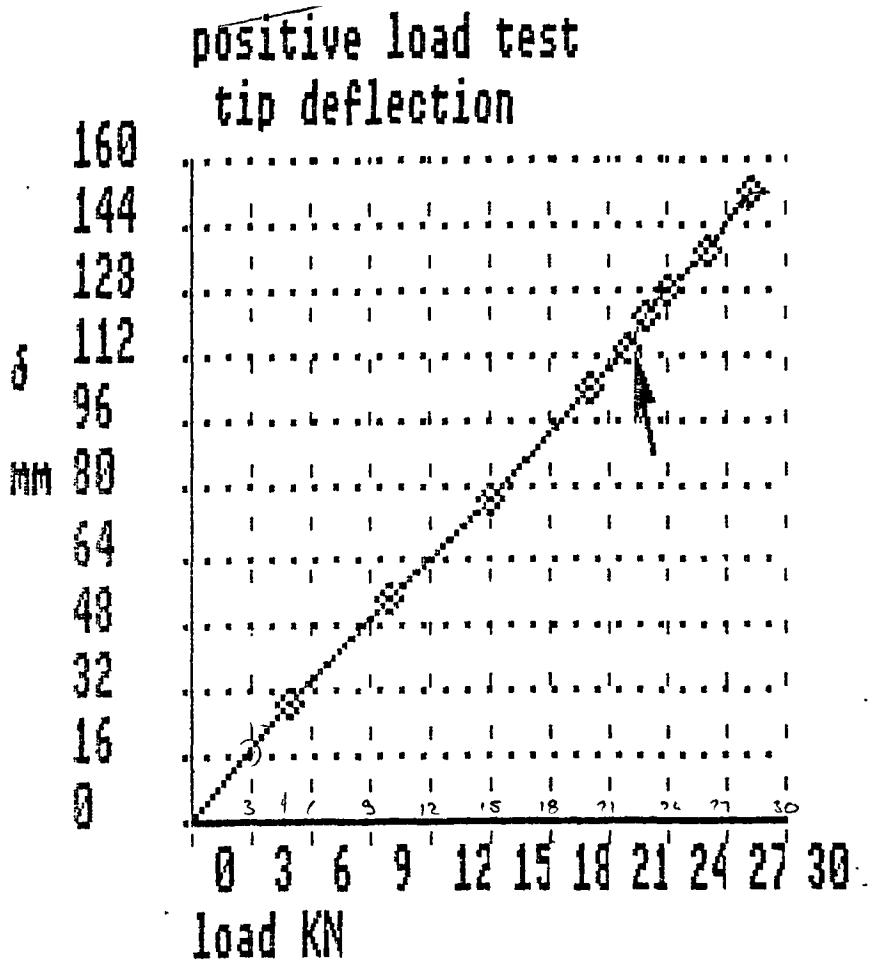

Figure 11.9.

Mid span deflection at station 1981 mm of the wing for the positive load case. This is the point at which the wing box is kinked.

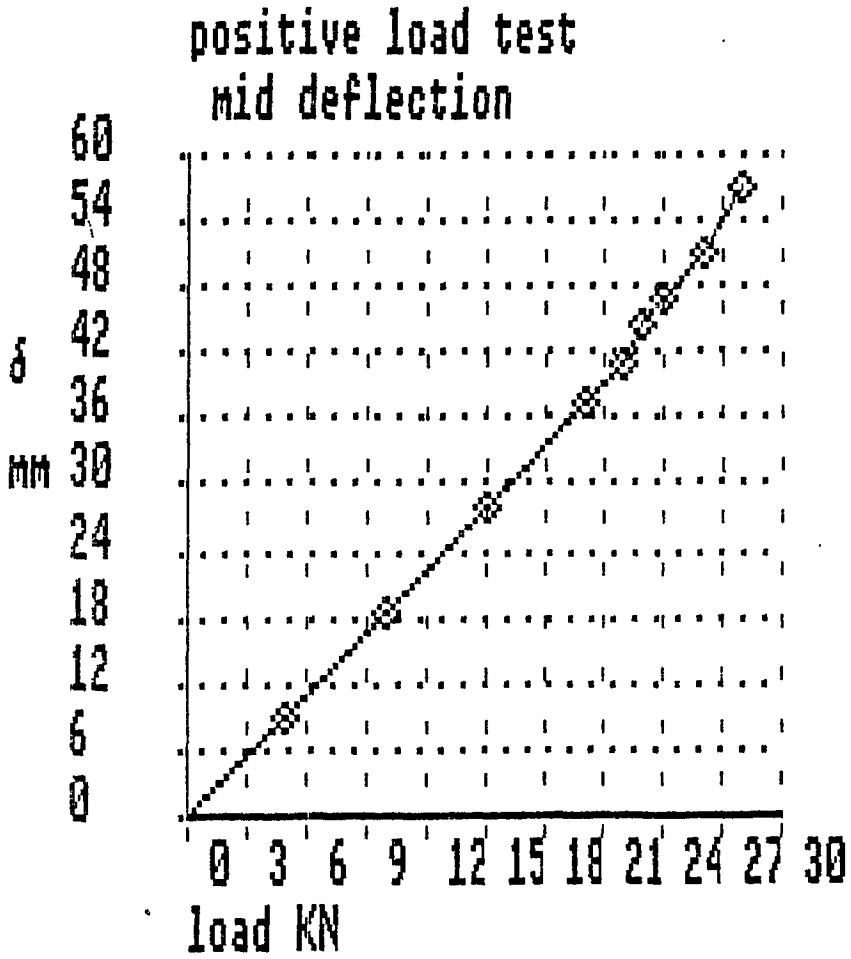

loss of stiffness above 19 kN. These readings must however be taken in context with the root deflections where the mounting flange meets the box. An interesting result here is shown in fig 11.10. A distinct jump can be seen at 19 kN (arrowed). This is the stage in the loading where the loud 'bang' occured. The jump may have been due to the shock wave disturbing the dial gauge, or it could be due to a localised failure of the flange at this point. At the leading spar (fig. 11.11) a more gradual loss of stiffness is indicated, with no jump.

The wing box washed out by 0.1 degrees during the test. This is due to the structural layout and sweep of the wing. This result shows that aeroelastic divergence should not be present.

11.4. Negative load test.

The negative load case could be exceeded without expecting root attachment problems. The design of the underskin is different from the top as seen in the main drawing A1-CFRP-01 in Appendix H. The skin changes at stn 1981 from four woven layers to two. The change occurs one bay further inboard than in the top skin. Also, a smaller quantity of unidirectional material is present in the lower skin laminate than the top.

11.4.1 Maximum strain.

The maximum strain recorded at -9G was 0.304% in gauge 40, situated on the compression skin near the root. This strain was partially due to postbuckling. The corresponding inner surface gauge 39 showed 0.148% strain. By taking the average, this gives a membrane strain of 0.226% . See Appendix F for full details.

11.4.2 Postbuckling behaviour.

Broadly similar results were obtained as for the positive load test. Postbuckling was generally more pronounced, the greatest degree of buckling being in the area of gauge 53. This gauge is internally mounted, with an external gauge mounted at the same spot. Fig 11.12 clearly shows inward buckling of the

Figure 11.10.

Root trailing spar deflection at the junction between the end of the mounting flange and the wing box for the positive load case. The arrow shows the distinct jump at the point where the bang was heard.

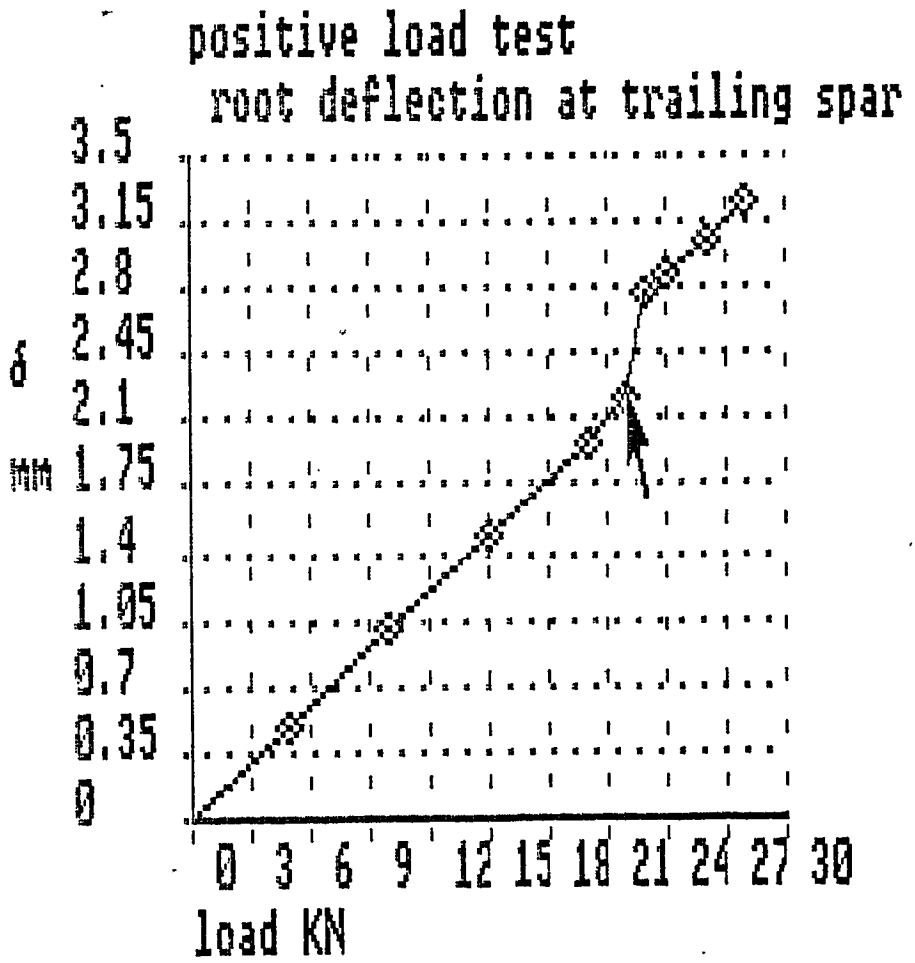

Figure 11.11.

Leading spar root deflection at the junction between the wing box and flange for the positive load case.

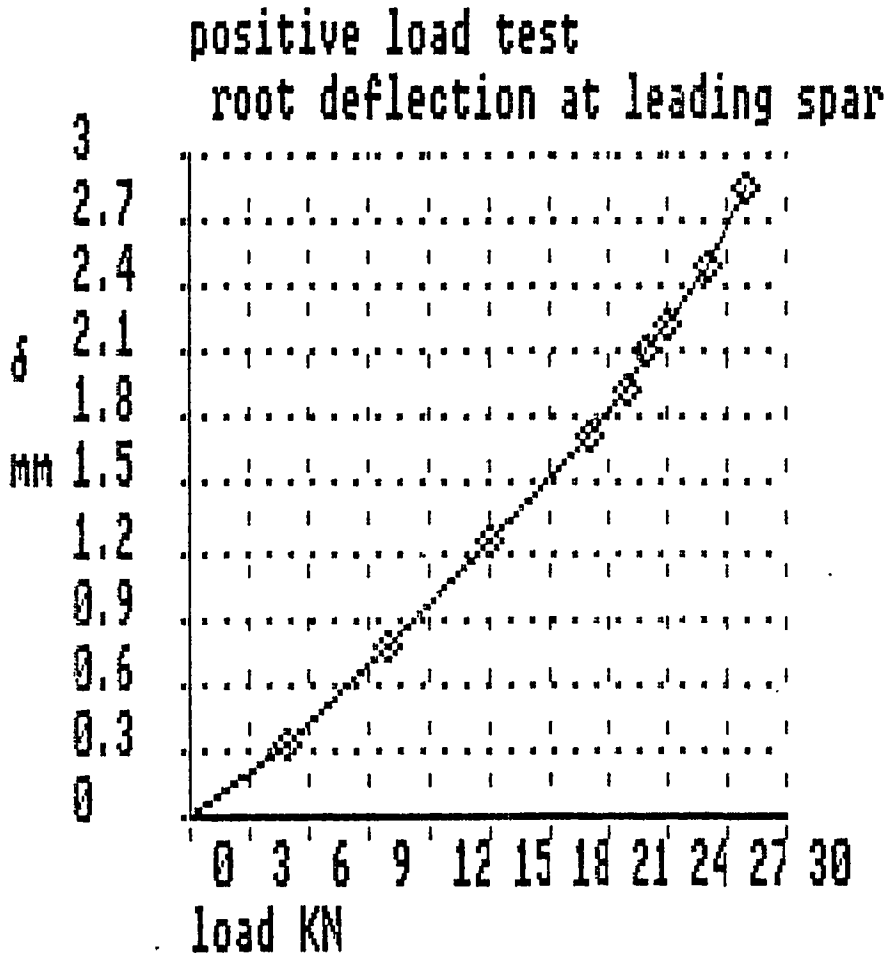

Figure 11.12.

Bifurcation of compression strains in the negative load case for gauge 53 (internal and external skin surfaces).

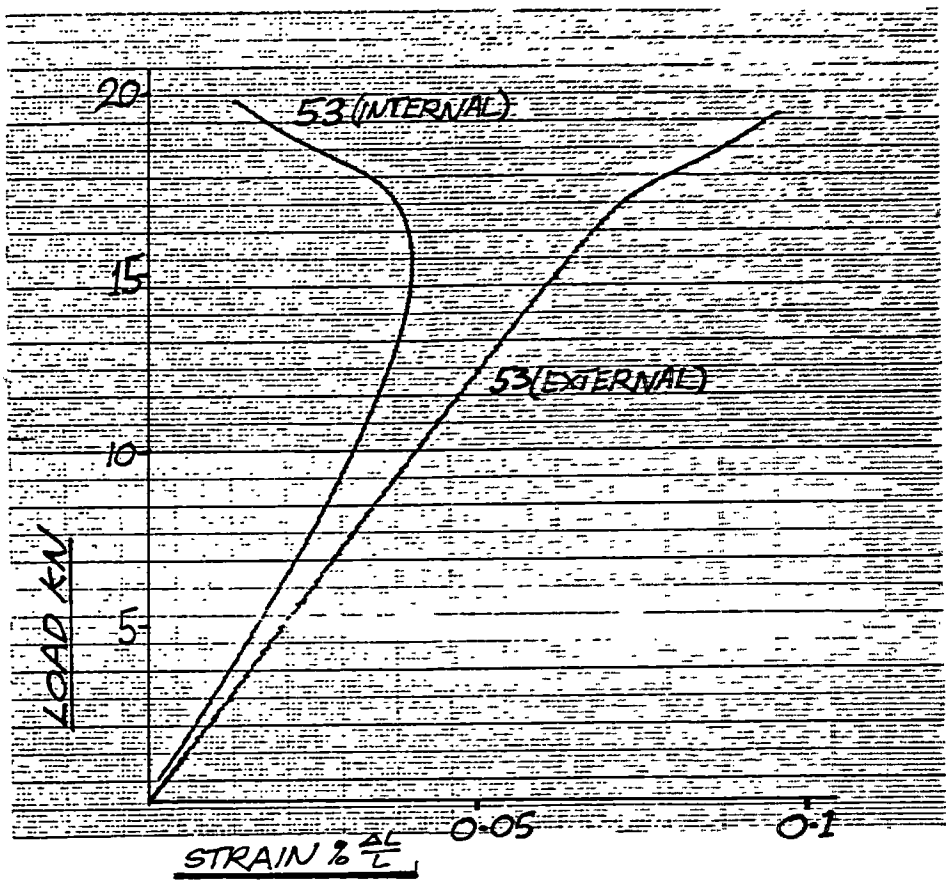

skin here. More buckling was seen towards the leading edge than in the positive case. This is shown in fig 11.13, from gauges 54 and 55.

Some of the gauges in the postbuckled panels near the trailing spar such as gauge 47 record an interesting buckling behaviour. The effect, as seen in fig 11.14, shows that the strains of the top and bottom surfaces diverge as usual. Taking the mean strain of the upper and lower surfaces to be the membrane strain, the membrane strain ceases to increase after the onset of local buckling. This behaviour reinforces the assumption used for the effective width analysis used to predict postbuckled amplitude. It was noticed during the testing that some of the skin buckles tended to be skewed. The skewing became more pronounced towards the trailing spar, as shown in fig 11.15. This skewing shows the presence of shear load.

In the negative load case, postbuckling continues in bay 1981-2556. This is because the skin includes only two outer woven plies here. Postbuckling is suppressed between ribs 868 and 1981 by the increased skin thickness. Non-linear effects re-emerge near the root as in fig. 11.16, gauges 39 and 40. The root area is again influenced by end constraint effects. The compression skin at the root can be seen under load in fig 11.17. The skin appears to bow inwards near the flange, whilst the stiffeners protrude. A general view of the postbuckling of the skin is given in fig 11.18.

11.4.3 Load/deflection results.

The load/deflection curves for the negative case are linear, as shown in figs 11.19 and 11.20.

11.5. Torsion tests.

To simplify the testing, the full aileron load was applied at stn 3706. The rib at this station was specially designed to withstand the load and transmit it to the structure. Ref. 32 shows that the maximum load due to full aileron deflection is 9.007 kN. The aileron load is limited by the maximum control stick force. However, the aerodynamic load does not all act at the aileron hinge line. Ref. 32 also shows the chordwise pressure distribution due to aileron. From

Figure 11.13.

Bifurcation of compression strain in skin panels near the leading edge at gauges 54 and 55. Negative load case.

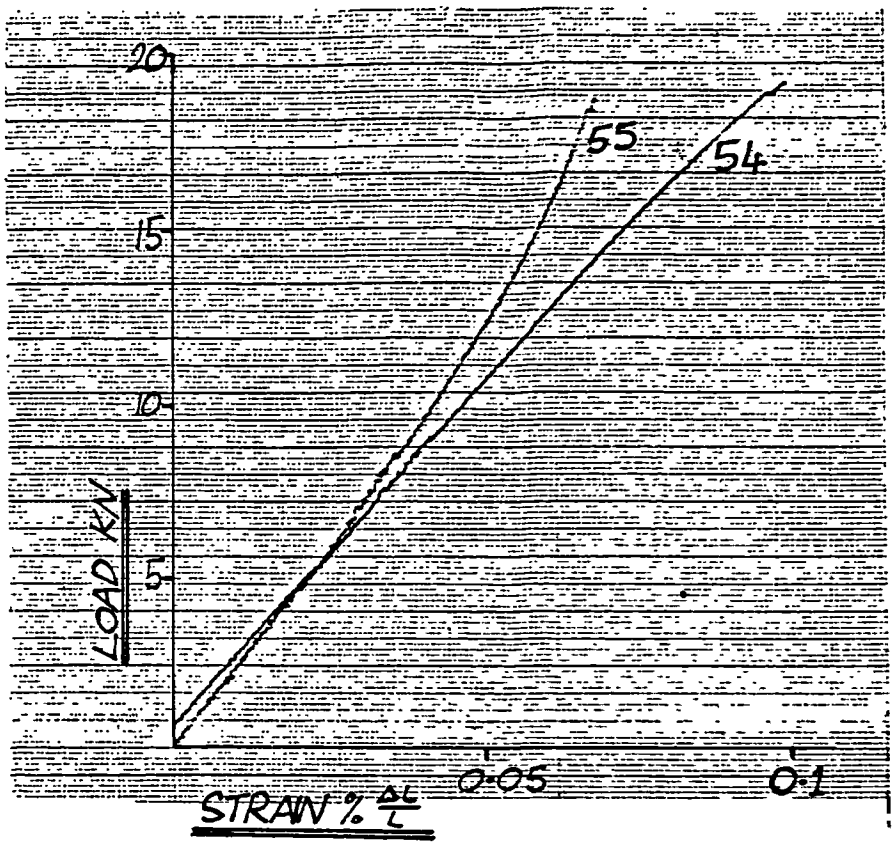

Figure 11.14.

For the compression gauges 47 in the negative case, the membrane strain ceases to rise once the panel has buckled.

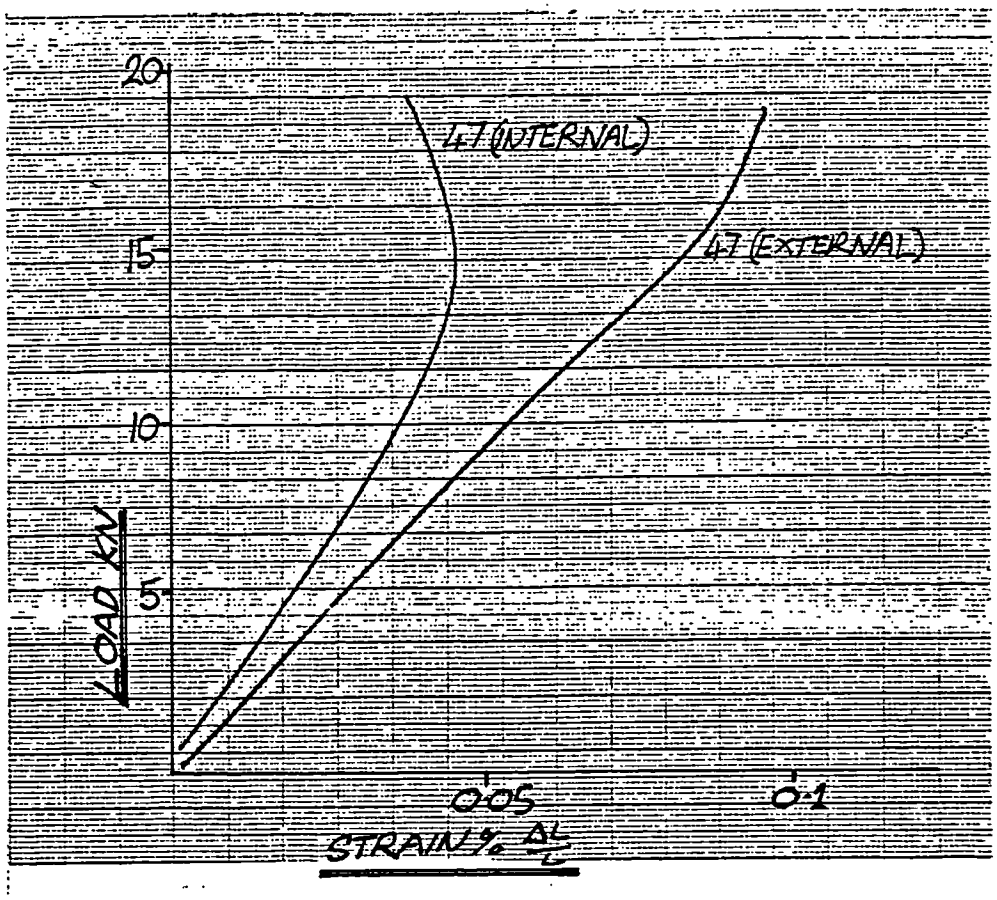

Figure 11.15.

Postbuckling of the skin in bays 1981-2556 in the negative load case. Note the skewing of the buckles due to shear forces. This skewing becomes more pronounced towards the trailing spar.

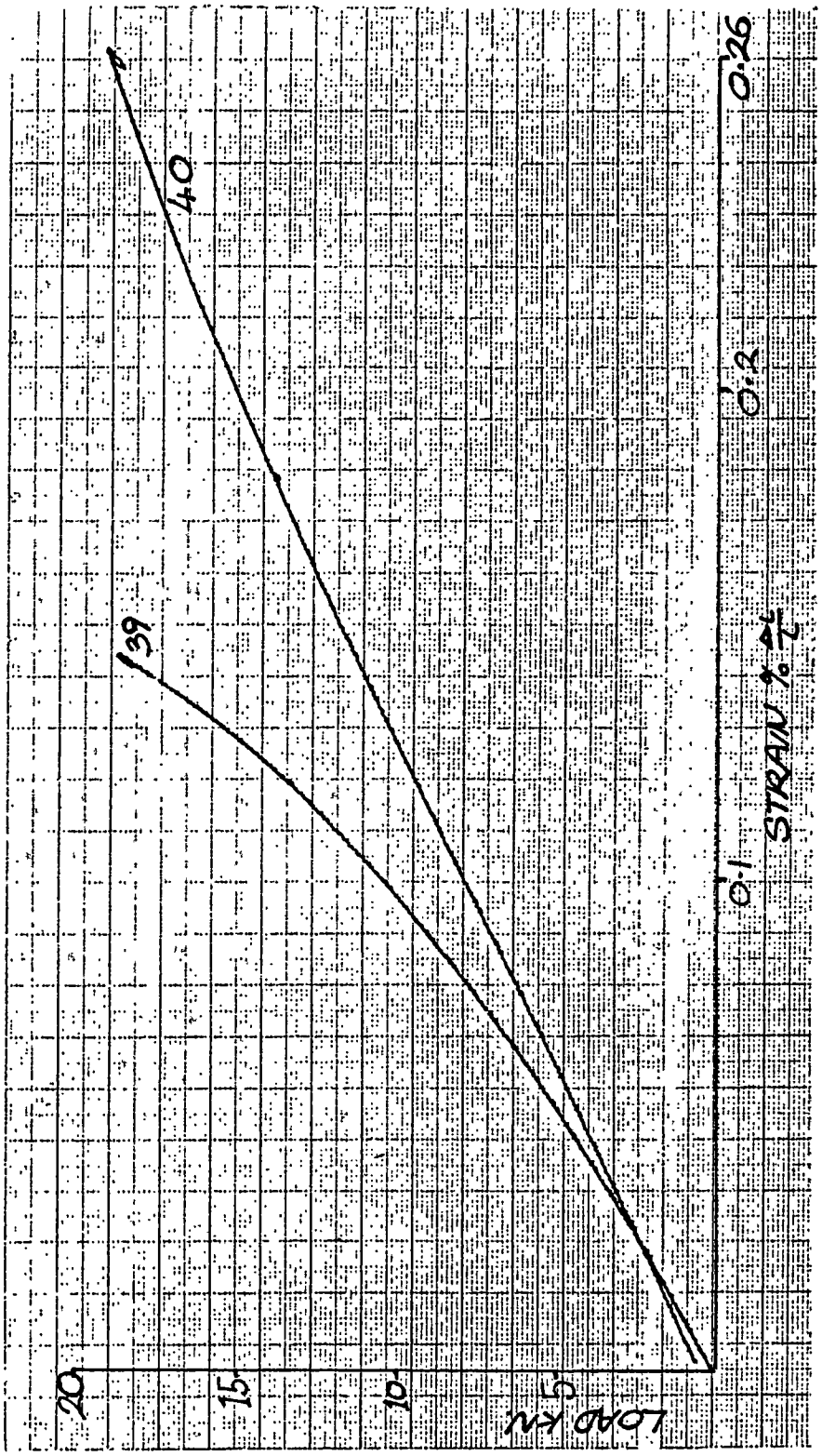

Figure 11.16.

Bifurcation of compression strain is shown at the wing root for the negative load case by gauges 39 and 40.

Figure 11.17.

The root area during the negative load test. The concave bowing of the skin panels between the stiffeners can be seen.

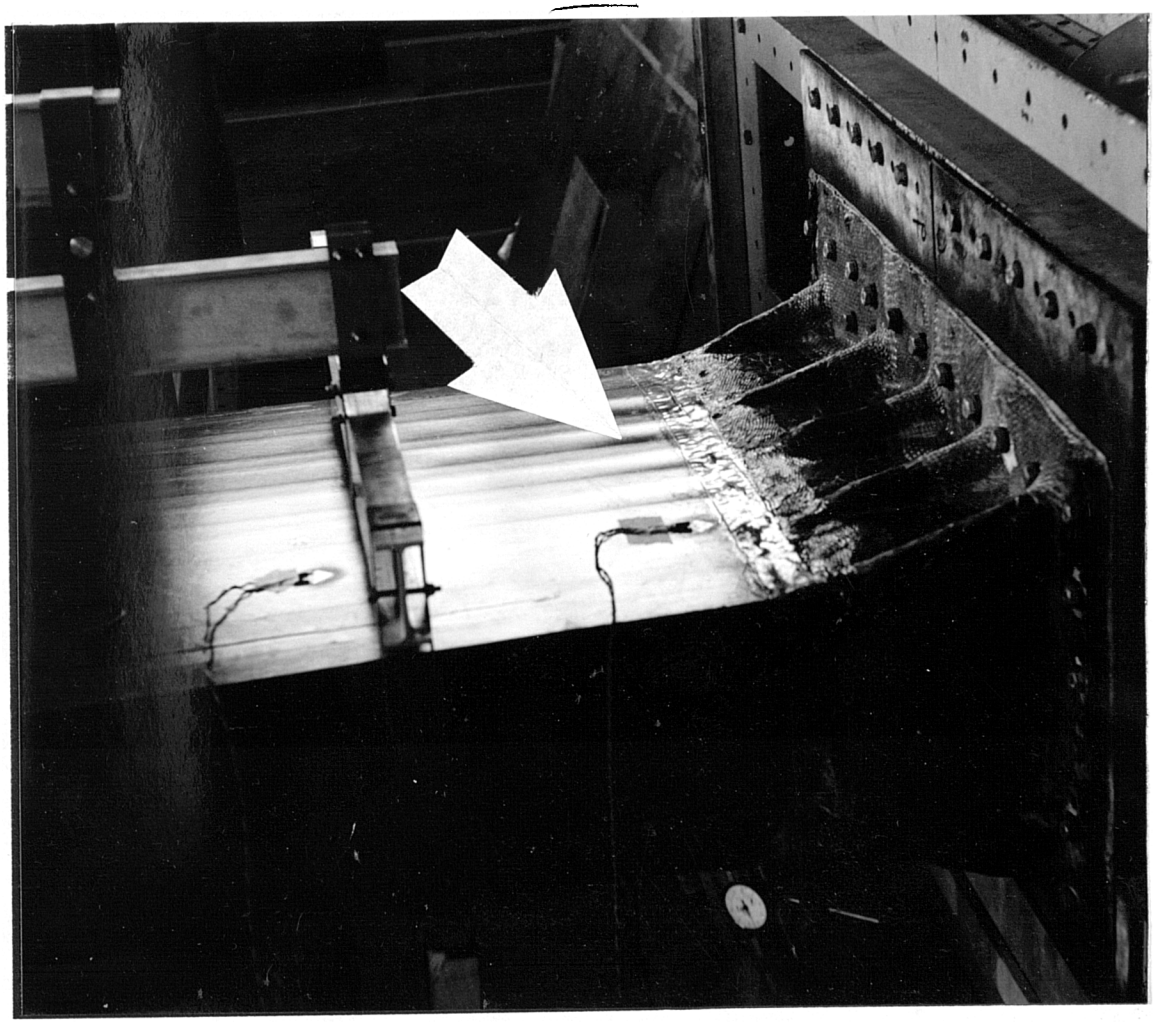

Figure 11.18.

A general view of the skin postbuckling from the top of the test rig.

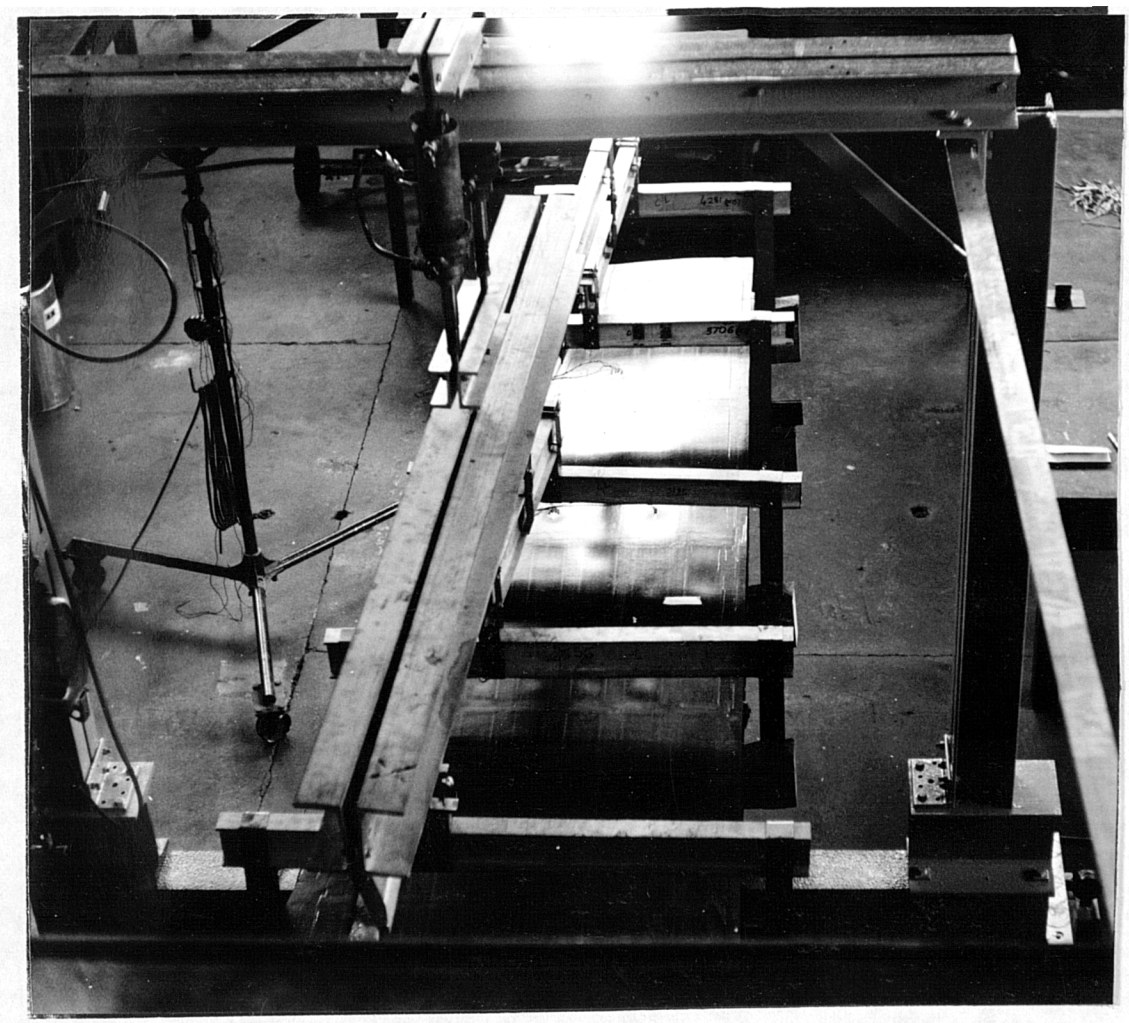

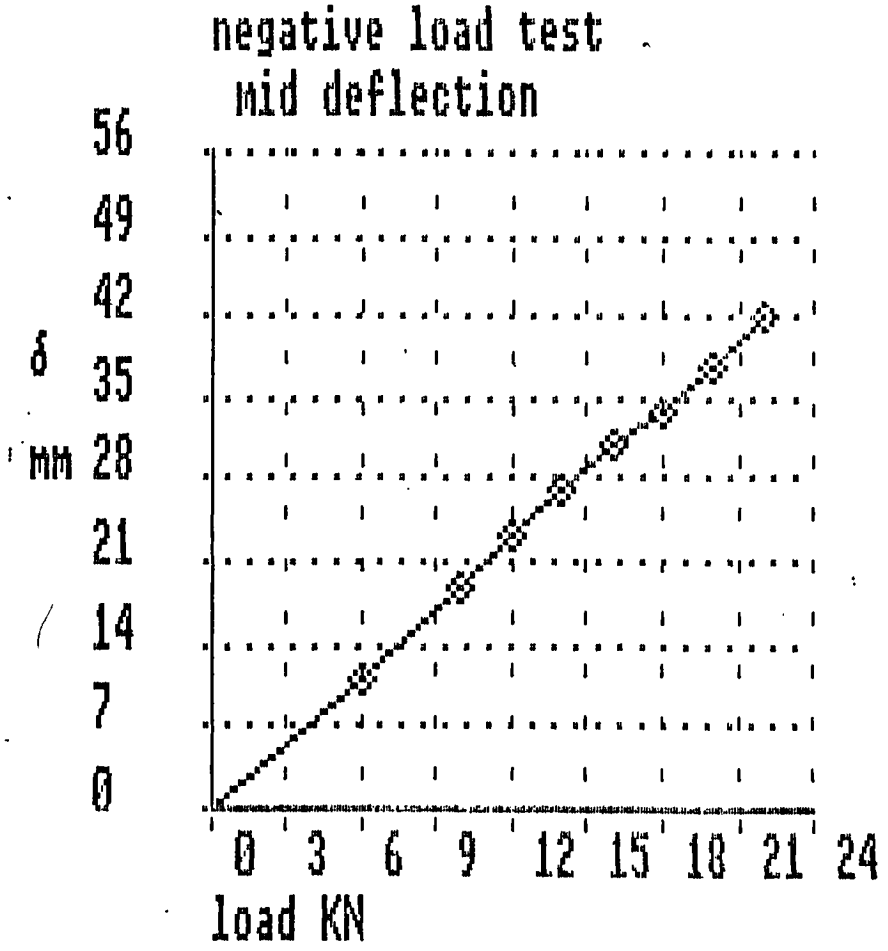

Figure 11.19.

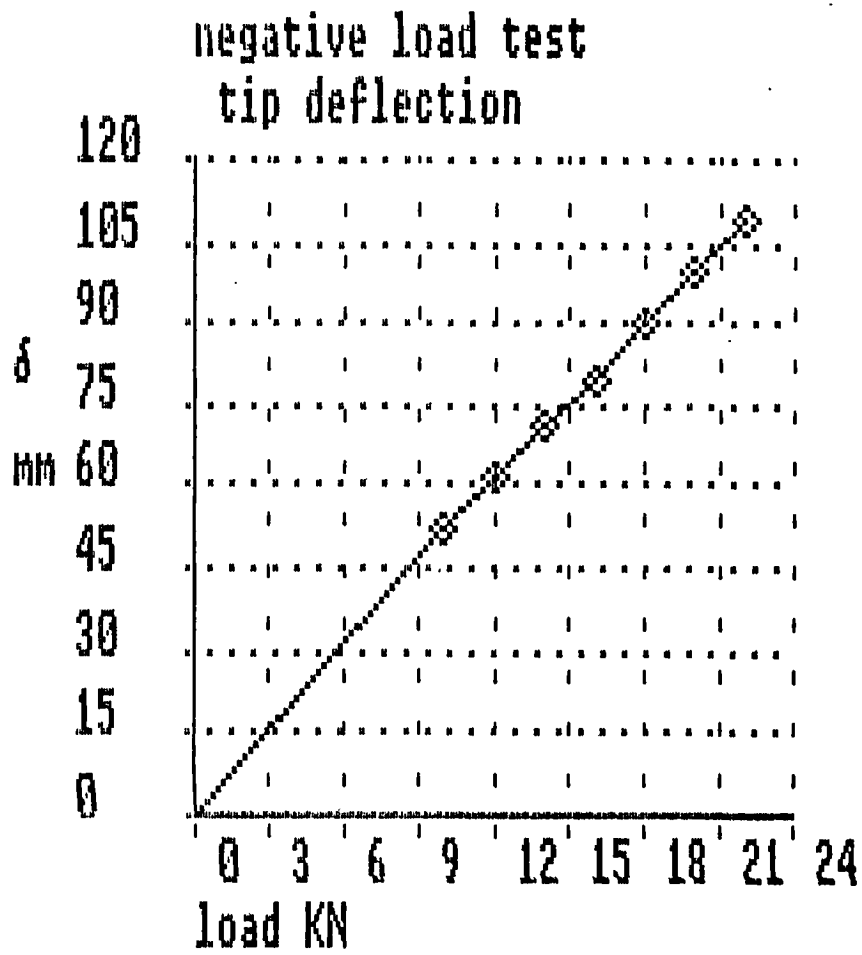

Figure 11.20.

this it was calculated (Appendix C) that the roll at zero 'G' case could be simulated by:

1) 5.35 kN at the aileron hinge station 3706.
2) 9.14 kN applied at the same load distribution as for positive or negative bending.

The 5.35 kN would normally be distributed between the aileron pickups. Three pickups are intended for the CFRP wing design, at stations 1981, 3706 and 4902. For this reason the testing was more severe than would be realised in practice.

11.5.1 Twisting of the wing.

The twisting of the wing due to aileron loads was measured by an inclinometer attached to the tip of the box. It was found that the twist was the same whether or not wing bending was combined with the aileron pickup load. The twist is shown in fig 11.21 for a range of aileron pickup loads. The maximum twist of 0.5 degrees shows that the wing is very stiff torsionally. Aileron reversal should not present a problem.

11.5.2 Strain gauge results.

Strain gauges 53 and 53A, axis 2, were monitored during the torsion tests. Shear postbuckling can be seen in the area of gauge 53 in fig 11.22. Fig 11.23 shows the strain recorded by gauges 53 and 53A. After bifurcation of inner and outer skin surface strains, a tension strain develops on both skin surfaces. The bifurcation marks the onset of shear postbuckling. After the skin panel has buckled in shear, a tension field develops.

11.6. Torsion combined with bending.

The most severe test to which the wing was subjected was the full roll case combined with + 0.67 x 13G in bending. The combined load was simulated by:

1) 5.35 kN applied to the aileron pickup at stn 3706.
2) 19.27 kN applied in lift through the whiffle tree.

Figure 11.21.

Washout measured at the wing tip for a load of 5.35 kN at the aileron pickup station 3706.

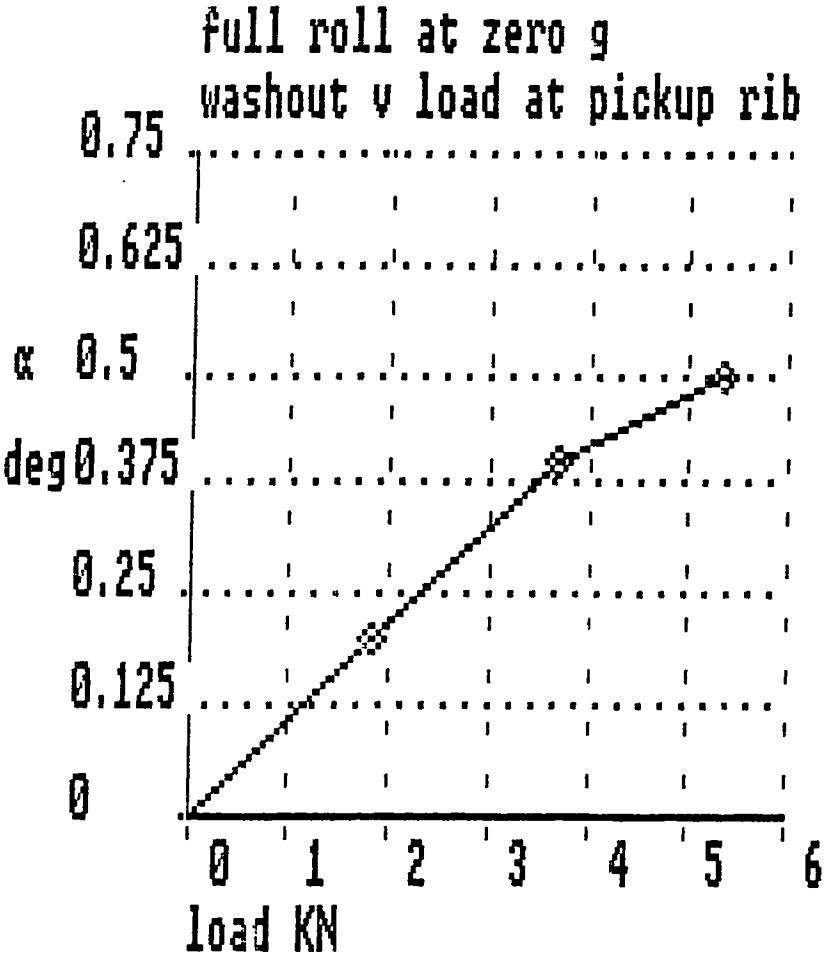

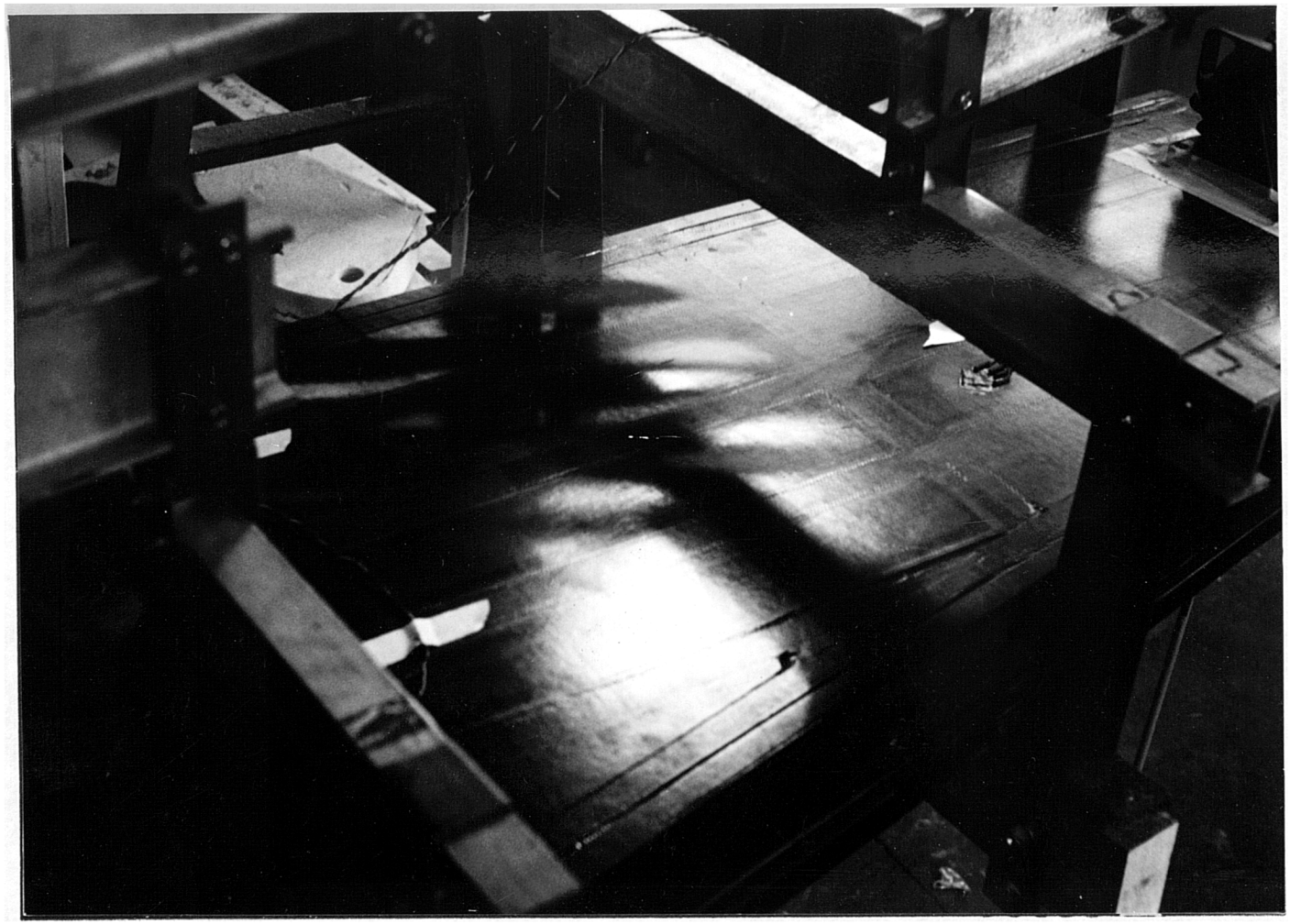

Figure 11.22.

The skin panels between stations 3131 and 3706 were postbuckled in snear that was caused by the aileron loading.

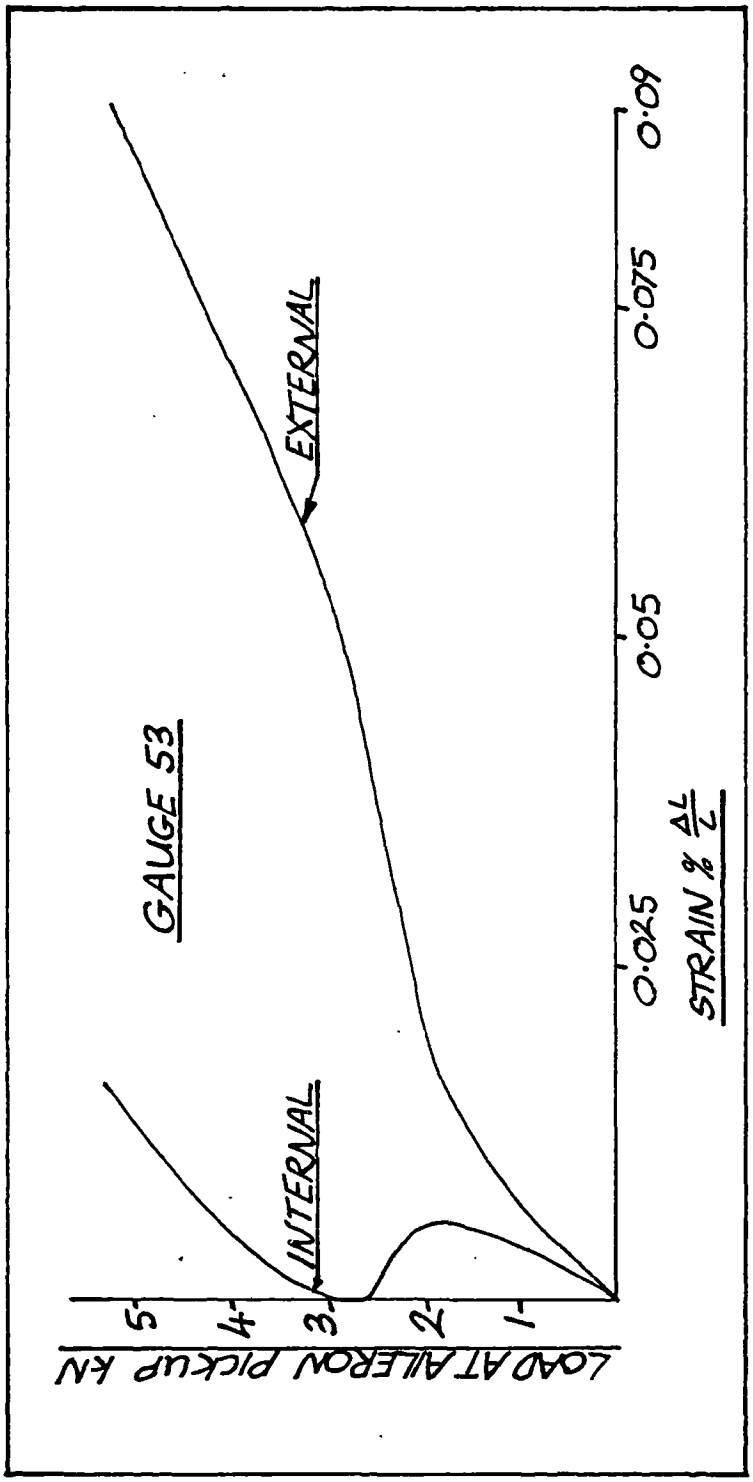

Figure 11.23.

Internal and external skin surfaces in tension due to shear at gauge 53. The effect caused by postbuckling in shear is shown.

The wing was subjected to the above case in the inverted position. Lift was applied via the whiffle tree in the same direction as the lift at the aileron pickup. The deflection at the tip caused by the combined load case is shown in fig. 11.24.

The combined load case had the effect of shifting the postbuckling inboard and towards the leading edge. Almost all of the wing compression surface was then postbuckled, as shown in fig 11.25.

11.7. A comparison of results with theory.

The wing box was compared with a linear finite element model of the structure for the positive load case at +13G. It can be seen from the table below that the F.E results predict lower strains than those recorded by test due to the effect of postbuckling. However, the results agree quite closely between rib stations 868 and 2556, where little or no buckling was recorded under test.

Postbuckled strains were calculated by taking the running loads acting on the skin structure from the F.E. model and applying the OPTIMIST program to predict the strains and the extent of postbuckling. The program predicted postbuckling ratios of 2 and 1.2, with buckle peak amplitudes of 1.5 and 1mm in bays 3131 and 3706 respectively. The strains predicted by OPTIMIST are shown in the OPT column in the table below.

Table 11.1 Comparison of test results with finite element model prediction.

Station mms	deflection mms		Typ. axial comp. strain %		
	FE	TST	FE	OPT	TST
431	0	0	.21	.21	.25
868	6	–	.14	.14	.13
1411	16	–	.11	.13	.16
1981	31	48	.07	.105	.11
2556	49	–	.07	.1	.1
3131	71	–	.05	.06	.06
3706	93	–	.02	.05	.07
4281	116	132	–	–	

Figure 11.24.

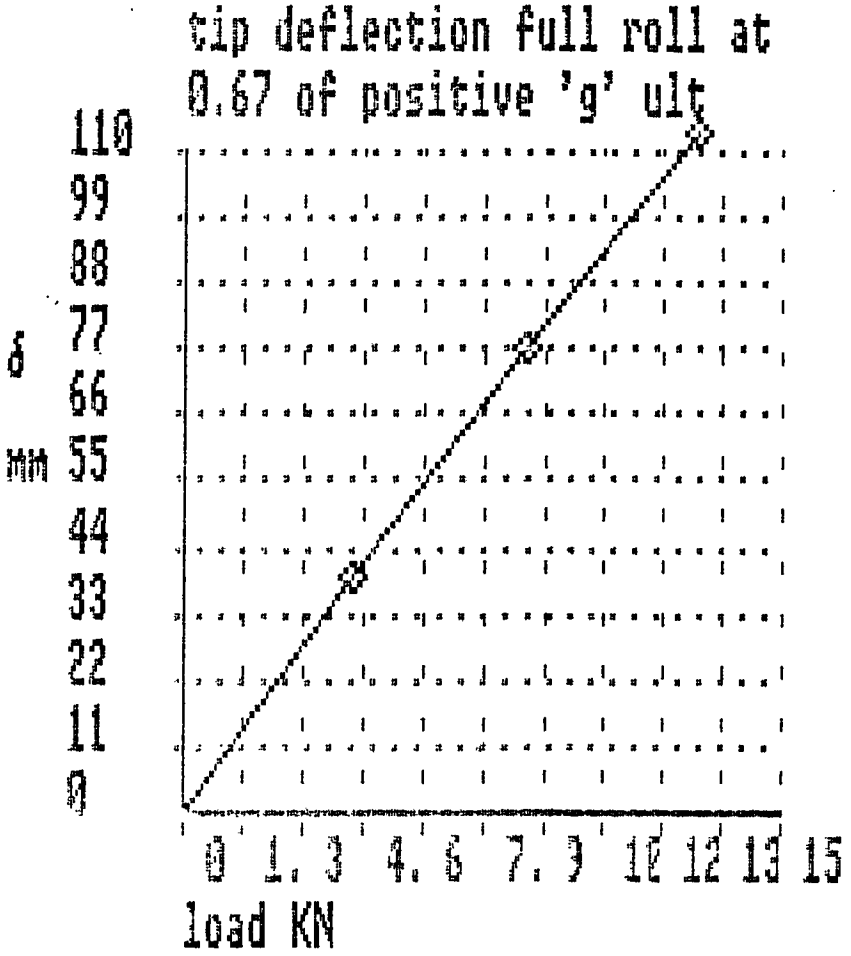
tip deflection full roll at
0.67 of positive 'g' ult
110
99
88
77
δ
66
mm 55
44
33
22
11
0
0
1.3
4.6
7.9
10
12
13
15
load KN

Figure 11.25.

When the wing was loaded in combined bending and torsion, virtually the whole top surface was postbuckled.

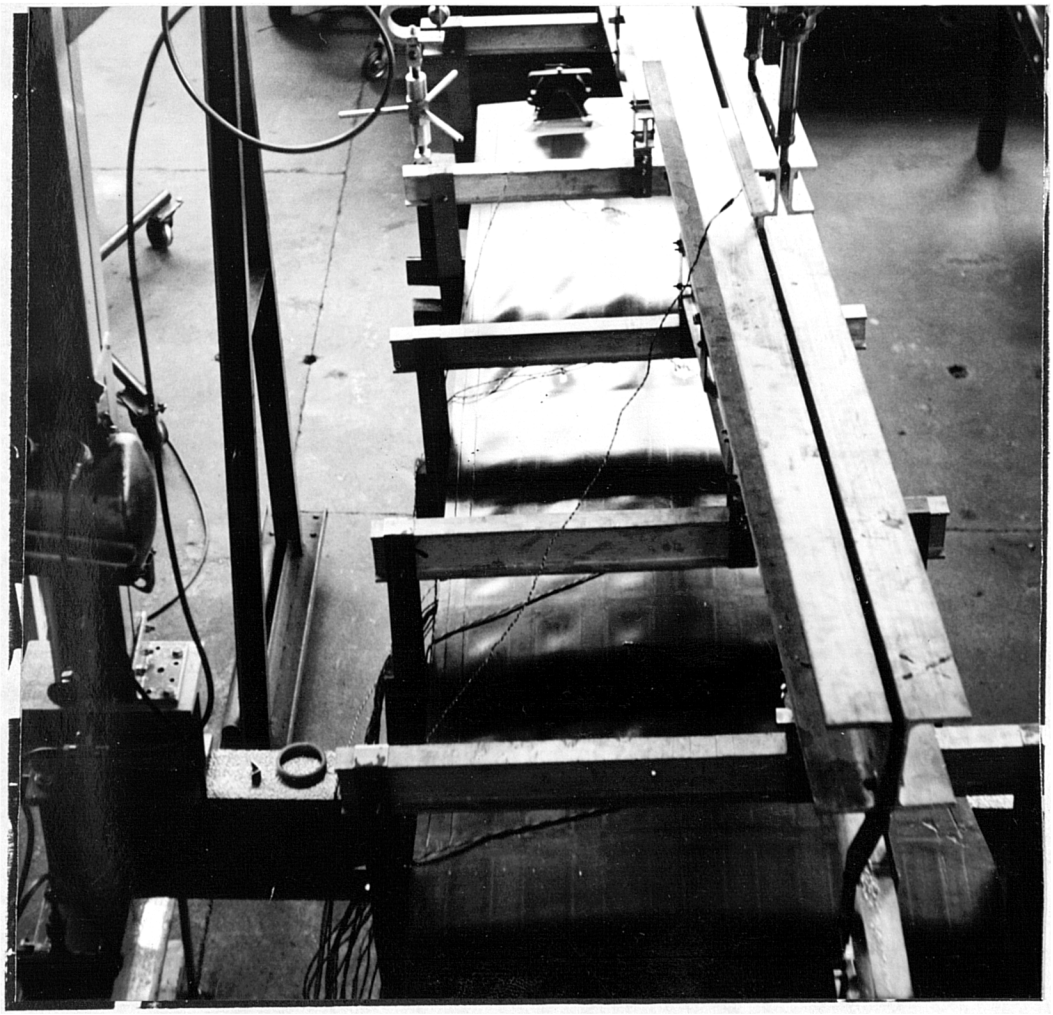

Chapter 12.
Discussion of the work and suggestions for further research.

12.1. General.

This project has demonstrated that a postbuckled CFRP wing structure is a practical proposition. The structure produced is 25% lighter than its aluminium alloy counterpart. The additional material has also added to the stiffness of the wing as well as the weight. Since the intended strain levels have not been reached at ultimate design loads, there is potential for removing some material. Because the wing is lighter, when considered as part of an overall aircraft design, the wing could be reduced in size. This would allow some further weight reductions.

12.2. Design Techniques.

The advantages and disadvantages of non-linear finite element analysis have been highlighted in chapter 3. The scope of the method, and the computer capability generally available will continue to grow. At present, the analysis time and computer usage restrict it to small problem areas.

Finite strip methods such as that proposed by Azzizan and Dawe (46) could be very useful. The finite strip technique could allow economical analysis of postbuckled prismatic panels. However, these techniques generally lose their appeal when shear loading is considered.

It is felt that there will always be a place for simplified design methods such as in chapter 4. These allow the designer some physical insight into the problem. They also give rapid results with modest computer usage. However, to work well they need valid assumptions, gained from non-linear finite element work, and from experiment.

12.3. Discussion of the design analysis developed in chapter 4.

12.3.1. Compression buckling.

Techniques for designing the structure have been

developed and shown to work. For compression buckling of stiffened panels, determination of the correct boundary conditions has been shown to be vital. The approach used in this work was to assume simple support at the stiffener centrelines.

With a torsionally flexible stiffener, this is a reasonable assumption. However, with the closed section stiffeners used, the panel tends to behave differently. It behaves as if simple support exists at the stiffener sidewall junctions. The incorporation of the anti-peel strip appears to change the boundary conditions further. It provides a more restrained edge condition. This may be due to the anti-peel strip stopping transverse shearing of the laminate at the stiffener junctions.

These effects tended to reduce the extent of the postbuckling in the wing. The extra material incorporated for joining features, and anti-peel strips also increased the wing stiffness. The results for stiffness fall between the two overall linear finite element analyses. The inner wing tends towards the non-buckled state, whilst the outer wing is more postbuckled.

12.3.2. The effect of shear.

Once local buckling has started, the effective width methods used in the design program give good results. At present, the effect of shear is considered only as an effect which reduces compression buckling loads. The presence of shear changes the nature of the postbuckling. The simplest assumption which could be made on the reduced stiffness in postbuckled shear is due to Wagner, described by Timoshenko (41). The approach assumes that only the tension fibres are taking load. If the shear stress is at $+-45^{o}$, the postbuckled stiffness becomes 0.5. This should give a satisfactory lower bound. It gives no information regarding buckle size and buckle induced strains however.

12.3.3. The calculation of weight.

This was based on a simple panel without having included the extra material required for practical manufacture. The extra material is needed to form joints and to allow an overlap at the stiffener caps.

This resulted in the weight being 8% greater than that originally predicted.

12.4. The construction method used.

The development of the co-cured skin/stiffener/rib flange system was worthwhile. Experience gained during the course of this programme has shown the need to match construction techniques to material characteristics carefully. Incorporation of special joining features into the construction has allowed the postbuckling to be exploited. The construction techniques developed also allow production without a very high tooling cost. The production cost is further reduced because the structure slots together, which allows it to be assembled without the use of expensive clamping jigs.

12.5. Tooling methods.

A method of tooling has been developed which could be used in production. The wing structure is quite economic in its tooling considering the extent of co-curing. Few major problems were experienced in moulding the wing. Those which did arise, such as the wrinkling near the spar joints, are discussed in chapter 7.

The existing tooling should last for an estimated 10-20 cycles. For volume production the quality of some of the tooling materials would need improvement. For example, a prepreg skin tool of high stiffness would be best for volume production. The rib tooling would also last longer in prepreg CFRP. The segmented stiffener tooling works well although it involves so many components. A reinforced rubber material such as 'Airpad' or 'Tygapad' could be used instead of the folded steel stiffener tool sections. Such a material would also be suitable for the stiffener runoff areas.

12.6. Testing.

The specially designed test rig has been successful. The wing has been tested and shown to meet or exceed the strength and stiffness of the original design. Postbuckled strength has been repeatedly demonstrated in all the load cases. The structure has

withstood application of the ultimate positive load case 19 times. No detectable change in its properties can be measured.

Exceeding the positive ultimate load case will probably result in failure at the root flange area. The acoustic emission equipment has recorded a high level of activity here. Failure at the root of the box is of little interest.

Because of the potential flange failure if the positive load case is exceeded, the box has been inverted. It should be possible to considerably exceed the negative load case of -9G without root flange failure occurring.

Currently, the box has been loaded to 25.1 kN negatively. This is approximately -12G. It seems quite feasible for the box to withstand the positive load case negatively. Taking the box to failure in negative loading will be of great interest for postbuckling research. This should preferably be done with multi-channel acoustic emission monitoring.

The torsion and torsion with bending cases are also interesting. Here, although the test cases have been covered, more data could be collected. This is especially true of the shear monitoring axes of the skin gauges. These areas need to be evaluated before the wing is tested to failure in negative bending.

12.7. Conclusions and suggestions for further work.

i. The effect of the anti-peel strips on the boundary conditions of the skin panels needs investigation. Some panel testing is required to see how this feature affects postbuckled strength.

ii. The effects of combined compression and shear in postbuckling are not well understood. Combined loads need some more investigation by testing the wing structure. Non-linear finite element techniques could be used to model selected panels under this loading.

iii. From the above data a simple design method, such as that based on Timoshenko (41), needs evaluation. A means of predicting postbuckling-induced bending strain then needs to be developed for shear loading.

iv. Many of the design features for postbuckling are also good for impact damage tolerance. For example, the skin/stiffener and skin/spar joints have been

designed to resist delamination. Also, the multiple load paths should be able to divert the load around a damaged area. The woven material for the outer plies was selected partly for its resistance to delamination. The wing structure could be used to investigate damage tolerance with postbuckling.

v. The slotted joints for a subsequent structure should incorporate a lead-in feature, which would allow much easier assembly.

vi. The use of hot-curing paste adhesives allows more time for assembly. The joint strength may also be better.

vii. Because the spar and rib shear webs are not directly connected, assembly has been greatly simplified.

References.

1. Buckling, postbuckling and crippling of materially nonlinear laminated composite plates.
R.R. Arnold and J. Mayers, Stanford University. International Journal of Solids & Structures, Vol 20, No9/10, pp863-880, 1984.

2. Postbuckling of Long Orthotropic Plates in Combined Shear and Compression. Manuel Stein, Nasa Langley Research Centre. AIAA Journal, Vol 23,No.5, 1984.

3. Compressive Buckling Strength of Graphite/Epoxy Laminated Curved Panels. Shigeo Kobayashi et al, University of Tokyo. Proceedings of ICAS conference, London, September 1986.

4. On the Use of The Effective Width Concept for Composite Plates. J. Rhodes and I.H. Marshall. Composite Structures, Applied Science Publishers, 1981.

5. Buckling of Rectangular Specially Orthotropic Plates. ESDU 80023. Engineering Sciences Data Unit, 1980.

6. Composites Design Course Notes No. Des 8050. R. Butler. Cranfield Institute of Technology 1984.

7. Composite Engineering Laminates. Deitz, M. I. T. press.

8. Anisotropic Plates. S.G. Lekhnitski, Gordon & Breach, 1968.

9. Design of Stiffened Composite Panels in the Post-Buckling Range. Dickson, Cole & Wang, Fibrous Composites in Structural Design. Lenoe et al, Plenum Press, 1980.

10. Recent Developments in the Design, Testing and Impact Damage Tolerance of Stiffened Composite Panels. Willams, Anderson et al, Nasa Langley Research Centre. Fibrous Composites in Structural Design, Lenoe et al, Plenum Press, 1980.

11. PASCO Panel Analysis and Sizing Code, Capability and Analytical Foundations, Anderson, Henessy & Stroud. Nasa TM 80181 , 1980.

12. Users' guide to VIPASA. F.W. Williams. Department of Civil Engineering,University of Birmingham, 1973.

13. International Journal of Numerical Methods in Engineering, R.J. Plank and W.H. Wittrick, vol. 8, page 323, 1974.

14. Aeronautical Quarterly, G.J. Turvey and W.H. Wittrick, vol 24, no.1, 1973.

15. Buckling and Vibration of Anisotropic or Isotropic Plate Assemblies Under Combined Loadings. W.H. Wittrick, International Journal of Mechanical Sciences, Vol 16, p209, 1974.

16. The Design, Manufacture and Test of Stiffened Aircraft Compression Panels Using Advanced Materials. G. Belgrano, Cranfield Institute of Technology Structural Design Msc. Thesis, 1983.

17. Initial Buckling Performance of some CFRP Structures and the Validity of Classical Plate Theory Assumptions. M.B. Snell. RAE Technical Report 79128. 1979.

18. The Behaviour in Compression Buckling of Stability Critical Curved Panels of Carbon Fibre Reinforced Plastic. M.B. Snell, RAE Technical Report 84052, May 1984.

19. Compression Buckling of Curved Stiffened CFRP Panels, L. Hussain, Cranfield Institute of Technology Msc. Thesis, 1984.

20. Buckling Loads for Stiffened Panels Subjected to Combined Longitudinal Compression and Shear Loadings: Results Obtained With PASCO, EAL and STAGS Computer Programs. W.J. Stroud, Greene & Anderson. NASA TM-83194, 1981.

21. Initial Buckling of Curved Panels of Generally Layered Composite Materials. Y. Zhang and F.L. Matthews, International Journal of Composite Structures, 1, January 1983.

22. A Finite Strip Method for the Post-Locally Buckled Analysis of Plate structures. T.R. Graves Smith and S. Sridharan. International Journal of Mechanical Science ,vol 20, pp833-842. 1978.

23. Non-Linear Analysis of Thin Sections in Compression. G. J. Hancock. Structural Division, proceedings of the American Society of Civil Engineers, vol 107, no. st3, March, 1981.

24. The Finite Element Method, 3rd. Edition, O.C. Zienkiewicz. McGraw-Hill. 1977.

25. LUSAS User's Manual. Finite Element Analysis Ltd, 1986.

26. The Compression Buckling Behaviour of Cylindrically Curved Unstiffened CFRP Panels Including the Effect of Imperfections. M.B. Snell. RAE Technical Report 86048. 1986.

27. The Design of an Aerobatic Aircaft. Potter and Ward. Msc thesis, Cranfield Institute of Technology, 1969.

28. Design note 23, wing shear force and bending moment diagrams for the Cranfield A1. Cranfield Institute of Technology.

29. Design note 16, A1 manoeuvre envelopes.

30. Design note 21, tail loads.

31. Design note 22, ground loads.

32. Design note 24, wing torque cases.

33. Design note 25, tail stressing.

34. Design note 26, yawed flight conditions.

35. Design note 148, longitudinal balance.

36. An Assessment of the Potential of Woven CFRP for High Performance Applications. P. Curtiss, S.M. Bishop. Composites, volume 15 no.4.

37. Structural Composites Airworthiness in Civil Aircraft. J.W. Bristow. Proceedings of 6th Sampe conference, Netherlands, 1985.

38. The WEIGHTS Computer Program. N. Murphy. Phd thesis, to be submitted 1987.

39. Scarf Repair Joints in C F Reinforced Plastic Strips. J.P.H. Webber. Journal of Adhesion, vol 12 pp. 257-281, 1981.

40. Weight-Strength Analysis of Aircraft Structures. F. Shanley. Mc.Graw Hill, 1952.

41. The Theory of Elastic Stability. S. Timoshenko,Mc Graw Hill, 1961.

42. Translaminar Reinforcement of Epoxy Impregnated Woven Carbon Fibre by Stitching and its Effect on Strength. T.G.N. Sleath. Msc Thesis, Cranfield Institute of Technology, 1986.

43. Design of the Spar to Wing Skin Joint, R.Copes and R. Pipes. Fibrous Composites in Structural Design, Lenoe et al. Plenum Press, 1978.

44. A1 Aerobatic Aircraft - Wing Proof Test. Test Report TR/A1/17. Cranfield Institute of Technology, 1978.

45. Postbuckling Failure of Composite Panels. Buskell, Davies and Stephens. Imperial College of Science and Technology, London. Composite Structures 3, I. Marshall. Elsevier, 1983.

46. Post Buckled Stiffness of Rectangular Orthotropic Composite Laminates. Z.G. Azizan and D.J. Dawe. Composite Structures 4, I. Marshall. Elsevier, 1987.

Appendix A.

Data input for LUSAS finite element models.

i) Non-linear finite element analysis of a stiffened CFRP panel with two foam-filled hat section stiffeners. This model and the results are described in chapter 3.

ii) Linear finite element model of the whole wing box. This data input contains all the co-ordinates for the structure. A shortened version is presented, as the input is produced by the WEIGHTS software. Since each individual element and its topology are defined separately, the full data is too voluminous to include here. The model is described in chapter 5.

```
CTHIS IS  THE DATA INPUT USED FOR A GEOMETRICALLY NON-LINEAR BUCKLING
ANALYSIS OF A STIFFENED CARBON FIBRE COMPOSITE PANEL SUBJECT TO
AXIAL COMPRESSION, USING LUSAS. THIS IS A FINITE ELEMENT MODEL OF PANEL C2
DESCRIBED IN REFERENCE 1.]
CNOTE- ALL COMMENTS ENCLOSED IN SQUARE BRACKETS THUS [] ARE NOT PART OF THE
INPUT DATA REQUIRED. THE COMPUTER USED IS A DEC VAX750 WITH DIGITAL VT101
TERMINALS.]

PROBLEM TITLE PANEL C2 SEMILOOF NONLINEAR
UNITS N MM
OPTIONS 12  32 34 40 80 87 133 [ THESE OPTIONS ARE USED FOR NON-LINEAR ANALYSIS]
QSL8 ELEMENT TOPOLOGY  [ THESE ARE 8-NODED SEMILOOF THIN SHELL ELEMENTS]
FIRST 1 1 2 3 23 34 33 32 22 [INCREMENTAL DATA GENERATION IS USED WHERE PRACTICABLE]
INC 13 31 31 31 31 31 31 31 31 10
FIRST 2 3 6 10 26 41 37 34 23
INC 13 31 31 31 31 31 31 31 31 10 [ NOTE ELEMENT TOPOLOGY HERE DEFINES
FIRST 4 3 4 5 24 36 35 34 23          LOCAL AXIS SYSTEM FOR MATERIAL ORTHOTROPY]
INC 13 31 31 31 31 31 31 31 31 10
FIRST 5 5 7 8 25 39 38 36 24
INC 13 31 31 31 31 31 31 31 31 10
FIRST 6 8 9 10 26 41 40 39 25
INC 13 31 31 31 31 31 31 31 31 10
FIRST 7 10 11 12 27 43 42 41 26
INC 13 31 31 31 31 31 31 31 31 10
FIRST 8 12 15 19 30 50 46 43 27
INC 13 31 31 31 31 31 31 31 31 10
FIRST 10 12 13 14 26 45 44 43 27
INC 13 31 31 31 31 31 31 31 31 10
FIRST 11 14 16 17 29 48 47 45 28
INC 13 31 31 31 31 31 31 31 31 10
FIRST 12 17 18 19 30 50 49 48 29
INC 13 31 31 31 31 31 31 31 31 10
FIRST 13 19 20 21 31 52 51 50 30
INC 13 31 31 31 31 31 31 31 31 10
HX20 ELEMENT TOPO  [ THESE ARE SOLID 20 NODED ELEMENTS USED FOR STIFFENER CORES]
FIRST 3 5 7 8 9 10 6 3 4 24 25 26 23 36 38 39 40 41 37 34 35
INC 13 31 31 31 31 31 31 31 31 31 31 31 31 31 31 31 31 31 31 31 10
FIRST 9 14 16 17 18 19 15 12 13 28 29 30 27 45 47 48 49 50 46 43 44
INC 13 31 31 31 31 31 31 31 31 31 31 31 31 31 31 31 31 31 31 31 10
NODE COORDINATES  [ DIMENSIONS ARE IN MILLIMETRES ]
1 0 0 0
311 0 473 0
2 12.5 0 0
312 12.5 473 0
3 25 0 0
313 25 473 0
4 27.75 0  12.7
314 27.75 473 12.7
5 30.5 0 25.4
315 30.5 473 25.4
6 40.5 0 0
316 40.5 473 0
7 40.5 0 25.4
317 40.5 473 25.4
8 50.5 0 25.4
318 50.5 473 25.4
9 53.25 0 12.7
319 53.25 473 12.7
10 56 0 0
320 56 473 0
11 81 0 0
321 81 473 0
12 106 0 0
```

```
322 106 473 0
13 108.75 0 12.7
323 108.75 473 12.7
14 111.5 0 25.4
324 111.5 473 25.4
15 121.5 0 0
325 121.5 473 0
16 121.5 0 25.4
326 121.5 473 25.4
17 131.5 0 25.4
327 131.5 473 25.4
18 134.25 0 12.7
328 134.25 473  12.7
19 137 0 0
329 137 473 0
20 149.5 0 0
330 149.5 473 0
21 162 0 0
331 162 473 0
22 0 23.65 0
301 0 449.35 0
23 25 23.65 0
302 25 449.35 0
24 30.5 23.65 25.4
303 30.5 449.35 25.4
25 50.5 23.65 25.4
304 50.5 449.35 25.4
26 56 23.65 0
305 56 449.35 0
27 106 23.65 0
306 106 449.35 0
28 111.5 23.65 25.4
307 111.5 449.35 25.4
29 131.5 23.65 25.4
308 131.5 449.35 25.4
30 137 23.65 0
309 137 449.35 0
31 162 23.65 0
310 162 449.35 0
SPACING
1 311 31 10*47.3 CNODES ARE EQUALLY SPACED FROM TOP TO BOTTOM OF MESH 1
2 312 31 10*47.3
3 313 31 10*47.3
4 314 31 10*47.3
5 315 31 10*47.3
6 316 31 10*47.3
7 317 31 10*47.3
8 318 31 10*47.3
9 319 31 10*47.3
10 320 31 10*47.3
11 321 31 10*47.3
12 322 31 10*47.3
13 323 31 10*47.3
14 324 31 10*47.3
15 325 31 10*47.3
16 326 31 10*47.3
17 327 31 10*47.3
18 328 31 10*47.3
19 329 31 10*47.3
20 330 31 10*47.3
21 331 31 10*47.3
22 301 31 9*47.3
23 302 31 9*47.3
```

```
24 303 31 9*47.3
25 304 31 9*47.3
26 305 31 9*47.3
27 306 31 9*47.3
28 307 31 9*47.3
29 308 31 9*47.3
30 309 31 9*47.3
31 310 31 9*47.3
QSL8 GEOMETRIC PROPERTIES (NOTE UNIT THICKNESS USED WHEN USING SHELL RIGIDITIES )
1 323 1 1 1 1 1 1 1 1 1
 MATERIAL PROPERTIES (THESE ARE ISOTROPIC PROPERTIES FOR STIFFENER CORES )
3 120 13 92 .3 70E-9 0
9 126 13 92 .3 70E-9 0
SHELL RIGIDITIES (THESE ARE FOR THE ORTHOTROPIC ELEMENTS )

C THE FOLLOWING ARE PROPERTIES OF THE MAIN SKIN PANELS )
1 118 13 74E3 43E3 35E3 32E3 .62E3 .66E3 .54E3 .5E3  90 0 0 0 0 0 0 0 0
2 119 13 74E3 43E3 35E3 32E3 .68E3 .66E3 .54E3 .5E3  90 0 0 0 0 0 0 0 0
7 124 13 74E3 43E3 35E3 32E3 .68E3 .66E3 .54E3 .5E3  90 0 0 0 0 0 0 0 0
8 125 13 74E3 43E3 35E3 32E3 .68E3 .66E3 .54E3 .5E3  90 0 0 0 0 0 0 0 0
13 130 13 74E3 43E3 35E3 32E3 .68E3 .66E3 .54E3 .5E3  90 0 0 0 0 0 0 0 0

C THE FOLLOWING ARE FOR THE STIFFENER VERTICAL WALLS )
4 121 13 20E3 20E3 17E3 16E3 .43E3 .43E3 .35E3 .33E3 90 0 0 0 0 0 0 0 0
6 123 13 20E3 20E3 17E3 16E3 .43E3 .43E3 .35E3 .33E3 90 0 0 0 0 0 0 0 0
10 127 13 20E3 20E3 17E3 16E3 .43E3 .43E3 .35E3 .33E3 90 0 0 0 0 0 0 0 0
12 129 13 20E3 20E3 17E3 16E3 .43E3 .43E3 .35E3 .33E3 90 0 0 0 0 0 0 0 0

C THE FOLLOWING ARE FOR THE STIFFENER CAPS )
5 122 13 15E4 29E3 21E3 18E3 .19E5 .88E4 .7E4 .64E4 90 0 0 0 0 0 0 0 0
11 128 13 15E4 29E3 21E3 18E3 .19E5 .88E4 .7E4 .64E4 90 0 0 0 0 0 0 0 0

SUPPORT NODES ( THE END NODES ARE FULLY RESTRAINED AND DISPLACED 1MM INITIALLY )
1 21 1 R R R R R 0 0 0 0
311 331 1 R R R R R 0 -1 0 0 0
52 300 31 F F R R R 0 0 0 0 0
31 310 31 F F R R R 0 0 0 0 0
22 301 31 F F R R R 0 0 0 0 0
32 280 31 F F R R R 0 0 0 0 0

LOAD CASE ( DUMMY LOAD OF ZERO TO SATISFY THE SYSTEM )
GL
311 331 1 0 0 0 0
ELEMENT OUTPUT CONTROL ( SUPPRESSES OUTPUT FOR ALL ELEMENTS )
1 13 1 1 0
 NONLINEAR CONTROL ( PARAMETERS FOR NON LINEAR ANALYSIS STARTING WITH NUMBER OF
 10 5 1 0 0 1 1 0 1  ITERATIONS PER INCREMENT )
 PLOT FILE ( TO OBTAIN THE FORM AT THE INITIAL DISPLACEMENT )

SUPPORT NODES ( EACH SUBSEQUENT CYCLE INCREMENTS THE DISPLACEMENT .05MM. TO SAVE
1 21 1 R R R R R 0 0 0 0 0           TIME, THIS IS ONLY DONE OVER THE RANGE FROM
311 331 1 R R R R R 0 -.05 0 0 0     JUST BEFORE BUCKLING TO AS FAR INTO THE
52 300 31 F F R R R 0 0 0 0 0        POST BUCKLED RANGE AS DESIRED. PLOT FILES
31 310 31 F F R R R 0 0 0 0 0        ARE NOT PRODUCED FOR EACH INCREMENT TO SAVE
22 301 31 F F R R R 0 0 0 0 0        SPACE AND TO REDUCE RUN TIME.)
32 290 31 F F R R R 0 0 0 0 0
LOAD CASE
GL
311 331 1 0 0 0 0 0
SUPPORT NODES
1 21 1 R R R R R 0 0 0 0 0
311 331 1 R R R R R 0 -.05 0 0 0
52 300 31 F F R R R 0 0 0 0 0
```

```
 31 310 31 F F R R R 0 0 0 0 0
 22 301 31 F F R R R 0 0 0 0 0
 32 280 31 F F R R R 0 0 0 0 0
 LOAD CASE
 CL
 311 331 1 0 0 0 0 0
 SUPPORT NODES
 1 21 1 R R R R R C 0 0 0 C
 311 331 1 R R R R R 0 -.05 0 0 0
 52 300 31 F F R R R 0 0 0 0 0
 31 310 31 F F R R R 0 0 0 0 0
 22 301 31 F F R R R 0 0 0 0 0
 32 280 31 F F R R R 0 0 0 0 0
 LOAD CASE
 CL
 311 331 1 0 0 0 0 0
 PLOT FILE
 SUPPORT NODES
 1 21 1 R R R R R C 0 0 0 C
 311 331 1 R R R R R 0 -.05 0 0 0
 52 300 31 F F R R R 0 0 0 0 0
 31 310 31 F F R R R 0 0 0 0 0
 22 301 31 F F R R R 0 0 0 0 0
 32 280 31 F F R R R 0 0 0 0 0
 LOAD CASE
 CL
 311 331 1 0 0 0 0 0
 SUPPORT NODES
 1 21 1 R R R R R C 0 0 0 C
 311 331 1 R R R R R 0 -.05 0 0 0
 52 300 31 F F R R R 0 0 0 0 0
 31 310 31 F F R R R 0 0 0 0 0
 22 301 31 F F R R R 0 0 0 0 0
 32 280 31 F F R R R 0 0 0 0 0
 LOAD CASE
 CL
 311 331 1 0 0 0 0 0
 SUPPORT NODES
 1 21 1 R R R R R C 0 0 0 C
 311 331 1 R R R R R 0 -.05 0 0 0
 52 300 31 F F R R R 0 0 0 0 0
 31 310 31 F F R R R 0 0 0 0 0
 22 301 31 F F R R R 0 0 0 0 0
 32 280 31 F F R R R 0 0 0 0 0
 LOAD CASE
 CL
 311 331 1 0 0 0 0 0
 PLOT FILE
 SUPPORT NODES
 1 21 1 R R R R R C 0 0 0 C
 311 331 1 R R R R R 0 -.05 0 0 0
 52 300 31 F F R R R 0 0 0 0 0
 31 310 31 F F R R R 0 0 0 0 0
 22 301 31 F F R R R 0 0 0 0 0
 32 280 31 F F R R R 0 0 0 0 0
 LOAD CASE
 CL
 311 331 1 0 0 0 0 0
 SUPPORT NODES
 1 21 1 R R R R R C 0 0 0 C
 311 331 1 R R R R R 0 -.05 0 0 0
 52 300 31 F F R R R 0 0 0 0 0
 31 310 31 F F R R R 0 0 0 0 0
```

```
22 301 31 F F R R R 0 0 0 0 0
32 280 31 F F R R R 0 0 0 0 0
LOAD CASE
CL
311 331 1 0 0 0 0 0
SUPPORT NODES
1 21 1 R R R R R C 0 C 0 C
311 331 1 R R R R R 0 -.05 0 0 0
52 300 31 F F R R R 0 0 0 0 0
31 310 31 F F R R R 0 0 0 0 0
22 301 31 F F R R R 0 0 0 0 0
32 280 31 F F R R R 0 0 0 0 0
LOAD CASE
CL
311 331 1 0 0 0 0 0
PLOT FILE
SUPPORT NODES
1 21 1 R R R R R C 0 C 0 C
311 331 1 R R R R R 0 -.05 0 0 0
52 300 31 F F R R R 0 0 0 0 0
31 310 31 F F R R R 0 0 0 0 0
22 301 31 F F R R R 0 0 0 0 0
32 280 31 F F R R R 0 0 0 0 0
LOAD CASE
CL
311 331 1 0 0 0 0 0
SUPPORT NODES
1 21 1 R R R R R C 0 C 0 C
311 331 1 R R R R R 0 -.05 0 0 0
52 300 31 F F R R R 0 0 0 0 0
31 310 31 F F R R R 0 0 0 0 0
22 301 31 F F R R R 0 0 0 0 0
32 280 31 F F R R R 0 0 0 0 0
LOAD CASE
CL
311 331 1 0 0 0 0 0
SUPPORT NODES
1 21 1 R R R R R C 0 0 0 C
311 331 1 R R R R R 0 -.05 0 0 0
52 300 31 F F R R R 0 0 0 0 0
31 310 31 F F R R R 0 0 0 0 0
22 301 31 F F R R R 0 0 0 0 0
32 280 31 F F R R R 0 0 0 0 0
LOAD CASE
CL
311 331 1 0 0 0 0 0
PLOT FILE
SUPPORT NODES
1 21 1 R R R R R C 0 C 0 C
311 331 1 R R R R R 0 -.05 0 0 0
52 300 31 F F R R R 0 0 0 0 0
31 310 31 F F R R R 0 0 0 0 0
22 301 31 F F R R R 0 0 0 0 0
32 280 31 F F R R R 0 0 0 0 0
LOAD CASE
CL
311 331 1 0 0 0 0 0
PLOT FILE
SUPPORT NODES
1 21 1 R R R R R C 0 0 0 C
311 331 1 R R R R R 0 -.05 0 0 0
52 300 31 F F R R R 0 0 0 0 0
31 310 31 F F R R R 0 0 0 0 0



22 301 31 F F R R R 0 0 0 0 0
32 280 31 F F R R R 0 0 0 0 0
LOAD CASE
CL
311 331 1 0 0 0 0 0
PLOT FILE
END
```

Coordinates, geometric properties, material properties and support nodes for the linear finite element model.

NODE COORDINATES

NODE NO.	COORDINATE IN X-DIRECTION	COORDINATE IN Y-DIRECTION	COORDINATE IN Z-DIRECTION

GLOBAL CARTESIAN COORDINATES

NODE NO.	COORDINATE IN X-DIRECTION	COORDINATE IN Y-DIRECTION	COORDINATE IN Z-DIRECTION
1	0.000000E+00	-0.812300	0.182090
2	0.000000E+00	-0.720000	0.176040
3	0.000000E+00	-0.600000	0.166014
4	0.000000E+00	-0.480000	0.153890
5	0.000000E+00	-0.360000	0.140030
6	0.000000E+00	-0.240000	0.124676
7	0.000000E+00	-0.120000	0.107990
8	0.000000E+00	0.000000E+00	0.900000E-01
9	0.000000E+00	0.000000E+00	-0.681400E-01
10	0.000000E+00	-0.120000	-0.807400E-01
11	0.000000E+00	-0.240000	-0.921200E-01
12	0.000000E+00	-0.360000	-0.102180
13	0.000000E+00	-0.480000	-0.110700
14	0.000000E+00	-0.600000	-0.117500
15	0.000000E+00	-0.720000	-0.122290
16	0.000000E+00	-0.812300	-0.124240
17	0.431000	-0.812800	0.168354
18	0.431000	-0.720000	0.166619
19	0.431000	-0.600000	0.156926
20	0.431000	-0.480000	0.146626
21	0.431000	-0.360000	0.134258
22	0.431000	-0.240000	0.120168
23	0.431000	-0.120000	0.104600
24	0.431000	0.000000E+00	0.876483E-01
25	0.431000	0.000000E+00	-0.663906E-01
26	0.431000	-0.120000	-0.787901E-01
27	0.431000	-0.240000	-0.898690E-01
28	0.431000	-0.360000	-0.994784E-01
29	0.431000	-0.480000	-0.107333
30	0.431000	-0.600000	-0.113129
31	0.431000	-0.720000	-0.116399
32	0.431000	-0.812800	-0.116661
33	0.868000	-0.812800	0.154457
34	0.868000	-0.720000	0.153046
35	0.863000	-0.600000	0.147697
36	0.868000	-0.480000	0.139228
37	0.868000	-0.360000	0.128357
38	0.868000	-0.240000	0.115537
39	0.868000	-0.120000	0.101090
40	0.868000	0.000000E+00	0.851792E-01
41	0.868000	0.000000E+00	-0.645573E-01
42	0.868000	-0.120000	-0.767604E-01
43	0.868000	-0.240000	-0.875418E-01
44	0.868000	-0.360000	-0.967038E-01
45	0.868000	-0.480000	-0.103895
46	0.868000	-0.600000	-0.108688
47	0.868000	-0.720000	-0.110434
48	0.868000	-0.812800	-0.109005
49	1.41100	-0.812800	0.137149
50	1.41100	-0.720000	0.138634
51	1.41100	-0.600000	0.136202
52	1.41100	-0.480000	0.130014
53	1.41100	-0.360000	0.121008
54	1.41100	-0.240000	0.109768
55	1.41100	-0.120000	0.967186E-01
56	1.41100	0.000000E+00	0.821041E-01
57	1.41100	0.000000E+00	-0.622739E-01
58	1.41100	-0.120000	-0.742327E-01
59	1.41100	-0.240000	-0.846435E-01
60	1.41100	-0.360000	-0.932482E-01
61	1.41100	-0.480000	-0.996127E-01
62	1.41100	-0.600000	-0.103157
63	1.41100	-0.720000	-0.103005
64	1.41100	-0.812800	-0.994707E-01
65	1.98100	-0.812800	0.119000
66	1.98100	-0.720000	0.123500
67	1.98100	-0.600000	0.124110
68	1.98100	-0.480000	0.120300
69	1.98100	-0.360000	0.113240
70	1.98100	-0.240000	0.103650
71	1.98100	-0.120000	0.920600E-01
72	1.98100	0.000000E+00	0.788000E-01
73	1.98100	0.000000E+00	-0.598100E-01

74	1.98100	-0.120000	-0.715200E-01
75	1.98100	-0.240000	-0.815500E-01
76	1.98100	-0.360000	-0.895800E-01
77	1.98100	-0.480000	-0.950900E-01
78	1.98100	-0.600000	-0.973400E-01
79	1.98100	-0.720000	-0.952200E-01
80	1.98100	-0.812800	-0.895000E-01
81	2.55600	-0.699958	0.105240
82	2.55600	-0.583299	0.109916
83	2.55600	-0.466639	0.108950
84	2.55600	-0.349979	0.103933
85	2.55600	-0.233319	0.959344E-01
86	2.55600	-0.116660	0.856093E-01
87	2.55600	0.000000E+00	0.734022E-01
88	2.55600	0.000000E+00	-0.579070E-01
89	2.55600	-0.116660	-0.689725E-01
90	2.55600	-0.233319	-0.781444E-01
91	2.55600	-0.349979	-0.849931E-01
92	2.55600	-0.466639	-0.888546E-01
93	2.55600	-0.583299	-0.886893E-01
94	2.55600	-0.699958	-0.828572E-01
95	3.13100	-0.587117	0.914791E-01
96	3.13100	-0.469693	0.957925E-01
97	3.13100	-0.352270	0.940633E-01
98	3.13100	-0.234847	0.881802E-01
99	3.13100	-0.117423	0.792875E-01
100	3.13100	0.000000E+00	0.680044E-01
101	3.13100	0.000000E+00	-0.560040E-01
102	3.13100	-0.117423	-0.666465E-01
103	3.13100	-0.234847	-0.748847E-01
104	3.13100	-0.352270	-0.801147E-01
105	3.13100	-0.469693	-0.811889E-01
106	3.13100	-0.587117	-0.762143E-01
107	3.70600	-0.474360	0.777171E-01
108	3.70600	-0.355770	0.816293E-01
109	3.70600	-0.237180	0.791808E-01
110	3.70600	-0.118590	0.724727E-01
111	3.70600	0.000000E+00	0.625867E-01
112	3.70600	0.000000E+00	-0.540747E-01
113	3.70600	-0.118590	-0.640681E-01
114	3.70600	-0.237180	-0.708657E-01
115	3.70600	-0.355770	-0.733912E-01
116	3.70600	-0.474360	-0.695515E-01
117	4.28100	-0.361194	0.639091E-01
118	4.28100	-0.240796	0.675468E-01
119	4.28100	-0.120398	0.646618E-01
120	4.28100	0.000000E+00	0.571574E-01
121	4.28100	0.000000E+00	-0.521478E-01
122	4.28100	-0.120398	-0.610096E-01
123	4.28100	-0.240796	-0.652166E-01
124	4.28100	-0.361194	-0.628729E-01
125	4.90200	-0.240000	0.491500E-01
126	4.90200	-0.120000	0.535000E-01
127	4.90200	0.000000E+00	0.514000E-01
128	4.90200	0.000000E+00	-0.501500E-01
129	4.90200	-0.120000	-0.562400E-01
130	4.90200	-0.240000	-0.557800E-01

TOTAL NUMBER OF NODES = 130
LARGEST NODE NUMBER = 130

DATA STORAGE LOCATIONS USED = 520

GEOMETRIC PROPERTIES

FIRST ELEMENT IN SERIES	LAST ELEMENT IN SERIES	DIFFERENCE BETWEEN ELEMNTS	THICKNESS AT 1ST NODE	THICKNESS AT 2ND NODE	THICKNESS AT 3RD NODE	THICKNESS AT 4TH NODE
SMI4 ELEMENTS						
64	70	1	0.2000E-02	0.2000E-02	0.2000E-02	0.2000E-02
80	86	1	0.1750E-02	0.1750E-02	0.1750E-02	0.1750E-02
96	102	1	0.1750E-02	0.1750E-02	0.1750E-02	0.1750E-02
112	118	1	0.1500E-02	0.1500E-02	0.1500E-02	0.1500E-02
128	133	1	0.1500E-02	0.1500E-02	0.1500E-02	0.1500E-02
143	147	1	0.1250E-02	0.1250E-02	0.1250E-02	0.1250E-02
156	159	1	0.1000E-02	0.1000E-02	0.1000E-02	0.1000E-02
167	169	1	0.1000E-02	0.1000E-02	0.1000E-02	0.1000E-02
176	177	1	0.7500E-03	0.7500E-03	0.7500E-03	0.7500E-03
TSM3 ELEMENTS						
134	0	0	0.1500E-02	0.1500E-02	0.1500E-02	
148	0	0	0.1250E-02	0.1250E-02	0.1250E-02	
160	0	0	0.1000E-02	0.1000E-02	0.1000E-02	
170	0	0	0.1000E-02	0.1000E-02	0.1000E-02	
178	0	0	0.7500E-03	0.7500E-03	0.7500E-03	
SMI4 ELEMENTS						
56	62	1	0.1500E-02	0.1500E-02	0.1500E-02	0.1500E-02
72	78	1	0.1500E-02	0.1500E-02	0.1500E-02	0.1500E-02
88	94	1	0.1250E-02	0.1250E-02	0.1250E-02	0.1250E-02
104	110	1	0.1250E-02	0.1250E-02	0.1250E-02	0.1250E-02
120	126	1	0.1250E-02	0.1250E-02	0.1250E-02	0.1250E-02
136	141	1	0.1000E-02	0.1000E-02	0.1000E-02	0.1000E-02
150	154	1	0.7500E-03	0.7500E-03	0.7500E-03	0.7500E-03
162	165	1	0.7500E-03	0.7500E-03	0.7500E-03	0.7500E-03
172	174	1	0.5000E-03	0.5000E-03	0.5000E-03	0.5000E-03
TSM3 ELEMENTS						
121	0	0	0.1250E-02	0.1250E-02	0.1250E-02	
137	0	0	0.1000E-02	0.1000E-02	0.1000E-02	
151	0	0	0.7500E-03	0.7500E-03	0.7500E-03	
163	0	0	0.7500E-03	0.7500E-03	0.7500E-03	
173	0	0	0.5000E-03	0.5000E-03	0.5000E-03	
SMI4 ELEMENTS						
71	0	0	0.1000E-02	0.1000E-02	0.1000E-02	0.1000E-02
87	0	0	0.1000E-02	0.1000E-02	0.1000E-02	0.1000E-02
103	0	0	0.1000E-02	0.1000E-02	0.1000E-02	0.1000E-02
119	0	0	0.1000E-02	0.1000E-02	0.1000E-02	0.1000E-02
135	0	0	0.1000E-02	0.1000E-02	0.1000E-02	0.1000E-02
149	0	0	0.7500E-03	0.7500E-03	0.7500E-03	0.7500E-03
161	0	0	0.7500E-03	0.7500E-03	0.7500E-03	0.7500E-03
171	0	0	0.7500E-03	0.7500E-03	0.7500E-03	0.7500E-03
179	0	0	0.5000E-03	0.5000E-03	0.5000E-03	0.5000E-03
63	0	0	0.1000E-02	0.1000E-02	0.1000E-02	0.1000E-02
79	0	0	0.1000E-02	0.1000E-02	0.1000E-02	0.1000E-02
95	0	0	0.1000E-02	0.1000E-02	0.1000E-02	0.1000E-02

111	0	0	C.1000E-02	C.1000E-02	C.1000E-02	0.1000E-02
127	0	0	C.1000E-02	0.1000E-02	C.1000E-02	0.1000E-02
142	0	0	C.7500E-03	C.7500E-03	C.7500E-03	0.7500E-03
155	0	0	C.7500E-03	0.7500E-03	C.7500E-03	0.7500E-03
166	0	0	C.7500E-03	0.7500E-03	0.7500E-03	0.7500E-03
175	0	0	C.5000E-03	C.5000E-03	0.5000E-03	0.5000E-03
1	7	1	C.1500E-02	0.1500E-02	0.1500E-02	0.1500E-02
8	14	1	0.1500E-02	0.1500E-02	0.1500E-02	0.1500E-02
15	21	1	C.1500E-02	0.1500E-02	0.1500E-02	0.1500E-02
22	28	1	C.1500E-02	0.1500E-02	0.1500E-02	0.1500E-02
29	35	1	C.1500E-02	0.1500E-02	C.1500E-02	0.1500E-02
36	41	1	C.1500E-02	0.1500E-02	C.1500E-02	0.1500E-02
42	46	1	C.1500E-02	0.1500E-02	0.1500E-02	0.1500E-02
47	50	1	C.1250E-02	0.1250E-02	0.1250E-02	0.1250E-02
51	53	1	C.1000E-02	0.1000E-02	C.1000E-02	0.1000E-02
54	55	1	C.1000E-02	0.1000E-02	0.1000E-02	0.1000E-02

G E O M E T R I C P R O P E R T I E S

FIRST ELEMENT IN SERIES	LAST ELEMENT IN SERIES	DIFFERENCE BETWEEN ELEMNTS	AREA OF SECTION AT 1ST NODE	AREA OF SECTION AT 2ND NODE	AREA OF SECTION AT 3RD NODE
	BRS2 ELEMENTS				
188	195	1	C.5600E-04	0.5600E-04	
204	211	1	C.5600E-04	0.5600E-04	
220	227	1	C.5600E-04	0.5600E-04	
236	243	1	C.5600E-04	0.4900E-04	
252	259	1	C.4900E-04	0.4200E-04	
267	273	1	C.3750E-04	0.3100E-04	
280	285	1	C.3100E-04	0.2200E-04	
291	295	1	0.2200E-04	0.1375E-04	
300	303	1	C.1375E-04	0.1100E-04	
	BRS2 ELEMENTS				
180	187	1	C.5200E-04	0.5200E-04	
196	203	1	C.5200E-04	0.5200E-04	
212	219	1	C.4800E-04	0.4800E-04	
228	235	1	C.4800E-04	0.4500E-04	
244	251	1	C.4500E-04	0.3900E-04	
260	266	1	C.3900E-04	0.3900E-04	
274	279	1	C.3400E-04	C.2500E-04	
286	290	1	C.2500E-04	0.1700E-04	
296	299	1	C.1700E-04	0.5000E-05	

WARNING CERTAIN VALUES OVERWRITTEN SYSTEM USES LATEST APPEARANCE OR EXTRA VALUES SPECIFIED (RDGPPR PROCESSOR)

TOTAL NUMBER OF ELEMENT GEOMETRIC PROPERTIES = 308
LARGEST ELEMENT NUMBER = 303

DATA STORAGE LOCATIONS USED = 490

M A T E R I A L P R O P E R T I E S O R T H O T R O P I C

FIRST ELEMENT	LAST ELEMENT	DIFFERENCE									
1	179	1	EX=	0.5500E+03	EY=	0.2300E+08	GXY=	0.1269E+08	NUXY=	0.7400E+00
			AX=	0.0000E+00	AY=	0.0000E+00	AXY=	0.0000E+00	NU=	0.0000E+00

M A T E R I A L P R O P E R T I E S

FIRST ELEMENT IN SERIES	LAST ELEMENT IN SERIES	DIFFERENCE BETWEEN ELEMNTS	MODULUS OF ELASTICITY	POISSONS RATIO	DENSITY	COEFFICIENT OF THERMAL EXPANSION	HYSTERETIC DAMPING FACTOR
180	303	1	0.1200E+09	0.3000	0.1600E-02		

TOTAL NUMBER OF PROPERTIES OR RIGIDITIES = 303
LARGEST ELEMENT NUMBER = 303

DATA STORAGE LOCATIONS USED = 27

S U P P O R T N O D E S

F=FREE
R=RESTRAINED OR RESTRAINED WITH PRESCRIBED DISPLACEMENT
S=SPRING

FIRST NODE	LAST NODE	DIFFRNCE	SUPPORT CONDITION	SPRING SUPPORT CONSTANT / OR PRESCRIBED DISPLACEMENT ALONG X-AXIS	SPRING SUPPORT CONSTANT / OR PRESCRIBED DISPLACEMENT ALONG Y-AXIS	SPRING SUPPORT CONSTANT / OR PRESCRIBED DISPLACEMENT ALONG Z-AXIS
1	0	0	R F F	0.0000000E+00	0.0000000E+00	0.0000000E+00
2	0	0	R F F	0.0000000E+00	0.0000000E+00	0.0000000E+00
3	0	0	R F F	0.0000000E+00	0.0000000E+00	0.0000000E+00
4	0	0	R F F	0.0000000E+00	0.0000000E+00	0.0000000E+00
5	0	0	R F F	0.0000000E+00	0.0000000E+00	0.0000000E+00
6	0	0	R F F	0.0000000E+00	0.0000000E+00	0.0000000E+00
7	0	0	R F F	0.0000000E+00	0.0000000E+00	0.0000000E+00
8	0	0	R F F	0.0000000E+00	0.0000000E+00	0.0000000E+00
9	0	0	R F F	0.0000000E+00	0.0000000E+00	0.0000000E+00
10	0	0	R F F	0.0000000E+00	0.0000000E+00	0.0000000E+00
11	0	0	R F F	0.0000000E+00	0.0000000E+00	0.0000000E+00
12	0	0	R F F	0.0000000E+00	0.0000000E+00	0.0000000E+00

13	0	0	R F F	0.000000E+00	0.000000E+00	0.000000E+00
14	0	0	R F F	0.000000E+00	0.000000E+00	0.000000E+00
15	0	0	R F F	0.000000E+00	0.000000E+00	0.000000E+00
16	0	0	R F F	0.000000E+00	0.000000E+00	0.000000E+00
17	0	0	F R R	0.000000E+00	0.000000E+00	0.000000E+00
21	0	0	F F R	0.000000E+00	0.000000E+00	0.000000E+00

TOTAL NUMBER OF SUPPORT NODES = 18
LARGEST NODE NUMBER = 21

DATA STORAGE LOCATIONS USED = 126

S U M M A R Y C F D A T A

TOTAL NUMBER OF ELEMENTS = 303
TOTAL NUMBER OF NODES = 130
TOTAL NUMBER OF SUPPORT NODES = 18
TOTAL NUMBER OF LOADING CASES = 1

LOCATIONS USED DURING DATA PROCESSING = 3424
LOCATIONS AVAILABLE = 499541

MAXIMUM FRONT WIDTH OF STIFFNESS MATRIX = 390
MAXIMUM HALF BANDWIDTH OF STIFFNESS MATRIX = 96
TOTAL NUMBER OF ACTIVE NODES = 130
TOTAL NUMBER OF EQUATIONS = 390

LOCATIONS USED DURING PRE-SOLUTION PROCESS = 8569
LOCATIONS AVAILABLE = 500000

S O L U T I O N B Y F R O N T A L S P A R S E M A T R I X T E C H N I Q U E

MACHINE CODE INNER LOOPS IN OPERATION

LOCATIONS REQUIRED DURING SOLUTION PROCESS = 80785
LOCATIONS AVAILABLE = 500000

LOCATIONS USED DURING POST-SOLUTION PROCESS= 2062
LOCATIONS AVAILABLE = 500000

LOAD CASE 1

S T R E S S E S A N D S T R A I N S I N E L E M E N T S

R E L A T I V E T O L O C A L A X E S

STRESS OR STRAIN COMPONENTS
MEMBRANE STRESSES SX,SY,SXY

Appendix B.

The OPTIMIST design program for the analysis of postbuckled CFRP stiffened panels.

The theoretical basis for the program is given in chapter 4. This appendix includes:

i) Operation of the program.

ii) A typical output.

iii) A listing of the program.

Operation of the OPTIMIST program.

The program as listed is written in BASIC to run on an Amstrad PC 1512 personal computer. It can, however, be modified to run on any other machine having 32K or more of memory. The program works interactively. It calculates the component sizes and best configuration for one bay of the wing box on each run.

A typical program run.

1) Options for output.
When the program is run, options are given for screen, disc file or printer output.

2) Rib sizing cycle.
The program runs in two cycles. These are the rib sizing cycle, and the skin sizing cycle. The program first enters the rib sizing cycle. The program asks for:

i) the depth of the wing box section,

ii) the desired axial skin panel strain,

iii) the running compression load in the top skin,

iv) the wing box chord.

From the above information the program calculates the rib crushing load (Nz). The program also contains the dynamic pressure loading for the A1 aircraft at +9G. The pressure loading is used to calculate the rib shear (Nxz) and the rib flange load caused by rib bending (Ny).

A laminate is chosen from the menu for the rib shear web. The laminates available are different combinations of 0° and $+-45^{\circ}$ plies. The angles are relative to the compression loading axis. If desired, a new kind of laminate can be specified in the data statement at lines 120-145. Usually, a simple $+-45^{\circ}$ laminate would be used.

The rib is considered to have vertical stiffeners. The program asks for the spacing between these stiffeners.

For a trial rib thickness of 1mm, the program first calculates the pure compression and pure shear buckling loads. The compression buckling half wavelength is also calculated.

The buckling loads for the combined shear and compression loads are then computed.

The minimum rib thickness required for the rib to withstand buckling is then calculated.

The compressive strain at buckling is also calculated.

3. Skin sizing cycle.

The program then enters the skin sizing cycle. The following information is input at this stage.

i) The desired skin thickness.

ii) The simply supported panel pitch between the skin stiffeners.

Another laminate is then chosen for the skin from the menu. For a highly loaded skin, a laminate could be selected incorporating some unidirectional material.

A compression to shear loading ratio is then input for the skin.

The program calculates the buckling loads for the skin in the same way as for the rib panels. The critical compression strain at buckling is computed.
A desired strain for the skin panel is then input, which will take the panel into the post buckled range.

The postbuckling strain ratio is output. The program calculates the reduced stiffness of the skin panel after buckling. From the reduced stiffness, the load carried by the panel at the desired strain is calculated.

The out-of-plane buckle amplitude is calculated. The surface strain due to bending of the plate is also calculated at the edge and the centre.

The program calculates how much unidirectional CFRP to add to the panel to achieve the desired skin compression load. The unidirectional material is assumed to be in the stiffener caps.

4. Optimisation of configuration.

Starting from a small rib spacing, the program calculates the weight per metre span of the box. The stiffeners are assumed to be of square cross-section and filled with foam of 51kg/m↑3. For each rib spacing, the stiffener depth that will just ensure column stability is calculated. The effect of transverse air loading on the stiffeners is also considered. For each rib spacing, a rib thickness is used that will just resist buckling.

At each rib spacing, a plot is produced of weight versus rib spacing. When the optimum weight is reached, the following are output:

i) The optimum weight per unit span.

ii) The minimum depth of the stiffeners required for column stability.

iii) The optimum rib spacing.

iv) The minimum thickness of rib required to resist buckling.

5. Optimisation of the skin thickness.

As shown, the program will calculate an optimum configuration of ribs and stiffener sizes. The actual skin thickness and stiffener spacing is under interactive control. The program runs quickly enough to be able to try different layouts and compare weights. In general, the wider the stiffener spacing and the thinner the skin, the lighter the structure. The constraints are in postbuckling amplitude, and torsional stiffness.

'OPTIMIST' SIZING & OPTIMISATION FOR
COMPOSITE POSTBUCKLED BOX BEAMS

rib sizing cycle

section depth m	0.2
strain in skin panels	0.0025
Nx KN/m skin compression load	250
structural box chord	1
for a trial rib spacing of 0.1 m	
Nz crush KN/m	0.17
Nyz shear KN/m	1.98
Ny flange KN	0.10
ratio of crush to shear	0.0835
effective s.s. panel pitch	0.35
laminate layup is 45sym	
pure comp. kn/m	1.88
half wave, m	0.35
pure shear kn/m	2.03
comp buckling kn/m	0.16
shear buckling kn/m	1.97
rib thickness required	
for no buckling mm	1.00
crit strain	0.000010

****

skin sizing cycle

laminate thickness mm	1.2
effective s.s. panel pitch	0.14
laminate layup is 45(2)0sym	
pure comp. kn/m	19.95
half wave, m	0.14
pure shear kn/m	21.45
compression to shear ratio	10
comp buckling kn/m	19.79
shear buckling kn/m	1.98
crit strain	0.000300
pb strain ratio	8.34
load/metre KN/m	73.71
post/pre buckled stiffness	0.371
stiffener area required mm^2	510.0

****

buckling amplitude

amplitude mm	4.2
max surface strain due to buckling	
at centre of plate	-.001250
at edge of plate	0.007452

****

has reached optimum

weight kg/m span	4.45
depth of stiffeners mm	27.00
crit. rib spacing mm	617.3
required rib thickness mm	1.836

```
   5 REM "OPTIMIST" STRUCTURAL SIZING & OPTIMISATION PROGRAM
 REM  FOR CFRP POSTBUCKLED BOX BEAMS
 REM  by W. Brooks 1987.
 CLS
 INPUT "choose screen=1 , printer=0 or disc file=3 ",pr
 IF pr=3 THEN INPUT "filename ?",o$
 IF pr=3 THEN OPEN #3 OUTPUT o$
 PRINT #pr "'OPTIMIST' SIZING & OPTIMISATION FOR":PRINT #pr " COMPOSITE POSTBUCKL
 ED BOX BEAMS":PRINT  "note spar shear webs not included"
 PRINT  "see thesis for analysis methods,":PRINT  " assumptions &  operation"
 PRINT "use sreen dump with MS-DOS and":PRINT " GRAPHICS/R function for graph out
 put"
 PRINT
 PRINT #pr
 7 DIM u(2): DIM p(10): DIM r(10)
   10 DIM s(10)
   20 DIM x(5): DIM w(6)
   25 DIM y(8)
   30 DIM t(5):DIM d(6,6)
   35 DIM e(10)
   40 LET g=0
   45 LET v=0
   50 LET t=0
   52 LET r$="y": PRINT #pr "rib sizing cycle"
 PRINT #pr "_____"
 REM r$ used to control operation of program.

   53 INPUT "section depth m", dep
 PRINT #pr"section depth m              ",dep
   55 PRINT  "type of laminate"
 57 LET d=1e12
   60 PRINT  "45 svm","1","45(4)0sym","2","45(2)0sym","3","45(2)0(2)svm","4","45,
 3)0(3)svm","5"
   65 INPUT b$
 PRINT  "laminate type                  ",b$
 IF r$="y" THEN t=1:GOTO 100
   80 PRINT  "laminate thickness mm"
   85 INPUT t
 PRINT #pr "laminate thickness mm       ",t
   100 IF r$="y" THEN PRINT "rib sizing cycle": GOSUB 865
   105 PRINT "effective s.s. panel pitch"
   110 INPUT b
 PRINT #pr "effective s.s. panel pitch  ",b
   115 RESTORE
   120 READ n$,a$,d(1,1),d(1,2),d(2,2),d(3,3),e(1),e(2),g,v
   125 DATA "1","45sym",.3417e-2,.2617e-2,.3417e-2,.2806e-2,.169e8,.169e8,.33e8,.
 745
   130 DATA "2","45(4)0sym",.00347,.002597,.003395,.00278,39.6e6,23.4e6,27.8e6,.7
 4
   135 DATA "3","45(2)0sym",.00369,.002527,.003318,.002716,55e6,23e6,24e6,.717
   140 DATA "4","45(2)0(2)sym",.004351,.002316,.003084,.002505,74e6,21e6,19e6,.67
   145 DATA "5","45(2)0(3)sym",.005031,.002087,.002841,.002286,85.7e6,19.7e6,16.3
 e6,.645
   150 IF n$<>b$ THEN  GOTO 120
   155 LET d(1,1)=d(1,1)*t^3
   160 LET d(1,2)=d(1,2)*t^3
   165 LET d(2,2)=d(2,2)*t^3
   170 LET d(3,3)=d(3,3)*t^3

 175 PRINT #pr "laminate layup is          " a$
 PRINT #pr "_____"
```

```
180 LET t=t/1000
185 FOR f=.5 TO 10 STEP .5
190 LET a=f*b
195 LET x(1)=(PI/b)^2
200 LET x(2)=(b/a)^2
205 LET x(3)=(a/b)^2
210 LET p=x(1)*(d(1,1)*x(2)+2*(d(1,2)+2*d(3,3))+d(2,2)*x(3))
215 IF p<q THEN  LET n=a
220 IF p<q THEN  LET q=p
225 IF f<10 THEN  GOTO 240
230 PRINT #pr "pure comp. kn/m         ",USING "##.##",q
235 PRINT #pr "half wave, m            ",USING "##.##",n
240 NEXT f
245 GOSUB 565
250 REM u crit
255 LET u=j/(t*e(1)/n)
260 LET ecr=u/n
265 PRINT #pr "crit strain              ",USING "##.######",ecr


270 REM ********************
275 REM post buckling
280 REM ********************
295 LET h=1/g-2*v/e(1)
305 LET r(1)=2+(1+e(1)*h*(b/n)^2+3*e(1)/e(2)*(n/b)^4)
310 LET e(3)=e(1)*((2+r(1))/(2+3*r(1)))
IF r$="y" THEN u(1)=(u/n):GOTO 325
315 IF r$<>"y" THEN LET u(1)=e
325 IF r$<>"y" THEN PRINT #pr "ob strain ratio          ",USING "##.##",u(1)/(u/n
)
330 LET p(3)=j+(u(1)-u/n)*e(3)*t
335 IF r$<>"y" THEN PRINT #pr "load/metre KN/m         ",USING  "##.##",p(3)
340 IF r$<>"y" THEN PRINT #pr "post/pre buckled stiffness",USING "##.###",e(3)/e
(1)
345 REM ******************
350 REM stiffeners
355 REM ******************
357 IF r$="y" THEN GOTO 426
 IF p(3)>enx THEN PRINT "****************************":PRINT "panel too thick or"
:PRINT" strain too high- stiffeners zero area":STOP
LET e(4)=120e9:REM stiffener cap modulus
360 LET s(1)=0
370 LET s(2)=s(1)/3: REM stiffener sidewall area
395 LET p(4)=(s(1)*e(4)+s(2)*e(1)*1000)*u(1)
410 LET p(5)=w*p(3)+p(4)/1000
IF (p(5)/w)<enx THEN LET s(1)=s(1)+5e-6:GOTO 370
415 PRINT #pr "stiffener area required mm^2",USING "####.#",s(1)*1e6

425 IF r$<>"y" THEN GOSUB 833: REM for buckle amplitude
426 IF r$="y" THEN LET r$="n":PRINT #pr "**************************************
**":PRINT #pr "skin sizing cycle":PRINT #pr "_____________________________________
______": GOTO 55

450 REM ******************
455 REM overall buckling
460 REM ******************

INPUT "return to continue",x$:CLS
470 LET w(4)=1e6
475 LET w(5)=1e6
480 LET d=1
500 LET d=d/1000
505 LET d=d+.0005
515 LET ij=.9*s(1)*(d/2)^2*e(4)
520 LET ik=t*w*(d/2)^2*e(3)
523 LET bc=1: REM beam column factor
525 LET lcr=SQR (PI^2*(ij+ik)/((p(5)*bc)*1000))
530 LET mocap=((nz/1)*1000*w*lcr^2/8)
```

```
535 LET uf=PI/2*SQR(p(5)/(p(5)*bc))
536 LET lamda=2*(1-COS(uf))/(uf^2*COS(uf))
537 LET mx=mocap*lamda
545 LET str=(mx/d/s(1))/e(4)
550 IF str+u(1)>=.004 THEN LET bc=bc+.01:GOTO 525

555 GOTO 700
560 REM ******************
565 REM shear
570 REM ******************
575 IF (d(1,1)*d(2,2))<(d(1,2)+2*d(3,3))^2 THEN  GOTO 585
580 GOTO 600
585 LET y(1)=SQR (2*d(2,2)*(d(1,2)+2*d(3,3)))/((b/2)^2*t)
590 LET y(2)=d(1,1)*d(2,2)/((d(1,2)+2*d(3,3))^2)
595 LET y(3)=d(1,1)^2*d(2,2)^2/((d(1,2)+2*d(3,3))^4)
600 LET t(1)=y(1)*(8.3+1.525*y(2)-.493*y(3))
605 LET y(4)=((d(1,1)*d(2,2)^3)^.25)/((b/2)^2*t)
610 LET y(5)=SQR ((d(1,2)+2*d(3,3))^2/(d(1,1)*d(2,2)))
615 LET y(6)=((d(1,2)+2*d(3,3))^2/(d(1,1)*d(2,2)))
620 LET t(1)=y(4)*(8.125+5.64*y(5)-.6*y(6))
625 LET t(3)=t(1)*t
630 REM sh kn/m
635 PRINT #pr "pure shear kn/m          ",USING "##.##",t(3)
640 REM ********************
645 REM interaction
650 REM ********************
IF r$="y" THEN r=rcs:GOTO 665
655 PRINT"comp/snear ratio"
660 INPUT r
PRINT #pr "compression to shear ratio       ",r
663 FOR j=1e-4 TO (q+t(3)) STEP (q+t(3))/1000
670 IF j/q+((j/r)/t(3))^2>=1 THEN  GOTO 680
675 NEXT j
680 PRINT #pr "comp buckling kn/m        ",USING "##.##",j
685 PRINT #pr "shear buckling kn/m       ",USING "##.##",j/r
IF r$<>"y" THEN GOTO 690

688 LET tg=(nz*(t*1000)^3/j)^.3333

689 PRINT #pr " rib thickness required":PRINT #pr " for no buckling mm  ",USING
"##.##",tg

LET rk=tg^3/l:REM ratio of rib thickness^3 to spacing


690 RETURN
695 REM ******************
700 REM weight/m
705 REM ******************

710 LET ol=w(4)+w(5)
715 LET w(1)=w*100*t*100*100*1.61/1000
720 LET w(2)=(s(1)+s(2))*10000*100*1.61/1000
725 LET w(3)=d^2*71*w/b
730 LET w(4)=w(1)+w(2)+w(3)
735 REM rib weight
737 LET tr=(tg^3*lcr/l)^.333
740 LET w(5)=1.61*tr*dep*w*(1/lcr)
745 LET w(5)=w(5)*1.1
750 REM joints
752 LET inc=inc+1

755 LET nw=w(4)+w(5)
760 IF nw >8 AND lcr > 0.8 THEN GOTO 765
IF nw<8 AND lcr <0.8 THEN PLOT  lcr*5000 +800;nw*500+800 MARKER 2 SIZE 1
```

```
765 IF nw>o1 THEN GOTO 777
770 GOTO 505
777 REM graphics
LINE 800;800,5000;800,800;800,800;5000
FOR n=0 TO 7
LINE 800;n*500+800,600;n*500+800
LINE n*500+800;800,n*500+800;600
 MOVE n*500+800;500:PRINT USING".#";n/10
 MOVE 200;n*500+800:PRINT USING "#.#";n
NEXT n
MOVE 10;4500: PRINT "weight kg/m"
MOVE 800;200: PRINT "rib spacing m"
MOVE 7000;4500
INPUT  "continue ?",x$:CLS
780 PRINT #pr " ********************************************************": PRINT #
pr "has reacned optimum"
PRINT #or "-----------------------------------------"
795 PRINT
800 PRINT #pr
805 PRINT
810 PRINT #pr "weight kg/m span      ",USING "##.##";w(4)+w(5)
815 PRINT #pr "depth of stiffeners mm", USING "##.##";d*1000
820 PRINT #pr "crit. rib spacing mm",USING "###.#";1cr*1000
822 PRINT #or "required rib thickness mm",USING "#.###": tr
PRINT "run comoleted"
IF pr=3 THEN CLOSE #3 o$
STOP
END


830 REM ************************
835 REM buckle amolitude
840 REM ************************
LET inc=PI/200
LET a=PI/200
LET q1=0
LET k=10
LET 1a=PI/2
856 LET d1=0
LET 12=PI/2+(u(1)-ecr)*PI/2
LET dx=PI/2/k
FOR x=0 TO PI/2 STEP PI/2/k
LET dy= (a*SIN(x+dx)-a*SIN(x))
LET q=ATN(dy/dx)
LET es=(0.5*t/n)*PI*SIN(q-q1)
LET f1=es/(SQR(dx^2+dy^2))
IF f1=>0 THEN LET f1c=f1:REM for plate edge bending strain
LET q1=q
LET d1=d1+SQR(dx^2+dy^2)
NEXT x
IF d1<12 THEN LET a=a+inc: GOTO 856
PRINT #pr "************************************************":PRINT #pr "buckling
amplitude"
PRINT #pr "-----------------------------------------"
PRINT #pr "amplitude mm                          ", n/PI*1000*a
PRINT #pr "max surface strain due to buckling"
PRINT #pr "at centre of plate                    ",USING"#.######",f1
PRINT #pr "at edge of plate                      ",USING"#.######",f1c
858 RETURN

860 REM ************************
865 REM "rib loadings"
870 PRINT "strain in skin panels"
875 INPUT e
PRINT #pr "strain in skin panels                 ",e
```

```
880 LET r=dep/(2*e)
885 PRINT "Nx KN/m skin compression load"
890 INPUT enx
PRINT #pr "Nx KN/m skin compression load      ",enx
900 LET l=0.1: REM starting rib spacing
905 PRINT  "chord"
910 INPUT w
PRINT #pr "structural box chord               ",w
915 LET p=enx/r
920 LET pl=7.9
925 REM ult airloadpress. at 13.5g
930 LET nz=(p-pl)*l
931 LET nz =ABS(nz)
PRINT #pr "for a trial rib spacing of 0.1 m"
935 PRINT #pr "Nz crush  KN/m           ",USING "##.##",nz
940 LET nyz=((pl*l*w)/2)/dep
945 PRINT #pr "Nyz shear KN/m           ",USING "##.##".nyz
950 LET mo=(nz*w^2)/8
955 LET ny=mo/dep
960 PRINT #pr "Ny flange KN             ",USING "##.##",ny
963 LET rcs=nz/nyz
964 PRINT #pr "ratio of crush to shear ",USING "##.####",rcs
965 RETURN
970 STOP
```

Appendix C.

Loading and initial design stressing of some detail areas.

Contents:

1. Transmission of shear from ribs to spars.

2. Transmission of shear from stiffened skin to spar shear webs.

3. Spar shear web buckling.

4. Torque loading of the wing box due to aileron deflection.

5. Design of the aileron load pickup rib stations 3706 and 1981.

6. Torsional stiffness.

7. Decrease in aileron effectiveness at Vd caused by wing twist.

1. Transmission of shear from ribs to spars.

Taking the most highly loaded rib station 2556mm from the centreline:

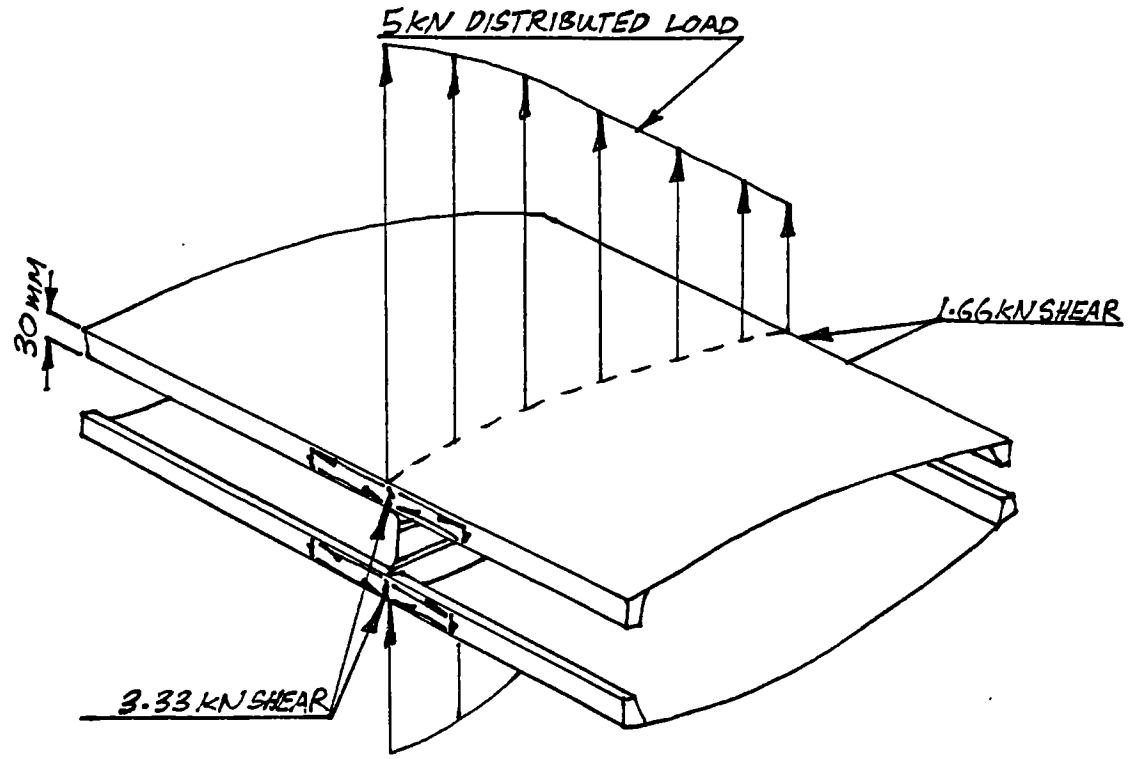

FIG C.1.

The rib is assumed to carry the distributed airloading from the wing skins one half rib bay each side of the rib. It then transmits the shear load into the mainspar shear webs.
In this design the rib shear webs are not directly bonded to the spar shear webs. Instead, the ribs transfer the shear load to the leading and trailing

stiffener side faces. These faces transmit the shear to the spars by means of a continuous slotted joint.

Assuming a bond shear strength of 20 MPa from test results in appendix G, and an applied load of 3.3kN, the bond area required is:

3,300/20 = 165mm↑2

The actual spar to skin joint on the stiffener sidewall is 30mm high and of double lap cofiguration. Hence, the width of the joint required to transfer the load is:

165/60 = 2.75mm.

Since the joint is continuous along the span, and the shear load can be diffused along the spar because the stiffeners are stiff in bending, this load case is not critical.

2. Transmission of shear from stiffened skin to spar shear webs.

The shear load taken by the spar web along the span varies from 150 to 30 kN/M at the ultimate positive loading.

The joint depth is the same as the stiffener height and varies from 30 to 20mm.

Taking an adhesive shear strength of 20 MPa, and assuming a continuous double lap joint, the joint capability at the root is:

30 x 2 x 20 = 1200 N/mm = 1200 kN/m.

Giving a reserve factor of 1200/150 = 8.

The joint is only loaded to 12.5% of its ultimate capability. Alternatively, only 12.5% of the joint depth needs to be effectively bonded.

3. Spar shear web buckling.

A check was made on web buckling using ESDU 67024. It takes into account the shear deformation of the sandwich core. The deformation considerably reduces the buckling load from that given by a simple plate buckling equation analysis.

Web wrinkling was analysed by the equation:

$0.43 \times t \times (Ef \times Ec \times Gc)^{.33} = Nxy,$

where t = thickness of each faceplate,
Ef = Young's modulus of faceplates,
Ec = Young's modulus of the core,
Gc = shear modulus of the core.

With woven 913-815 carbon fibre woven faceplates at 0.34mm thick per ply, a quasi-isotropic Ef value of 65,000 N/mm^2 was used.

The sandwich core is assumed to be 5mm thick Rohacell wf51 foam where Ec = 70 N/mm^2 and Gc = 21 N/mm^2.

With these properties the following table was constructed:

Station. mm	Shear load. N/mm	Spar depth. mm	Layup each face.	Buckle. Nxy N/mm	Wrinkle. Nxy N/mm.
431	150	240	+-45°(2)	214	265
1411	140	210	+-45°(2)	210	265
1981	140	140	+-45°(2)	210	265
3131	100	100	+-45°	136	132
4281	50	70	+-45°	139	132

The table was constructed on the basis that all the shear load was taken by the leading spar.

4. The torque loading of the wing box.

From ref 28, the proof load due to the full deflection of the aileron, stick force limited, is 9 kN. The ultimate case is therefore 9 x 1.5=13.5 kN.

This load acts at a chordwise position given in ref. 32. The limit wing torque about the wing 25% chord line is 1.83 kN/m. The distance of the 25% chord line from the aileron pickup at stn. 3706 is 0.495m. Thus

the limit load required at the aileron pickup is:

1.83/0.495 = 3.69kN.

In the ultimate case this is 3.69 x 1.5 = 5.54 kN.

The spanwise centre of pressure on the aileron itself due to aileron deflection is 3706mm outboard of the centreline. The total assymmetric load produced by the wing acts at 3017mm outboard. In the ultimate case, the additional bending moment applied to the wing is:

(13.5 x 3.017)-(5.54 x 3.706) = 20.1 kN/m.

The whiffle tree is constructed so that the spanwise centre of pressure is at 2.63m outboard. Thus the load required to generate the bending moment is:

20.1/2.63 = 7.67 kN.

Therefore the ultimate aileron loading case at zero G is simulated by 7.67 kN applied through the whiffle tree combined with 5.54 kN applied at the aileron pickup at station 3706mm outboard.

4.1 Combined bending and torque cases.

Full aileron is applied at +6G in the limit case. From des.23 a maximum root bending moment of 39.4 kN/m is given for this load case. This bending moment includes the load applied to the aileron at the hinge line. The aileron load is 3.69kN at 3.706m as before. Thus the ultimate bending moment applied is:

(39.4 x 1.5)-(3.69 x 1.5 x 3.706) = 38.58 kN/m.

Since the whiffle tree load is applied at 2.63m outboard, the whiffle tree load required is:

38.58/2.63 = 14.6 kN

This is again combined with 5.54kN applied at the aileron pickup point stn. 3706 acting in the same direction.

In the negative load condition, the aileron load is the same but reversed in sign. The bending load is

factored by:
-9/13.5 = -0.666

which is the ratio of negative to positive manoeuvring load factors, n2 and n1. Thus for the negative loading case, the load applied by the whiffle tree is:

-0.666 x 14.6 = -9.72 kN.

This is combined with the -5.54 kN aileron load applied at stn. 3706.

5. Design of the aileron load pickup ribs station 3706.

The rib is constructed as shown below. It is designed to take the aileron loading into the structure.

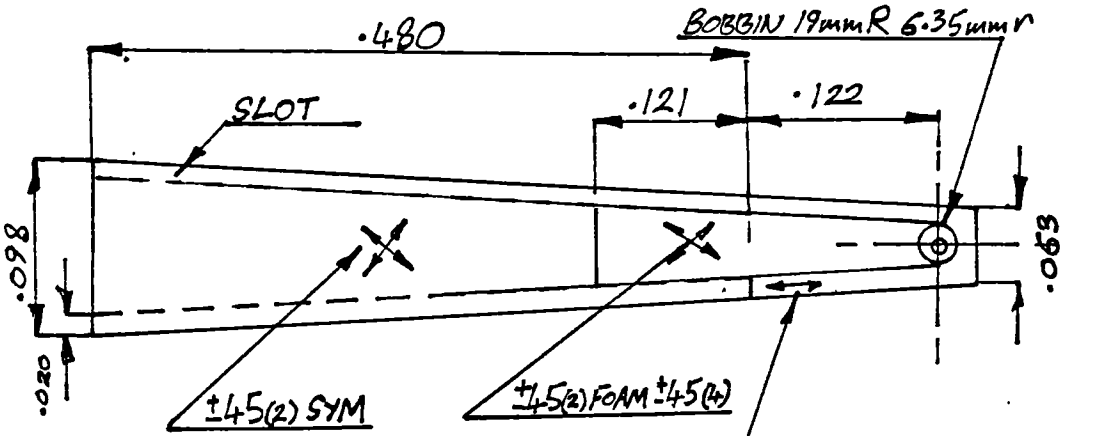

FIG C.2

5.1 The aileron loading is transferred to the rib by means of a bobbin which is bonded into position. The area of the bobbin side faces which join to the faces of the rib is:

$$\pi R^2 - \pi r^2 = \pi 19^2 - \pi 6.35^2 = 1007\ mm^2.$$

Taking the bond strength to be 20 MPa from testing,

the load that can be taken is:

1007 x 20 x 2 = 40,280 N.

Giving a reserve factor of 40.28/5.5 = 7.3.

5.2 Shear loading of the sandwich side faces.

The side faces are of a total combined thickness of 2.04mm of +-45° woven CFRP. The depth of the shear webs is 63mm and the applied load is 5.5 kN. Assuming the side faces take only the shear loading, the running shear load is:

5.5/.063 = 87kN/m.

The 2.04mm thick laminate under a shear loading of 87kN/m was analysed by means of "ANALAM", the author's laminate analysis program.
The program gave a shear strain of 0.129%. The strain in the material axes was +- 0.064%. This is well within the capability of the material. The maximum allowable value in the material axes is 0.4%, giving a reserve factor of:

0.4/.064 = 6.25.

Comparison of the sandwich panel shear web thickness with the spar shear web shows that neither shear buckling nor wrinkling are critical.

5.3 Direct strains due to bending.

The bending moment applied to the rib is:

5.5 x .122 = .671 kN/m.

The depth of the rib is .063m, so the direct load taken by the caps is:

.671/0.063 = 10.65kN.

If it is assumed that the direct load due to bending is taken by a 20mm deep strip of cap material, then a running compression load on this strip exists of:

10.65/.02 = 532kN/m.

The cap material layup is +-45°(2),0°(4),+-45°(4). The 45° layers are woven CFRP at 0.34mm/ply, the unidirectional CFRP is 0.127mm/ply.
When analysed by the "ANALAM" program, a compression strain value of 0.35% was given. This gives a reserve factor of:

0.4/0.35 = 1.14.

5.4 Transmission of the rib load into the structure.

The direct load in the edges of the rib web is transmitted to the rib flanges by means of slotted joints. These joints are 20mm deep. How much length of joint is required to transmit the load by adhesion?
The end load in the rib web edges is a maximum of 10.65kN at the trailing spar. The bond strength is 20MPa. The area required for bonding is therefore:
10650/20 = 532mm↑2.
The joint is 20mm deep and acts in double shear. The minimum length required is:

532/40 = 13.3mm.

Since the joint extends for the whole rib length of 480mm, this load can easily be carried. This analysis does not take into account the stress concentration of the adhesive at the joint edges. See appendix G for one possible approach.

6. Torsional stiffness.

The rate of twist is given by:

in radians/metre span. $$\frac{d\theta}{dz} = \frac{T}{4A^2}\oint\frac{ds}{Gt}$$

The torque T applied about the shear centre, taken to be half way between the spars, is:

5.5 x (.122+.24) = 1.9 kN/m.

The cross sectional area A is, (assuming constant dimensions from rib station 3706):

.48 x (.098 + .063) x .5 = .038 m↑2.

The skin thickness is taken to be .0015m.
The modulus of rigidity is 33 x 10↑9 N/m↑2.
The distance around the perimeter of the section is :

$\oint \delta s$ = (.48 x 2) + .098 + .063 = 1.21m.

The rate of twist in rads/m is then:

(1900/(4 x (.038)↑2)) x (1.21/(33 x 10↑9 x .0015)) = 0.00804

This is 0.46° per metre.

The box is expected to be considerably stiffer than this because both the cross sectional area and the thickness increase towards the root.(Actual testing has since shown the twist to be 0.4 over the span from stn. 481 to stn. 3706)

7. Decrease in aileron effectiveness at Vd caused by wing twist.

When the ailerons are instantaneously deflected, the wing structure twists. The twist reduces the overall assymmetric lift. At a certain combination of twist and speed, aileron reversal will occur. The lift produced by each wing is:

$$L = \frac{1}{2}\rho V^2 C_L S$$

The lift coefficient is assumed to be in linear proportion to the wing incidence.

The lift curve slope is: $\frac{dC_L}{d\alpha^\circ} = .0733$

The area, S, is 7.47m↑2.
The speed, Vd, is 121.9 m/sec.
The air density, ρ , is 1.23 kg/m↑3.

If the wing twist is 0.46 /m, then for the 3.7m inboard of the aileron pickup the average incidence change is:

0.46° x 3.7 x 0.5 = 0.85°.

The lift due to this effective incidence change is then:

$$1.23 \times .5 \times 121.9^2 \times .85 \times .0733 \times 7.47 = 4253\,N$$

If this lift acts at the same spanwise position as the

total assymmetric lift due to aileron, 3.01 m outboard, then the reduction in bending moment is:

4.253 x 3.01 = 12.8 kN/m.

The rolling moment provided by the aileron is:

9 x 1.5 x 3.01 = 40.6 kN/m.

The reduction in effectiveness of the ailerons at Vd is then:

12.8/40.6 x 100 = 31%.

This is obviously a very simple examination. Nevertheless, it does show the reduction in aileron effectiveness at high speed due to a comparatively small wing twist. (The reduction in aileron effectiveness caused by the actual measured twist will be $0.4/2 \times 1/.85^{\circ} \times 31\% = 7.3\%$ by the same analysis.)

Appendix D.

Rejected design approaches.

A description of the separate wing ribs that were designed for the first test box.

Appendix D.

Rejected design approaches.

During the development of the wing, some design schemes were unsuccessful. These have been covered in the main text with the exception of the wing ribs. The ribs were initially designed to be flanged, and separate from the skin. The rib was similar to that in a typical metal structure. The idea behind the scheme was to allow the wing skin to be produced as a flat panel that could be curved to shape.

The design was rejected for four reasons:

i) A bonded joint had to be made between the rib flange and the skin inside surface. The joint was subjected to peeling loads from postbuckling of the skin panels. This could lead to separation and failure.

ii) Because of the complex geometry of the skin/stiffener inside surface, it was very difficult to maintain a good fit between the rib flange and the skin. Expensive matched tooling would be required.

iii) Clamping of the joint for bonding was very difficult to achieve. The simplest method was to use blind rivets, which involved drilling holes in the postbuckling skin. This was considered a poor solution because of the stress concentrations the holes would produce. The rivets would also spoil the clean aerodynamic surface that should be an advantage of a composite structure.

iv) Due to the relatively complex geometry of the A1 wing, curving the skin panels to shape would be very difficult. Because the wing has a kinked leading spar, the stiffeners would be forced to bend along their length. This was unacceptable.

The first test box was constructed with separate ribs, an example of which is shown in fig. D.1. The ribs were produced in a simple semi-matched tooling system in the following way:

i) From a wooden mock-up of the rib, a wet-laminated glass/epoxy female mould was made.

ii) In the mould a wet-laminated male mould was produced. The male mould was then cut into quarters.

iii) A woven carbon/epoxy prepreg kit was placed into the mould, which was covered with a PTFE release cloth.

iv) The PTFE coated male mould was positioned over the prepreg. The mould acted as a form of matched pressure intensifier. Because the mould had been cut into quarters, the segments could be pushed against the rib inner surface by a vacuum bag.

v) The whole assembly was covered in a breather cloth and enclosed inside a vacuum bag.

vi) The rib was autoclave cured at 80 psi.

The technique produced high-quality mouldings which were of a complex shape. Although the ribs were rejected for the final wing design, the lessons learnt in producing them were valuable. The ribs enabled the development of simple semi-matched tooling methods using composite materials.

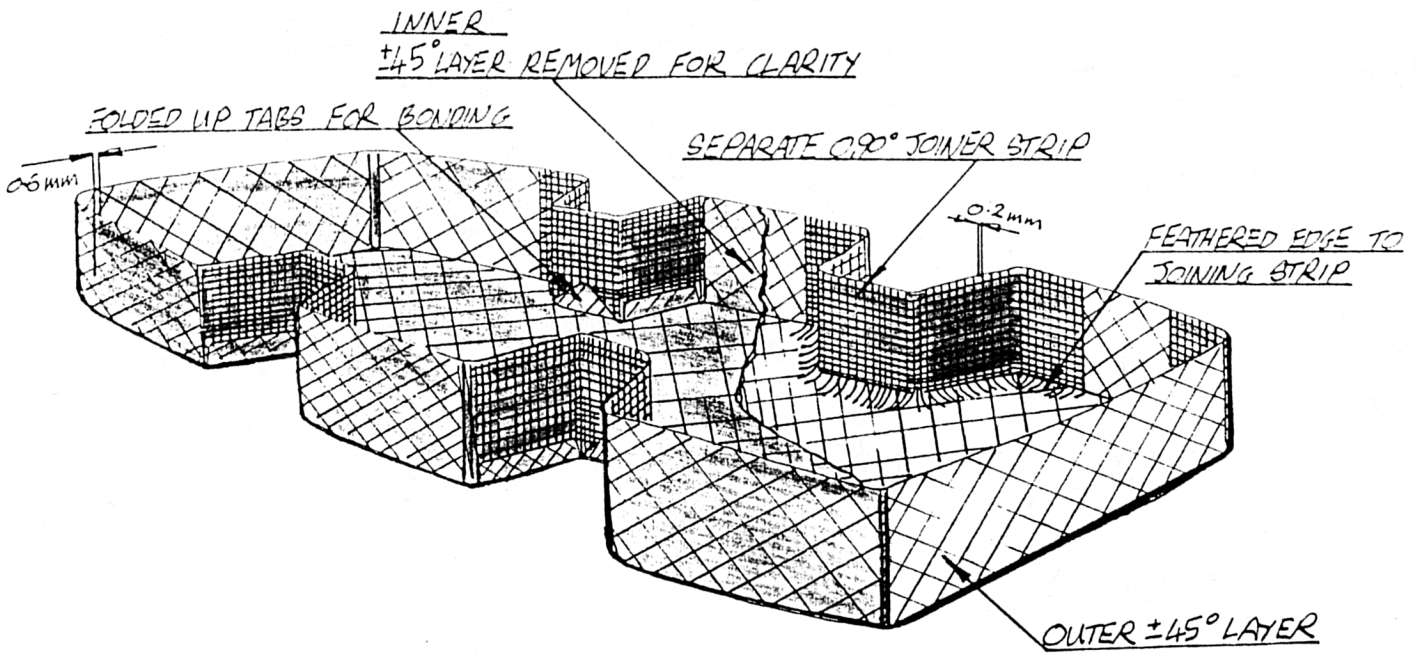

Figure D.1.

The laminating method and general layout of the separate, flanged ribs.

Appendix E.

Published Papers.

Two papers were written for presentation at international conferences.

i) The Design and Construction of a Post Buckled Carbon Fibre Wing Box Structure. ICAS conference proceedings, held in London, September 1986. This paper is mainly concerned with design techniques.

ii) The Construction of a Post Buckled Carbon Fibre Wing Box. Published in " Composite Structures 4", I.H. Marshall, Elsevier, 1987. The paper was presented at the ICCS IV conference, Paisley, September 1987. The paper deals mainly with construction techniques.

THE DESIGN AND CONSTRUCTION OF A POST BUCKLED CARBON FIBRE WING BOX STRUCTURE

W. G. Brooks,
Aircraft Design,
College of Aeronautics,
Cranfield Institute of Technology,
Wharley End,
Bedfordshire, England.

Abstract.

Design and construction techniques are developed for a post buckled carbon fibre reinforced plastic (cfrp) wing box to be used on an aerobatic light aircraft. Following studies of post buckled stiffened panel behaviour and the evaluation of various design techniques, a wing box structure has been designed. Construction techniques have then been developed and appraised so that the wing box can be manufactured easily and that the expected high structural efficiency can be realised in practice.

Notation.

P_{CR} Buckling load of skin element.
P_x Load in x direction (major loading axis)
P_y load in y direction
T_{CR} critical shear load
P_s load due to stiffeners
P_{tot} total panel load
a length of skin elements
b width of skin elements
t skin thickness
D_{11}-D_{33} bending stiffness matrix terms for skin
H elastic constant defined by eq.7
E_s stiffener cap material modulus
E_{11} major loading axis modulus
E_{22} transverse modulus
E_* effective post buckled modulus
ν_{12} poissons ratio
G_{12} shear modulus
W total panel width
A_s stiffener cross sectional area per unit width
d stiffener depth
EI total panel column stiffness
ϵ strain
u displacement

Introduction.

Post buckled wing box structures in composite materials can provide significant weight savings compared to non buckled designs. This is due to the technique of locating the wing bending material in concentrated areas of unidirectional fibres. The skin panels can then be allowed to buckle without overall failure of the structure occuring, as the stiffeners take proportionally more load than the skin. Loading can then be increased until column failure of the stiffeners occurs. This mode of failure may interact with the local buckling of the panel to reduce the buckling load. Failure may also occur because of skin/stiffener delamination due to excessive local buckling of the skin panels causing peeling loads, or due to failure of the material itself.

Design techniques.

The first requirement for designing such a structure is to be able to predict the behaviour of postbuckled stiffened panels. It is desirable that any design technique to be used in the initial stages should be quick and simple to use, so that parametric studies can be made of structural configuration. The initial design technique may also be used as part of an opimisation loop to find the best layout. Data generated from experimental work by Belgrano (1) was used in assessing the accuracy of three design techniques.

Finite element methods.

Using the finite element program LUSAS, one of the experimental panels was modelled. Semiloof 8 noded thin shell elements were used to model the skins and stiffener walls. Isotropic 20 noded solid semiloof elements were employed to model the stiffener cores as shown in fig. 1.

A geometrically non-linear analysis was performed using incremental displacement of the panel ends. This is an analysis technique where the stiffness matrix of the structure is updated at each incremental end displacement. Although imperfections were not introduced, the model started buckling as a result of out of plane bowing. This was caused by the difference in stiffness between the stiffener caps and the panel skin. This method gave a detailed insight into the performance of the panel with good accuracy as can be seen in fig. 2. The reactions from the panel end nodes could be analysed, showing the way in which the stiffeners took up increased loading after the skin panels had buckled, as shown in fig. 3.

The disadvantage of this form of

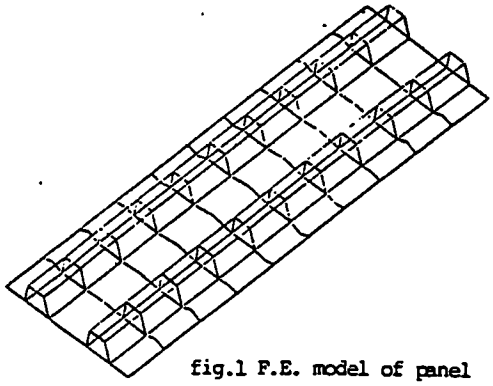

fig.1 F.E. model of panel

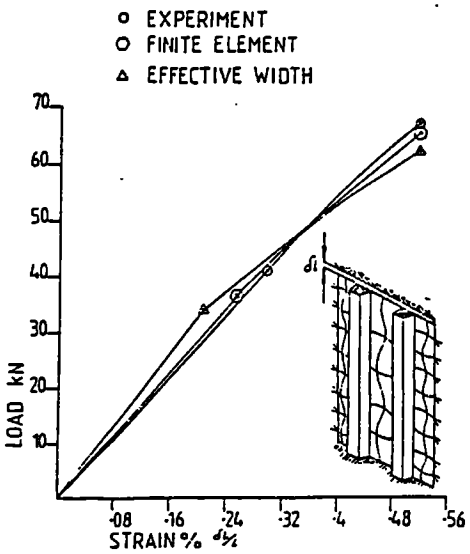

fig.2 3 design methods for panels

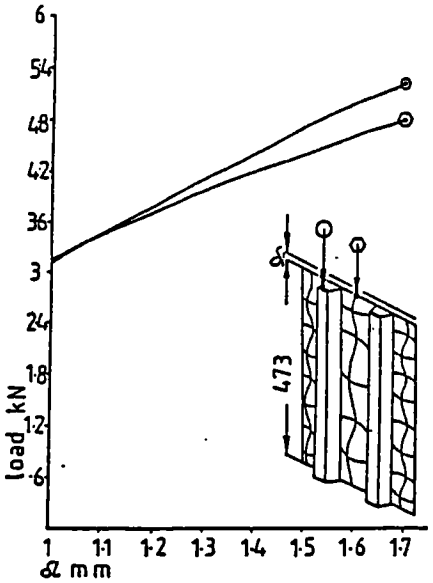

fig.3 F.E. node reactions

analysis at present is in the long computer processing time and large memory requirements required. This is because the structure has to be solved at each incremental displacement in order to build up the load/displacement curve. This factor made it impractical to analyse a box structure in this way, as the DEC VAX750 machine took 13 hours of CPU time to analyse the panel only.

Finite strip analysis.

The computer program PASCO was also used (4). This uses a finite strip method to determine the buckle shape across the plate. The plate is built up from repeating elements which are then linked together to form the desired cross section. PASCO is a program which incorporates VIPASA, the actual buckling analysis, in a method of structural optimisation. This can be used to optimise the panel at the point of buckling. The design solution tends towards the use of deep, very closely spaced stiffeners if allowed to optimise without constraints.
This program is quick to use and accurate at the point of buckling. The disadvantage is that the program cannot analyse post buckled panels.

Orthotropic plate equation with effective width concept for post buckling.

This analysis was used by the author as a means of quickly sizing post buckled specially orthotropic panels for initial design purposes. As a program for use on a 48k microcomputer, it was later developed to optimise the spacing of ribs and stiffeners. It was found to give results to a good engineering accuracy.
In the experimental results for all of the test panels in ref.1 it was noticed that due to the torsionally stiff nature of the stiffener design, they tended to remain stable up to overall column failure. The only effect of the stiffeners was in taking up relatively more of the panel loading as the skin panels buckled. For these reasons it was assumed that the stiffeners could be considered to be a linear - elastic part of the structure until overall failure occured.
The behaviour of the whole stiffened panel was thus approximated to be that of a series of plates which would locally buckle, held in simple support at each side by a series of linear - elastic stiffeners.

Buckling of the skin panels.

Compression.

The length of the panel is allowed to vary, and the buckling load is determined for simple-support conditions by the equation below, which has been derived from the differential equation

describing the free vibration of a specially orthotropic plate.

$$P_{CR} = \frac{\pi^2}{b}\left\{D_{11}\left(\frac{b}{a}\right)^2 + 2(D_{12}+2D_{33}) + D_{22}\left(\frac{a}{b}\right)^2\right\} \quad (1)$$

Shear.

The critical load on the plate for shear buckling is given by the equations below, also derived from the overall plate differential equation, from ref.2.

When $D11D22 > (D12+2D33)\uparrow 2$,

$$T_{CR} = \sqrt{\frac{2D_{22}(D_{12}+2D_{33})}{(b/2)^2 t}}\left\{8.3 + 1.525\frac{D_{11}D_{22}}{(D_{12}+2D_{33})^2} - .493\frac{D_{11}^2 D_{22}^2}{(D_{12}+2D_{33})^4}\right\} \quad (2)$$

When $D11D22 < (D12+2D33)\uparrow 2$,

$$T_{CR} = \frac{\sqrt[4]{D_{11}D_{22}^3}}{(b/2)^2 t}\left\{8.125 + 5.64\sqrt{\frac{(D_{12}+2D_{33})^2}{D_{11}D_{22}}} - .6\frac{(D_{12}+2D_{33})^2}{D_{11}D_{22}}\right\} \quad (3)$$

Interaction.

From Leknitski (5) it has been shown that the plate buckles when:

$$\frac{P_x}{P_{xCR}} + \frac{P_y}{P_{yCR}} + \frac{P_{xy}}{P_{xyCR}}^2 \geq 1 \quad (4)$$

Displacement and strain.

The displacement of the plate in compression at buckling is given by:

$$u_{CR} = P_{xCR}\frac{a}{t E_{11}} \quad (5)$$

from which the strain at buckling follows from:

$$\varepsilon_{CR} = \frac{u_{CR}}{a} \quad (6)$$

Post buckled stiffness.

This is analysed using the approach found in ref.3.

First the elastic constant H is found:

$$H = \left(\frac{1}{G_{12}} - \frac{2\nu_{12}}{E_{11}}\right) \quad (7)$$

This is applied to the following equation for the reduced stiffness of a simply supported plate:

$$\frac{E^*}{E} = \frac{2 + \left(1 + E_{11}H(b/a)^2 + 3\frac{E_{11}}{E_{22}}\left(\frac{b}{a}\right)^4\right)}{2 + 3\left(1 + E_{11}H(b/a)^2 + 3\frac{E_{11}}{E_{22}}\left(\frac{b}{a}\right)^4\right)} \quad (8)$$

The effect of stiffeners.

The stiffener areas and properties are then superimposed on those for the skin panels to obtain the whole plate stiffness. This can be determined at the point of buckling, and for any desired strain level above this.

The stiffener area is assumed to be 90% unidirectional fibres in the stiffener cap only. The area neglected is assumed to be 45 degree fibres in the stiffener sides, which constitute shear webs. These are assumed to carry insignificant compression load, as shown in the finite element analysis.

The loading due to the stiffeners is thus:

$$P_s = A_s E_s u \qquad N/M \quad (9)$$

so that the total panel loading per unit width is given by:

$$P_{tot} = \frac{P_s}{1000} + WP_{SW} \qquad KN/M \quad (10)$$

Overall buckling of the panel.

Here the stiffener/skin combination is considered to act as a beam in the overall Euler mode. The skin and stiffener caps are assumed to be thin so that the second moments of area are calculated from the centroids of their areas.

The second moment of area of the panel is:

$$EI = A_s\left(\frac{d}{2}\right)^2 E_s + tw + \left(\frac{d}{2}\right)^2 E_{11} \quad (11)$$

From which the critical length for overall panel failure is found from:

$$L = \sqrt{\frac{\pi^2 EI}{P_{tot}\times 1000}} \qquad M \quad (12)$$

This is used to determine the rib pitch required.

Weight of the panel.

The stiffeners are assumed to be of square cross section, and to be filled with 71 kg/m^3 foam. The stiffener walls are assumed to be half the thickness of the skin panels, and the stiffener caps to be 1.5 times as thick. These ratios are close to those employed in the stiffened panels which have been optimised in ref.1.

Knowing the density of the composite material, the weight of the panel per unit area is easily determined.

This technique was used to size the skin panels from running loads obtained by engineers' bending theory. It was also used to find the degree of reduced stiffness of the skin panels after buckling. These skin sizes and reduced stiffness values were then applied to a linear finite element analysis of the whole structure to check deflections and strain levels under load when in a post buckled condition, as seen in fig. 4.

These methods have been used to size the structure prior to finite element analysis of the complete wing box. The finite element model (fig 4) incorporated reduced stiffness

properties for the skin panels derived from the above analysis. By this means the effect of buckling could be modelled over the whole structure.

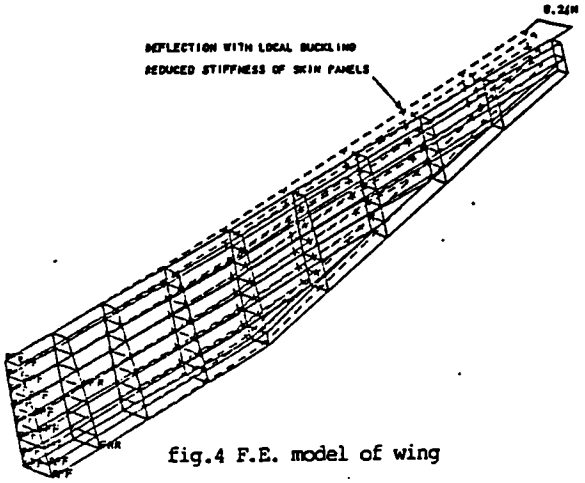

fig.4 F.E. model of wing

Design philosophy.

The post buckled concept is central to this work, and so a configuration of buckled skin panels stabilised by ribs, stiffeners and spars had to be realised in practice. In the case of this wing, the values of shear loading in the spar shear webs is low so that a multiple spar design would result in impractically thin guages for the shear webs. For these reasons a single cell torsion and bending box with stiffened skin panels was designed to take the major loads.

Construction techniques.

Panels.

The construction techniques for producing panels incorporating co-cured, foam cored, trapezioidal section stiffeners have been well proven in ref 1. The use of an enclosed section for the stiffeners in post buckled design is important. Due to the high torsional stiffness of the stiffeners, stiffener rolling and consequent failure due to modal interaction of local and stiffener flexural buckling may be avoided. The desired mode of failure is by column buckling at or near to 0.4% axial strain.

Construction of these foam cored stiffeners is relatively straightforward as the foam is used as tooling to maintain the desired cross section during curing. After cure, the foam remains in position and helps to stabilise the stiffener walls. In order to acheive good compaction of the laminate at the stiffener/panel junction, silicone rubber presssure intensifiers are used. A layer of polytetraflouroethylene (PTFE) cloth release film is placed between these and the laminate to avoid silicone contamination of the epoxy matrix.

Ribs.

The original design concept was to produce a box structure by curving flat skin/stiffener panels over ribs. The ribs would then be bonded to the skins along the rib flanges. The ribs were designed as flanged mouldings in CFRP at +-45 degrees to the fore and aft axis as it was intended that the bending material would be built into the panel skins at the rib stations. The rib flange was continuous so that a bond could be made to the panel and stiffener surfaces, so maximising the bond area.

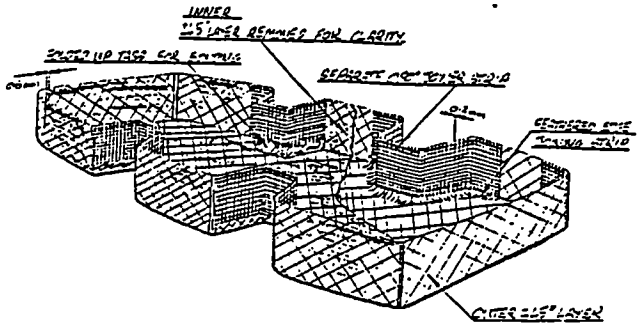

fig.5 rib design

Using channel section spars, the ribs were firstly bonded to these components by using a high viscosity cold curing epoxy adhesive. This operation was easy, but the bonding of the ribs to the skin presented more difficulty. Problems were encountered in build-up of tolerances between the rib flange and stiffener profiles. Difficulty was also experienced in clamping the joint effectively. Eventually blind rivets were used here to close the joint, with aerodynamic penalties.

Co cured design.

To solve these problems a new means of construction has since been developed whereby the rib flanges are produced integrally with the stiffened panels. Tooling for these is produced by means of setting a template of the desired rib flange against the tool surface which has sections of dummy stiffeners placed onto it (fig 6).

Starting with a very fine tissue of glass rovings, a wet laminated glass or carbon fibre contact moulding is produced which follows the form of the rib/stiffener/skin junctions. The moulding is then cut at the apex of each stiffener into segments, so that variations in thickness of the CFRP part to be produced can be accomodated. The stiffened panel is then produced as shown in fig 7. The panel skin laminations are firstly positioned on the tool, followed by the stiffener cores, stiffener cap unidirectional

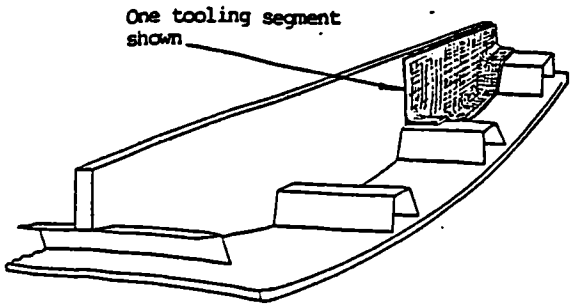

fig.6 tooling for ribs

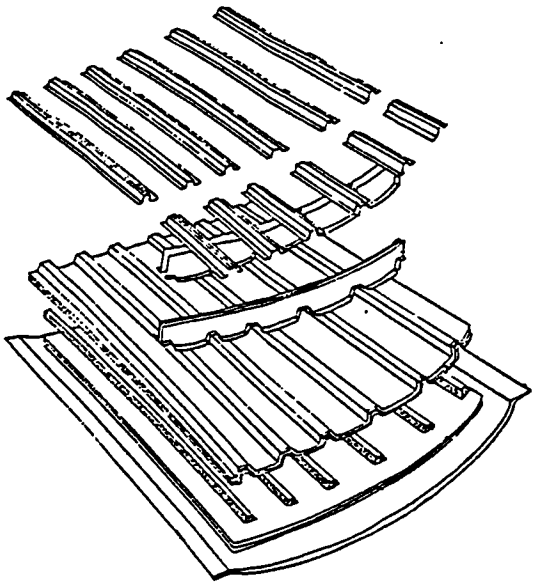

fig.7 panel components

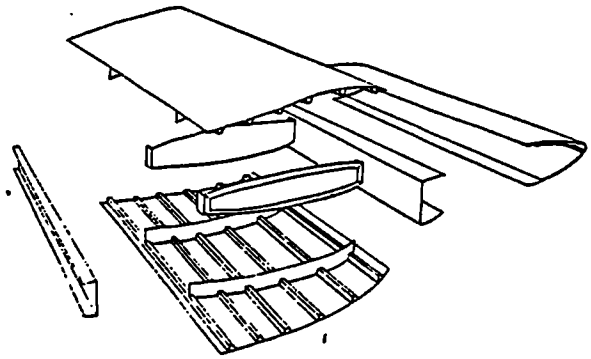

fig.8 box assembly

material, the rest of the skin laminations and finally the rib flange laminations. The flange laminations spread out in both directions on contact with the panel to prevent peel failure of the joint. The rib tools are then placed in position, spray coated with a PTFE release agent. These are followed by a PTFE release cloth and the pressure consolidators for the panel stiffeners. After these parts have been positioned, the whole assembly is covered in a glass wool bleeder pad to ensure equalisation of the vacuum and to prevent vacuum bag failure through bursting against sharp edges. The fact that the vacuum bag bridges across the corners at the stiffener/rib junctions is of no consequence as the pressure is carried by the tooling in these areas. The whole assembly is enveloped in a vacuum bag for subsequent autoclave curing at a pressure of 40-50 psi and 120 degrees C.

Assembly of the box.

Although production of the skin panels is more complex, assembly of the box is much simplified and structural integrity improved by this process, as shown in fig 8. The ribs are now joined to the panels at their shear webs, where a large shear loaded bond can be readily made. Location and clamping devices such as rivets can be incorporated without compromise to the aerodynamic performance of the wing.
Once the panels have been joined to the ribs, the leading and trailing spars are added. To avoid the problem of bondline failure caused by local buckling of the adjacent skin panel, the spars join the skin at panel stiffeners. In this way the bond area is stabilised against peeling loads. The stiffeners here are also specially shaped so that the spars bond to the stiffener sidewall as well as the panel skin.

Spars.

A foam stabilised spar is being used following problems experienced when shear buckling of the spar shear web interacted with compression buckling of the adjacent compression panel. This effect tended to increase the problem of peel loads arising at the spar flange to skin bond.

Experimental programme.

A box structure has been constructed and tested to the original design, with results shown in fig 9. This showed that post-buckled structure has potential in practice, as full elastic recovery was demonstrated through several load/unload cycles to proof load. The fatigue life of such a structure should also be better than in aluminium because of the superior fatigue charecteristics of the material itself and the bonded construction.
Following experience gained with this box, a second structure incorporating the co-cured techniques described above has been constructed, which is currently under test. The work will culminate in the production of a full scale wing box 4m long for static load, acoustic emission and damage tolerance testing.

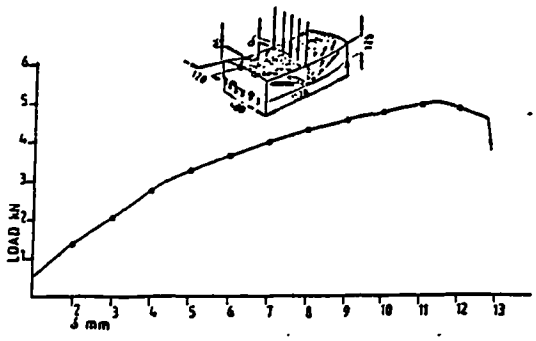

fig.9 test box results

references.

1. The design, manufacture and testing of stiffened aircraft compression panels using advanced materials.
G.Belgrano.
Cranfield Institute of technology
College of Aeronautics
Structural design Msc thesis
1984.

2. Composite engineering laminates.
A. Deitz
M.I.T. press.

3. On the use of the effective width concept for composite plates.
Rhodes & Marshall.
Composite structures
I.H. Marshall
Applied science publications
1981.

4. Pasco. Capability and analytical foundation.
M. Anderson et al,
NACA technical memorandum no.
80181.
1980.

5. Anisotropic Plates.
S.G. Lekhnitskii.
Gordon & Breach,
1968.

12

The Construction of a Postbuckled Carbon Fibre Wing Box

W. G. BROOKS

College of Aeronautics, Cranfield Institute of Technology, Wharley End, Bedfordshire MK43 0AL, UK

ABSTRACT

A postbuckled carbon fibre structure requires special design considerations to avoid delamination failures. A practical design for a postbuckled wing box is presented. The design features incorporated have been proven in the author's testing programme. This is leading to the testing of a full-scale wing box for an aerobatic light aircraft. Various means of improving the strength of skin/stiffener junctions are described, including the use of Kevlar stitching at this critical area.

A co-curing technique is used to form all the joints made directly to the skin surfaces. Tooling suitable for low volume production has been developed to form these joints. Final assembly of the structure is by adhesive bonding. Different configurations of joint are evaluated. A type of slotted joint is developed which uses features incorporated into the co-cured mouldings. This type of joint allows the structure to be assembled without the use of expensive clamping jigs.

1. THE WING DESIGN

The wing has been designed as a box beam structure using ten ribs, as seen in Fig. 1. It has two full-depth spars. There are eight stiffeners across the chord at the root and three at the tip, including the spar caps. It is designed to withstand 13·5 g at the aircraft's aerobatic weight. It is intended to allow the wing skins to postbuckle in order to maximise the strength/weight ratio.

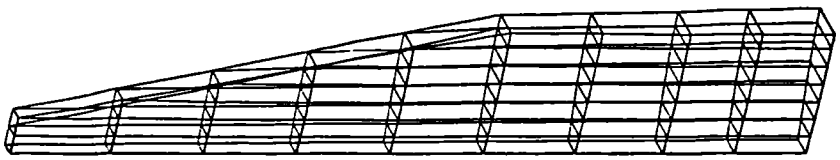

FIG. 1. Finite element wing box model.

The design methods used to size the structure and optimise the configuration have been described in Ref. 1.

The wing is constructed from a 120°C curing prepreg carbon fibre/epoxy system, Ciba-Geigy 913. High strength unidirectional fibres are used for the stiffener caps and skin mid-plies with a cured thickness of 0·127 mm per ply. A woven five-harness satin cloth reinforcement is used for the $\pm 45°$ outer skin layers. The cured thickness of this material is 0·34 mm. A woven reinforcement was chosen for ease of handling.

2. PROBLEM AREAS OF POSTBUCKLED DESIGN IN COMPOSITES

2.1. Skin/Stiffener Joints

To avoid modal coupling between stiffener torsional buckling and plate local buckling a closed section stiffener has been used. The type of stiffener shown by the program PASCO (Ref. 2) to give the highest panel compression buckling load for a given weight is of a closed trapezium section (Fig. 2).

These stiffeners can be produced by means of a Rohacell foam core of the required cross-section. Some form of tooling is required to produce the external form of the stiffener. The foam then provides a reaction to the tooling, allowing the laminate to be consolidated. This foam core is designed to stay in place after curing of the panel.

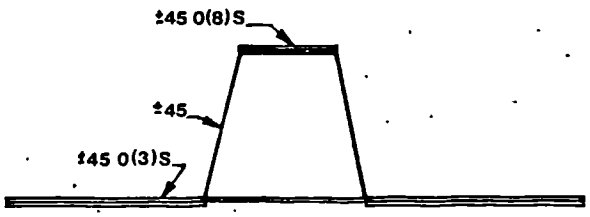

FIG. 2. Typical stiffener.

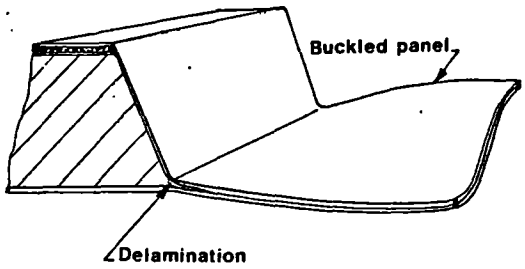

FIG. 3.

One cause of failure of the panels in Ref. 3 was separation of the skin from the stiffeners due to the effects of local buckling. As the skin panels buckle, both bending and peeling loads are generated at the skin/stiffener junction. These panels had the stiffeners co-cured to the skin as integral members. However, they were constructed in such a way as to produce a weak peel-loaded junction between the stiffener and the skin, as shown in Fig. 3. Three methods have been explored to prevent or delay this mode of failure.

2.1.1. The corrugated method

This method of panel lay-up is shown in Fig. 4. It was intended to prevent stiffener separation from the skin by putting most of the skin plies into the stiffener sidewalls. In this way continuous fibre paths would exist across the junction. This method was used in the construction of the first testbox. This box was representative of the outer wing and developed a postbuckling ratio of 5.

The main disadvantage of this scheme arises when the panel has more than two stiffeners. It then becomes extremely difficult to form the prepreg

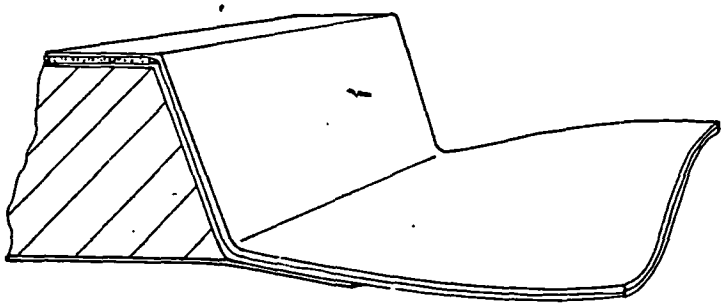

FIG. 4. Corrugated method.

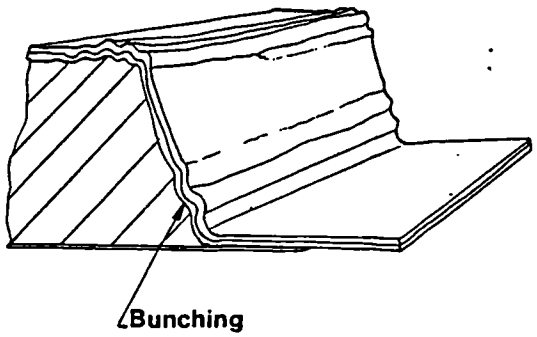

FIG. 5.

so that it conforms exactly to each stiffener profile. Excess material is forced to bunch together, usually at the stiffener corners (Fig. 5). This occurred despite the use of tooling that was completely successful when used on a single stiffener panel.

There are also a large proportion of $\pm 45°$ fibres placed into the stiffener walls by this method. These fibres are used in the skin panels to give a high buckling load. These are not required in the stiffeners, which are essentially beam-columns. Their function is to take up axial loading as the skin panels buckle, and to provide structural stability in the long column and torsional modes. For this purpose unidirectional material is required at the stiffener top and base. Thin shear webs are required between them to provide a torsionally stiff section.

2.1.2. The stiching method

Stitching of the panel at the skin/stiffener junction was seen as a means of achieving two aims. These were to make the prepreg conform tightly to the stiffener profile at the lay-up stage, as well as to improve the strength of the joint. A standard industrial sewing machine was used. A 70-tex spun Kevlar thread was used with an ultimate tensile load of 57 N. Due to the limited throat of the machine, a lay-up technique had to be developed which used subassemblies. These were then co-cured together. An interleaving technique was devised for this purpose, as shown in Fig. 6. This technique has the advantage of allowing adjustment of the stiffener spacing on the tool. Any excess material could move in the interleaves instead of bunching during the cure. The compression skin panel of testbox 2 was successfully produced and tested using this method. This testbox, as shown in Fig. 7, is representative of the wing root area and has a postbuckling ratio of 2·5.

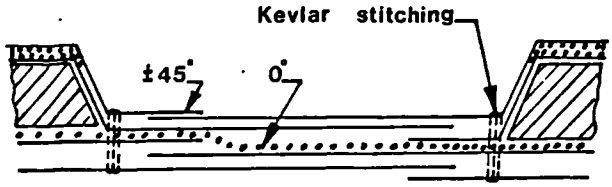

FIG. 6. Interleaving and stitching.

Although this method was successful, the manufacturing process is rather labour intensive. Slow stitching rates have to be used to allow the viscous resin to flow as the needle passes through, typically 150 stitches/min at 20°C. Faster speeds result in more damage as more fibres are broken rather than flowing around the needle. Increasing the temperature of the prepreg reduces the viscosity but increases the resin pick-up on the needle. A solvent pad can then be used to keep the needle clean but with the risk of the solvent affecting the prepreg.

2.1.3. Co-cured joint design

The function strength can be considerably improved by the incorporation of an anti-peel bridging strip, as shown in Fig. 8. A single ply of woven ±45° carbon has a great effect on the peeling strength compared with the simple joint. This bridging strip can be incorporated into the construction under the stiffener foam core, bending upwards into the stiffener sidewall. The void at the junction between the strip, the stiffener sidewall and the skin is filled with resin or a bundle of unidirectional fibres. Reference 4 shows that increasing the corner radii here increases the joint peeling strength.

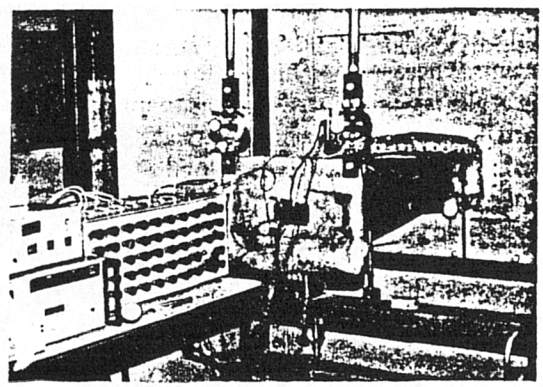

FIG. 7. Testbox 2.

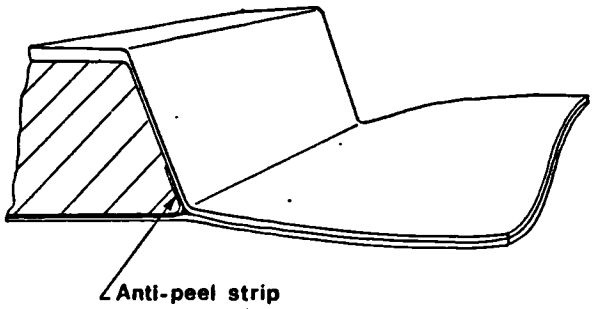

FIG. 8.

To solve the problems of stiffener spacing adjustment and float of excess material, the stiffener sidewall plies have been designed to overlap at the stiffener cap. The stiffener cap is a structurally stable area. A joint here is not liable to failure through delamination caused by local buckling effects.

2.2. Testing of the Skin/Stiffener Joints

A special test coupon has been devised to duplicate the peeling and bending loads at the junction, as seen in Fig. 9. Using this method, various configurations of co-cured joint were tested with results shown in Table 1. In the case of the stitched joints it was found that the stitching pitch had to be in the order of 1 mm or less to realise an advantage over the plain control specimen. The stitches had also to be made within 0·5 mm of the junction in order to provide an improvement.

The very great improvement in strength from the use of an anti-peel strip can be seen. It allows the interlaminar tensile loads to be distributed over a large area instead of the load acting on the stress concentration at the joint in the brittle matrix.

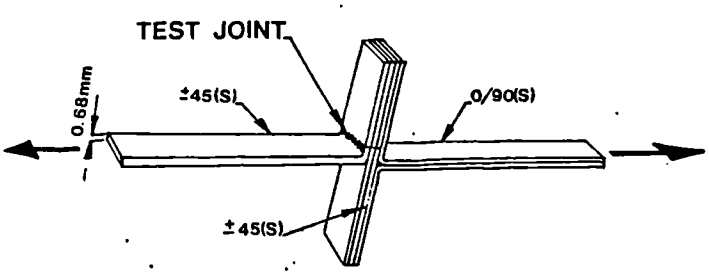

FIG. 9. Peel test coupon.

TABLE 1
Skin/stiffener junction results

Specimen	Load/width (N/mm)
Control-simple co-cured peeling joint	78
Zigzag stitched, 0·6 mm feed, 1·8 mm wide stitches using 70-tex spun Kevlar. Delaminated under the stitching	100
With anti-peel strip one ply woven CFRP at junction. Did not peel—delaminated under the joint	104
With anti-peel strip (two plies woven CFRP at junction). Delaminated under the junction	118

3. THE POSITIONING OF ASSEMBLY JOINTS

Correct location of bonded assembly joints in a postbuckled structure is of great importance. The prime consideration is to avoid placing these joints adjacent to buckled components. Good and bad methods of joining a spar to a postbuckled skin panel are shown in Fig. 10. Joint geometry should also be simple unless the two components to be joined have been produced

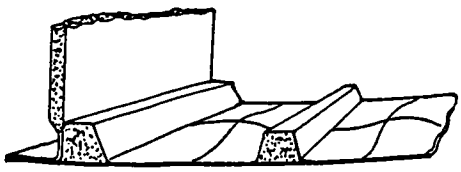

Good

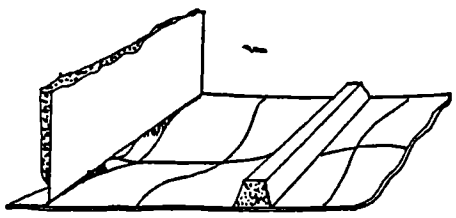

Bad

FIG. 10. Spar to skin joints.

on very precise matched tooling. This is one reason why it has been found better to co-cure the rib flanges with the skin. The box structure can then be completed by the use of rib shear webs.

3.1. Clamping of Simple Lap Joints

Clamping of lap joints for assembly, particularly if one side is blind, can be a major problem. This is particularly true for thin sections where the clamping force has to be distributed along the length of the component. The spar joints of testbox 2 were clamped by means of a partial vacuum drawn inside the box, as shown in Fig. 11. This technique is acceptable for

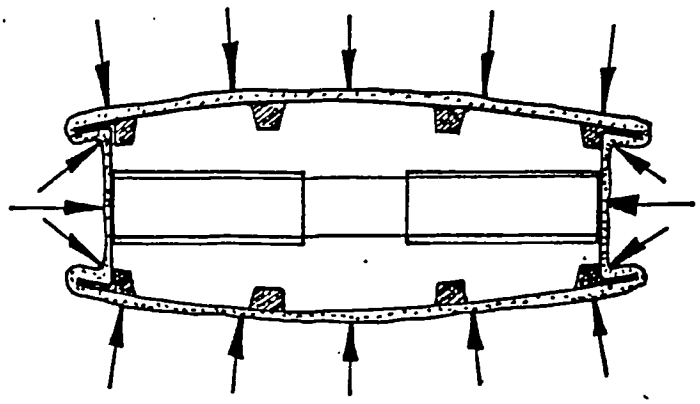

FIG. 11. Vacuum clamping.

boxes of near square section. Boxes of long chord require reinforcement to avoid crushing. An alternative solution is to design a large clamping jig, the cost of which is too high to justify for a one-off structure. This type of simple lap joint also incorporates no means of controlling the bondline thickness. Over-clamping can result. This results in the bondline being too thin with a consequent reduction in strength.

3.2. Slotted Joints

These disadvantages led the author to investigate slotted joints, as shown in Fig. 12. This type of joint can be co-cured as a feature into the structure. It can be designed to be self-clamping with bondline thickness control. It can also locate the components together in the desired position. These joints load the adhesive in pure shear without the peeling effects which can occur in single lap joints.

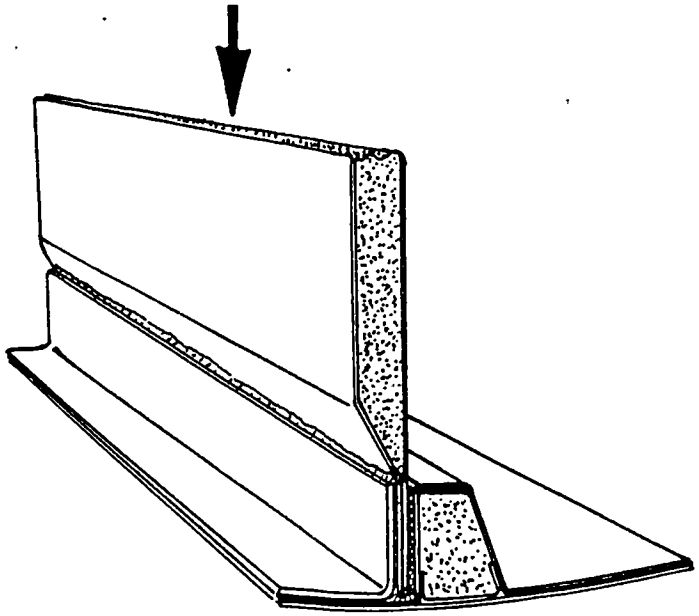

FIG. 12. Slotted joint.

3.3. Spar Joints

For these reasons continuous slotted joints are used to join each spar shear web to the stiffened skin panels. In this design a sandwich stabilised shear web is used. This is designed not to buckle. This 'slot together' joint concept could work particularly well with a sine wave stabilised shear web, requiring very little strength from the adhesive.

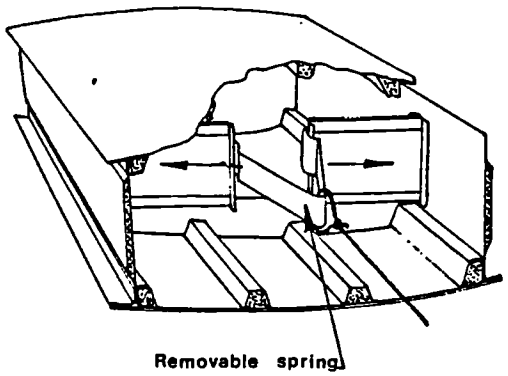

FIG. 13. Rib to spar bonding.

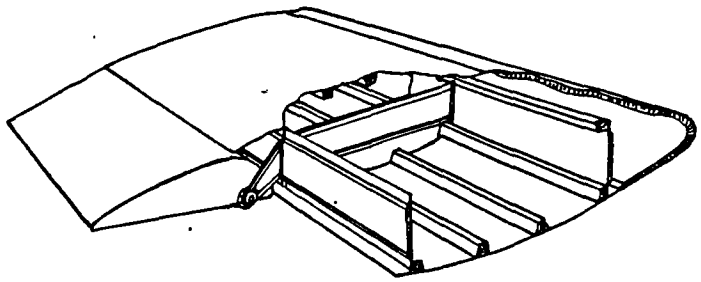

FIG. 14. Pickup rib detail.

3.4. Rib Joints

The ribs are joined together by means of a slotted joint similar to that of the spars. However, in the case of the ribs there can be a need to form a bond between the ribs and the spar shear web (Fig. 13). This is accomplished by cutting the rib into two sections. The bond clamping force is then provided by means of a removable hairpin spring. This spring slides the two rib sections apart along their slotted joints.

Where pickup points such as those for the aileron hinges are required, the solution is to cut the spar at this point. This allows the rib web to come through as a continuous member. The rib then diffuses the load from the ribs into skin shear through the slotted joints and co-cured rib flanges (Fig. 14). Since only the spar shear web has been cut, no problems exist with discontinuity of the spar caps.

4. TOOLING

There are many advantages of using composite materials in the tooling. Complex forms such as the rib tooling can be produced at low cost. The coefficient of thermal expansion can be the same as that of the component to be produced. Tooling can be produced which is of high stiffness with comparatively low weight. The tooling system for this test structure is shown in Fig. 15. For this one-off test structure all the composite tooling is produced by the wet laminating process. A high temperature resin system, SP690/590, is used which cures at room temperature. A slow postcuring cycle is then required to give the resin a heat deflection temperature of 130°C. By using a 120°C curing prepreg for the final structure, this wet laminated tool can be used directly to produce the component. This was a major reason for choosing Ciba-Geigy 913 prepreg material.

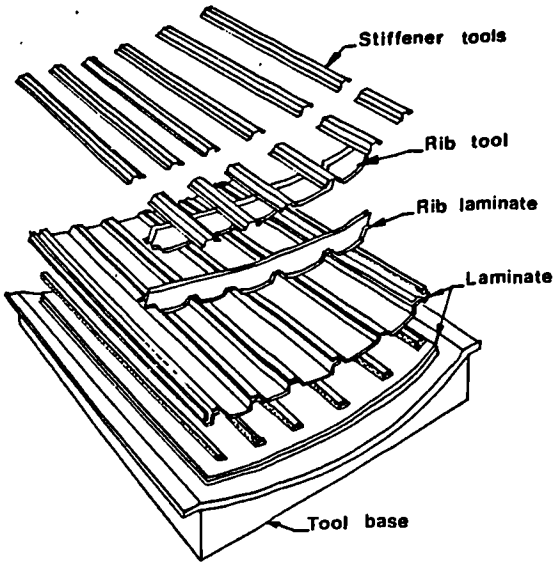

FIG. 15. Tooling system.

4.1. Skin Tooling

The tooling used to produce the co-cured skin panels is of carbon/epoxy. A specially orthotropic laminate 6 mm thick of woven material at 0/90° to the rear spar is used. An 'egg box' type of stiffening structure has been laminated to the undersurface of the tool. The depth of this should be at least $\frac{1}{30}$ of the tool length for adequate stiffness.

4.1.1. Ribs

The tooling for the rib flanges was produced from wet laminated mouldings taken from the tool surface. Using a dummy rib and stiffeners, a carbon/epoxy moulding was made, as shown in Fig. 16. These mouldings were cut at the apex of each stiffener. This allows each part of the moulding to distribute the autoclave pressure evenly on to the co-curing panel.

4.1.2. Stiffeners

The stiffeners were originally produced using silicone pressure intensifiers. This material can cause contamination of the CFRP surface, and so is no longer used. A system of folded steel sections is now used to consolidate the prepreg.

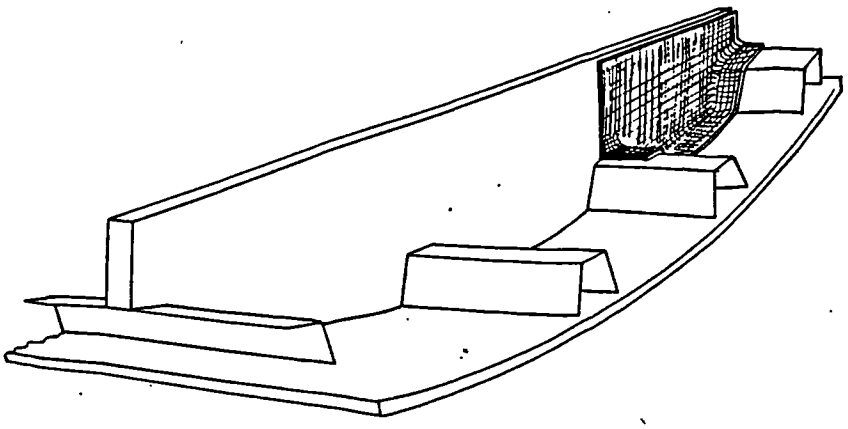

FIG. 16. Rib tool moulding technique.

4.1.3. Jointing features

The slotted joints are formed by inserting PTFE-coated light alloy strips into the moulding. These are removed after cure to reveal a slot. The slot is then prepared for bonding with an abrasive. A layer of textured peel-ply could be used here for the purpose of forming a good bond.

5. CONCLUSIONS

Critical problem areas of postbuckled design in composites have been identified. These are mainly in joint areas between stiffeners and buckled skin panels. Three methods of preventing failure by skin/stiffener separation have been described. Of these, the method of including an anti-peel strip into the junction is the simplest and most effective.

Stitching of the laminate in this area is effective but is a laborious process due to the small stitching pitch required. The technique was not used in the final design on these grounds. However, an upper bound to the process where failure occurs by fibre breakage at the junction has not yet been found.

The location and type of bonded assembly joints has been found to be important for success. It has been shown that joints should be made at structurally stable parts of the structure to avoid debonding.

Other features of the design have been developed to simplify production. These include the overlapping technique at the stiffener caps to avoid

bunching; the slotted joints at the ribs and the slotted spar joints. These last two features allow assembly of a bonded structure without the need for expensive clamping systems.

ACKNOWLEDGEMENT

This work is supported by the Royal Aircraft Establishment, Farnborough.

REFERENCES

1. BROOKS, W. G., The design and construction of a post buckled carbon fibre wing box structure, *ICAS Conference Proceedings*, College of Aeronautics, Cranfield Institute of Technology.
2. PELGRANO, G., The design, manufacture and testing of stiffened aircraft compression panels using advanced materials, M.Sc. structural design thesis, Cranfield Institute of Technology, 1984.
3. ANDERSON, M. *et al.*, PASCO panel analysis and sizing code, capability and analytical foundations, NACA Technical Memorandum 30181, January 1980.
4. COPES, R. and PIPES, R., Design of the spar to wingskin joint, Centre for Composite Materials, University of Delaware: LENOE *et al.*, *Fibrous Composites in Structural Design*, New York, Plenum Press, 1978.

Appendix F.

The complete strain gauge test data. Refer to drawing A1-CFRP-04 in appendix H for strain gauge positions.

POSITIVE LOAD TEST RESULTS

LOAD KN	0.000	4.986	9.987	14.909	19.906
S.G. NO.	STRAIN EACH LOAD %				
1/1	0.000	0.005	0.008	0.013	0.019
1/2	0.000	-0.004	-0.008	-0.013	-0.016
1/3	0.000	0.005	0.011	0.017	0.023
2/1	0.000	0.002	0.002	0.002	0.003
2/2	0.000	-0.001	-0.003	-0.004	-0.006
2/3	0.000	0.003	0.004	0.005	0.005
3/1	0.000	0.001	0.001	0.001	0.001
3/2	0.000	-0.000	-0.001	-0.001	-0.001
3/3	0.000	0.004	0.004	0.005	0.005
4/1	0.000	0.004	0.006	0.007	0.009
4/2	0.000	-0.000	-0.001	-0.003	-0.004
4/3	0.000	0.002	0.002	0.003	0.004
5/1	0.000	0.003	0.002	0.000	-0.001
5/2	0.000	0.003	0.003	0.002	0.001
5/3	0.000	-0.001	-0.002	-0.003	-0.005
6/1	0.000	0.004	0.006	0.006	0.007
6/2	0.000	0.002	0.002	0.001	0.001
6/3	0.000	0.003	0.003	0.003	0.003
7/1	0.000	0.006	0.007	0.008	0.008
7/2	0.000	-0.001	-0.002	-0.002	-0.003
7/3	0.000	0.005	0.005	0.006	0.007
8/1	0.000	-0.022	-0.024	-0.018	-0.019
8/2	0.000	-0.001	-0.002	-0.003	-0.003
8/3	0.000	0.006	0.007	0.007	0.007
9/1	0.000	0.001	0.001	0.002	0.002
9/2	0.000	0.002	0.003	0.004	0.005
9/3	0.000	0.005	0.007	0.010	0.012
10/1	0.000	0.006	0.010	0.015	0.018
10/2	0.000	0.017	0.017	0.014	0.014
10/3	0.000	0.010	0.018	0.026	0.035
11/1	0.000	0.009	0.018	0.025	0.033
11/2	0.000	-0.004	-0.011	-0.017	-0.023
12/1	0.000	-0.006	-0.012	-0.019	-0.025
12/2	0.000	0.009	0.018	0.027	0.037
13/1	0.000	0.006	0.012	0.019	0.024
13/2	0.000	-0.006	-0.011	-0.016	-0.020
14/1	0.000	-0.006	-0.012	-0.018	-0.024
14/2	0.000	0.003	0.008	0.013	0.018
15/1	0.000	-0.004	-0.010	-0.015	-0.021
15/2	0.000	0.010	0.018	0.025	0.033
16/1	0.000	0.008	0.012	0.016	0.020

POSITIVE LOAD TEST RESULTS

LOAD KN	0.000	4.986	9.987	14.909	19.906
S.G. NO.		STRAIN EACH LOAD %			
16/2	0.000	-0.004	-0.008	-0.012	-0.017
17/1	0.000	-0.011	-0.022	-0.032	-0.042
17/2	0.000	0.011	0.020	0.029	0.037
18/3	0.000	-0.016	-0.033	-0.047	-0.060
19/3	0.000	-0.027	-0.057	-0.090	-0.127
20/3	0.000	-0.038	-0.078	-0.121	-0.169
21/3	0.000	0.141	0.121	0.103	0.085
22/3	0.000	-0.027	-0.053	-0.077	-0.102
23/3	0.000	-0.025	-0.051	-0.076	-0.100
24/3	0.000	-0.024	-0.048	-0.070	-0.093
25/3	0.000	-0.027	-0.054	-0.081	-0.107
26/3	0.000	-0.028	-0.058	-0.089	-0.119
27/3	0.000	-0.017	-0.034	-0.051	-0.067
28/3	0.000	-0.020	-0.039	-0.058	-0.076
29/3	0.000	-0.022	-0.042	-0.062	-0.081
30/3	0.000	-0.014	-0.027	-0.036	-0.039
31/3	0.000	-0.014	-0.027	-0.039	-0.049
32/3	0.000	-0.014	-0.034	-0.052	-0.072
33/3	0.000	-0.007	-0.016	-0.022	-0.026
34/3	0.000	-0.012	-0.024	-0.036	-0.047
35/3	0.000	-0.012	-0.023	-0.032	-0.042
36/3	0.000	-0.010	-0.019	-0.028	-0.036
37/3	0.000	-0.014	-0.028	-0.038	-0.048
58	0.000	-0.020	-0.041	-0.062	-0.083
59	0.000	-0.005	-0.015	-0.025	-0.035
60	0.000	-0.014	-0.030	-0.045	-0.060
61	0.000	-0.006	-0.017	-0.027	-0.037
62	0.000	-0.005	-0.014	-0.021	-0.029
63	0.000	-0.009	-0.023	-0.036	-0.049
64	0.000	-0.001	-0.006	-0.010	-0.014
38/3	0.000	0.027	0.052	0.074	0.097
39/3	0.000	0.038	0.076	0.117	0.159
67	0.000	0.031	0.059	0.090	0.122
37/3	0.000	-0.006	-0.016	-0.024	-0.032

POSITIVE LOAD TEST RESULTS

LOAD KN	21.867	22.751	23.835	25.813	28.017
S.G. NO.	STRAIN EACH LOAD %				
1/1	0.022	0.021	0.022	0.025	0.027
1/2	-0.018	-0.005	-0.006	-0.007	-0.008
1/3	0.025	0.030	0.031	0.033	0.034
2/1	0.003	0.004	0.004	0.004	0.004
2/2	-0.006	-0.012	-0.013	-0.013	-0.015
2/3	0.005	0.004	0.004	0.007	0.008
3/1	0.001	0.000	0.001	0.000	0.001
3/2	-0.001	-0.003	-0.003	-0.004	-0.004
3/3	0.006	0.005	0.005	0.006	0.006
4/1	0.009	0.009	0.010	0.010	0.011
4/2	-0.004	-0.006	-0.006	-0.007	-0.007
4/3	0.004	0.004	0.004	0.004	0.005
5/1	-0.001	-0.002	-0.002	-0.003	-0.003
5/2	0.001	0.000	0.000	-0.000	-0.000
5/3	-0.006	-0.007	-0.007	-0.008	-0.008
6/1	0.007	0.006	0.007	0.007	0.008
6/2	0.001	0.000	0.000	0.000	0.000
6/3	0.004	0.002	0.003	0.003	0.003
7/1	0.008	0.007	0.007	0.007	0.008
7/2	-0.003	-0.004	-0.004	-0.005	-0.005
7/3	0.007	0.006	0.006	0.006	0.007
8/1	-0.020	-0.018	-0.018	-0.018	-0.021
8/2	-0.003	-0.005	-0.005	-0.005	-0.005
8/3	0.008	0.006	0.007	0.007	0.007
9/1	0.002	0.001	0.001	0.001	0.001
9/2	0.005	0.004	0.004	0.004	0.005
9/3	0.013	0.012	0.012	0.013	0.014
10/1	0.020	0.020	0.021	0.023	0.024
10/2	0.014	0.012	0.010	0.011	0.010
10/3	0.038	0.039	0.041	0.044	0.048
11/1	-0.736	0.040	0.042	0.045	0.047
11/2	-0.025	-0.031	-0.033	-0.034	-0.036
12/1	-0.028	-0.031	-0.032	-0.036	-0.040
12/2	0.041	0.027	0.027	0.029	0.031
13/1	0.027	0.027	0.028	0.030	0.033
13/2	-0.022	-0.023	-0.024	-0.026	-0.028
14/1	-0.027	-0.029	-0.030	-0.033	-0.035
14/2	0.020	0.020	0.021	0.023	0.026
15/1	-0.023	-0.025	-0.026	-0.029	-0.031
15/2	0.035	0.036	0.037	0.040	0.043
16/1	0.022	0.022	0.023	0.024	0.026

POSITIVE LOAD TEST RESULTS

LOAD KN	21.867	22.751	23.835	25.813	28.017
S.G. NO.	STRAIN EACH LOAD %				
16/2	-0.018	-0.020	-0.021	-0.023	-0.024
17/1	-0.046	-0.049	-0.051	-0.055	-0.059
17/2	0.040	0.041	0.043	0.046	0.050
18/3	-0.064	-0.071	-0.074	-0.080	-0.086
19/3	-0.142	-0.154	-0.163	-0.180	-0.200
20/3	-0.190	-0.207	-0.219	-0.242	-0.269
21/3	0.078	0.074	0.070	0.063	0.056
22/3	-0.112	-0.112	-0.117	-0.126	-0.135
23/3	-0.111	-0.110	-0.115	-0.125	-0.135
24/3	-0.102	-0.104	-0.109	-0.118	-0.127
25/3	-0.116	-0.120	-0.125	-0.134	-0.145
26/3	-0.131	-0.136	-0.143	-0.155	-0.170
27/3	-0.073	-0.075	-0.078	-0.084	-0.091
28/3	-0.083	-0.085	-0.089	-0.096	-0.104
29/3	-0.088	-0.091	-0.095	-0.103	-0.112
30/3	-0.039	-0.037	-0.037	-0.037	-0.036
31/3	-0.053	-0.053	-0.055	-0.058	-0.060
32/3	-0.080	-0.083	-0.087	-0.096	-0.108
33/3	-0.026	-0.025	-0.024	-0.024	-0.022
34/3	-0.052	-0.053	-0.055	-0.059	-0.065
35/3	-0.046	-0.063	-0.048	-0.052	-0.056
36/3	-0.039	-0.047	-0.041	-0.044	-0.048
37/3	-0.053	-0.059	-0.062	-0.065	-0.070
58	-0.091	-0.085	-0.089	-0.095	-0.103
59	-0.039	-0.037	-0.039	-0.043	-0.047
60	-0.066	-0.068	-0.071	-0.077	-0.084
61	-0.041	-0.042	-0.044	-0.048	-0.052
62	-0.033	-0.033	-0.035	-0.038	-0.042
63	-0.054	-0.055	-0.058	-0.063	-0.069
64	-0.016	-0.016	-0.017	-0.019	-0.021
38/3	0.106	0.119	0.125	0.137	0.150
39/3	0.176	0.200	0.211	0.230	0.254
67	0.135	0.076	0.078	0.081	0.089
37/3	-0.036	-0.036	-0.038	-0.041	-0.045

NEGATIVE LOAD TEST

LOAD KN	0.000	6.012	9.994	11.984	13.939
S.G. NO.	STRAIN EACH LOAD IN %				
1/1	0.000	0.004	0.007	0.007	0.006
1/2	0.000	-0.003	-0.002	-0.001	-0.001
1/3	0.000	-0.007	-0.009	-0.010	-0.011
2/1	0.000	-0.003	-0.003	-0.004	-0.005
2/2	0.000	0.001	0.002	0.003	0.003
2/3	0.000	0.000	0.001	0.000	-0.000
3/1	0.000	0.006	0.007	0.007	0.006
3/2	0.000	-0.000	0.001	0.001	0.001
3/3	0.000	0.008	0.011	0.011	0.011
4/1	0.000	-0.002	-0.001	-0.001	-0.001
4/2	0.000	0.006	0.008	0.009	0.010
4/3	0.000	-0.001	-0.001	-0.001	-0.001
5/1	0.000	0.000	0.002	0.003	0.003
5/2	0.000	0.000	0.002	0.002	0.002
5/3	0.000	-0.002	-0.004	-0.006	-0.007
6/1	0.000	0.002	0.007	0.007	0.007
6/2	0.000	0.005	0.007	0.006	0.007
6/3	0.000	0.000	0.001	0.001	0.001
7/1	0.000	-0.000	0.000	0.000	0.000
7/2	0.000	0.000	0.002	0.002	0.002
7/3	0.000	-0.003	-0.002	-0.003	-0.003
8/1	0.000	-0.325	-0.325	-0.325	-0.325
8/2	0.000	-0.000	-0.001	-0.001	-0.001
8/3	0.000	-0.001	-0.001	-0.002	-0.002
9/1	0.000	0.003	0.003	0.002	0.002
9/2	0.000	0.002	0.002	0.002	0.002
9/3	0.000	-0.001	-0.001	-0.001	-0.001
10/1	0.000	0.005	0.006	0.007	0.009
10/2	0.000	-0.132	-0.134	-0.135	-0.134
10/3	0.000	0.008	0.013	0.016	0.018
11/1	0.000	-0.013	-0.018	-0.022	-0.026
11/2	0.000	0.010	0.019	0.021	0.025
12/1	0.000	0.006	0.013	0.014	0.017
12/2	0.000	-0.014	-0.023	-0.029	-0.033
13/1	0.000	-0.009	-0.015	-0.018	-0.021
13/2	0.000	0.007	0.014	0.016	0.018
14/1	0.000	0.009	0.016	0.019	0.022
14/2	0.000	-0.009	-0.012	-0.014	-0.016
15/1	0.000	0.006	0.011	0.013	0.016
15/2	0.000	-0.011	-0.018	-0.022	-0.025
16/1	0.000	-0.003	-0.005	-0.007	-0.008

LOAD KN	0.000	6.012	9.994	11.984	13.939
S.G. NO.	STRAIN EACH LOAD IN %				
16/2	0.000	0.005	0.012	0.014	0.016
17/1	0.000	0.015	0.026	0.031	0.035
17/2	0.000	-0.012	-0.018	-0.022	-0.025
38/3	0.000	-0.024	-0.036	-0.041	-0.045
39/3	0.000	-0.059	-0.090	-0.103	-0.115
40/3	0.000	-0.077	-0.127	-0.151	-0.177
41/3	0.000	0.177	0.156	0.146	0.135
42/3	0.000	-0.043	-0.072	0.043	-0.101
43/3	0.000	-0.041	-0.067	-0.080	-0.093
44/3	0.000	-0.027	-0.042	-0.050	-0.059
45/3	0.000	-0.032	-0.054	-0.066	-0.077
46/3	0.000	-0.034	-0.059	-0.071	-0.084
47/3	0.000	-0.024	-0.037	-0.042	-0.045
48/3	0.000	-0.030	-0.047	-0.056	-0.064
49/3	0.000	-0.033	-0.054	-0.065	-0.076
50/3	0.000	-0.019	-0.029	-0.034	-0.039
51/3	0.000	-0.023	-0.036	-0.042	-0.048
52/3	0.000	-0.027	-0.043	-0.051	-0.059
53/3	0.000	-0.019	-0.031	-0.036	-0.039
54/3	0.000	-0.030	-0.051	-0.062	-0.072
55/3	0.000	-0.026	-0.043	-0.051	-0.058
56/3	0.000	-0.010	-0.016	-0.018	-0.021
57/3	0.000	-0.012	-0.016	-0.019	-0.021
66	0.000	-0.020	-0.031	-0.039	-0.045
67	0.000	0.258	0.237	0.225	0.213
68	0.000	-0.013	-0.022	-0.027	-0.031
69	0.000	-0.021	-0.036	-0.044	-0.052
70	0.000	-0.014	-0.025	-0.031	-0.037
71	0.000	-0.008	-0.013	-0.016	-0.019
72	0.000	-0.024	-0.039	-0.047	-0.054
73	0.000	-0.007	-0.011	-0.014	-0.015
47EXT	0.000	-0.033	-0.055	-0.067	-0.081
50EXT	0.000	-0.022	-0.035	-0.042	-0.049
53EXT	0.000	-0.024	-0.041	-0.050	-0.059

NEGATIVE LOAD TEST

LOAD KN	13.939	15.978	17.914	19.896	21.881
S.G. NO.	STRAIN EACH LOAD IN %				
1/1	0.006	0.006	0.006	0.006	0.006
1/2	-0.001	0.000	0.001	0.002	0.004
1/3	-0.011	-0.011	-0.011	-0.011	-0.009
2/1	-0.005	-0.005	-0.006	-0.007	-0.007
2/2	0.003	0.003	0.004	0.004	0.004
2/3	-0.000	0.000	-0.000	-0.000	0.000
3/1	0.006	0.007	0.006	0.007	0.007
3/2	0.001	0.001	0.001	0.001	0.001
3/3	0.011	0.012	0.011	0.011	0.012
4/1	-0.001	-0.001	-0.001	-0.002	-0.002
4/2	0.010	0.011	0.011	0.012	0.013
4/3	-0.001	-0.001	-0.001	-0.001	-0.000
5/1	0.003	0.004	0.005	0.005	0.006
5/2	0.002	0.002	0.002	0.003	0.003
5/3	-0.007	-0.009	-0.011	-0.013	-0.014
6/1	0.007	0.008	0.007	0.007	0.008
6/2	0.007	0.007	0.007	0.007	0.007
6/3	0.001	0.001	0.001	0.001	0.002
7/1	0.000	0.000	0.000	0.000	0.000
7/2	0.002	0.003	0.003	0.003	0.004
7/3	-0.003	-0.003	-0.003	-0.003	-0.324
8/1	-0.325	-0.325	-0.325	-0.325	-0.325
8/2	-0.001	-0.001	-0.001	-0.001	-0.001
8/3	-0.002	-0.002	-0.002	-0.002	-0.002
9/1	0.002	0.002	0.003	0.003	0.003
9/2	0.002	0.001	0.001	0.001	0.001
9/3	-0.001	-0.000	-0.000	-0.000	0.000
10/1	0.009	0.010	0.012	0.014	0.015
10/2	-0.134	-0.132	-0.131	-0.131	-0.132
10/3	0.018	0.021	0.024	0.027	0.030
11/1	-0.026	-0.029	-0.034	-0.038	-0.043
11/2	0.025	0.028	0.030	0.033	0.036
12/1	0.017	0.019	0.021	0.023	0.025
12/2	-0.033	-0.038	-0.043	-0.049	-0.054
13/1	-0.021	-0.024	-0.027	-0.030	-0.032
13/2	0.018	0.021	0.023	0.025	0.027
14/1	0.022	0.025	0.028	0.031	0.034
14/2	-0.016	-0.018	-0.020	-0.022	-0.024
15/1	0.016	0.018	0.021	0.023	0.026
15/2	-0.025	-0.028	-0.032	-0.035	-0.038
16/1	-0.008	-0.010	-0.012	-0.014	-0.015

LOAD KN	13.939	15.978	17.914	19.896	21.881
S.G. NO.	STRAIN EACH LOAD IN %				
16/2	0.016	0.019	0.020	0.022	0.024
17/1	0.035	0.040	0.044	0.049	0.053
17/2	-0.025	-0.029	-0.032	-0.036	-0.039
38/3	-0.045	-0.047	-0.048	-0.048	-0.047
39/3	-0.115	-0.125	-0.133	-0.141	-0.148
40/3	-0.177	-0.204	-0.234	-0.268	-0.304
41/3	0.135	0.125	0.115	0.105	0.096
42/3	-0.101	-0.114	-0.128	-0.142	-0.155
43/3	-0.093	-0.106	-0.118	-0.131	-0.143
44/3	-0.059	-0.067	-0.076	-0.084	-0.092
45/3	-0.077	-0.089	-0.100	-0.111	-0.122
46/3	-0.084	-0.096	-0.109	-0.122	-0.134
47/3	-0.045	-0.043	-0.038	-0.033	-0.027
48/3	-0.064	-0.071	-0.078	-0.083	-0.091
49/3	-0.076	-0.087	-0.099	-0.112	-0.121
50/3	-0.039	-0.043	-0.045	-0.046	-0.047
51/3	-0.048	-0.054	-0.060	-0.066	-0.070
52/3	-0.059	-0.068	-0.076	-0.085	-0.094
53/3	-0.039	-0.041	-0.038	-0.015	-0.000
54/3	-0.072	-0.083	-0.095	-0.109	-0.122
55/3	-0.058	-0.064	-0.070	-0.075	-0.077
56/3	-0.021	-0.023	-0.026	-0.029	-0.031
57/3	-0.021	-0.023	-0.026	-0.028	-0.030
66	-0.045	-0.053	-0.061	-0.068	-0.076
67	0.213	0.199	0.186	0.172	0.159
68	-0.031	-0.036	-0.041	-0.046	-0.050
69	-0.052	-0.061	-0.069	-0.077	-0.085
70	-0.037	-0.043	-0.049	-0.055	-0.061
71	-0.019	-0.022	-0.024	-0.027	-0.030
72	-0.054	-0.061	-0.068	-0.076	-0.083
73	-0.015	-0.017	-0.019	-0.021	-0.023
47EXT	-0.081	-0.093	-0.099	-0.103	-0.105
50EXT	-0.049	-0.056	-0.063	-0.067	-0.062
53EXT	-0.059	-0.068	-0.078	-0.102	-0.118

TORSION TEST AT ZERO BENDING

(LOAD APPLIED TO AILERON PICKUP 3706)

LOAD KN		1	2	3	4
S.G. NO.	STRAIN EACH LOAD IN %				
1/1	0.000	0.004	0.004	0.002	0.002
1/2	0.000	0.001	0.002	0.001	0.001
1/3	0.000	-0.001	-0.002	-0.003	-0.003
2/1	0.000	0.000	0.000	-0.001	-0.001
2/2	0.000	0.005	0.006	0.007	0.007
2/3	0.000	0.003	0.003	0.003	0.003
3/1	0.000	-0.001	-0.001	-0.002	-0.002
3/2	0.000	0.004	0.005	0.005	0.005
3/3	0.000	0.002	0.001	0.001	0.001
4/1	0.000	0.000	0.000	-0.001	-0.001
4/2	0.000	-0.002	-0.002	-0.002	-0.002
4/3	0.000	0.003	0.003	0.002	0.002
5/1	0.000	-0.003	-0.004	-0.005	-0.005
5/2	0.000	-0.000	-0.000	-0.000	0.000
5/3	0.000	0.002	0.002	0.001	0.001
6/1	0.000	0.004	0.004	0.003	0.003
6/2	0.000	-0.000	-0.001	-0.001	-0.001
6/3	0.000	-0.001	-0.001	-0.001	-0.001
7/1	0.000	-0.003	-0.003	-0.003	-0.002
7/2	0.000	0.001	0.002	0.001	0.001
7/3	0.000	-0.324	0.000	-0.000	-0.324
8/1	0.000	0.016	0.016	0.016	0.014
8/2	0.000	-0.003	-0.005	-0.007	-0.010
8/3	0.000	-0.001	-0.002	-0.003	-0.003
9/1	0.000	-0.001	-0.000	0.000	0.001
9/2	0.000	0.004	0.004	0.002	0.000
9/3	0.000	0.002	0.003	0.003	0.003
10/1	0.000	0.001	0.002	0.003	0.003
10/2	0.000	0.161	0.162	0.162	0.161
10/3	0.000	0.004	0.005	0.005	0.005
11/1	0.000	0.001	-0.001	-0.006	-0.010
11/2	0.000	0.003	0.005	0.007	0.010
12/1	0.000	-0.001	0.003	-0.003	-0.004
12/2	0.000	0.006	0.007	0.007	0.007
13/1	0.000	-0.002	-0.004	-0.007	-0.010
13/2	0.000	-0.001	0.000	0.002	0.004
14/1	0.000	0.003	0.003	0.002	0.003
14/2	0.000	0.001	0.001	0.000	0.000
15/1	0.000	-0.001	-0.000	0.000	0.000
15/2	0.000	0.001	0.002	0.001	0.000
16/1	0.000	-0.003	-0.007	-0.012	-0.017

LOAD AT AILERON PICKUP 3706

LOAD KN		1	2	3	4
S.G. NO.	STRAIN EACH LOAD IN %				
16/2	0.000	0.009	0.013	0.018	0.022
17/1	0.000	0.004	0.007	0.010	0.012
17/2	0.000	0.004	0.002	-0.001	-0.004
38/3	0.000	0.001	-0.004	-0.012	-0.020
39/3	0.000	-0.006	-0.016	-0.031	-0.044
40/3	0.000	-0.003	-0.015	-0.033	-0.051
41/3	0.000	-0.052	-0.058	-0.069	-0.079
42/3	0.000	-0.002	-0.009	-0.022	-0.034
43/3	0.000	-0.001	-0.008	-0.020	-0.032
44/3	0.000	-0.002	-0.008	-0.017	-0.026
45/3	0.000	-0.001	-0.008	-0.019	-0.030
46/3	0.000	0.000	-0.008	-0.020	-0.032
47/3	0.000	-0.000	-0.007	-0.016	-0.024
48/3	0.000	-0.000	-0.007	-0.016	-0.025
49/3	0.000	-0.003	-0.012	-0.023	-0.035
50/3	0.000	0.007	0.011	0.016	0.023
51/3	0.000	-0.009	-0.015	-0.024	-0.029
52/3	0.000	-0.003	-0.010	-0.018	-0.024
53/3	0.000	0.003	0.004	0.006	0.009
54/3	0.000	-0.008	-0.012	-0.016	-0.018
55/3	0.000	-0.002	-0.009	-0.018	-0.026
56/3	0.000	-0.004	-0.010	-0.018	-0.025
57/3	0.000	0.004	0.004	0.002	0.001
66	0.000	-0.000	-0.009	-0.021	-0.032
67	0.000	0.009	0.012	0.002	0.009
68	0.000	-0.004	-0.015	-0.097	-0.155
69	0.000	0.001	-0.012	-0.052	-0.074
70	0.000	0.004	0.004	0.003	0.002
71	0.000	-0.007	-0.018	-0.032	-0.047
72	0.000	-0.009	-0.022	-0.039	-0.058
73	0.000	-0.002	-0.005	-0.006	-0.004
47EXT	0.000	0.003	0.007	0.012	0.020
50EXT	0.000	-0.006	-0.014	-0.025	-0.032
53EXT	0.000	0.005	0.006	0.006	0.005

TORSION TEST AT ZERO BENDING
LOAD APPLIED TO AILERON PICKUP 3106

LOAD KN	2	3	4	5	6
S.G. NO.	STRAIN EACH LOAD IN %				
1/1	0.004	0.002	0.002	-0.325	0.001
1/2	0.002	0.001	0.001	0.002	0.002
1/3	-0.002	-0.003	-0.003	-0.004	-0.004
2/1	0.000	-0.001	-0.001	-0.001	-0.002
2/2	0.006	0.007	0.007	0.008	0.009
2/3	0.003	0.003	0.003	0.003	0.003
3/1	-0.001	-0.002	-0.002	-0.002	-0.002
3/2	0.005	0.005	0.005	0.006	0.007
3/3	0.001	0.001	0.001	0.001	0.002
4/1	0.000	-0.001	-0.001	-0.001	-0.001
4/2	-0.002	-0.002	-0.002	-0.001	-0.001
4/3	0.003	0.002	0.002	0.002	0.002
5/1	-0.004	-0.005	-0.005	-0.005	-0.005
5/2	-0.000	-0.000	0.000	0.001	0.001
5/3	0.002	0.001	0.001	0.000	-0.000
6/1	0.004	0.003	0.003	0.004	0.004
6/2	-0.001	-0.001	-0.001	-0.001	-0.001
6/3	-0.001	-0.001	-0.001	-0.000	-0.000
7/1	-0.003	-0.003	-0.002	-0.002	-0.002
7/2	0.002	0.001	0.001	0.000	-0.000
7/3	0.000	-0.000	-0.324	0.003	0.004
8/1	0.016	0.016	0.014	0.018	0.012
8/2	-0.005	-0.007	-0.010	-0.013	-0.015
8/3	-0.002	-0.003	-0.003	-0.001	0.001
9/1	-0.000	0.000	0.001	0.001	0.001
9/2	0.004	0.002	0.000	-0.001	-0.002
9/3	0.003	0.003	0.003	0.005	0.006
10/1	0.002	0.003	0.003	0.004	0.005
10/2	0.162	0.162	0.161	0.161	0.159
10/3	0.005	0.005	0.005	0.006	0.006
11/1	-0.001	-0.006	-0.010	-0.013	-0.015
11/2	0.005	0.007	0.010	0.013	0.015
12/1	0.003	-0.003	-0.004	-0.005	-0.005
12/2	0.007	0.007	0.007	0.008	0.008
13/1	-0.004	-0.007	-0.010	-0.013	-0.015
13/2	0.000	0.002	0.004	0.006	0.008
14/1	0.003	0.002	0.003	0.003	0.002
14/2	0.001	0.000	0.000	0.000	0.001
15/1	-0.000	0.000	0.000	0.001	0.001
15/2	0.002	0.001	0.000	-0.001	-0.001
16/1	-0.007	-0.012	-0.017	-0.021	-0.025

LOAD APPLIED TO AILERON PICKUP 3706. TORSION ONLY TEST

LOAD KN	2	3	4	5	6
S.G. NO.	STRAIN EACH LOAD IN %				
16/2	0.013	0.018	0.022	0.026	0.030
17/1	0.007	0.010	0.012	0.015	0.016
17/2	0.002	-0.001	-0.004	-0.006	-0.008
38/3	-0.004	-0.012	-0.020	-0.025	-0.029
39/3	-0.016	-0.031	-0.044	-0.056	-0.064
40/3	-0.015	-0.033	-0.051	-0.067	-0.079
41/3	-0.058	-0.069	-0.079	-0.087	-0.094
42/3	-0.009	-0.022	-0.034	-0.044	-0.053
43/3	-0.008	-0.020	-0.032	-0.042	-0.050
44/3	-0.008	-0.017	-0.026	-0.033	-0.040
45/3	-0.008	-0.019	-0.030	-0.039	-0.047
46/3	-0.008	-0.020	-0.032	-0.043	-0.052
47/3	-0.007	-0.016	-0.024	-0.029	-0.027
48/3	-0.007	-0.016	-0.025	-0.032	-0.038
49/3	-0.012	-0.023	-0.035	-0.045	-0.054
50/3	0.011	0.016	0.023	0.031	0.041
51/3	-0.015	-0.024	-0.029	-0.029	-0.023
52/3	-0.010	-0.018	-0.024	-0.026	-0.020
53/3	0.004	0.006	0.009	0.011	0.015
54/3	-0.012	-0.016	-0.018	-0.020	-0.021
55/3	-0.009	-0.018	-0.026	-0.033	-0.038
56/3	-0.010	-0.018	-0.025	-0.033	-0.041
57/3	0.004	0.002	0.001	-0.001	-0.003
66	-0.009	-0.021	-0.032	-0.043	-0.053
67	0.012	0.002	0.009	0.018	0.027
68	-0.015	-0.097	-0.155	-0.204	-0.246
69	-0.012	-0.052	-0.074	-0.091	-0.104
70	0.004	0.003	0.002	-0.001	-0.003
71	-0.018	-0.032	-0.047	-0.061	-0.076
72	-0.022	-0.039	-0.058	-0.076	-0.094
73	-0.005	-0.006	-0.004	0.001	0.011
47EXT	0.007	0.012	0.020	0.028	0.036
50EXT	-0.014	-0.025	-0.032	-0.038	-0.040
53EXT	0.006	0.006	0.005	0.003	0.000

Appendix G.

Tests of different adhesives and surface preparations for joining CFRP.

This appendix also contains a method of analysis for adhesively bonded lap joints.

Tests of different adhesives and preparations for joining CFRP.

Four single lap shear test specimens were produced, 30 mm wide with a joint overlap of 15mm. The layup used was +-45(2),0 SYM using 0.34mm Ciba-Geigy 913-815 woven prepreg with XAS-913 unidirectional material 0.125mm thick.
Two of the coupons were prepared by lightly abrading the surface to a matt finish using 600 grade silicon carbide paper, followed by degreasing in acetone. The other two were left with no preparation at all apart from the degreasing.

Two adhesives were tested, both made by Ciba-Geigy Ltd. They were both paste type room temperature curing epoxy materials. One was Redux 403, an adhesive developed for improving the fatigue life of riveted joints in aluminium. This material is widely used in the College of Aeronautics for bonding of aluminium end tags to CFRP coupons for tensile testing.
The other adhesive was Araldite 2005, a commercial high peel strength adhesive. Both adhesives have a claimed shear strength of around 30 MPA for metals.

Results:

Stress MPA	Adhesive	Surf. Prep.	Remarks
25.3	2005	light abrasion	Fibres broken on surface - good.
23.5	2005	none	Adhesive itself sheared.
10.4	403	light abrasion	Adhesive separated- little trace left on one side.
12.4	403	none	Adhesive sheared- traces left on each half.

Theory:

A stress concentration approach was used to determine the strength of the joint from:

$$\frac{l}{k} = L\sqrt{\frac{G}{Et\delta}}$$

Where: δ = bondline thickness,
G = shear modulus of the adhesive,
t = adherend thickness,
E = adherend extentional modulus,
L = length of joint,
τ_{MAX} = maximum shear stress of the adhesive.

Stress concentration $= n = \frac{\tau_{MAX}}{\tau_m} = \frac{1}{k} \coth \frac{1}{k}$

From this the failure load $F = \frac{\tau_{MAX}}{n}$

This method gave a predicted joint strength of 3.3 KN using Araldite 2005 properties, which is rather conservative.

Reference:

Metal to metal adhesive bonding,
S. Semerdjiev,
Business books Ltd, London.

Appendix H.

Drawings.

A1-CFRP-01.	Wing composite stiffened skin panels top and bottom.
A1-CFRP-02.	A1 CFRP spars.
A1-CFRP-03.	A1 CFRP wing ribs.
A1-CFRP-04.	A1 CFRP wing strain gauge positions, wiring, types.
A1-CFRP-05.	CFRP wing box whiffle tree test rig.
A1-CFRP-06.	Wing skin tooling details for top and bottom skins.
A1-CFRP-07.	Leading and trailing spar tools.
A1-CFRP-08.	Dummy tooling stiffener sections.
A1-CFRP-09.	Leading spar slot tooling.
A1-CFRP-10.	Stiffener tooling caul plates.
A1-CFRP-11.	Trailing spar slot and stiffener tooling.
A1-CFRP-12.	Common and leading stiffener tooling sections.

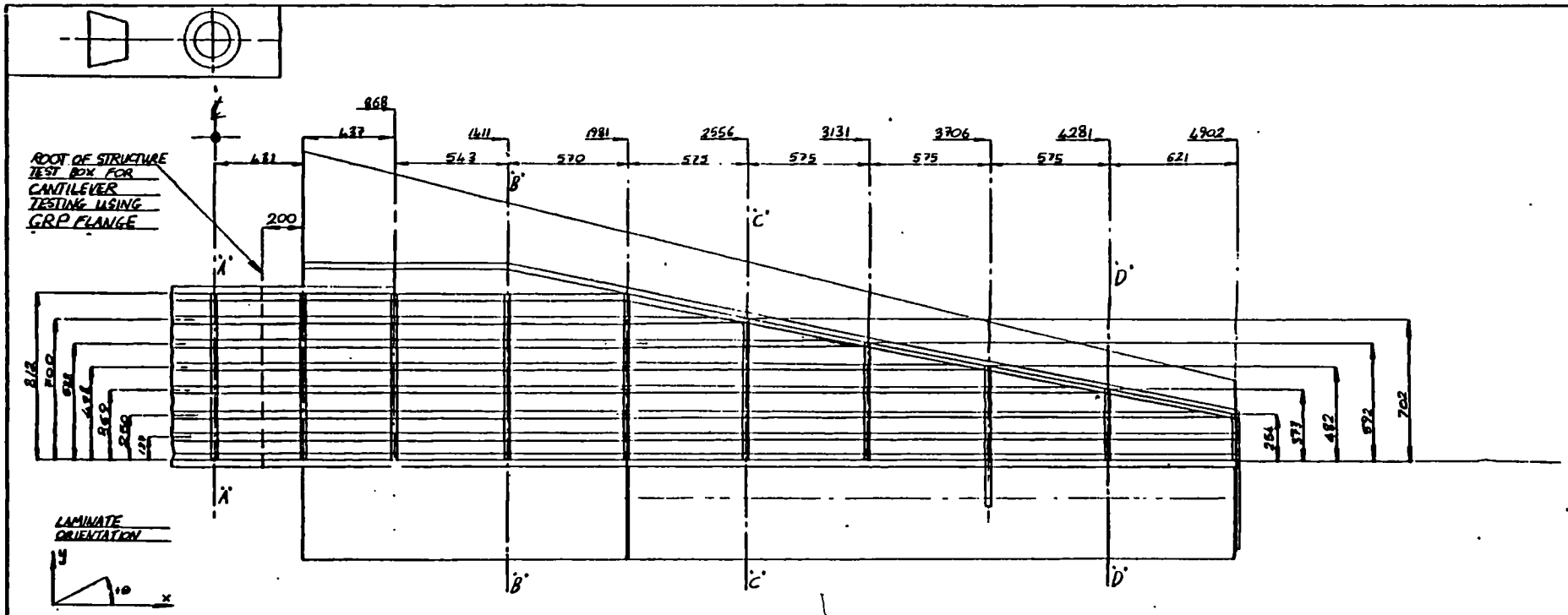

LAMINATE	STN 0 - 431	STN 431 - 868	STN 868 - 1411	STN 1411 - 1981	STN 1981 - 2556	STN 2556 - 3131	STN 3131 - 3706	STN 3706 - 4281	STN 4281 - 4902
Top Skin	±45(2) 0(2)S = 1.87mm	±45(2) 0(2)S = 1.87mm	±45(2) 0(2)S = 1.87	±45, 0 S = 1.61mm	±45, 0 S = 1.61mm	±45 0 S = 0.73mm	±45 = 0.73mm	±45 = 0.88mm	±45 = 0.88mm
Top Stiff. Side Wall	±45(2)	±45(2)	±45(2)	±45(2)	±45(2)	±45	±45	±45	±45
Top Stiff. Cap	±45, 0(2) ±45	±45, 0(2) ±45	±45, 0(2) ±45	±45, 0(2) ±45	±45, 0(2) ±45	±45, 0(2)	±45, 0(2)	±45, 0(2)	±45, 0(2)
Top Stiffener Height	27mm	27mm	27mm	27 mm	27 — 35.5 mm	23.5 — 30 mm	30 mm	30 mm	30 mm
Bottom Skin	±45(2) 0 S	±45 0 S	±45 0 6	±45(2) 0 6	±45 0 S	±45 0 S	±45 S	±45 S	±45 S
Bot. Stiff. Side Wall	±45(2)	±45(2)	±45(2)	±45(2)	±45	±45	±45	±45	±45
Bot. Stiff. Cap	±45, 0(2) ±45	±45, 0(2) ±45	±45, 0(2) ±45	±45, 0(2) ±45	±45, 0(2)	±45, 0(2)	±45, 0(2)	±45, 0(2)	±45, 0(2)
Bot. Stiffener Height	27mm	27mm	30 mm	27 mm	30 - 23.5 mm	23.5 - 30 mm	30 mm	30 mm	30 mm

MATERIAL	APPLICATION	THICKNESS
CIBA 913-815-35	ALL ±45° PLIES	0.34 mm
CIBA XAS-913-12	ALL 0° PLIES	0.127 mm
COMPOSITE MFG	STIFFENER CORES	

CURING
CURE TO CIBA - GEIGY 913 SCHEDULE
USING 40 PSI AUTOCLAVE PRESSURE

"A-A" STIFFENERS 2-7 FULL SCALE

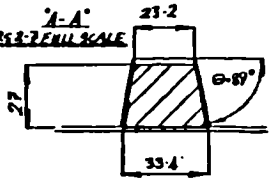

"B-B"

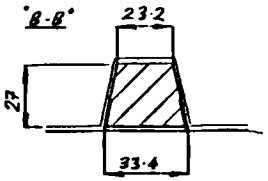

"C-C"

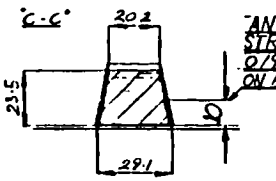

"ANTI-PEEL" STRIP 1 PLY 0/90° WOVEN ON ALL STIFFENERS

"D-D"

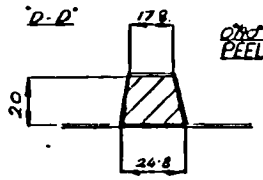

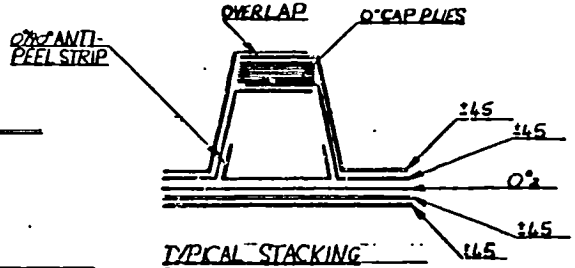

TYPICAL STACKING SEQUENCE AT ROOT

VALUES OF ANGLE Θ FOR L.E (NO. 8) AND T.E (NO. 1) STIFFENERS FOR JOINING TO SPAR SHEAR WEBS

	STN 0	STN 431	868	1384	1981	2556	3131	3706	4281	4902
ΘL	86° 6'	86° 6'	87° 6'	89° 46'	92° 19'	92° 11'	91° 54'	93° 28'	93° 6'	93° 6'
ΘT	98° 57'	98° 57'	98° 9'	97° 32'	96° 29'	95° 18'	95° 8'	94° 10'	93° 6·6'	91° 36'

TYP TRAILING EDGE STIFFENER

R.S

TYP LEADING EDGE STIFFENER (NEAR ROOT)

SLOT TO JOIN TO SPAR WEB

F.S

DRAWN	CHK'D	APP'D	SCALE	TITLE:- WING COMPOSITE STIFFENED SKIN PANELS TOP & BOTTOM
N. ROBERTSON			1/10	
COLLEGE OF AERONAUTICS CRANFIELD INSTITUTE OF TECHNOLOGY CRANFIELD				DRAWING No. A1-CFRP-01 SHT 1 OF 12 SHEETS

F.S

LEADING SPAR

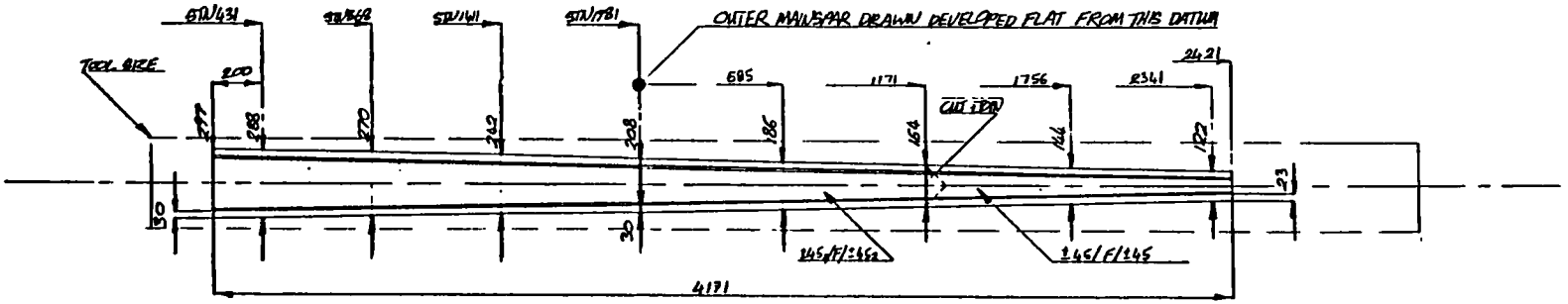

TRAILING SPAR

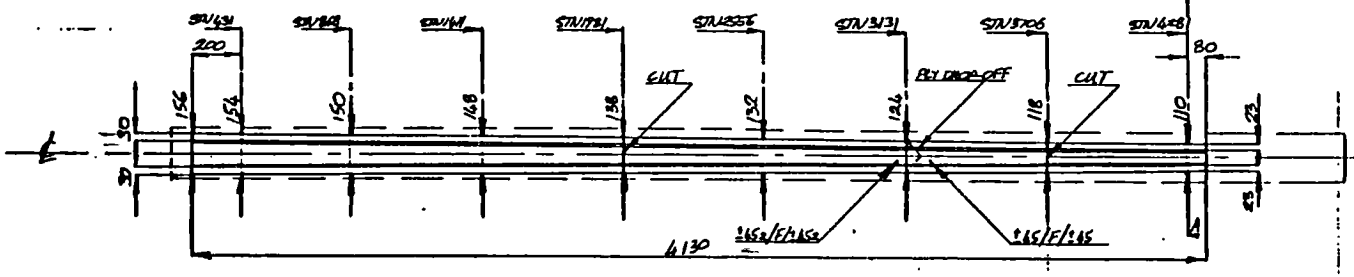

R.S

THYCAL SPAR SECTION A-A.

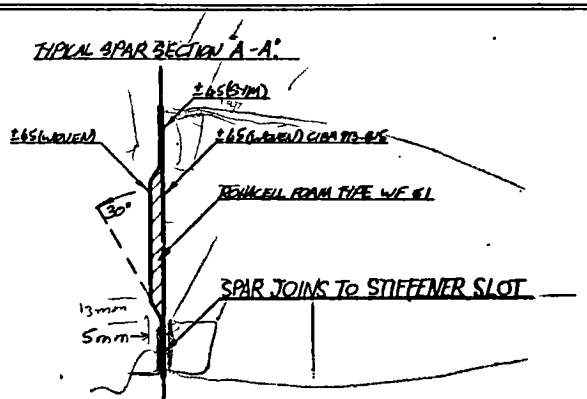

11 CFRP SPARS	
1/10 SCALE 26/1/87	
W.J BROOKS	
SHEET 2 OF 12	11-CFRP-02

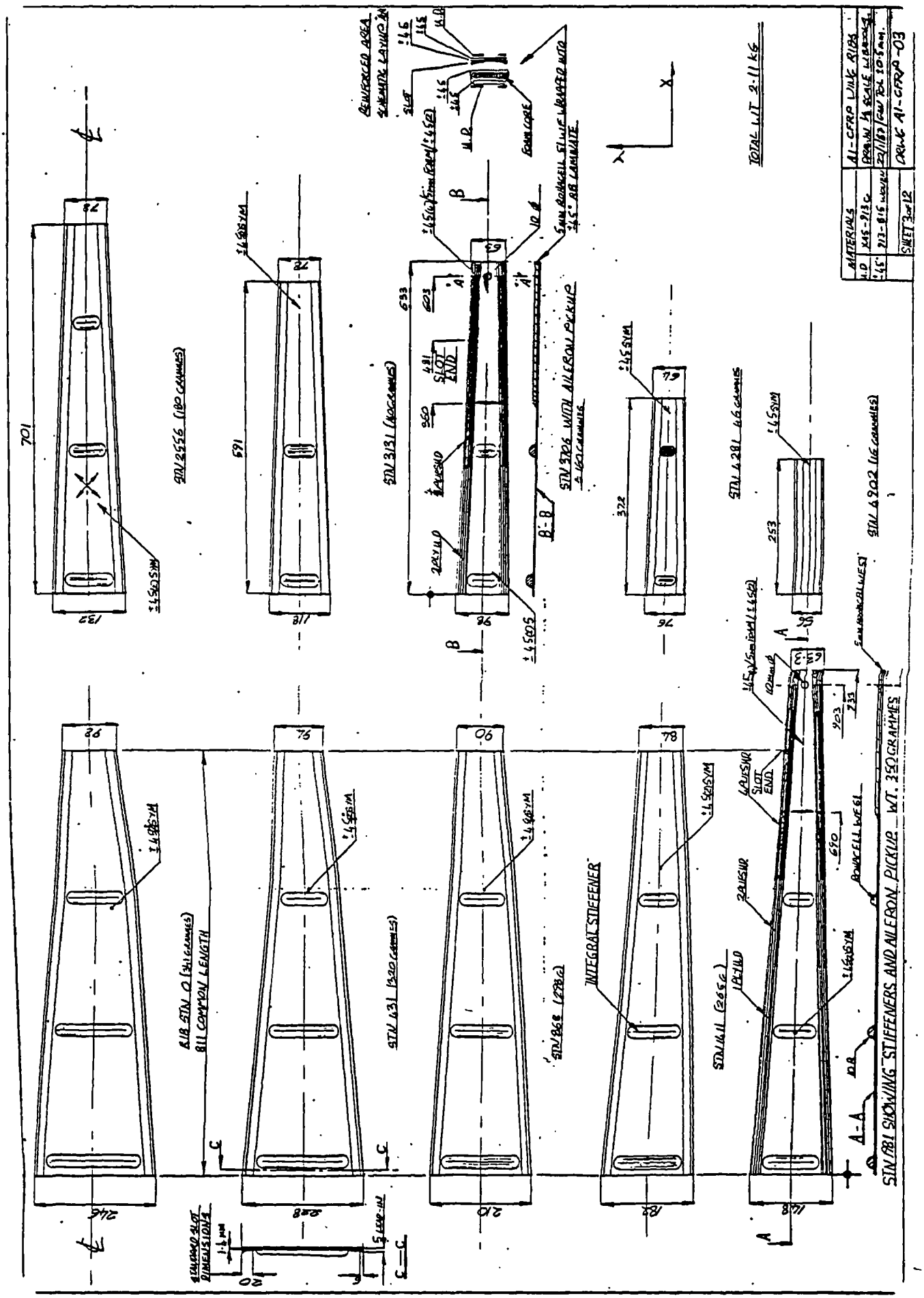
STN 2556 (100 GRAMMES)
STN 3131 (160 GRAMMES)
STN 3206 WITH AILERON PICKUP (160 GRAMMES)
STN 4281 (46 GRAMMES)
STN 8902 (16 GRAMMES)
STN 431 (320 GRAMMES)
STN 8868 (278 GRAMMES)
STN 8411 (265 GRAMMES)
AIR STN O (311 GRAMMES)
BILL CONTROL LENGTH
INTEGRAL STIFFENER
STIFFENER SLOT DIMENSIONS
SECTION A-A
SECTION B-B
SECTION C-C
REINFORCED AREA SCHEMATIC LAYUP
45° AB LAMINATE
FOAM CORE
TOTAL WT. 2·11 KG
MATERIALS
A1-CFRP LIKE RIBS
DRAWN 1/4 SCALE WEIGHTS
SHEET 3 OF 12
DRWG A1-CFRP-03

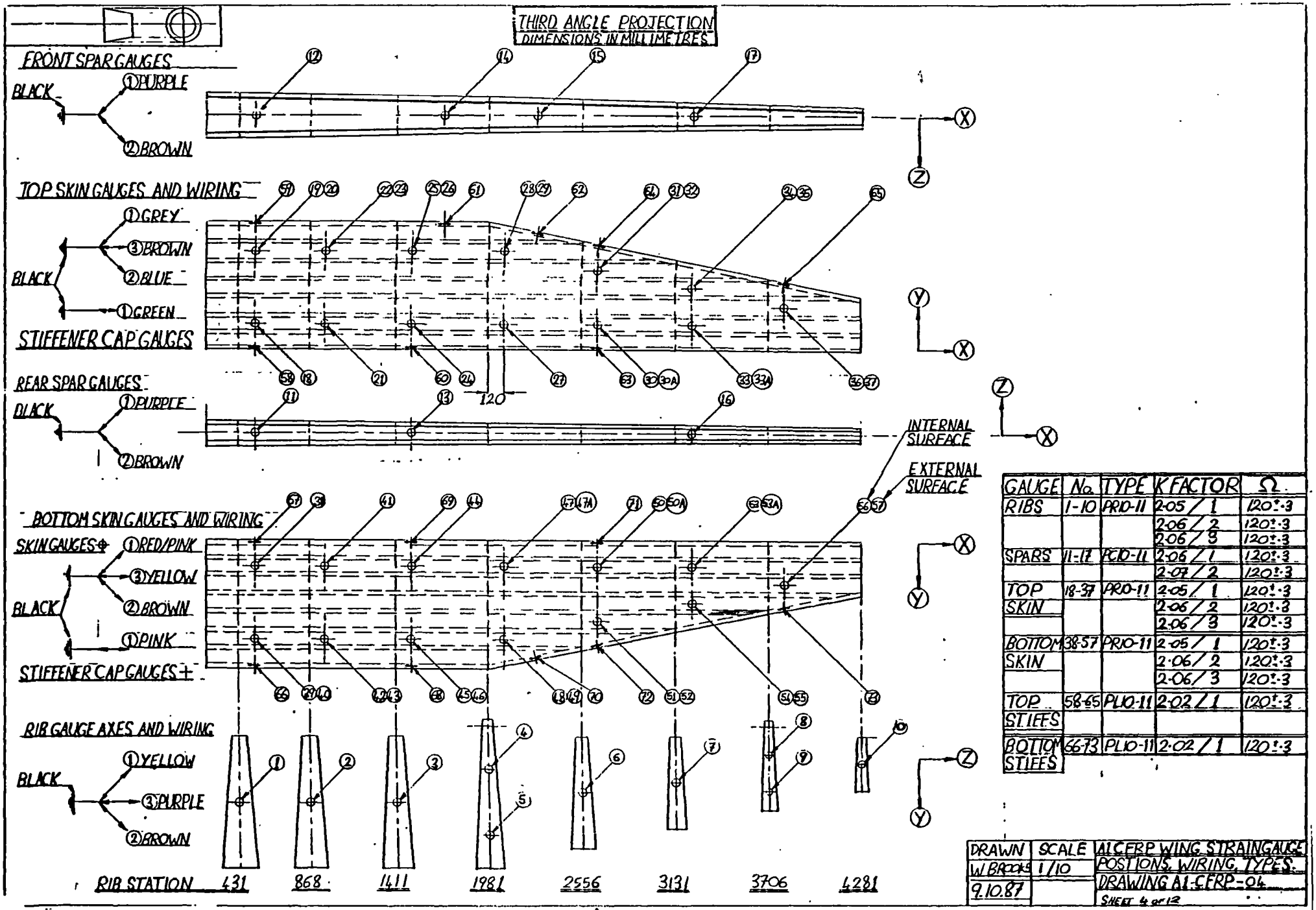

GAUGE	No.	TYPE	K FACTOR	Ω
RIBS	1-10	PRD-11	2·05 / 1	120±·3
			2·06 / 2	120±·3
			2·06 / 3	120±·3
SPARS	11-17	PCD-11	2·06 / 1	120±·3
			2·07 / 2	120±·3
TOP SKIN	18-37	PRD-11	2·05 / 1	120±·3
			2·06 / 2	120±·3
			2·06 / 3	120±·3
BOTTOM SKIN	38-57	PRD-11	2·05 / 1	120±·3
			2·06 / 2	120±·3
			2·06 / 3	120±·3
TOP ST.FFS	58-65	PLD-11	2·02 / 1	120±·3
BOTTOM STIFFS	66-73	PLD-11	2·02 / 1	120±·3

DRAWN	SCALE	AIRCERP WING STRAINGAUGE
W BROOKS	1/10	POSITIONS, WIRING, TYPES.
9.10.87		DRAWING AI-CERP-04
		SHEET 4 OF 12

SECTION A-A

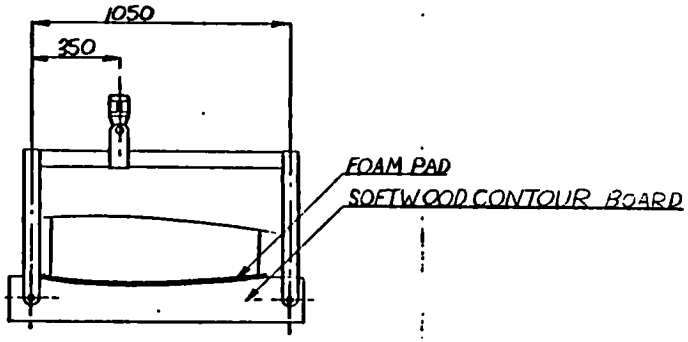

TYPICAL BEAM

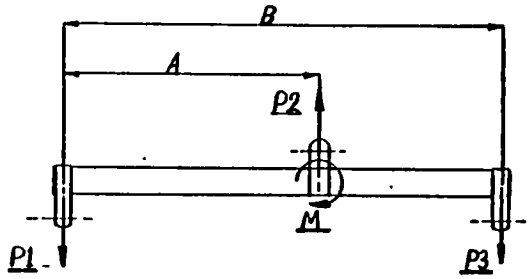

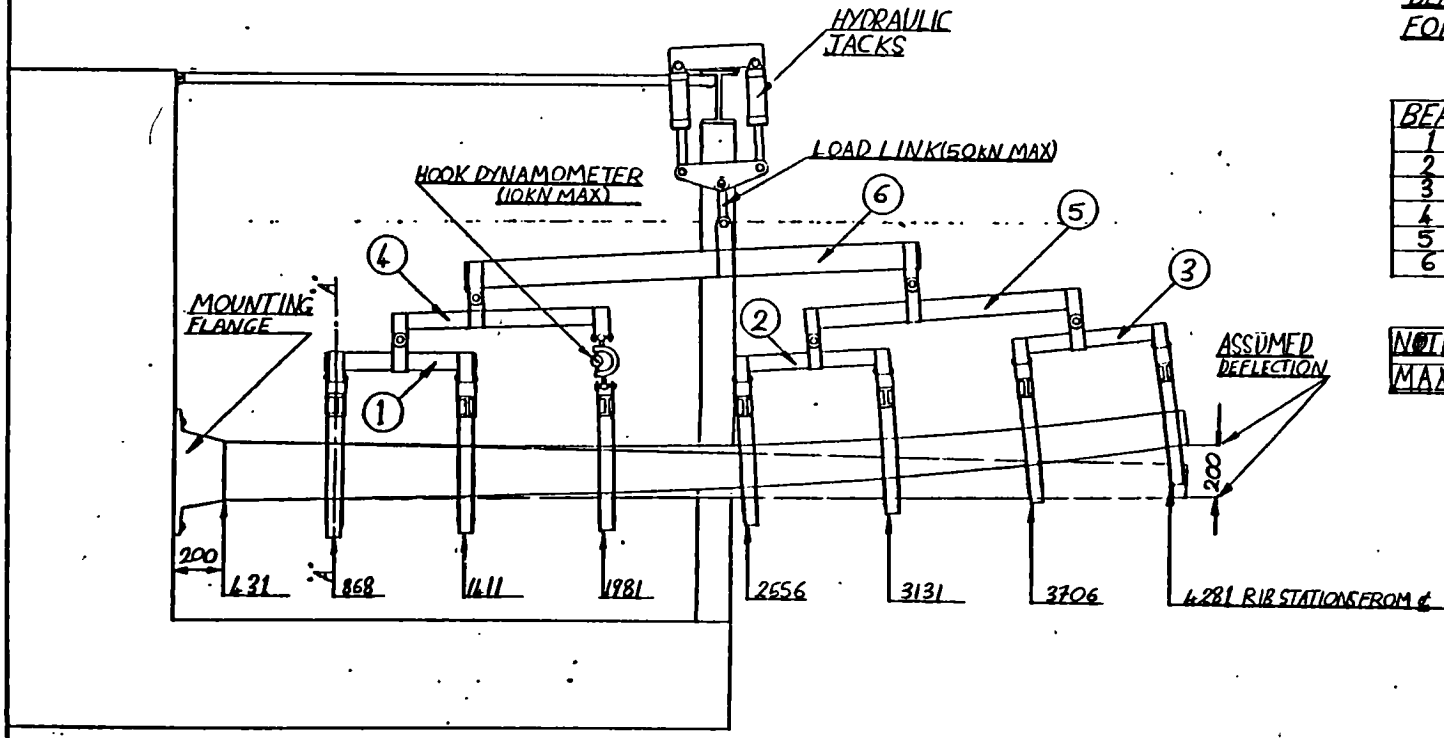

BEAM DIMENSIONS AND FORCES FOR THE POSITIVE ULTIMATE LOAD OF 28·25 kN.

BEAM	A mm	B mm	P1 kN	P2	P3	M kNm
1	253	543	4	7·5	3·5	1·012
2	287	575	5	10	5	1·43
3	280	575	3·75	6·25	2·5	0·86
4	307	820	7·5	12	4·5	2·306
5	411	1070	10	16·25	6·25	4·115
6	1003	1745	12	28·25	16·25	12·036

NOTE
MAXIMUM LOAD CAPABILITY 30 kN

SCALE 1/10	CFRP WING BOX WHIFFLE TREE TEST RIG.
W BROOK 9.10.87	DRWG A1-CFRP-05 SHEET 5 OF 12

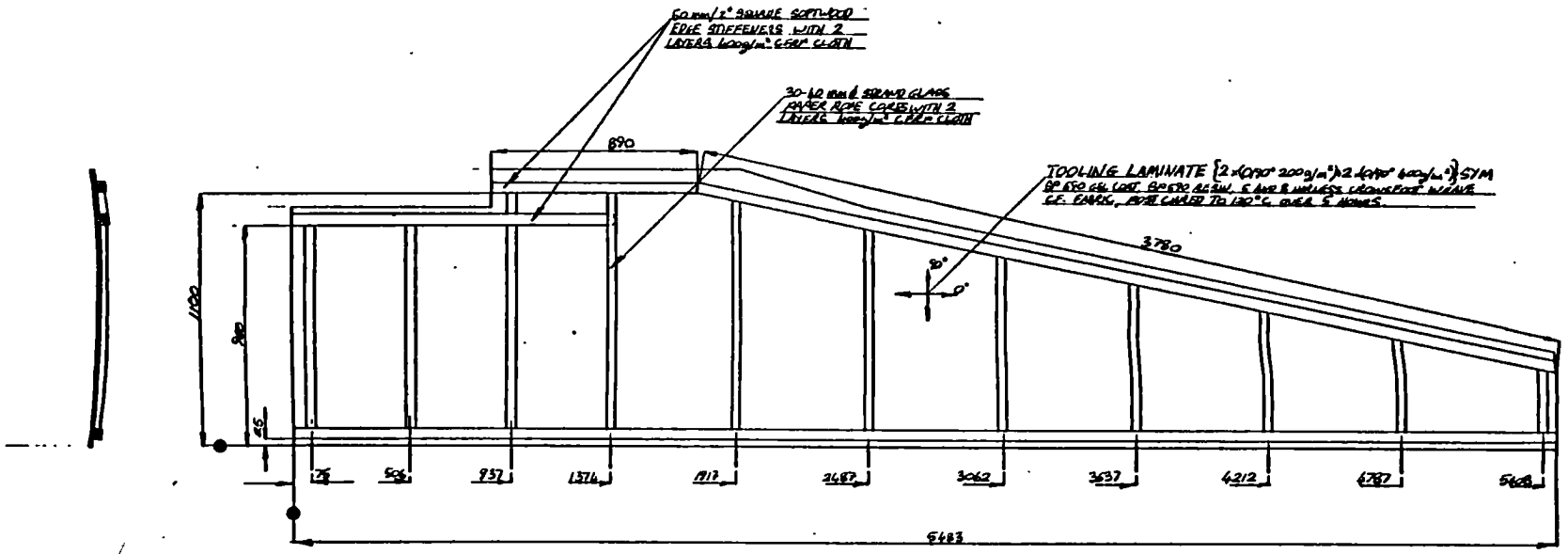

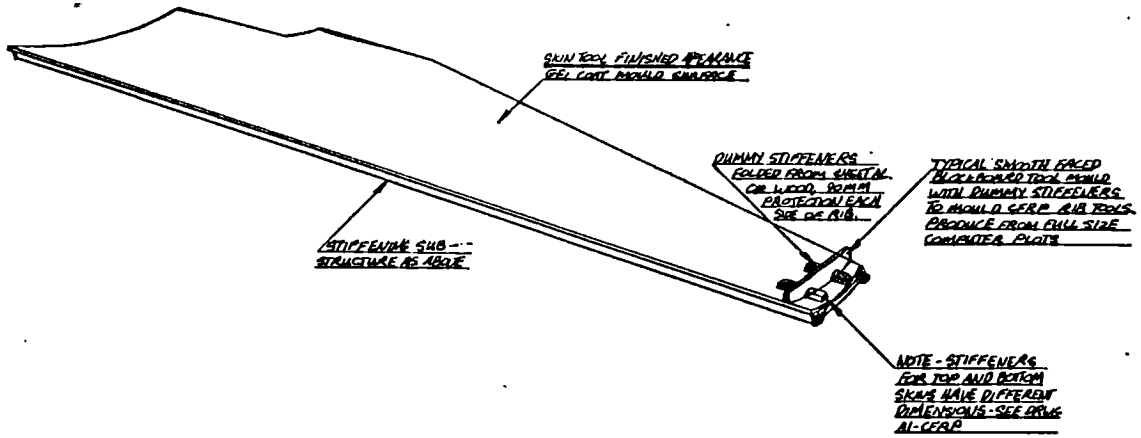

ALL DIMENSIONS MM. GEN TOL ± 0.10 mm

DRAWN	CHK'D	APP'D	SCALE
WE [illegible]			1/10

TITLE:- WING SKIN TOOLING DETAILS FOR TOP AND BOTTOM SKINS.

COLLEGE OF AERONAUTICS
CRANFIELD INSTITUTE OF TECHNOLOGY
CRANFIELD.

DRAWING No. A1-CFRP-06

SHT 6 OF 12 SHEETS

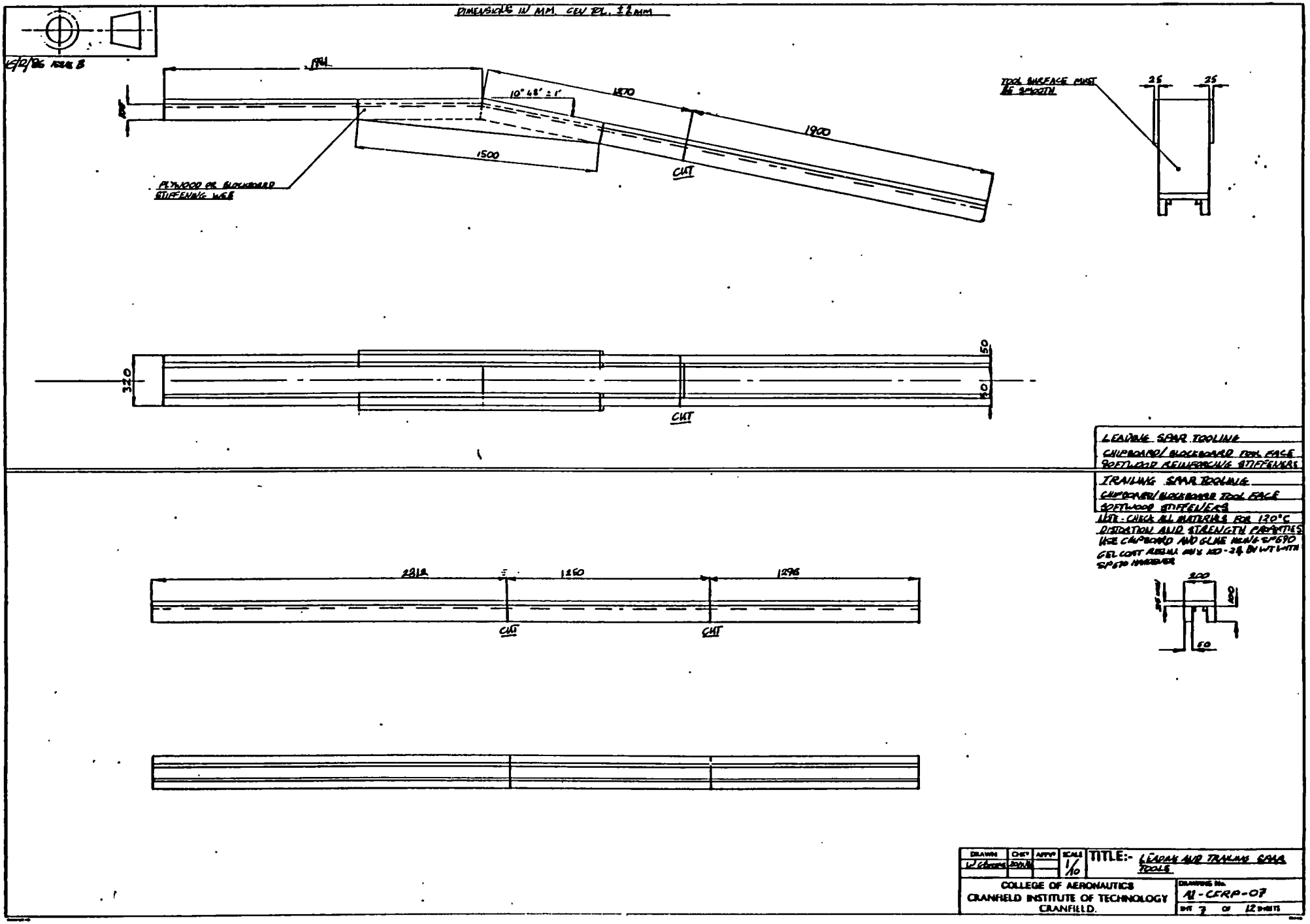
DIMENSIONS IN MM. GEN TOL. ±½MM
6/12/86 ISSUE B
194
10° 48' ± 1°
1670
1900
1500
CUT
PLYWOOD OR BLOCKBOARD STIFFENING WEB
TOOL SURFACE MUST BE SMOOTH
25
25
320
50
50
CUT
LEADING SPAR TOOLING
CHIPBOARD/BLOCKBOARD TOOL FACE
SOFTWOOD REINFORCING STIFFENERS
TRAILING SPAR TOOLING
CHIPBOARD/BLOCKBOARD TOOL FACE
SOFTWOOD STIFFENERS
NOTE - CHECK ALL MATERIALS FOR 130°C
DISTORTION AND STRENGTH PROPERTIES
USE CHIPBOARD AND GLUE MIX SP690
GEL COAT RESIN MIX 100 - 3% BY WT WITH
SP610 HARDENER
2318
1260
1296
CUT
CUT
200
100
50
DRAWN
CHK'D
APP'D
SCALE 1/10
TITLE:- LEADING AND TRAILING SPAR TOOLS
COLLEGE OF AERONAUTICS
CRANFIELD INSTITUTE OF TECHNOLOGY
CRANFIELD.
DRAWING No. A1-CERP-07
SHT 7 OF 12 SHEETS

DIMENSIONS IN MM'S

INNER WING
STIFFENER DUMMY
32 OFF
4M CLOSE-GRAIN WOOD
EG TEKTONG

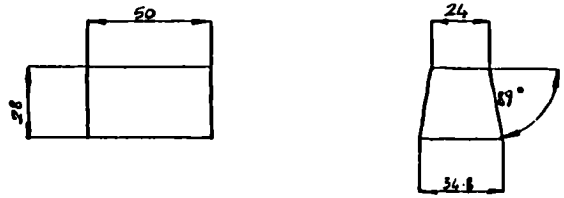

MID-WING STIFFENER DUMMY
30 OFF

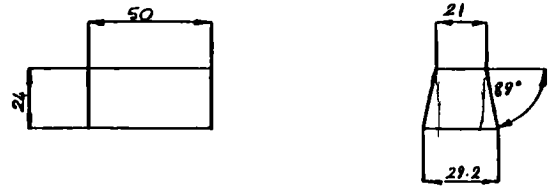

OUTER WING STIFFENER DUMMY
22 OFF

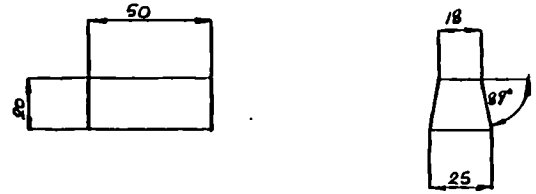

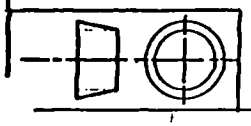

SCALE	TITLE
FULL	DUMMY TOOLING STIFFENER SECTIONS
11.11.86	
THIRD ANGLE PROJ	DRWG A1-CFRP-08

SHEET 8 OF 12

ALL DIMENSIONS IN MMS.

OUTER WING LEADING SPAR SLOT TOOL
FOLD FROM 20 SWG M.S (3mm BEND RADIUS)
2 OFF (MIRROR IMAGE)

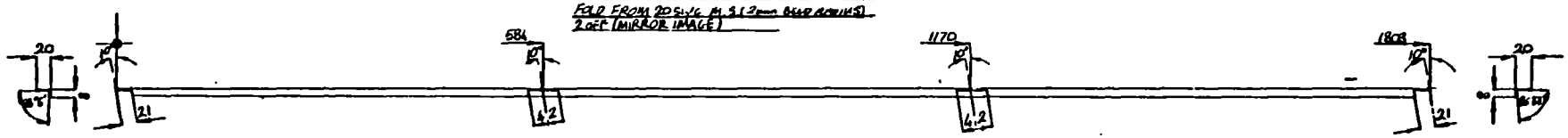

MID WING LEADING SPAR SLOT TOOL
FOLD FROM 18 SWG M.S
2 OFF (MIRROR IMAGE)

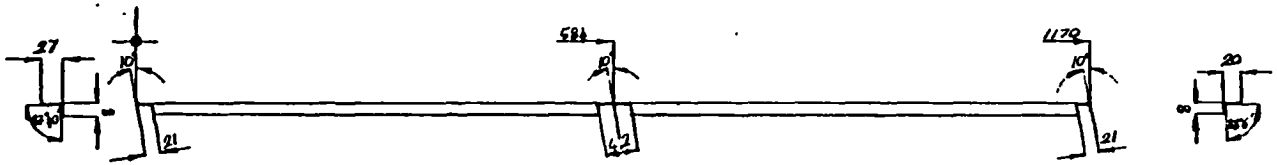

INNER WING LEADING SPAR SLOT TOOL
FOLD FROM 18 SWG M.S.
2 OFF (MIRROR IMAGE)

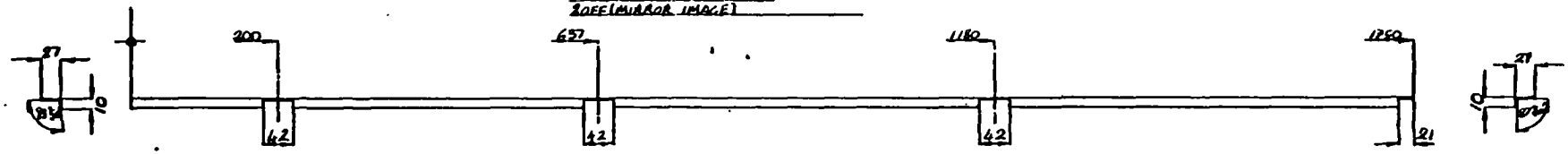

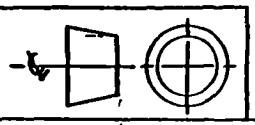

SCALE	TITLE
1/3	LEADING SPAR SLOT TOOLING
FINISH	
MAT.	DRWG. No AI-CFRP-09

SHEET 9 of 12

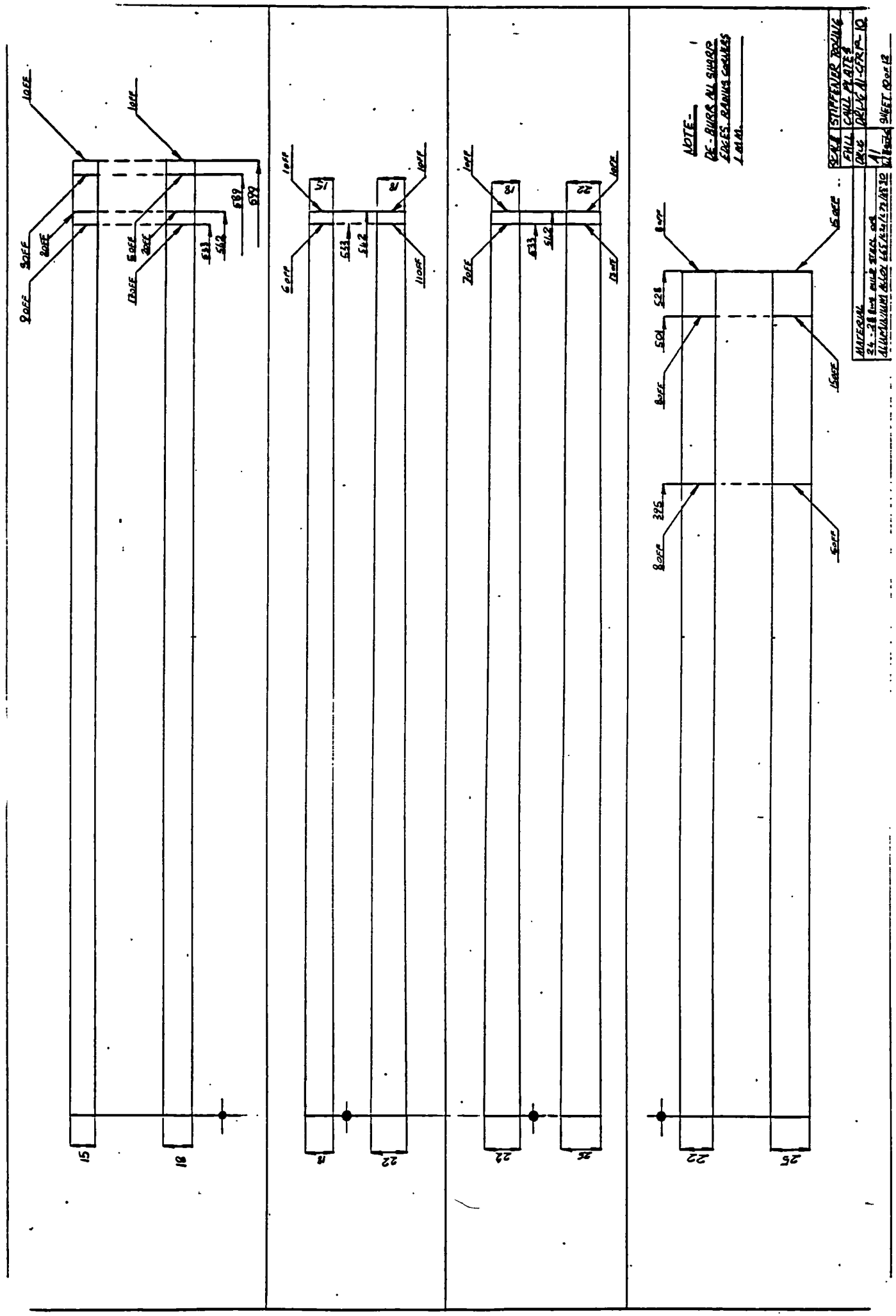
STIFFENER TOOLING
FULL CAUL PLATES
DELVE AI-GFR PA-10
MATERIAL
24-28 ply CMH STAGE 2A
ALUMINUM BLOCK 6061-T6 OR 2024-T3
SHEET 10 of 12
NOTE:
DE-BURR ALL SHARP EDGES. BRING CORNERS TO A RADIUS.

ALL DIMENSIONS IN MILLIMETRES UNLESS OTHERWISE STATED.

WING OUTER TRAILING STIFFENER TOOLING - 3 OFF REQ'D
MIRROR IMAGE. STBD LOWER SHOWN 18 SWG M.S

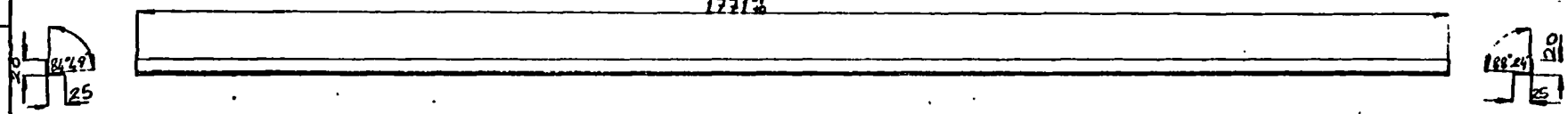

WING MID TRAILING STIFFENER TOOLING - 2 OFF (MIRROR IMAGE) 18 SWG M.S

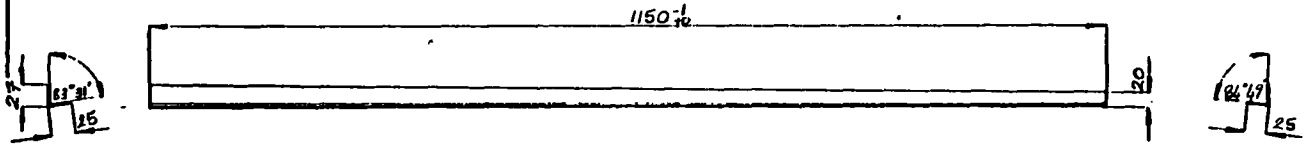

WING INNER TRAILING STIFFENER TOOLING - 2 OFF (MIRROR IMAGE) 18 SWG M.S.

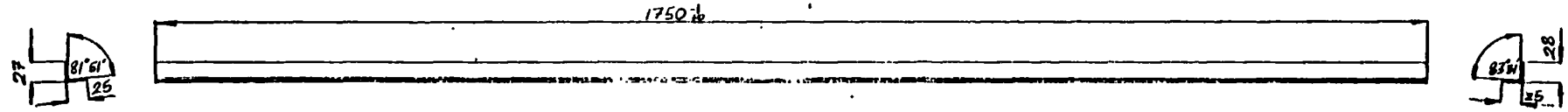

INNER TRAILING SPAR SLOT TOOL - 2 OFF (MIRROR)

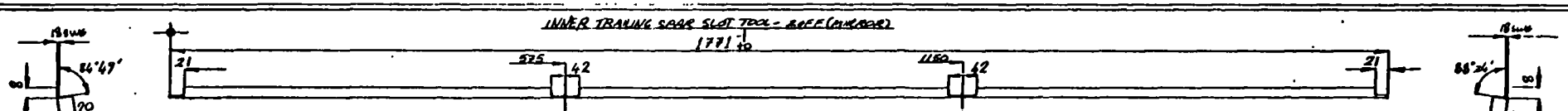

MID TRAILING SPAR SLOT TOOL - 2 OFF (MIRROR)

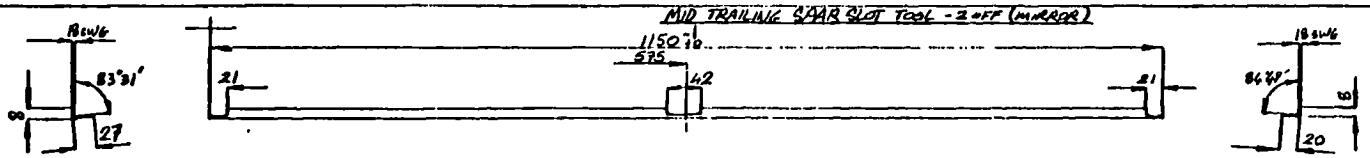

OUTER TRAILING SPAR SLOT TOOL - 3 OFF (MIRROR)

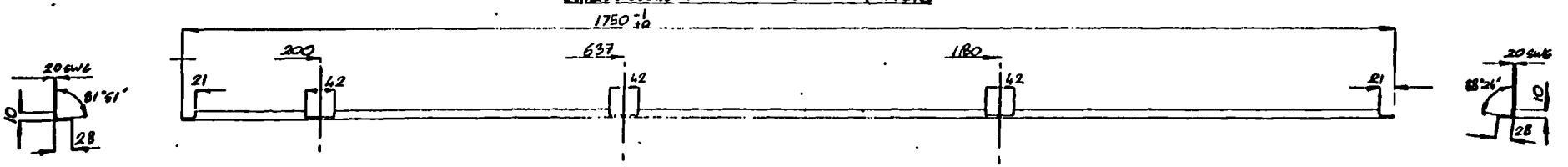

ISSUE	MODIFICATION										

ITEM	PART No.	DESCRIPTION				No. OFF	MAT'L	SPEC.	REMARKS
		DRAWN	CHK'D	APPV'D	ISSUE STATUS				
		W Bates							

THIRD ANGLE PROJECTION

GENERAL TOLERANCE ON DIMENSIONS
MACHINED
UNMACHINED
OTHER DIMENSIONS AS STATED
WELD SHAPE SHOWN THUS
MACHINE SHAPE SHOWN THUS

JOB No. | No. OF SETS REQ'D | USED ON DRG

SHEET SIZE A1
SCALE 1/3
FINISH NAT.

TITLE:- BOX TRAILING SPAR SLOT AND STIFFENER TOOLING

ISSUED BY
CRANFIELD INSTITUTE OF TECHNOLOGY
CRANFIELD.

DRAWING No. A1-CFRP-11

SHT. 11 OF 12 SHEETS

ALL DIMENSIONS IN MILLIMETRES UNLESS OTHERWISE STATED.

ISSUE	DESCRIPTION
B	10 DEC'86

COMMON STIFFENER TOOLING SECTIONS

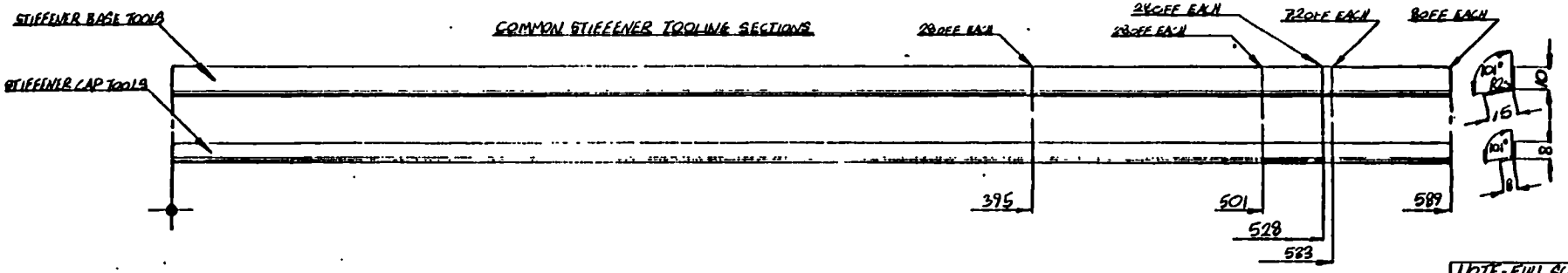

NOTE: FULL SCALE

NOTE - ½ SCALE

OUTER WING LEADING STIFFENER TOOLING - 2 OFF (MIRROR IMAGE) REQUIRED - UPPER SHOWN (STBD)

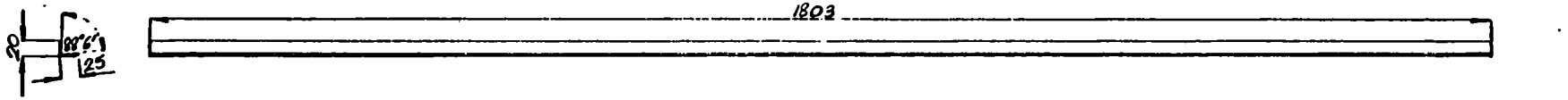

MID WING LEADING STIFFENER TOOLING 2 OFF (MIRROR IMAGE) REQUIRED - UPPER SHOWN (STBD)

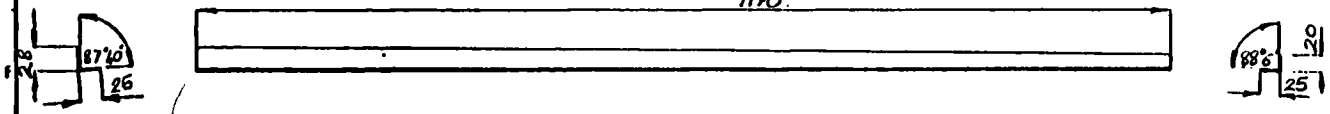

INNER WING LEADING STIFFENER TOOLING - 2 OFF (MIRROR IMAGE) REQUIRED - UPPER SHOWN (STBD)

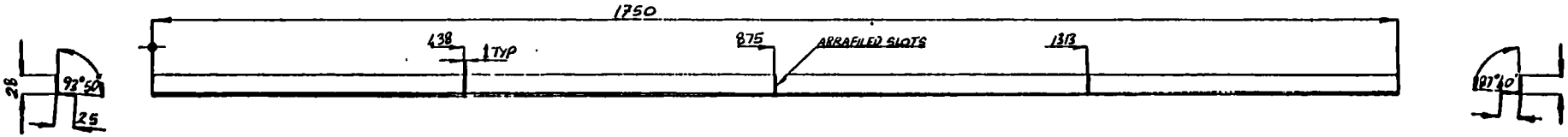

NOTE
ALL PARTS 20SWG MS COLD FORMED
BEND RADIUS 2mm
DEBURR ALL EDGES
CORNER RADIUS 2mm

THIRD ANGLE PROJECTION			A1	ISSUE	PART No.	DESCRIPTION	No. OFF	DATE	SPEC. REMARKS
GENERAL TOLERANCE ON DIMENSIONS: MACHINED / UNMACHINED / OTHER DIMENSIONS AS STATED / EDGES SHOWN THUS ∧∧ / SURFACE FINISH SHOWN THUS √	JOB No.	No. OF SETS REQ'D	FULL 1/8	DRAWN L.J.BROOKS	CHK'D 18/12/86	APPV'D	ISSUE ISSUE	TITLE:- COMMON & LEADING STIFFENER TOOLING SECTIONS	
			FINISH MAT.	ISSUED BY CRANFIELD INSTITUTE OF TECHNOLOGY CRANFIELD.				DRAWING No. A1-CFRP-12-: SHT. 12 OF 12 SHEETS	